Rescuing the paralysed phenotype of *unc-18 (e81)* null mutant *C. elegans*

Thesis submitted in accordance with the requirements of the University of Liverpool for the degree of Doctor in Philosophy by Khoula Afzal

May, 2023

Table of Contents

Abstract

Title: Rescuing the paralysed phenotype of *unc-18 (e81)* null mutant *C. elegans*

Author: Khoula Afzal

Munc-18 (also known as STXBP1) functions as a core component of the fusion machinery at the presynapse, with a role in several stages of the vesicle cycle. In humans, heterozygous *de novo* mutations in Munc18-1 are associated with infantile epileptic encephalopathy, however, there is currently no cure for the disorder. This investigation was interested in whether the function of Munc18-1 could be bypassed if it was completely dysfunctional. As null mutations in Munc18-1 and its homologues in several organisms such as yeast and mammals are unviable, the *C. elegans* nematode was chosen as the model organism. *C. elegans* remain viable yet demonstrate a severely paralysed phenotype. Prior to this work, ethyl methanesulfonate mutagenesis (EMS) of *unc-18 (e81)* null mutants led to the discovery of a mutant, termed *unc-18* rescue, in which locomotion appeared indifferent from wild-type. Whole genome SoLiD sequencing confirmed the presence of the *unc-18 (e81)* mutation in the *unc-18* rescue mutant, as well as two novel mutations in *dgk-1 (ulv1)* and *sorf-2 (ulv2),* and a third mutation in *sorf-2 (ulv3),* which were all hypothesised to be putatively involved in the *unc-18* rescue phenotype. In this investigation, behavioural analysis confirmed that locomotion of *unc-18* rescue mutants was successfully restored to wild-type levels when on a surface, but not when in solution. Expression of wild-type *dgk-1* in *unc-18* rescue mutants reversed improvements in locomotion, confirming the necessity of the *dgk-1 (ulv1)* for the *unc-18* rescue phenotype. However, diacylglycerol kinase (DGK) inhibition or elevated diacylglycerol (DAG) in *unc-18 (e81)* null mutants did not improve locomotion suggesting the necessity of another gene. Transgenic expression of wild-type *sorf-2* reduced the rate of locomotion and confirmed the necessity of *sorf-2*. Together, *sorf-2* RNAi and *dgk-1* inhibition successfully improved locomotion in *unc-18 (e81)* null mutants, but not in *unc-18 (e81)* null mutants lacking the *sorf-2 (ulv3)* mutations, or in alternative *unc-18* null mutants, suggesting *unc-18 (e81)* null specificity for the rescue phenotype. Further, ^{1}H nuclear magnetic resonance (NMR) spectroscopy was able to successfully identify differences in lipid and polar metabolite abundance between wild-type, *unc-18 (e81)* null, and *unc-18* rescue worms, highlighting the importance of lipid pathways in physiological processes. Together these findings confirmed the necessity of the *dgk-1 (ulv1)* and *sorf-2 (ulv2 and ulv3)* mutations in the *unc-18* rescue phenotype and suggest that the *unc-18* rescue phenotype is produced by the combined efforts of proteins and lipids which bypass the function of *unc-18* in synaptic vesicle fusion.

Acknowledgements

The research for this thesis has been aided by a collection of people, who have either directly helped me throughout my PhD or have supported me through the process. Firstly, I would like to thank my funding body, DiMeN, who trusted in me and allowed me to pursue my interest in scientific research. My supervisor, Jeff, who has been more than patient with me throughout the years. Jeff provided me the support and space I needed to develop as an independent researcher. He has continuously helped me critically think about my research and work through my mistakes, without knocking my confidence. Alan, who has always provided me with an alternative perspective. I am grateful for all the suggestions for analysis provided by Alan in my supervisory meetings, which have allowed me to better understand the project. Marie Phelan and Zain Ghanameh, who taught me all I needed to know, and more, about NMR. I am grateful for the help that they both provided me, especially given that this part of my PhD was conducted during the COVID-19 pandemic. Starting off with no NMR knowledge, I now leave confident in the theory and analysis involved with the technique. Liz Seward - although plans to work with Liz did not work out, I am grateful for the enthusiasm and suggestions she provided towards my project. And Lee and Nordine, who provided me with valuable help and suggestions throughout the years of my thesis, as well as memorable Christmas parties.

Working in red block has been incredible and a place where I have met amazing scientists, and life-long friends. Ali, the worm expert who kindly took me under his wing in my first year and kept the lab entertained with his dad jokes. Rick, who had worked in red block since the lab opened and could always be relied on for social plans, making my time in the lab memorable. Nitika, the official red block genius, without whom I could not have finished my PhD. I am extremely grateful for having Nitika's support from day one until the end, our study sessions during writeup, and being able to procrastinate with each other when needed. Liam, my lab brother, who would wind me up more than anyone, but who I could also rely on for a morning Greggs run. Ellie, who understood my *C. elegans* struggles, and who has a work ethic I could only dream of. Robin, my fellow Barclay crew, is one of the nicest people I've met and impressed me with his amazing patching skills. Ami and Amy, who despite starting in my final few months, made those months hilariously fun. I

was grateful to hand over my bench to Amy, who managed to keep as chaotic as I had. Marie, who was only in red block during my first year, but remained supportive of me throughout my PhD.

I would also like to thank my family, who continued to support me despite still thinking I have coursework and exams. Last but not least, I would like to thank my partner Malik, who joined me on the journey from early on and has supported me continuously until the end.

Abbreviations

5-HT=5-hydroxytryptamine

AAA= ATPases Associated with diverse cellular Activities

ACh=acetylcholine

AChE=acetylcholinesterase

AcN=acetonitrile

ADP=adenosine diphosphate

AMP=adenosine monophosphate

ANOVA=analysis of variance

AP2=adaptor protein 2

ARA=arachidonic acid

ATGL=adipose triglyceride lipase

ATP=adenosine triphosphate

AUC=area under the curve

BDCP=Beige and Chediak-Higashi domain containing protein

BEACH=Beige and Chediak-Higashi

BSA=bovine serum albumin

Ca^{2+}=calcium

$CaCl_2$=calcium chloride

CaMb=calmodulin-binding

CAMRQ2=cerebellar ataxia, mental retardation, and disequilibrium syndrome

CAPS=Ca^{2+}-dependent activator protein for secretion

cDNA=complementary deoxyribonucleic acid

CDP-choline=cytidine-diphosphocholine

CDP-DAG=cytidine diacylglycerol

C. elegans=Caenorhabditis elegans

CGC=Caenorhabditis Genetics Center

CHS=Chediak-Higashi Syndrome

CNS=central nervous system

COPI=constitutive photomorphogenic 1

COPII=constitutive photomorphogenic 2

CPMG=Carr-Purcell-Meiboom-Gill

CRISPR=clustered regularly interspaced palindromic repeats

CRS=Correlation Reliability Score

CSP=cysteine string protein

DAG=diacylglycerol

DAGK=diacylglycerol kinase

DAGL=diacylglycerol lipase

DCV=dense-core vesicle

DGAT=diglyceride acyltransferase

dgk-1=diacylglycerol kinase-1

DHA=docosahexaenoic acid

dH_2O=distilled water

DMF=N,N-dimethylformamide

DMSO=dimethyl sulfoxide

DNA=deoxyribonucleic acid

DRS=Dent's Ringer solution

E. coli=Escherichia coli

EDTA=ethylenediaminetetraacetic acid

EMS=ethyl methanesulfonate

EPA=eicosapentaenoic acid

EPG=electropharyngeogram

ER=endoplasmic reticulum

ERGIC=endoplasmic reticulum-Golgi intermediate compartment

FRET=fluorescence resonance energy transfer

GABA=γ-aminobutyric acid

GFP=green fluorescent protein

Gof=gain-of-function

HEPES=4-(2-hydroxyethyl)-1-piperazineethanesulfonic acid)

HIC=hypersensitive to cholinesterase inhibitors

HSL=hormone-sensitive lipase

$Ins(1,4,5)P_3$=inositol (1,4,5)-trisphosphate

IPI=inter-pump interval duration

IPTG=isopropyl β-d-1-thiogalactopyranoside

KH_2PO_4=monopotassium phosphate

LB=Luria-Bertani

LRBA=lipopolysaccharide-responsive, beige-like anchor

LYST=lysosomal trafficking regulator

MAG=monoacylglycerol

MARCKS=myristoylated alanine-rick C kinase substrate

MFS=major facilitator superfamily

MGAT=monoacylglycerol-O-acyltransferase

$MgCl_2$=magnesium chloride

$MgSO_4$=magnesium sulfate

MS=mass spectrometry

ms=millisecond

MUFA=monounsaturated fatty acids

Munc13= mammalian uncoordinated-13

Munc18=mammalian uncoordinated-18

NAC=N-acetylcysteine

NaCl=sodium chloride

NAD=nicotinamide adenine dinucleotide

NADP=nicotinamide adenine dinucleotide phosphate

NADPH=nicotinamide adenine nucleotide phosphate

NA_2HPO_4=disodium phosphate

NaOH=sodium hydroxide

NBEA=neurobeachin

NBEAL1=neurobeachin-like 1

NBEAL2=neurobeachin-like 2

NDMA=N-nitrosodimethylamine

NGM=nematode growth medium

NMJ=neuromuscular junction

NMR=nuclear magnetic resonance

Noesy=Nuclear Overhauser Effect Spectroscopy

NSF= N-ethylmaleimide-sensitive factor

NSMAF=neutral sphingomyelinase activation-associated factor

PA=phosphatidic acid

PC=principal components

PCA=principal component analysis

PCR=polymerase chain reaction

PH=pleckstrin homology

PI=phosphatidylinositol

PI3K=phosphoinositide 3-kinase

PKC=protein kinase C

PKD=protein kinase D

PLA2=phospholipase A2

PLC=phospholipase C

PLD=phospholipase D

PLS=partial least squares

PLS-DA=partial least squares discriminant analysis

PMA=phorbol 12-myristate 13-acetate

PQN=probabilistic quotient normalisation

PS=phosphatidylserine

PSD=phosphorylation site domain

$PI(4,5)P_2$=phosphatidylinositol 4,5-bisphosphate

PIP_3=phosphatidylinositol (3,4,5)-biphosphate

PUFA=polyunsaturated fatty acid

QC=quality control

qPCR=quantitative polymerase chain reaction

Rab=Ras-associated binding

RHO-1=Ras homolog 1

RIC=resistance to cholinesterase inhibitors

RIMS=Rab3-interacting molecules

RNA=ribonucleic acid

RNAi=RNA interference

ROC=receiver operating characteristic

Rop=Ras opposite

SAM=sterile α motif

SD=standard deviation

SE=standard error

SM=Sec1/Munc18

SMS=sphingomyelin synthase

SNAP-25=synaptosomal-associated protein of 25 kDa

SNAPS=soluble NSF-attachment proteins

SNARE=soluble N-ethylmaleimide-sensitive factor activating protein receptor

SNR=signal to noise ratio

SoC=super optimal broth with catabolite repression

SoLiD=sequencing by oligonucleotide ligation and detection

sorf-1=suppressor of organelle function 1

sorf-2=suppressor of organelle function 2

STXBP1=syntaxin binding protein-1

TEA=tris-acetate EDTA

TG=triglycerides

TMAO=trimethylamine N-oxide

TSP=trimethylsilyl-$^2H_4$-propionate

UDP=uridine diphosphate

UFA=unsaturated fatty acid

unc-13=uncoordinated-13

unc-18=uncoordinated-18

VAMP=vesicle associated membrane protein

VIP=variable importance in projection

Vps33p=vacuolar protein sorting-associated protein 33

Vps45p=vacuolar protein sorting-associated protein 45

WD=tryptophan-aspartic acid

WDFY3=WD and FYVE zinc finger domain-containing protein 3

WDFY4=WD and FYVE zinc finger domain-containing protein 4

WDR81=WD repeat domain 81

WT=wild-type

Chapter 1. Introduction

1.1 Thesis overview

Munc-18 (also known as STXBP1) functions as a core component of the fusion machinery at the presynapse, with functions in several stages of the vesicle cycle (1–4). Through interactions with key proteins on the vesicle membrane (synaptobrevin 2) and on the target membrane (syntaxin-1 and synaptosomal-associated protein 25), Munc18-1 regulates the fusion and release of synaptic vesicles (5–7). In humans, heterozygous *de novo* mutations in Munc18-1 were first described in early infantile epileptic encephalopathy (8) and have since been linked to intellectual disorders, neurodegeneration, and movement disorders. To date, there have been more than 100 different variants of STXBP1 identified in patients with epileptic encephalopathies, including missense mutations, truncating mutations, and partial or whole gene deletions (9). Due to lack of understanding of STXBP1-related disorders, there is no cure for epileptic encephalopathies, which results in high mortality and morbidity (10). This investigation aimed to investigate whether the function of Munc18-1/*unc-18* could be bypassed if it is completely dysfunctional. Null mutations in Munc18-1 and it's homologues in several organisms have been found to be unviable (11–13). However, null mutations in the *C. elegans* homologue, *unc-18,* result in paralysis yet the worms remain viable. Therefore, *C. elegans* was chosen as the model organism for this investigation. Prior to the work described in this thesis, ethyl methanesulfonate (EMS) mutagenesis of *unc-18 (e81)* null mutants was carried out to identify novel mutants with differing phenotypes. EMS mutagenesis led to the discovery of a mutant, termed *unc-18* rescue, in which locomotion had been restored. Whole genome SoLiD sequencing confirmed the presence of the *unc-18 (e81)* mutation in the *unc-18* rescue mutant, as well as two novel mutations in *dgk-1 (ulv1)* and *sorf-2 (ulv2),* which were hypothesised to be putatively involved in the

16

unc-18 rescue phenotype. Through a series of behavioural, pharmacological and metabolomic approaches, the work in this thesis aimed to address the following aims:

- validate successful restoration of locomotion in *unc-18* rescue mutants relative to locomotion in wild-type *C. elegans*

- identify whether the *dgk-1 (ulv1)* mutation is required for the restoration in locomotion, and explore whether it would be sufficient to produce the rescue phenotype

- identify whether the *sorf-2 (ulv2)* is required for the restoration in locomotion, and explore whether it would be sufficient to produce the rescue phenotype

- investigate the molecular mechanism involved in the restoration of locomotion.

1.2 The secretory pathway

Eukaryotic organisms rely on a process of membrane trafficking to maintain cellular functions. Key to this process is the secretory pathway; the transport of molecules from the cellular to the extracellular space. The ability of eukaryotic organisms to secrete neurotransmitters, hormones and other secretory substances is vital for survival. Particularly for multi-cellular eukaryotes, careful regulation is required for the complex organisation and function of the various tissues and organs. In humans, the function of the secretory pathway is essential for maintaining normal physiology. Dysfunction of this pathway can give rise to several diseases, such as cancer, diabetes, congenital neurodegenerative disorders, as well as Parkinson's disease (14).

The transport of vesicles relies on two key processes – the formation of transport vesicles, and the fusion of the vesicle carriers with appropriate organelles (15). At the end of the vesicle transport pathway is the process of exocytosis through which the contents of the vesicles are released into the extracellular space. Exocytosis can either occur in a constitutive or regulated manner. Constitutive exocytosis occurs in all eukaryotic cell types and provides a continuous flow of secretory molecules. In this form of exocytosis, vesicles undergo exocytosis as soon as they reach the plasma membrane, in absence of any stimuli. Conversely, in regulated exocytosis, vesicles cluster beneath the cell membrane until exocytosis is triggered by a signal (16), which allows the release of a high abundance of molecules in a short period of time. Regulated exocytosis can occur as two types; slow onset release, which usually occurs for the release of hormones, or fast onset which is limited to

membrane fusion at neuronal synapses (17). Slow onset release occurs over a large

cell surface area for a longer period, ranging from seconds to minutes (18), while fast

exocytosis release occurs at distinct locations at the plasma membrane, releasing

standardised amounts of neurotransmitters within milliseconds (17). These two types

of exocytosis also differ in terms of the vesicles that transport the cargo. For slow

onset release, vesicles known as secretory granules tend to have variable sizes but

are generally large with diameters >100 nm, while synaptic vesicles are smaller and

more uniform in size with diameters of approximately <50 nm (5). Generally,

regulated exocytosis is triggered by Ca^{2+} influx through voltage gated Ca^{2+} channels

following depolarisation of the membrane. This commonly occurs in nerve and

endocrine cells, however in other cell types, exocytosis is triggered by hormones and

intracellular messengers (19,20). For synaptic vesicle exocytosis, rapid

depolarisation and repolarisation produces an action potential which travels to the

presynaptic terminal (21). Once arrived at the presynaptic terminal, the onset of

exocytosis occurs within 100 μs (22). For this to occur, a pool of readily releasable

vesicles must be available at the plasma membrane (19). Regardless of differences,

regulated exocytosis, in any form, is carefully mediated by molecular machinery

which allows the successful release and recycling of vesicles.

1.2.1 The secretory stages leading to exocytosis

Before exocytosis can occur, vesicle cargo must first be synthesised and packaged

into the vesicles. Once packaged, vesicles are transported to the plasma membrane,

ready for their release. The majority of transmembrane proteins, except those of the

mitochondria, will reach their final destination through this pathway, which comprises

the endoplasmic reticulum (ER), Golgi complex, and plasma membranes. In yeast

and plant cells, vacuoles also make up the pathway, while mammalian cells contain lysosomes (23). The main entry site for most secretory pathway proteins is the ER, which creates an appropriate environment for the folding, assembly, maturation and degradation of soluble and membrane proteins. It is an extensive membrane-bound organelle made up of a network of cisternae which stretch through the cytoplasm and can be subdivided into two structurally distinct domains: the rough ER, covered by ribosomes, and the smooth ER. While the cisternae of the two domains can be connected and contain similar proteins, some proteins, such as the yeast Sec16p complex, are localised only to the rough ER (23,24). This mechanism also applies to the control of the secretory pathway for synaptic vesicle secretion, however, there are differences in the organisation and distribution of organelles due to the larger distances involved (25,26). In addition to the components already mentioned, the synaptic vesicle secretory pathway also comprises additional membrane-bound intermediates that allow transport between compartments in a highly regulated manner (27). Several electron microscopy studies have revealed the presence of a continuous endomembrane network of ER spanning the soma, dendrites, axons, and even reaching within dendritic spines in some cases (28–31). The ER-Golgi intermediate compartment (ERGIC) is composed of structures which form sorting stations of anterograde and retrograde cargoes that are interconnected by highly mobile elements. Individual ERGIC units communicate laterally through rapidly forming and dissipating tubules and vesicles. Important for the activity at the ERGIC are protein coats such as COPI and COPII, which function in the early stages of the secretory pathway. COPII controls transport from the ER to the ERGIC, while the subsequent sorting within the ERGIC is controlled by COPI (32). Furthermore, present at the ER are several mechanisms which retain the 'home' proteins while

allowing other proteins to exit the ER and make their way to the next stage in the

secretory pathway, which occurs at the Golgi complex (23). Proteins enter the Golgi

complex at its *cis* face (entry face) which is usually oriented towards the nucleus

(33). They are then transported through the complex and undergo post-translational

modification by processing enzymes such as glycosyltransferases and

sialyltransferases (34). Following modification, the proteins exit the Golgi through its

trans face (exit face), packaged in vesicles which are formed by budding. In

mammalian cells, the complex consists of stacks of cisternae which are connected

by tubulovesicular regions (35,36). In some yeast however, such as *Saccharomyces*

cerevisiae, there are scarce cisternae, and instead, the Golgi units are made up of

tubular networks (37,38). The role of the Golgi complex is to further process and sort

proteins for transport to their designated destinations, such as lysosomes or the

plasma membrane (27).

1.2.2 Synaptic vesicle exocytosis

Neurotransmitter release is initiated through an action potential, which depolarised

the resting membrane potential, and results in the opening of voltage-gated Ca^{2+}

channels in the presynaptic membrane. Following the opening of these channels, a

rapid influx of Ca^{2+} into the presynaptic terminal facilitates the fusion of synaptic

vesicles to the presynaptic membrane, which then results in the release of

neurotransmitters into the synaptic cleft. The neurotransmitters diffuse through the

cleft, binding to their respective receptors on the post-synaptic membrane and

producing a post-synaptic electrical signal (4). Current models of synaptic vesicle

exocytosis segment the process into several steps – docking, priming, fusion, and

exocytosis – which are carefully regulated by proteins that are present on, and in close proximity to the synaptic vesicle and the presynaptic membrane (4,39). Before exocytosis can occur, vesicles move towards the presynaptic plasma membrane where they are docked and primed for fusion (39,40). The process of docking and priming includes a subset of proteins including Rab proteins, CAPS protein, Munc18, and tomosyn (41). Following the docking of vesicles to the presynaptic membrane, priming alters vesicles from a fusion-incompetent state to a fusion-competent state after which they become responsive to Ca^{2+} (4). Synaptic vesicle exocytosis is restricted to the active zone (Figure 1.1), a section of the presynaptic membrane, which lies at the interface between the presynaptic membrane and synaptic cleft. Here, core synaptic proteins are concentrated and function to transform a presynaptic action potential into the release of neurotransmitter signal (21). These proteins include Munc18, soluble N-ethylmaleimide-sensitive factor activating protein receptor (SNARE) proteins (synaptosomal-associated protein of 25 kDa (SNAP-25), synaptobrevin (VAMP), and syntaxin-1) (4,42,43); as well as Rab6 interacting protein (ELKS), RIM, and Munc13 (21,44) (Figure 1.1).
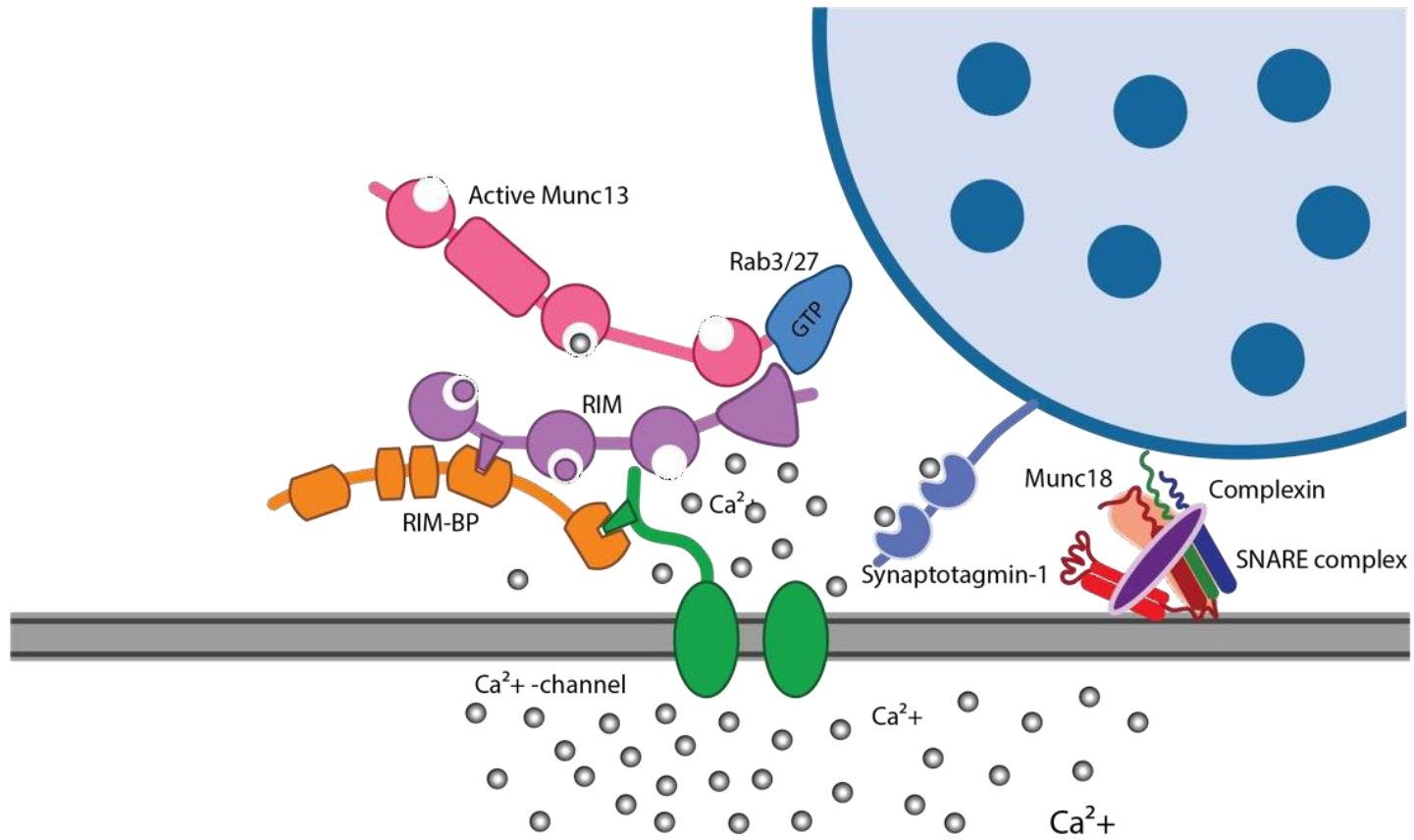
Figure 1.1. Schematic of the active zone with key proteins involved in synaptic vesicle fusion. At the active zone, vesicles are docked and primed before fusing with the presynaptic membrane and releasing their neurotransmitter contents. An in-depth description of the proteins involved in these processes has been provided in the text. Ca^{2+}=calcium; GTP=guanosine triphosphate; RIM=rab interacting molecule; RIM-BP=RIM binding proteins; SNARE=soluble N-ethylmaleimide-sensitive-factor attachment protein receptor. Adapted from Sudhof et al, 2012.

1.3 Soluble N-ethylmaleimide-sensitive factor attachment protein receptor (SNARE) proteins

Soluble N-ethylmaleimide-sensitive factor attachment protein receptor (SNARE) proteins are characterised by the presence of approximately 60-70 residues in length, known as a SNARE motif. Since their first discovery in the late 1980s, SNARE proteins have been established as key components of intracellular membrane fusion machinery for both general and neuronal forms of exocytosis (45,46). Their function lies at the very last step of the vesicle transport cycle, in the priming and fusion of vesicles with the membrane (Figure 1.2) (41,47). The neuronal SNARE family has been best characterised and includes the proteins synaptobrevin (also known as vesicle-associated membrane protein; VAMP), synaptosome-associated protein of 25 kDa (SNAP-25), and syntaxin. Originally, these proteins were individually identified, but were later found to form a complex (48–53). Additionally, it was found that SNAREs are conserved across the secretory pathway of organisms, including *Saccharomyces cerevisiae* and *Drosophila* (50,54,55). Synaptobrevin encodes a 116-amino acid protein anchored to the vesicle membrane by its single transmembrane domain and is accordingly known as a v-SNARE. Syntaxin and SNAP-25 are known as t-SNARES, which are anchored to the plasma (or target) membrane by a single transmembrane helix and lipid anchors, respectively (56). The characteristic SNARE motif within these proteins has a high tendency to form a tetrahelical bundle. The formed SNARE core complex (also known as 'SNAREpin') comprise four α-helices, one belonging to synaptobrevin, one belonging syntaxin and two to SNAP-25 (42,43,57–59), and it's by formation of these complexes that SNARE proteins mediate synaptic vesicle exocytosis (5,6).
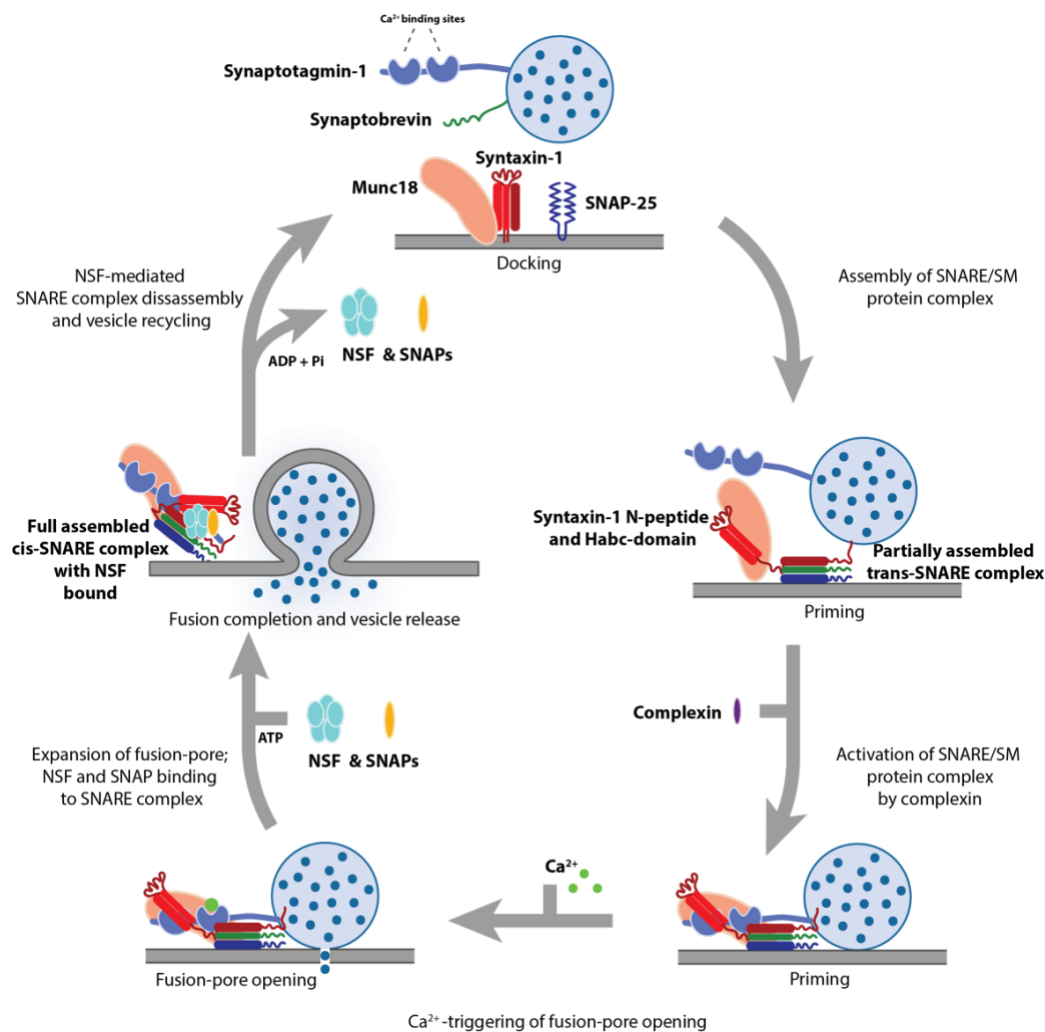
Figure 1.2. Schematic of synaptic vesicle fusion. Docking involves the process in which the vesicle and presynaptic membranes align in a fusion-ready state. Syntaxin-1 exists in a 'closed' conformation in which the Habc domain folds onto its SNARE motif. Munc18 binds to the N-peptide of syntaxin-1, enabling an 'open' conformation, which facilitates the formation of the SNARE complex. v-SNARE synaptobrevin forms a trans-SNARE complex with t-SNAREs syntaxin-1 and SNAP-25. Once the trans-SNARE complex is assembled, complexin binding increases priming of the SNARE/SM protein complex. These complexes then provide a substrate for Ca^{2+}-triggered fusion pore opening following Ca^{2+} binding to synaptotagmin. After the opening of the fusion pore, the resulting cis-SNARE complex are disassembled through function of NSF/SNAP ATPases. The vesicles then go through a process of recycling, ready for another round of fusion. ADP=adenosine diphosphate; ATP=adenosine triphosphate; CA2+=calcium; NSF=N-ethylmaleimide sensitive fusion protein; Pi=inorganic phosphate; SM=sec1/Munc18; SNAP=synaptosomal-associated protein of 25 kDa; SNARE=soluble N-ethylmaleimide-sensitive factor attachment protein receptor. Adapted from Sudhof et al, 2013.

1.3.1 SNARE complex formation

The importance of the SNARE complex in Ca^{2+} mediated synaptic vesicle exocytosis was demonstrated following evidence that targeted disruption of the SNAREs in mice, *Drosophila*, and *C. elegans* abolishes action potential evoked neurotransmitter release (60–65). The precise mechanisms that enable the formation of the SNARE complex have long been debated. Assembled complexes bridging two membranes are known as *trans*-SNARE complexes (46). It is proposed that SNAREs form a *trans* configuration through a zipper-like fashion from the N-terminal to the C-terminal region (66), through which the trans-SNARE configuration undergoes a conformational change to form a *cis*-SNARE complex (7). Formation of the *trans*-SNARE complex begins with the four N-terminal SNARE domains which become associated with each other. In the initial steps of SNARE complex formation, t-SNAREs syntaxin-1A and SNAP-25 form a 1:1 complex before interaction with synaptobrevin, acting as a receptor for v-SNAREs (67). However, *in vitro*, neuronal SNAREs syntaxin-1A and SNAP-25 were found to prefer a 2:1 complex (68,69). The four helical bundle formation, known as the SNARE core complex or 'SNAREpin', was discovered using electron paramagnetic resonance spectroscopy and X-Ray crystallography, altering the original idea that syntaxin-1A and synaptobrevin-2 align in parallel (59,70). This formation consists of 15 layers of interacting hydrophobic side chains, with a central ionic layer containing one residue from synaptobrevin-2 (arginine) and three residues from syntaxin-1A and SNAP-25 (glutamine) – a feature that is highly conserved and crucial for SNARE zippering. This discovery resulted in the reclassification of SNAREs as Q-SNAREs and R-SNAREs (47,54). Mutations at the C-terminus of the hydrophobic layers disrupt fast Ca^{2+}-triggered exocytosis *in*

vivo, and *in vitro*, and result in two-step thermal unfolding (71). In another study, introducing a small hydrophobic molecule, myricetin, into the SNARE complex, led to the discovery of a half-zippered SNARE complex in which the C-terminal was frayed (72). This half-zippered intermediate can be observed using nanodiscs in which synaptobrevin-2 is attached to one disc and a single t-SNARE (syntaxin or SNAP-25) attached to the other disc. The *trans*-SNARE complex is able to form between the two discs but is prevented from facilitating membrane fusion due to the rigid structure of the nanodiscs (73). This partially assembled state can be maintained under mechanical tension, which is interrupted by action of other synaptic proteins which facilitate the formation of the final SNARE complex and subsequently membrane fusion (73,74).

1.3.2 SNARE complex disassembly

After successful fusion, the SNARE complex must be disassembled, which allows the individual SNAREs to be recycled for another round of fusion. It is widely accepted that the process of SNARE complex disassembly occurs through the P-type adenosine triphosphatase (ATPase) activity of N-Ethylmaleimide Sensitive Factor (NSF), which binds to the core SNARE complex through soluble NSF adapter proteins (SNAPs). Initially, it was believed that NSF acted as a fusion protein (53), with evidence from microinjection experiments that the protein played a

role in regulating the kinetics of neurotransmitter release (76). However, disruption of ATPase activity of NSF in *Drosophila* resulted in SNARE complex accumulation in synaptic vesicles, highlighting the importance of NSF in SNARE complex disassembly (77). NSF forms a hexameric ring structure, with each subunit

containing three domains – an amino-terminus involved in substrate binding, and two AAA superfamily ATP-binding domains, D1 and D2 (78–80). The ATPase activity of the D1 domain is vital for the disassembly of the core complex, while the D2 domain exhibits little ATPase activity but plays an important role in hexamerisation. Six NSF molecules and four α-SNAP molecules bind to the SNARE core complex sequentially to form a super-complex referred to as the 20S complex (75). It is suggested that NSF, associated with ATP hydrolysis use SNAPs as a lever to untwist the tetrahelical bundle of the complex. Biochemical and electrophysiological experiments support this model with evidence that the tetrahelical bundle of the SNARE complex exists in a left-handed orientation, while the four α-SNAPs which surround it form a barrel in the opposite orientation suggesting a twist mechanism is involved in the core complex disassembly (81–83). However, questions still remain of the exact sequence of SNARE disassembly from the complex (82).

1.4 Regulation of exocytosis by Munc13 and related proteins

Munc13 and its homologues are large (approximately 200kDa) proteins, predominantly located within the cytoplasm of the presynaptic terminal. It plays a vital role in most forms of synaptic transmission, regulating the various processes through function of its multidomain architecture (41,84). Munc13-1 encodes the major neuronal mammalian isoform of Munc13, expressed in an active zone-specific manner (85). Within the N-terminal region lies a single C_2 (C_2A) domain and a calmodulin-binding (CaMb) sequence, while the C-terminal region contains a C_1 domain, two C_2 (C_2B and C_2C) domains and a MUN domain (86). The MUN domain is characterised as an elongated module which interacts with SNARE proteins (67,87). The CaMb region is involved in the regulation of Ca^{2+}-dependent forms of short-term plasticity (88). The C_1 domain binds to diacylglycerol (DAG), mediating DAG and phorbol ester-dependent potentiation of neurotransmitter release (89,90). The C_2A domain controls neurotransmitter release by forming a heterodimer with the Rab3 effectors, known as RIMs (91–93). The C_2B domain functions as a phosphatidylinositol 4,5-bisphosphate (PI(4,5)P_2)- and Ca^{2+}-dependent modulator of short-term plasticity (94), while the function of the C_2C domain remains enigmatic. The structure of Munc13 and its homologues is generally conserved in *Drosophila, C. elegans,* and all vertebrates, with the exception that *Drosophila* lacks the N-terminal C2 domain (95,96). Vertebrates contain three Munc13 genes (97), while in *C. elegans,* two isoforms of its homologue, *unc-13,* exist (98), differing by the presence of alternative amino termini. In *Drosophila*, on the other hand, one gene encodes three isoforms (95,96). In *C. elegans, unc-13* mutants demonstrate impaired neurotransmission despite having normal nervous system architecture and

densities of synapses and postsynaptic receptors at the neuromuscular junction (NMJ). The mutants also exhibit higher levels of synaptic vesicles at the NMJ with almost complete perturbation of evoked release at both GABAergic and cholinergic synapses. Additionally, vesicles are docked in these mutants but are not competent for release (98). Similar findings are observed in *Drosophila* and mice lacking Munc13-1 (96,99). Together these findings highlight the importance of Munc13 in synaptic transmission and implicate it in the priming step of the vesicle cycle.

Also important for Munc13 function is its interaction with DAG, highlighted by the highly conserved DAG binding C1 domain. The interaction between DAG and Munc13 was demonstrated in early work in *C. elegans*, finding that DAG binding drives the membrane association of Munc13 (100). It is this interaction which lowers the energy barrier for vesicle fusion and allow exocytosis to occur (89,90). Similar to interaction with RIM1, DAG-binding releases Munc13 from its autoinhibitory state, positively regulating synaptic transmission (84). Ca^{2+} influx following high-frequency stimulation activates phospholipase C (PLC), which increases levels of DAG and activates Munc13-1 (90). Once activated, the MUN domain facilitates the initial stages of the SNARE complex formation, involving a Munc18-1/syntaxin-1 complex (3,101,102). In *unc-13* mutant *C. elegans*, open syntaxin-1A is only able to partially restore neurotransmitter release (103), highlighting the close relationship of Munc13-1/*unc-13* and SNAREs. It is suggested that Munc13-1 also functions to enable the proper configuration of the syntaxin-1A/synaptobrevin-2 complex within the SNARE complex when using the syntaxin-1A/SNAP-25 complex as a starting point; a function that was identified in absence of Munc18-1 (3). The inclusion of the MUN domain in these studies increased the probability of Ca^{2+}-triggered fusion, which was

further increased by the presence of the DAG-binding C1 domain, and a $PI(4,5)P_2$-binding C2B domain. As the proper configuration of syntaxin-1A/SNAP-25 is produced from the syntaxin-1A/Munc18-1 complex, Munc13-1 and Munc18-1 cooperate to enable to proper configuration of the tertiary SNARE complex. Additionally, it is suggested that the role of Munc13-1 in facilitating SNARE complex assembly is enabled by the C2C domain and C1-C2B domains which interact with the vesicle and plasma membranes, respectively, forming a bridge through the MUN domain (104). It is this bridging action of Munc13-1 that is believed to facilitate interactions between synaptobrevin-2 and the Munc18-1/syntaxin-1 complex, and subsequently successful formation of the SNARE complex (86). Therefore, the functional importance of the distinct domains of Munc13 in exocytosis are well established.

Successful Munc13 function requires careful regulation by other proteins and second messengers. In addition to Munc13-1, RIM1 proteins are also localised to the active zone and function in priming through direct interactions with Munc13-1, the ubiquitously expressed Munc13-2, and Rab3a (91). However, while their roles in synaptic vesicle exocytosis are closely connected, unlike Munc13, RIM proteins are not essential for neurotransmitter release (105,106). *C. elegans* with mutant *unc-10* (RIM1 homologue) are viable yet demonstrate defective behaviours due to synaptic dysfunction (107), while Munc13-1 variants lacking RIM1 binding demonstrate reduced priming activity compared to the wild-type strain. It is therefore suggested that RIM1 positively regulates Munc13-1 (91,105). In addition to regulating priming, RIM1 has been found to be important for short- and long-term regulation of neurotransmitter release, as abolishing RIM1 expression in mice reduces release probability in excitatory neurons and increases release probability in inhibitory

neurons (108). Additionally, the important relationship between RIM1 and Munc13-1 is demonstrated by the reduction in Munc13-1 levels in mice following the deletion of RIM1 (105). Other studies of RIM1 in mice and its homologue (*unc-10*) in *C. elegans* have implicated it in determining the size of the readily releasable vesicle pool (105,106,109). It is suggested that RIM proteins activate the priming function of Munc13 by preventing its auto-inhibitory homodimerization (110). Thus, while RIM proteins may not be essential for synaptic vesicle exocytosis, they are important for normal Munc13 function.

1.5 Functions of other key synaptic proteins in synaptic vesicle exocytosis

The presynaptic machinery involves several protein components, many of which are conserved across species (111). Firstly involved in docking, the Rab proteins constitute a family of monomeric GTPases which regulate intracellular transport (4,41). In humans, there are over 60 identified Rab family members, while in *C. elegans*, 31 members of the Rab family exist, of which, 29 exist as human orthologues (112). *Drosophila melanogaster* has 26 members of the Rab family, and *Saccharomyces cerevisiae* has 11 members (113). Synaptic vesicles contain proteins from at least three families of Rab proteins – Rab3 (114), Rab5 (115), and Rab11 (116). Of these, Rab3 is most abundantly present, localised to synaptic and other secretory vesicles (4), and makes up approximately 25% of total Rab GTP binding within the brain (117). In *C. elegans*, neuronal *rab-3* is crucial for regulating synaptic vesicle-mediated release, with *rab-3* mutants exhibiting altered NMJ morphology and vesicle abundance at the synapse (118).

Additionally, two proteins with specialised roles in release are synaptotagmin and complexins. Synaptotagmin encodes a central vesicle protein which interacts directly with the SNARE complex, containing two C2 domains (C2A and C2B) which bind Ca^{2+} (119–121). Synaptotagmin-1 is the most abundant Ca^{2+}-sensing protein present on the surface of synaptic vesicles, making up approximately 7% of the total vesicle protein (121,122). Once vesicles are primed and ready for fusion, synaptotagmin acts as a Ca^{2+} sensor and facilitates the opening of the fusion pore (39). It has been found to bind five Ca^{2+} ions in total, three bound by the C2A domain, and two by the

C2B domain (123). Initial studies demonstrated the key function of synaptotagmin in secretion using anti-synaptotagmin antibodies and recombinant fragments of the gene (124–126). Further studies identified a post-docking function in exocytosis following evidence that peptides corresponding to conserved regions of the C2A and C2B domain result in a post-docking block in exocytosis (127). Studies in *Drosophila* demonstrated the importance of synaptotagmin as null mutants exhibited impaired Ca^{2+}-triggered release, while studies in mice demonstrated that synaptotagmin is required for fast release, but not asynchronous release (128–131). Particularly studies from invertebrates have shown that synaptotagmin facilitates SNARE complex formation, and Ca^{2+} acts through synaptotagmin to facilitate SNARE complex dimerization (119).

Like synaptotagmin, complexins also have a selective role in Ca^{2+}-triggering for release and bind directly to the SNARE complex. They contain unstructured sequences at the N- and C-terminus which flank an accessory and a central α-helix (132). The N-terminus region is vital for the activation of synaptic vesicle exocytosis and priming of synaptic vesicles (72,133,134), while the C-terminus region is important for clamping and priming (but not for the activation of synaptotagmin-mediated exocytosis) (135). The accessory α-helix is important for clamping synaptic vesicles, while the central α-helix binds SNARE complex and is important for all functions of complexin (134,136,137). Complexins are suggested to stabilise the primed state of vesicles, and/or increase the fusogeneicity of their primed state. Interestingly, complexins were not found to be involved in vesicle docking in mammals, however, *C. elegans* complexin nulls demonstrate impaired vesicle docking, suggesting functional differences between mammalian and invertebrate

complexins (138,139). With specialised roles, synaptotagmin and complexins act in concert to synchronise and promote Ca^{2+}-triggered synaptic vesicle exocytosis (140).

Tomosyn plays a role in regulating binding between syntaxin, SNAP-25 and synaptobrevin during synaptic vesicle priming. First isolated from the rat brain as a protein capable of interrupting the Munc18-syntaxin-1 complex (141), tomosyn has been implicated in both constitutive and regulated exocytosis. It comprises two functional domains – WD40 repeats located at the N-terminus, and a SNARE domain, located at the C-terminus; the latter of which shares sequence homology with the R-SNARE domain of synaptobrevin (142,143). Tomosyn inhibits synaptic release by forming an inhibitory SNARE complex with syntaxin and SNAP-25. Thus, *tom-1* mutant *C. elegans* demonstrate increased neurotransmitter release, an increased pool of primed vesicles and an increased abundance of *unc-13* at the synapse. Additionally, *tom-1* mutants also demonstrate increased neuropeptide release from dense core vesicles (144), highlighting an important function as a negative regulator of exocytosis.

Another relevant protein is the Ca^{2+}-dependent activator protein for secretion (CAPS). It is a multi-domain protein containing a dynactin 1 binding domain (DBD), a C2 domain, a pleckstrin homology (PH) domain, a Munc13 homology domain, and a dense-core vesicle (DCV)-binding domain (145). Each domain serves a different function for the protein. The dynactin-1 binding domain is necessary for CAPS sorting (146), while the C2 domain regulates Ca^{2+}-mediated binding to phospholipids (147). The PH domain on the other hand interacts with acidic phospholipids and binds to the plasma membrane (148). The Munc13 homology domain directly

interacts with syntaxin (87), while the DCV binding domain allows CAPS to target DCVs (149). In mammals, two isoforms of CAPS exist (CAPS1 and CAPS2), while *C. elegans* contain only one. The mammalian CAPS isoforms are different in their spatiotemporal expression, but demonstrate similar functions (146,150). In the *C. elegans* homologue, *unc-31*, the C2 domain has been found to be essential for the function of the nervous system as mutant worms with point mutations in the C2 domain demonstrate an uncoordinated phenotype (151). In mice, double-knockout of CAPS1 and CAPS2 results in priming defects in glutamatergic transmission (152), with similar results following loss of the *Drosophila* homologue dCAPS which reduces evoked glutamatergic transmission by almost 50% and leads to the accumulation of synaptic vesicles at active zones (153). The roles of Munc13 and CAPS are nonredundant in exocytosis, as Munc13 is unable to rescue exocytic defects in CAPS knockout neurons, and CAPS is unable to restore neurotransmitter release in Munc13 knockout neurons(152,154,155). More recently, structure-functional analysis of CAPS found that it plays two roles – one as an inhibitor of Munc13s ability to catalyse the opening of syntaxin-1, and one which stabilises open-state syntaxin-1 for SNARE complex formation (156). Like Munc13, CAPS functions in the regulation of SNARE proteins and SNARE complex formation.

1.6 Sec1/Munc18 (SM) proteins

While the SNARE proteins make up much of the core presynaptic machinery, the Sec1p/Munc18 (SM) proteins are also part of the key machinery. At least 4 SM proteins exist in yeast – Sec1p, Sly1p, Vps33p and Vps45p (11). Sec1p is involved in the fusion steps of protein secretion (157,158), while Sly1p functions in fusion for vesicles trafficked between the endoplasmic reticulum and Golgi apparatus (159). *vps33p* functions in transport from the Golgi complex to the vacuole (160), and the fourth SM protein, *vps45* is essential for vacuolar protein sorting (161). The first indication of the importance of SM proteins in membrane fusion was found following the observation that above a particular temperature, temperature-sensitive *sec1-1* mutants showed inhibition of invertase and acid phosphatase secretions, resulting in vesicle accumulation and disruption of cell growth (162). It was following this finding that the role of SM proteins in membrane fusion was solidified. *sly1* null mutations are lethal (163), while mutations in *vps45* result in defects in vacuolar protein sorting and intracellular vesicle accumulation (161). Evidence that the yeast homologues of syntaxin, SSO1 and SSO2 are multicopy suppressors of the temperature sensitive *sec1-1* mutation provided the first indication that SM proteins interact with syntaxin (164). Despite being mostly cytoplasmic, Sec1 proteins have high affinity with syntaxin. Following the finding that *in vivo*, the two proteins are not stably associated, it was suggested that their binding may be highly regulated (165).

The nematode worm *C. elegans unc-18* was the first metazoan Sec1 protein homolog to be discovered, sharing 22-28% sequence homology with the yeast Sec1 proteins. Brenner (1974) first generated an *unc-18* null mutant using EMS mutagenesis characterised by a partially paralysed and uncoordinated phenotype,

and partial resistance to acetylcholinesterase (AChE) inhibitors (166,167). *unc-18*

null mutants however exhibit normal morphology of GABA motorneurons (168).

These mutants also have a lower growth rate in comparison to wild-type *C. elegans*

(169). Initial ideas suggested that this was due to a defect in one of the final steps of

acetylcholine (ACh) vesicular transport affecting the membrane trafficking system of

the nerve terminal. A role of the gene in neural transmission was then further

supported by evidence from indirect immunofluorescence localisation experiments

which showed staining in all ventral cord neurons in newly hatched larva, regardless

of whether the neurons were GABAergic or cholinergic (170). In *unc-18* null mutants,

presynaptic terminals develop normal with distribution of synapses that is

indistinguishable from wild-type. However, these mutants exhibit reduction in the size

of the readily releasable pool and number of docked vesicles (168). These

physiological changes observed in *unc-18* mutant *C. elegans* support a role of the

gene in neural transmission and highlight the organism as a key model for

investigating the presynaptic molecular machinery.

The *Drosophila* homolog of *sec1*, named *rop* (*Ras opposite),* was discovered while

investigating the unrelated *Ras2* gene, as *rop* was found to be transcribed upstream

to the *Ras2* promoter region. The cloned product *rop* was found to share 58%

sequence identity with *unc-18*, and 21-27% sequence identity with *sec1, sly1* and

slp1 (171), and was expressed strongly within the embryonic central nervous system

(CNS), particularly in the neuropil, axon bundles and the synapse-rich termini

(13,171). In *Drosophila, rop* and syntaxin have been found to be involved in

successful neurotransmitter release through interaction with the SNARE complex *in*

vivo (172). Loss of function *rop* mutants exhibit unsuccessful secretion of cellular products in embryos, as well as reduced synaptic response to light stimuli in the compound eye. Both of these phenotypes can be rescued with an intact copy of exogenous *rop* (13). These findings demonstrate that as well as involvement in synaptic transmission, *rop* also functions in general secretion.

The mammalian *sec1* homologues were independently isolated by three different research groups. One group isolated the protein from rat brain lysate through a pull-down assay investigating proteins associated with syntaxin. This study consequently discovered the protein which they named Munc18, and confirmed its interaction with syntaxin (173). Pevsner et al (1994) and Garcia et al (1994) also isolated Munc18 using degenerate oligonucleotides which were based on sequence homologies among *sec1*, *unc-18* and *rop*. They termed the discovered protein n-sec1 (neuronal sec1) and rbSec1 (rat brain Sec1), respectively (165,174). Differential splicing of the C-terminus of the gene then generated the isoform rbSec1B (165). Electron microscopy and immunocytochemical localisation studies revealed strong expression of the rbSec1 protein in axon rich areas, including the mossy fiber terminal zone of the hippocampus and the corpus callosum (165). rbSec1 formed a 1:1 stochiometric complex with syntaxin, binding with a very high affinity which was found to be 1000-fold higher than the binding affinity of VAMP with syntaxin (175,176). It was through structural studies of the Munc18-1/syntaxin-1 complex that the three domains of Munc18-1 were revealed. Domain 1 exhibits α/β architecture, spanning 134 amino-terminal residues, and domain 2 has a similar architecture, spanning residues 135-245 and 480-592. Domain 3, which spans residues 247-479, comprises a large insertion between two strands of domain 2 and can be further categorised into two

subdomains. Subdomain 3a constitutes a mixture of α and β structures, and subdomain 3b comprises a mixture of α-helices. The three domains on Munc18-1 are organised in an arch shape with a central cavity lined by domains 1 and 3a. The crystal structure of Munc18-syntaxin binding revealed that it is the central cavity of Munc18-1 to which syntaxin-1 binds (177). Like the *Drosophila rop* gene, mammalian Sec1 proteins are not limited to the nervous tissue but also function in general secretion (11), and mutating Munc18-1 or its homologs result in defects in neurotransmitter release, or general vesicular secretion (11,178,179). Together, these observations from multiple species have implicated a key role of Munc18 in membrane fusion, however to date, its exact role remains elusive.

1.6.1 The role of Munc18 in exocytosis

The role of Munc18 in exocytosis has long been debated. The protein has been suggested to have three key functions. One is functioning as a molecular chaperone of syntaxin-1, allowing its appropriate localisation and expression (1,180,181). The second role is in priming through the promotion of SNARE complex-mediated membrane fusion (6,182,183), and the third function is in the docking of large dense-core vesicles to the plasma membrane (12,184).

Early studies suggested that Munc18-1 acts as a negative regulator of exocytosis from evidence that *n-sec1* binds with high affinity to syntaxin in a way that prevents it from binding to SNAP-25 or synaptobrevin, inhibiting the formation of the SNARE complex and thus membrane fusion (174). Binding of mammalian Munc18-1 to syntaxin was confirmed following the discovery that syntaxin also adopts a 'closed'

conformation in which the SNARE binding domain is blocked (176,177,185). The idea of Munc18-1 as a negative regulator of membrane fusion was supported by evidence that Munc18-1 inhibits syntaxin-1A interaction with synaptobrevin 1 and synaptobrevin 2 (186), as well as observations that it is excluded from co-immunoprecipitation studies of syntaxin-1A and other SNAREs (165). In *Drosophila*, neurotransmitter release increased following a mutation that reduces the affinity of syntaxin for *rop* (172), while overexpression of *rop* in *Drosophila* inhibited neurotransmitter release in a syntaxin-dependent manner (187,188). The idea that Munc18/*unc-18* was inhibitory remained prevalent despite the presence of data which supported a positive regulatory role of the protein. In one study, deletion of Munc18 reduced membrane fusion rather than producing an increase, as would be expected of negative regulators (179). In another, exocytosis increased in chromaffin cells following overexpression of Munc18-1 (12). Later, it was proposed that Munc18-1 binding to syntaxin stabilises it within its 'closed' conformation (189). This is one of three different binding modes for the Munc18-1/syntaxin-1A complex (177,190).

Evidence of the role of Munc18-1 as a chaperone for syntaxin-1 came from studies of mutant rat kidney fibroblast cells and other non-neuronal cells in which ectopically expressed syntaxin-1 remained trapped in the Golgi and/or endoplasmic reticulum. In these studies, co-transfection with Munc18-1 resulted in the localisation of syntaxin-1 at the plasma membrane (180,191,192). Munc18-1 knockdown in PC12 cells resulted in the mislocalisation and accumulation of syntaxin-1 in the perinuclear region, but not accumulation of t-SNARE SNAP-25. These defects in syntaxin-1 mislocalisation were rescued following expression of wild-type Munc18-1 (1). Similarly, in *unc-18* mutant *C. elegans,* anterograde transport of *unc-64* is disrupted (181). Together, these

findings led to the suggestion that Munc18-1 chaperones syntaxin-1 to the plasma membrane by preventing SNARE complex formation in the wrong cellular compartments (191,193). Despite all this evidence, the chaperone function of Munc18-1 for syntaxin does not seem to be an essential role in neurons or neuroendocrine cells (168,194,195). Expression of syntaxin-1A which is unable to bind Munc18-1 can still support exocytosis but produces slower release kinetics (194). Similarly in *C. elegans*, constitutively open form of syntaxin can fully support neurotransmission and can partially bypass a requirement for UNC-13 (196), but not the requirement for UNC-18 (168). This finding adds to the collective evidence that the role of Munc18-1 is not as simple as just facilitating a conformational change of syntaxin.

A role of Munc18-1 in SNARE complex formation was supported by comparing differences in crystal structures of isolated t-SNARE SSO1 to the Munc18-1/syntaxin-1 complex, suggesting that Munc18-1 may facilitate a conformational change of 'closed' conformation syntaxin (197). Structural studies initiated the idea that either Munc18-1/syntaxin-1 is dissociated by an unidentified factor, or that Munc18-1 facilitates core complex formation in a coordinated manner following a conformational change (189). Furthermore, studies revealed that Munc18-1 directly binds to SNARE complexes containing syntaxin-1 (182,183,198). This is supported by findings that yeast Sec1 will only bind to its cognate syntaxin when it is assembled into a binary or ternary SNARE complex (199). *In vitro* studies have identified that recombinant Sec1 and Munc18-1 are able to increase SNARE- dependent membrane fusion between synthetic liposomes. This effect requires the binding of Munc18-1 to the extreme N-terminus of syntaxin and the fully assembled SNARE complex (182,200).

The absence of Munc18-1 prevents the docking of dense-core vesicles to the plasma membrane in both chromaffin cells and mice (12), despite levels of synaptic vesicle docking remaining normal in mice (179). Furthermore, a Munc18-1 *gain-of-function* mutation (E466K) in chromaffin cells resulted in increased direct binding of Munc18-1 to Rab3a. As a result, an increase in exocytic events was observed; an effect that required binding of Munc18-1 to closed conformation syntaxin (201). It was suggested that this effect may be due to an increase in vesicle docking resulting from interactions between Rab3a and Munc18-1 (202). The same mutation (E466K) within domain 3b of UNC-18 results in increased sensitivity to aldicarb. This is consistent with increased fusion events observed using carbon fibre amperometry traces in chromaffin cells expressing the E466K mutation. Furthermore, a Glu379 insertion mutation in domain 3b of Munc18-1 disrupted binding to Mint1 and was found to reduce the frequency of exocytosis, as measured by amperometry traces (203).

Together, these findings suggest an important role of domain 3b in the recruitment and docking of vesicles. In *C. elegans unc-18* mutants, defects in vesicle tethering and proportion of docked synaptic vesicles are unable to be rescued through the expression of constitutively open syntaxin (168,204). Interestingly, an *unc-18;tom-1* double mutation is able to partially ameliorate the docking defects in *unc-18* mutants, possibly due to competition between TOM-1 and UNC-18 for syntaxin binding during the docking process (204). These findings highlight that Munc18-1/*unc-18* functions in multiple stages of the exocytic cycle.

More recently, findings from single-molecule fluorescence resonance energy transfer (FRET) assays suggested that Munc18-1 not only acts as a chaperone to syntaxin-1, but also the syntaxin-1/SNAP-25 t-SNARE complex, by inducing and modulating closed conformation syntaxin-1 (205). The formation of the Munc18-1/syntaxin-1 complex has been discussed in regard to the initial stages of SNARE complex formation, however, mechanisms of the subsequent steps remain controversial. One notion suggests a ternary complex formation between Munc18-1, syntaxin-1 and SNAP-25, which may act as an intermediate for binding with synaptobrevin (3,182,206). However, another notion suggests that the subsequent conformation is a template complex in which first Munc18-1 arranges syntaxin-1 and synaptobrevin in a cleft of Munc18-1 (102,207–209). The first model was supported by findings that Munc18-1 binds to the t-SNARE complex and induces the closed conformation of syntaxin-1 (205). Other studies supported the idea that Munc18-1 must first be dissociated for SNARE complex formation, identifying RIM (rab3 interacting molecule) and UNC-13/Munc13 as key molecules involved in the transition (102). It is suggested that when in a complex, Munc18-1 and syntaxin represent an 'off state', inhibiting each other, and are released through the action of Munc13 and RIM at the active zone (210). Furthermore, in *C. elegans*, UNC-13 displaces UNC-18 from syntaxin (169). This evidence supports a role of Munc18-1 in the priming and fusion stages of exocytosis. This is further supported by evidence that *unc-18* null mutants exhibit impaired evoked and spontaneous neurotransmitter release alongside a reduction in priming and total numbers of primed vesicles (168). The function of Munc18-1 in priming is suggested to involve its interaction with Munc13 and syntaxin, which has previously been discussed (Section 1.3) (101,211). In addition to Munc13, other factors have been suggested to be involved in Munc18- 1/syntaxin-1 complex disassembly. Tomosyn displaces Munc18-1 through binding to syntaxin-1

(141), while binding of syntaxin to Munc18-1 is inhibited following phosphorylation of Munc18-1 by protein kinase C (PKC), and cyclin-dependent kinase 5 (212). Phosphorylation of Munc18 by PKC reduces the amount of Munc18 that is bound to syntaxin (213). Specifically for regulated exocytosis, phosphorylation of Ser-306 and Ser-313 in Munc18 reduced affinity for syntaxin and was found to be important for regulating the kinetics of vesicle release. This finding suggested that PKC-mediated phosphorylation of Munc18 may allow faster release kinetics and vesicle recycling (214).

1.7 Diacylglycerol kinases (DGKs) in membrane trafficking

Diacylglycerol kinases (DGKs) modulate the balance between the two signalling lipids, diacylglycerol (DAG) and phosphatidic acid (PA), through the conversion of DAG to PA. DGK activity was first described by early work in the 1950s which identified a 'phospholipid effect' and characterised the phosphatidylinositol (PI) cycle. Key to this cycle, kinase activity which phosphorylated DAG into PA was identified (215). The mammalian DGK family is made up of ten distinct isoenzymes - α, β, γ, δ, ϵ, θ, ξ, η, ι, and κ. Between them, they share some common features. Each isoenzyme contains two or three C1 domains, similar to the structure of PKC, and a catalytic domain. The ten isoenzymes can be further divided into 5 subcategories according to their structural features. In the type 1 subgroup, DGKs α, β, and γ contain calcium-binding EF-hand motifs and a recoverin homology domain. The type 2 subgroup DGKs δ, η, and κ contain pleckstrin homology, and sterile α motif (SAM) domains, as well as a separated catalytic region. Unlike the other subgroups, type III DGKϵ has no recognisable regulatory domain other than the aforementioned C1 and catalytic domains. Type IV DGKs ξ and ι are categorised by the presence of a myristoylated alanine-rick C kinase substrate (MARCKS) phosphorylation site domain (PSD), and four ankyrin repeats, while type V DGKθ contains three C1 domains, a Gly/Pro-rich domain, and a PH-domain-like region containing an overlapping Ras-associating domain (216).

The catalytic domain resides at the C-terminal region, made up of approximately 325 amino acids, and has almost identical segments in all DGKs. In type II DGKs, the catalytic domain is separated into two regions which are interrupted by a long stretch

of non-conserved sequence which is made up of approximately 300 amino acids (217). Each catalytic domain contains an ATP binding site which has been found to be important for DGK function as mutation of a glycine to alanine or aspartate completely inhibits DGK function (218–220). The C1 domains contain approximately 50 amino acids with a conserved core structure which comprises six cysteines and two histidines. Like other C1 domain-containing proteins, it is this region that binds DAG.

Except for DGKs δ and ϵ, all DGKs are expressed within the brain at levels that are higher than or equivalent to in other tissues. Detected in a number of regions, such as the hippocampus (β, γ, ϵ, θ, ξ, ι), cerebellum (γ, ϵ, θ, ξ, ι), olfactory bulb (β, γ, θ, ξ), and the retina (γ, ϵ, ι) (221), it is evident that DGKs play an integral role within the nervous system. Various DGKs can also be found within the lungs, spleen, thymus, and several cultured white blood cells (216,221,222). For example, DGKα and ξ are expressed in T-lymphocytes, amongst other regions (223). DGK function is conserved through evolution as homologues of several DGK isoenzymes have also been identified in *C. elegans, Drosophila*, as well as in several plant species such as *Arabidopsis*, tobacco, wheat, and tomato. In addition to function within the nervous system, mammalian DGKs demonstrate a plethora of signalling functions, ranging from immune and inflammatory responses to diabetes, heart disease, and cancer (223).

The *C. elegans dgk-1* is a genetically tractable model which has been used to reveal the physiological functions of DGKs in neuronal processes. It is expressed in neurons and is 38% identical to the mammalian DGKθ. In response to dopamine and

serotonin, *dgk-1* phosphorylates DAG generated by Gαq signalling, reducing

neurotransmission (224). RHO-1 then binds to DGK-1, inhibiting its activity and

functioning as a presynaptic activator of neurotransmitter release (225). It is now well

established that *dgk-1* functions as a negative regulator of the Gαq pathway.

Accordingly, inhibition or loss of DGK-1 results in increased neurotransmission due

to the availability of DAG for Munc13. *Loss-of-function* mutations in the *C. elegans*

dgk-1 gene successfully restore DAG levels in *egl-30* (orthologue of the

heterotrimeric G protein alpha subunit Gq) and *egl-8* mutants (orthologue of

phospholipase C β4) (226). In *C. elegans dgk-1* mutants*,* phenotypic effects include

hyperactive locomotion and egg- laying, and hypersensitivity to aldicarb

(224,226,227). In *Drosophila*, DGK activity has been implicated in the mechanism of

retinal degeneration. rdgA, the *Drosophila* homologue of mammalian DGKι, induces

degeneration in a light-dependent manner, with observed photoreceptor destruction

in newborn flies. These defects are rescued in rdgA-Gαq double mutants (228,229),

adding to the evidence that DAG is an excitatory messenger. Overall, the DGK

pathway is important for the regulation of two key signalling lipids – DAG and PA - in

different biological functions, particularly within the nervous system.

1.8 Lipid signalling at the synapse

While research of synaptic function has largely focused on proteins involved in

exocytosis and endocytosis, over the last few decades the importance of lipids in

these processes has become evident. Lipids produce a dynamic environment in

which synaptic proteins can operate (230). During membrane fusion, lipid bilayers

undergo structural changes, which allows the formation of curved shapes when the

vesicle and plasma membranes come together (231–233). Importantly, lipid rafts,

formed by clusters of cholesterol and sphingolipids in discrete regions of the cell membrane (234,235) exist in a less fluid and more structured state compared to the glycerophospholipids-rich domains within the membrane (234). It is suggested that lipid rafts function in signal transduction pathways by facilitating protein-protein interactions (236), as well as in membrane traffic pathways, forming and regulating constitutive secretory vesicles (18).

Lipids are also involved in the recruitment of exocytic proteins to the plasma membrane, which requires carefully coordinated spatial regulation of lipid-protein interactions. Particularly, phosphoinositides play important roles in the spatial-temporal activation or deactivation of synaptic proteins. $PI(4,5)P_2$ has emerged as a key signalling molecule involved in the regulation of vesicle exocytosis and endocytosis, and the accompanying actin cytoskeletal rearrangement, with over 20 proteins involved in regulated exocytosis known to bind $PI(4,5)P_2$ (237–241). $PI(4,5)P_2$ levels have been found to determine the rate of vesicle priming, size of the readily releasable pool, and the continuous rate of exocytosis in stimulated cells (242–244). In the $PI(4,5)P_2$ pathway, phosphatidylinositol-4-phosphate produces $PI(4,5)P_2$, phospholipase D (PLD) produces phosphatidic acid, and phospholipase C (PLC) catalyses the production of DAG (241). Lipids such as phosphoinositides and DAG are enriched on specific membrane compartments and act as direct recruiters of proteins involved in membrane trafficking. $PI(4,5)P_2$ and DAG bind synaptotagmin and Munc13, respectively, recruiting the proteins to the plasma membrane and facilitating synaptic vesicle fusion (231). On the other hand, PA, which has been studied less extensively, binds to several synaptic proteins, including the SNARE protein syntaxin-1A. It is believed that through these interactions, PA regulates the

energetics of membrane fusion and the membrane architecture during fusion (245,246). Other proteins that are regulated in the $PI(4,5)P_2$ pathway include adaptor protein 2 (AP2), epsin, and dynamin, all of which function in exocytic or endocytic processes (245,247,248).

Another function of lipids lies in modifying the localisation and activity of secretory proteins. Exocytic proteins are typically palmitoylated, which involves the covalent attachment of a 16-carbon palmitate to the thiol group of one or many cysteines (231). Palmitoylation of SNAP-25 within four central residues may enhance the clustering of the SNARE protein in lipid rafts, and facilitating the formation of exocytic active sites (234,249,250). Palmitoylation of synaptobrevin-2 is observed in adult brains but not embryonic brains, suggesting that palmitoylation may not be required for membrane tethering, but is involved in developmental regulation (251). Additionally, palmitoylation of synaptotagmin-1 (120), and cysteine string protein (CSP) also occur (252), highlighting importance for the modification of proteins in the secretory process. The first report of direct interactions between SNARE proteins and signalling lipids was evidence that direct treatment with phospholipase A2 (PLA2) or administration of arachidonic acid (ARA) enhances SNARE complex formation in synaptic membrane preparations (253). Interestingly, ARA was able to interact with syntaxin-1 in the presence of Munc18, which is believed to stabilise syntaxin-1 (253,254). Further involvement of lipids in SNARE function includes interaction of sphingosine with synaptobrevin-2 (255), and in some studies, with syntaxin-1, which is thought to facilitate engagement with Munc18 (256). The multiple interactions of lipids with SNARE proteins are believed to assist SNARE complex formation and enhance vesicle secretion (257). Particularly,

sphingosine has been shown to modulate the frequency and fusion pore behaviour of vesicle exocytosis, suggesting that signalling lipids are important for not only modifying synaptic proteins but also controlling the amount of neurotransmitter released during secretion (258,259).

Moreover, synaptic vesicle membranes are unique due to the high abundance of polyunsaturated fatty acids (PUFAs), which generally act as precursors for second messengers, and function in the regulation of vesicle trafficking (240,258,260,261). This is evident in humans, as mutations in PUFA-related enzymes result in mental retardation (262). Similarly, *in C. elegans*, mutations of FAT-3, a gene encoding a fatty acid desaturase which is essential for the production of PUFAs, results in development and behavioural defects accompanied by reduced synaptic vesicles and neurosecretion (263,264). The activity of PLA2 releases lysophospholipids and free unsaturated fatty acids (UFAs) from the *sn-2* position of the phospholipid molecule (265). Free UFAs diffuse into the cytosol and interact with their targets. This is important in several forms of secretion, including neurotransmitter release (261,266,267). As such, the understanding of the molecular machinery involved in exocytosis is incomplete without understanding the extensive contribution that signalling lipids provide in the process.

1.9 The discovery of WDR81 and its potential function within neuronal processes

WDR81 is a protein that was recently implicated in cerebellar ataxia, mental retardation, and disequilibrium syndrome (CAMRQ2), a rare form of autosomal

recessive cerebellar ataxia following the identification of a missense mutation P856L in the gene of Turkish consanguineous family members suffering from the disease (268,269). It is predicted to be a transmembrane protein, containing an N-terminal BEACH domain, multiple WD repeats at the C-terminus and a major facilitator superfamily (MFS) domain. Although the presence of such features are characteristic of solute carrier transport proteins, the cellular function of WDR81 remains enigmatic.

In the original investigation, WDR81 was found to be highly expressed in the mouse cerebellum and corpus callosum with expression also observed in the Purkinje cell layer of the cerebellum. In the Turkish family, major structural abnormalities were observed in these regions (268,269), suggesting an important neuronal function. More recent investigations have found consistent findings with WDR81 expression in Purkinje and photoreceptor cells. In these studies, WDR81$^{nur5/nur5}$ mutant mice exhibited large, electron-dense, spheroid-like structures in the Purkinje cell dendrites. These structures were identified to be abnormal mitochondria with disorganised cristae. Additionally, mutating WDR81 in these mice led to early-onset photoreceptor cell loss and progressive Purkinje cell death, suggesting that the protein is required for the survival of these cells (270). The *C. elegans* homolog, *sorf-2*, has also been implicated in the regulation of phosphatidylinositol 3-phosphate (PtdIns3P) in early to late endosome conversion (271). SORF-2 was found to form a complex with SORF-1 (WDR91) which then interacts with the BEC-1 subunit of phosphoinositide 3-kinase (PI3K). Deletion of either *sorf-2* or *sorf-1* enriches BEC-1 on early endosomes and enhances the activity of PI3K. WDR81 and WDR91 were also found to regulate PtdIns3P levels by acting in a complex with Beclin1 and

suppressing P13K activity (271). In another study, ablation of WDR81 in adult neuronal progenitor cells resulted in impaired hippocampal neurogenesis and hippocampus-dependent learning owing to elevated levels of PtdIns3P. WDR81 was found to interact with VPS15 and Beclin1; an interaction that was proposed to inhibit the assembly of the class 3 PI3K (PI3K-III) complex and prevent the endosomal synthesis of PtdIns3P (272), consistent with previous findings. A negative regulatory role of WDR81 for the PI3K complex was further supported by evidence that WDR81 gene silencing increased exosome levels in human glioblastoma cells (273). Thus, there is ample evidence to suggest a role for the WDR81 and its homologues in autophagy.

Other studies of WDR81 demonstrate a role of the protein in aggrephagy as inactivation of WDR81 resulted in the accumulation of ubiquitinated proteins and autophagy receptor p62 in mouse brains and cells. Through interaction with p62, WDR81 was found to promote cargo recognition for aggrephagy. Additionally, WDR81 knockdown reduced the recruitment of LC3C to ubiquitinated proteins and was found to specifically interact with LC3C but not other family members. This suggests that WDR81 may coordinate p62-dependent recognition of ubiquitinated proteins with LC3C-mediated assembly of autophagosomes, facilitating the clearance of ubiquitinated proteins through autophagy. In contrary to the findings of WDR81 in PtdIns3P regulation, its function in aggrephagy seems independent of the endosomal WDR91-WDR81 complex, as WDR91 knockdown did not result in accumulation of ubiquitinated proteins and p62 loci (274). However, as the co-expression of GFP-WDR81 and mCherry-WDR91 perfectly colocalised with

endosomal structures, it was suggested that WDR91 may promote the recruitment of WDR81 to endosomes (274).

A substantial proportion of WDR81 however is not located on endosomes, suggesting that it has other functions in addition to intracellular trafficking (274). While there is limited available data about WDR81 and its homologues, the protein contains several distinct structures which have been investigated widely in other proteins. Like other BEACH-domain-containing proteins (BDCPs), WDR81 is a large protein containing a BEACH and WD repeat domains. Originally, the BEACH domain was identified as a conserved region within the lysosomal trafficking regulator (LYST) protein (275). To date, BEACH domains have been identified in eight other human proteins: neurobeachin (NBEA), neurobeachin-like 1 (NBEAL1), neurobeachin-like 2 (NBEAL2), lipopolysaccharide-responsive, beige-like anchor (LRBA) protein, WD and FYVE zinc finger domain-containing protein 3 (WDFY3), WD and FYVE zinc finger domain-containing protein 4 (WDFY4), neutral sphingomyelinase activation-associated factor (NSMAF), and WDR81 (276). Despite their large size and conservation of regions, the exact functions of BDCPs remain elusive. Generally, they have been implicated in diverse cellular mechanisms such as vesicular transport, apoptosis, membrane dynamics, and receptor signalling. The BDCP family demonstrate clinical significance as genetic variations within several of the genes have been associated with human disorders. In addition to the disorders associated with WDR81 mutations, LYST mutations cause Chediak-Higashi Syndrome (CHS) (275), LRBA has been associated with cancer growth (277) and generalised autoimmunity syndrome (278), NBEA is implicated in autism (279), NBEAL1 in glioma (280), NBEAL2 in gray platelet syndrome (281,282), and WDFY4

is associated with systemic lupus erythematosus (283). The disorders caused by LYST, LRBA, NBEAL2 and WDR81 all share the property that inheritance of the disorder is autosomal recessive and there is no obvious phenotype for heterozygous mutation carriers. The clinical outcomes following mutations in BDCPs make it evident that this family of proteins serve important physiological functions and suggest that WDR81 may serve an important role in normal neuronal processes.

1.10 *C. elegans* as a model organism for membrane trafficking

For decades, the *C. elegans* nematode has been utilised in research to advance the understanding of synaptic transmission. In the 1960s, Nobel laureate Sydney Brenner demonstrated the utility of *C. elegans* as an animal model with *in vivo* investigations of developmental and neuronal processes (284). These non-pathogenic animals have a life-span of approximately 20 days, and provide several benefits for exploring the neuronal mechanisms involved in ageing and neurodegeneration (285). Readily cultured in standard laboratory conditions, *C. elegans* can be easily genetically manipulated and characterised using a range of phenotypic assays. *Loss-of-function, gain-of-function*, and null mutations can be easily generated and maintained within the nematode (284,286). Additionally, *C. elegans* exist as two sexes, males and hermaphrodites. Hermaphrodites give rise to approximately 300 offspring, while males provide excellent tools for manipulating the genome though genetic crossing (285). Following mating, hermaphrodites produce hundreds of offspring, making the *C. elegans* an excellent model for easily reproducible experiments. The *C. elegans* nematode was the first multicellular organism to have the complete genome sequenced, and today, the complete nervous system of *C. elegans,* containing 302 neurons has been mapped, making *C.*

elegans a popular choice for studying the complex molecular mechanisms of synaptic transmission (287,288).

Several standardised techniques are available for the *C. elegans* organism, allowing for the investigation of proteins in more complex pathways. One of the most utilised behavioural assays in *C. elegans* is that of locomotion, in which the worm moves along a surface encompassed in a film of water which attaches its body to the surface through surface tension (287). Normal locomotion is maintained through carefully coordinated dorsoventral sinusoidal bends, which can be interrupted by several genetic manipulations resulting in an uncoordinated phenotype. The identification of these mutations has advanced the understanding of key molecular components of exocytosis, such as Munc18 (*unc-18*) and the SNARE protein syntaxin (*unc-64*) (284,286). In the neuromuscular junction of motoneurons, the three main components are the excitatory cholinergic synapse, the inhibitory GABAergic synapse, and the muscle (289). Synaptic transmission at the cholinergic synapse can be easily investigated using another common assay known as the aldicarb assay. Acetylcholine (ACh) is the major excitatory neurotransmitter released from the presynapse into the NMJ of over one-third of neurons in *C. elegans* (289). This release of ACh from excitatory motoneurons facilitates muscle contraction, and subsequently, locomotion. Aldicarb acts as an inhibitor of acetylcholinesterase, resulting in an accumulation of ACh in the NMJ which leads to hypercontraction, and eventually paralysis of the worm. Worms which are defective in neurotransmission will have low levels of ACh release from the presynapse, and will take longer to paralyse, exhibiting a phenotype known as resistance to cholinesterase inhibitors (RIC). Alternatively, mutants with elevated levels of neurotransmission and

acetylcholine release will reach paralysis more quickly. Thus, these mutants are referred to as hypersensitive to cholinesterase inhibitors (RIC) (290). Thus, aldicarb provides a simple method to quantitatively analyse synaptic transmission in mutant worms.

The pharynx of *C. elegans* has become well-utilised for the indirect investigation of neurotransmission. Several features of the pharynx make it suitable for understanding the cellular and molecular mechanisms of behaviour (291). It comprises 60 cells; 20 are muscle cells of 8 different anatomical types, 20 are neurons of 14 different anatomical types, and the remainder are structural and glandular cells. The pharyngeal neurons only make a connection with one bilaterally symmetric pair of extrapharyngeal neurons and so are almost organised as an autonomous nervous system (292). Within this region, activity consists of two motions – pumps and isthmus peristalses - which bring food into the pharyngeal lumen, grind it and pass it towards the intestine (293,294). Pharyngeal pumping can be measured using electropharyngeogram (EPG) recordings in which electrical events within the pharynx produce transient signals (291). An EPG recording is made up of five electrical transients. Positive transients are observed following activity of the cholinergic MC motorneurons and depolarisation of the pharynx, while repolarisation of the corpus and terminal bulb muscle produce negative transients. The depolarisation and repolarisation transients are separated by several negative transients corresponding to glutamate release from the M3 motorneurons. Thus, EPG recordings provide an excellent insight into electrical activity and synaptic transmission between neurons and muscle cells (291,295), albeit interpretations of the non-pharyngeal neurons is indirect.

Furthermore, metabolomic and lipidomic methods are ever evolving with increasing demand in research. The *C. elegans* organism has become a well-used model to investigate the genetic basis for the regulation of fatty acid synthesis and storage (296). While the physiologies between *C. elegans* and mammals are vastly different, the proteins involved in synthesizing, oxidising and transporting molecules are conserved (297). In recent years, metabolic network models for *C. elegans* were constructed (298,299), owing to accurate and robust metabolomics methods (300). The most used methods for metabolite analysis in *C. elegans* include gas chromatography (GC)-MS (301,302), and nuclear magnetic resonance (NMR) spectroscopy (302–304). As metabolomics techniques are highly sensitive, using the *C. elegans* model organism provides the most stringent experimental control when studying multicellular organisms (305). As a whole, *C. elegans* offer a great opportunity for genetic manipulation with the ability to sufficiently replicate results.

1.11 Work carried out before this project and the rationale for the current investigation

Work leading up to this project aimed to investigate whether it was possible to bypass the function of *unc-18* if there is a complete *loss-of-function* of the gene. *unc-18 (e81)* null mutants were chosen as the preferred strain to investigate the complete *loss-of-function* of *unc-18*. These mutants were originally created by Sydney Brenner (284) and are believed to be complete nulls due to the premature stop codon in the *e81* allele (2). *unc-18 (e81)* null mutant *C. elegans* were acquired from the Caenorhabditis Genetics Center (CGC) and were subjected to a suppressor screen in which worms were exposed to ethyl methanesulfonate (EMS) to introduce random mutations within the genome. EMS readily penetrates *C. elegans*, with newly hatched larvae producing progeny with several clones of mutants (Figure 1.3). The progeny were analysed for

reversion of *unc-18* paralysis, identifying a mutant worm (*unc-18* rescue) in which locomotion was indistinguishable from wild-type (WT). Using the original *unc-18 (e81)* null mutant strain as a reference, whole genome SoLiD sequencing of the *unc-18* rescue strain was carried out to identify mutations that were novel to *unc-18* rescue strain. As the *unc-18 (e81)* null mutation contains a host of several other background mutations, each mutation was carefully analysed. By subtracting mutations that occur in *unc-18 (e81)* null mutants, 367 single nucleotide point mutations were identified as specific to the *unc-18* rescue strain. While several of the mutations were located in non-coding regions, and deemed to be irrelevant, a few mutations were of interest for the investigation. These included mutations in *unc-104* (kinase-like motor protein required for anterograde axonal transport of synaptic vesicles), *unc-44* (ankyrin-like protein involved in axonal guidance during development), *unc-51* (protein kinase required for axonal outgrowth), and *pde-4* (cAMP phosphodiesterase involved in control of locomotion rate). However, closer analysis of where the mutations were located led to the conclusion that they were unlikely to be involved in the *unc-18* rescue phenotype. Analysis of the whole genome sequencing did however identify two novel mutations that are putatively involved in altering synaptic transmission in the *unc-18* rescue strain in addition to the original *unc-18 (e81)* mutation: a nonsense mutation in the kinase domain of a neuronal diacylglycerol kinase – *dgk-1 (ulv1)*, and a missense mutation in the WDR81 orthologue *sorf-2 – sorf-2 (ulv2).* The current investigation explored the involvement of the two novel mutations in the rescue of locomotion observed in *unc-18* rescue mutants through a series of behavioural and biochemical techniques.
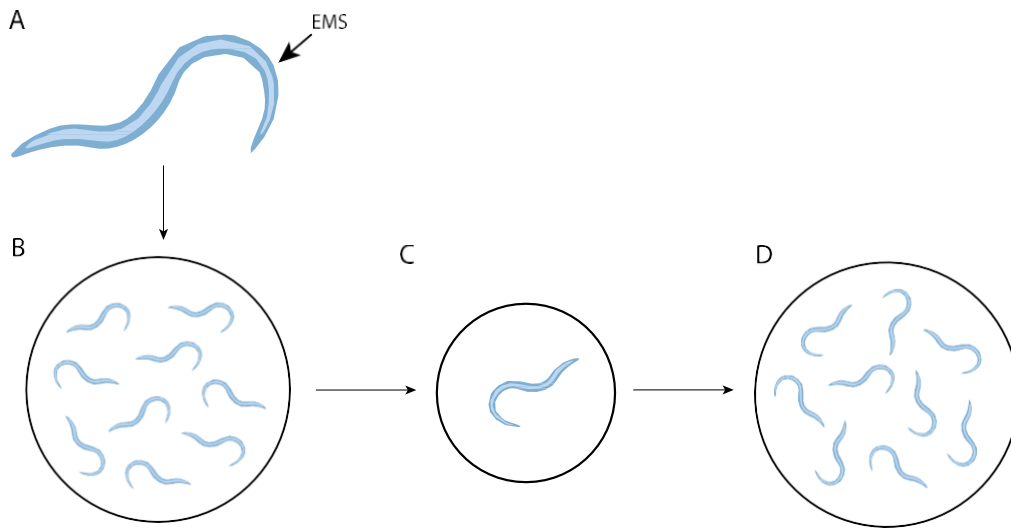
Figure 1.3. Ethyl methanesulfonate (EMS) mutagenesis of C. elegans. A) *C. elegans* are exposed to EMS and left to self-fertilise. B) Heterozygous F1 progeny are assessed for different phenotypes and individual worms of interest are isolated and left to self-fertilise. C) Homozygous F2 progeny are assessed to confirm phenotype.

Chapter 2. Materials and Methods

2.1 Materials

All materials were obtained from Sigma Aldrich (Poole, UK) unless stated otherwise in the text.

2.2 *C. elegans* Maintenance

All *C. elegans* were grown and maintained on nematode growth medium (NGM: w/v 2% agar, 0.25% peptone, and 0.3% NaCl) at 20°C. Sterile-filtered solutions at final concentrations of 1 mM $CaCl_2$, 1 mM $MgSO_4$, 25 mM KH_2PO_4, and 5 μg/ml cholesterol were added to molten NGM. Each 60 x 15 mm polystyrene Petri dish contained 10 ml NGM and small 35 x 10 mm polystyrene petri dishes contained 5 ml NGM, with *Escherichia coli* OP50 provided as food source. To maintain plates, worms were sub-cultured to freshly seeded plates every 3-4 days. In the event that worms had become starved, plates were maintained by excising a section of NGM from an old plate and placing it onto a freshly seeded plate. A summary of *C. elegans* strains used is shown in Table 1.

2.2.1 Freezing and revival

For long term storage of worms, plates were overgrown until worms were starved to obtain progenies at the L1 and/or L2 larval stages, which are best to survive freezing. Worms were washed off NGM agar plates with 2.5ml M9 buffer (22 mM KH_2PO_4, 1 mM $MgSO_4$, 86 mM NaCl, and 35 mM NA_2HPO_4) and transferred to a 15 ml Falcon tube with 2.5 ml of freezing solution (30 % w/v glycerol, 3 mM $MgSO_4$, 5.5 mM NaOH, 50 mM KH_2PO_4, and 100 mM NaCl). The worm suspension was then

vortexed briefly and aliquoted in 1 ml volumes among 2 ml cryotubes (Appleton Woods, Birmingham, UK). Worms were subjected to slow-freezing at -80°C overnight before transfer into polystyrene boxes for long-term storage at the same temperature. When required, frozen aliquots were thawed at room temperature. After a brief vortex, the contents were poured onto a freshly seeded NGM plates and left to grow.

2.2.2 Decontamination

If bacterial or fungal contamination occurred, worms were decontaminated in one of two ways. Either sections of the contaminated plates were excised and moved to freshly seeded plates, and worms further transferred onto fresh plates once they crawled off, or plates were bleached. For bleaching, worms were washed off contaminated plates with 3.5 ml dH_2O and transferred to a 15 ml Falcon tube with 0.5 ml 0.5 M NaOH (final concentration) and 1 ml 10% commercial alkaline hypochlorite bleach. The tube was briefly vortexed every 2 minutes for 10 minutes, and then centrifuged at 1000 g for 1 minute to pellet released eggs. The supernatant was aspirated to 100 μl, leaving just the pellet. The pellet was washed in 5 ml dH_2O, re-centrifuged at 1000 g for 1 minute and aspirated to 100 μl once more. The pelleted eggs were resuspended and pipetted onto a freshly seeded NGM plate.

Table 1. List of C. elegans strains used in study

Name	Strain	Gene (allele)	Description	Source
WT	Bristol N2	N/A	Wild-type	CGC
unc-18 (e81) null	CB81	unc-18 (e81)	Q to STOP mutation	CGC
unc-18 rescue	AMG199	unc-18 (e81); dgk-1 (ulv1); sorf-2 (ulv2); sorf-2 (ulv3)	unc-18 null containing point mutations	Made in house
unc-18 rescue + dgk-1	AMG337-339	unc-18 (e81); dgk-1(ulv1); sorf-2(ulv2); sorf-2 (ulv3); Ex[Prab-3::dgk-1; Prab-3::EGFP]	unc-18 rescue with transgenic expression of wt dgk-1	Made in house
dgk-1 + sorf-2	AMG349-351	dgk-1 (ulv1); sorf-2 (ulv2)	point mutations in dgk-1 and sorf-2	Made in house
unc-18 + DAG	AMG346-348	unc-18 (e81); egl-30 (js126)	unc-18 e81 null with js126 gof mutation	Made in house
rrf-3	NL2099	rrf-3 (pk1426)	Homozygous rrf-3 deletion	CGC
unc-18 true deletion	COP3885	N/A	full reading frame deletion	Knudra
unc-18 ulv12 null	AMG361-363	unc-18 (ulv12)	7 base pair deletion	Made in house (306)
rrf-3 + unc-18 true deletion	N/A	rrf-3 (pk1426); N/A	Contains deletions in rrf-3 and full reading frame deletion in unc-18	Made in house

rrf-3 + unc-18 ulv12 null	AMG727	*rrf-3 (pk1426); unc-18 (ulv12)*	Contains deletions in *rrf-3* and *unc-18*	Made in house
unc-18 (e81) null – *ulv3*		*unc-18 (e81);*	*unc-18* null, paralysed, slow growing	Made in house
dgk-1 null	VC1014	*dgk-1 (ok1462)*	Contains a deletion	CGC
unc-18 rescue + *sorf-2*	AMG726	*unc-18 (e81); dgk-1(ulv1); sorf-2(ulv2); Ex[Phsp-16.48::sorf-2]*	*unc-18* rescue with transgenic expression of *sorf-2* using a heat-shock promoter	Suny Biotech
sorf-2 heterozygous null	FX18261	tm5210/ht2	Lethal null of *sorf-2*, balanced by hT2 (qIs48)	Mitani lab
sorf-2 overexpression (global)	AMG520-522	N2;Ex[Pf52c9.1::f52c9.1 cDNA; Prab-3::GFP]	Overexpression of *sorf-2* under its endogenous promoter	Made in house
sorf-2 overexpression (neuronal)	AMG523-525	N2;Ex[Prab-3::f52c9.1 cDNA; Prab-3::GFP]	Overexpression of *sorf-2* under a *rab-3* promoter	Made in house

CGC= Caenorhabditis Genetics Center; N/A=not assigned

2.3 *C. elegans* assays

Unless otherwise mentioned, all behavioural assays were conducted in a temperature-controlled room (20–22°C) using young adult hermaphrodite worms picked from well-populated, non-starved plates.

2.3.1 Assessing locomotion in solution

Locomotion of *C. elegans* in solution was assessed by quantifying the rate of thrashing in Dent's Ringer solution (DRS; pH 7.4, 1 mM $MgCl_2$, 3 mM $CaCl_2$, 6 mM KCl, 10 mM HEPES, and 140 mM NaCl). A single thrash was identified as a head to tail sinusoidal movement. Single worms were placed in droplets of 0.1% (w/v) bovine serum albumin (BSA)/DRS and left for 5 minutes to recover. After recovery, the rate of thrashing was quantified for each worm over a period of one minute. Thrashing was assessed using a one-way analysis of variance (ANOVA), followed by Tukey's multiple comparison test.

2.3.2 Assessing locomotion on NGM agar

The body bend assay was based on the locomotion assay used by Tsalik and Hobert (2003) (307). Young adult hermaphrodite worms were moved from their original NGM plates to non-seeded plates and left for 5 minutes to recover. Locomotion was defined and quantified by counting the number of body bends (defined as one complete sinusoidal movement of the worms body from maximum amplitude, to minimum, and through to maximum amplitude again) performed by the worm within 1

minute. Thrashes were assessed using a one-way ANOVA, followed by Tukey's multiple comparisons test.

2.3.3 Acute aldicarb resistance assay

This assay was conducted as previously described by Lackner et al. (1999) and was used to measure indirectly the extent of cholinergic transmission at the neuromuscular junction. The aldicarb (Sigma Aldrich, Poole, UK) stock solution was dissolved in 70% ethyl alcohol at a concentration of 100 mM and then added to molten NGM for a final concentration of 1 mM. Approximately 25–50 worms were moved to the centre of 60 x 15 mm unseeded NGM plates containing 1 mM aldicarb. Acute sensitivity to aldicarb was measured as the time of paralysis onset following acute exposure to the drug. This was assessed by lightly prodding worms 3 times with a thin tungsten wire every 10 minutes, or every 5 minutes for mutants that are characteristically hypersensitive to aldicarb. Paralysis was confirmed after no physical response to prodding was observed. The assay was continued until all the worms had reached complete paralysis. Aldicarb sensitivity was assessed using a log rank test for Kaplan Meier followed by the Bonferroni corrections test.

When assessing aldicarb sensitivity in worms following pharmacological treatment, 1 mM aldicarb plates were made containing the relevant dose of drug under investigation. Following treatment with the drug on a separate NGM plate containing the drug only, worms were moved to drug-containing aldicarb plates. The aldicarb assay was then carried out as normal. Control aldicarb plates such experiments were made using 1 mM aldicarb and dimethyl sulfoxide (DMSO) at the equivalent concentration to the drug under investigation.

2.3.4 DGK inhibitor dose response test

1 M DGK inhibitor II (R59949; Sigma) solution was dissolved in DMSO to produce a 10 ml stock. The DGK inhibitor solution was added to molten NGM plates at varying concentrations (0, 0.001, 0.01, 0.1, 1, 10 and 100 μM) either with or without 1 mM aldicarb. The volume of NGM was adjusted accordingly to produce plates containing a final volume of 20 ml. Control plates were made with the corresponding concentration of DMSO only (final concentrations: 0, 0.001, 0.01, 0.1, 1, 10 and 100 μM). 30–50 WT worms were pre-treated for 2 hours on the NGM plates containing the DGK inhibitor II only, before being moved to NGM plates containing both the DGK inhibitor II and aldicarb. Care was taken to prevent worms escaping the plates during the pre-treatment. The acute aldicarb resistance assay was then carried out as previously described (Section 2.3.3).

2.3.5 Assessing locomotion following drug treatment

30–50 worms were pre-treated for 2 hours on NGM plates made up containing 2 μg/ml phorbol 12-myristate 13-acetate (PMA; Sigma) or containing 1 μM DGK inhibitor II. During this time, care was taken to prevent worms escaping. Following pre-treatment, the body bend and aldicarb assays were carried out as previously described (Section 2.3.2 and 2.3.3).

2.3.6 Electropharyngeogram (EPG) recordings

Prior to recording, worms were washed in M9 Buffer and then collected in a M9 Buffer and 25% v/v 5-hydroxytryptamine (5-HT; 10 mM) solution for 30 minutes. ScreenChips (InVivo Biosystems, Oregon, USA) were preloaded with the M9/5-HT

solution to stimulate pharyngeal pumping. Worms were gently loaded into the

ScreenChip using a syringe and polyethylene tubing. By applying gentle pressure

through the syringe, a single worm was loaded into the recording channel either

head-first or tail-first. Recordings were made for a minimum of three minutes per

worm using the NemAcquire Software and analysed using NemAnalysis Software

(InVivo Biosystems). Analysis conditions are listed in Table 2. Default pump

parameters set by the NemAcquire Software were used, unless stated otherwise.

EPG recordings were assessed using a one-way ANOVA, followed by Tukey's

multiple comparisons test.

Table 2. EPG analysis parameters used with NemAcquire Software

Analysis Parameters	
Minimum E SNR	1.8
Minimum R SNR	2.2
E Highpass cut-off (Hz)	20
R Highpass cut-off (Hz)	20
Minimum Absolute Threshold (uV)	10
Pump Parameters	
Minimum Pump Duration (ms)	40
Maximum Pump Duration (ms)	300
Minimum Intra-pump Distance (ms)	30

E=excitatory spike; EPG=electropharyngeogram; R=relaxatory spike; SNR=signal to noise ratio

2.3.7 Genetic crossing for creation of *unc-18* RNA interference (RNAi) sensitive strains

rrf-3 males were generated through crossing with Bristol N2 (WT) worms, and

subsequently backcrossing the resultant offspring with *rrf-3* hermaphrodites until

homozygosity was reached. 25 WT males were placed onto freshly seeded plates with 4–5 L4 stage *rrf-3* hermaphrodites. 25 *rrf-3* males were then crossed with 4–5 *unc-18* mutant worms and left to mate for 5 days. 1 F1 progeny hermaphrodite (non-paralysed) was then isolated and left to self-fertilise. Any paralysed F2 progeny were then isolated and allowed to self-fertilise before being genotyped for the *rrf-3* mutation.

2.3.8 RNAi by feeding

RNAi experiments were conducted according to standard feeding protocols (308). Bacterial cultures of the RNAi plasmid *sorf-2* (F52C9.1) (Source Bioscience) were made in Luria-Bertani (LB) medium containing 100 μg/ml ampicillin. NGM plates were made according to the standard protocol (Section 2.1) with addition of 1 mM isopropyl β-d-1-thiogalactopyranoside (IPTG) and 25 μg/ml carbenicillin. An empty vector (pG-L4440) was used as a negative control for the RNAi screen. Plates were left to dry at 20°C for 5–7 days before being seeded with 3 50μl droplets of RNAi bacterial cultures. Once dry, 5 L3–L4 worms were added to the seeded plates and left to self-fertilise. As RNAi plates lose efficacy of RNAi over time, fresh plates were prepared for each experiment. Unless otherwise mentioned, phenotypic and qPCR analysis was carried out on first-generation progeny fed with the indicated RNAi bacterial clones.

2.4 Molecular Biology

2.4.1 RNA extraction and cDNA synthesis

To perform RNA extraction, 100 *C. elegans* were picked into 100 μl of dH$_2$O in a microcentrifuge tube. After a brief centrifuge, 400 μl of TRIzol® was added and samples were frozen at -80°C for a minimum of 30 minutes before use. When required, samples were thawed at 37°C on a shaking block for 30–40 minutes. *C. elegans* RNA was extracted and purified using RNeasy mini kit and RNase-Free DNase Set (Qiagen, Manchester, UK) according to manufacturer's instructions. RNA concentration and purity was measured using a DS-11 spectrophotometer (DeNovix, USA). cDNA synthesis was then conducted using ProtoScript® II First Strand cDNA Synthesis Kit (NEB, Hitchin, UK). <1 μg RNA, 2 μl Random primer mix, 10 μl 2X ProtoScript II Reaction Mix, 2 μl 10X Protoscript II Enzyme mix, and dH$_2$O were mixed to a final volume of 20 μl. The components were incubated at 25°C for 5 minutes before being incubated at 42°C for 1 hr. The reaction was terminated by heating to 80°C for 5 min and samples were then stored at -80°C. All incubations were done in a thermal cycler.

2.4.2 Quantitative PCR reaction assembly and thermal cycling

1 μl of cDNA template was loaded into each well of a *Bio-Rad* 96-well hard-shell PCR plate with 5 μl Sybr green, 0.5 μl forward/ reverse primer, and 3 μl dH$_2$O making a total reaction mix of 10 μl. qPCR primers are listed in Table 3. Thermocycling was conducted using the Bio-Rad CFX Real-time PCR detection system. 40 cycles of thermocycling were conducted as follows: 95°C for 30 seconds,

95°C for 5 seconds, 58°C for 30 seconds. Melting curves were measured through an increase from 55 to 95°C by 0.5°C increments every 5 seconds. Data were analysed using two-way ANOVA, followed by Tukey's multiple comparisons test.

Table 3. Primer sequences for qPCR

Gene	Forward sequence	Reverse sequence	Annealing Temp (°C)	Amplicon size (bp)
unc-18	CATCACTCCACTTCT CCAT	GCATTCCTCAGCAAG ACT	58	349
sorf-2	CATCAATGGTATCA GCAATGGAAGTG	GATCTTAGTCGGAAT GTTGAGTCG	58	233
dgk-1	TCCTCTCATGATCAG CCACA	TTTGAGCACGTTTTCC CTCA	58	340
pmp-3	TGGTGTCGCGATTA CTGTAG	GATTTGTTGTCGCAG AGTGG	58	283

2.4.3 Genomic DNA extraction and single *C. elegans* PCR

For *C. elegans* genotyping, genomic DNA was extracted for sequencing. Individual animals were picked into 10 μl of lysis buffer (95 μl of 5X Phusion® HF Buffer (NEB) and 5 μl 20 mg/ml Proteinase K). Animals were picked into lids of 0.2 ml PCR tubes and briefly spun down in a microcentrifuge before being frozen at -80°C for at least 10 minutes or until they were required for lysis. *C. elegans* were freeze thawed before undergoing worm lysis using a standard protocol of incubation in a thermal cycler of 65°C for 90 minutes followed by 95°C for 15 minutes. 1 μl of the lysate was used for single *C. elegans* PCR and genotyping. Single *C. elegans* PCR was completed using Phusion® High-Fidelity DNA Polymerase (NEB) according to the manufacturer's instructions for a 20 μl reaction. 1 μl worm lysis product, and 1.25 μl

of each forward and reverse primer from a 10 μM stock were used for each reaction. Primers used for genotyping are described in Table 4. PCR products were separated and analysed as described ahead.

Table 4. Primer sequences used for *C. elegans* PCR

Gene	Forward sequence	Reverse sequence	Annealing Temp (°C)	Amplicon size (bp)
unc-18	CACACGAGCAAGTTT ACCAATCTTCCC	CTGTCGGACCCAATG ACGACTTC	60	412
sorf-2	GCGATTCTTGATGCC CGAAATGGAAAG	CTGGAGCCTATCAGA TAGGAGCAATTGAG	60	891
dgk-1	CGACTTCGTCTGGAA ATCAAACGG	GAGCTTGGATTGGAT GAGTCCCAG	59	956
rrf-3	CACGAGCTGCGTACG AAGAT	GATACTTGCAGCATG TCCAGACAC	60	625

2.4.4 Agarose gel electrophoresis

Agarose gel electrophoresis was used to separate DNA fragments. 6X DNA gel purple loading dye (Bio-Rad Laboratories Ltd, Hertfordshire, UK) was added to the samples before being loaded onto an agarose gel made up of 1% (w/v) agarose dissolved in Tris-acetate EDTA (TAE) buffer (40 Mm Tris, 20 mM acetic acid, 1 mM EDTA), with addition of 0.5 μl/ml Sybr® Safe (Invitrogen, UK). 1kb Hyperladder (Meridian Bioscience, USA) was loaded alongside the samples as a size reference. The gels were placed in tanks containing TAE buffer at 80 V for 45 minutes. The resolved DNA was then visualised under UV trans-illumination using a ChemiDoc™ XRS system (Bio-Rad), and desired fragments were purified using the Wizard® SV Gel and PCR Clean-Up System (Promega, Hampshire, UK) according to the manufacturer's instructions.

2.4.5 Plasmid transformation

Plasmid DNA was amplified by transformation into chemically competent *E. coli* strain DH5α using heat shock treatment. 50 μl of competent DH5α cells (Invitrogen) were thawed on ice before being incubated on ice with 1 μl of plasmid DNA for 30 minutes. The cells were then heat-shocked at 42°C in a water bath for 30 seconds and immediately re-placed on ice. 250 μl of super optimal broth with catabolite repression (SOC) media (0.5% w/v yeast extract, 2% w/v tryptone, 10 mM NaCl, 10 mM MgCl$_2$, 2.5 mM KCl, 20 mM glucose) was added and then incubated at 37°C for an hour while under continuous agitation at 220 rpm. The transformation was then plated out in varying quantities (typically 20 μl and 100 μl) on LB-agar plates (0.5% w/v yeast extract, 1% w/v tryptone, 1% w/v agar, 1% w/v NaCl) containing the appropriate antibiotic (100 μg/ml ampicillin or 50 μg/ml kanamycin). The plates were then incubated at 37°C overnight.

2.4.6 Plasmid DNA preparation

Single colonies of *E. coli* cells were picked from transformation plates into 8–10 ml LB media for mini-preparations, or 200 ml LB media for maxi-preparations. The LB media was mixed with the appropriate antibiotic – 100 μg/ml ampicillin or 50 μg/ml kanamycin. Cultures were grown overnight at 37°C while shaken at 220 rpm. Bacterial cultures were then pelleted by centrifugation at 12,000 g (mini-preps) or 4,000 g (maxi-preps) and then processed using either the PureYield™ Plasmid Miniprep System (Promega), or the PureLink™ HiPure Plasmid MaxiPrep Kit

(Invitrogen), each completed by following the manufacturer's protocols. Plasmid concentration and purity were quantified using a nanodrop spectrophotometer.

2.4.7 Sub-cloning of plasmids for transgenic expression

Phsp16.48::*sorf-2* plasmid for transgenic expression was created using T4 ligation followed by the Gateway cloning system. The phsp16.48 DNA to be inserted was first amplified by PCR using primers containing SacII and ClaI sites at the 5' and 3' ends respectively. Punc-17-A destination vector was digested to create complementary sticky ends. The two DNA fragments were resolved using agarose gel electrophoresis and extracted using methods previously described (Section 2.4.4). After measuring DNA concentration and purity, the two fragments were ligated using T4 ligase (Promega). Vector and insert were mixed in a 5:1 ratio, respectively, with addition of 1 μl 10X ligase buffer, 1 μl T4 ligase, and dH$_2$O to make a final concentration 20 μl. The reaction was incubated at room temperature for 2 hours before being heat inactivated at 65°C for 10 minutes. The destination vector was amplified using DH5α *E. coli* cells and plasmid purified as previously mentioned. Successful ligation was validated by restriction digest.

AttL flanking sequences within the entry clone allowed the DNA of interest (*sorf-2*) to be inserted into the destination vector, which contained AttR flanking sequences, using LR Clonse II (ThermoFisher) recombinase following the manufacturer's instructions. The resulting expression clone plasmids were amplified using DH5α *E. coli* cells and plasmid purified using the standard maxi-prep procedure previously described.

2.4.8 Transgenic expression of plasmids

Following successful sub-cloning, phsp16.48::*sorf-2* was injected, with a p*sur-5::sur-5*::NLSGFP reporter marker into *unc-18* rescue mutants, at a concentration of 5 ng/μl. Injections were performed by SunyBiotech (Fuzhou, China).

2.5 Analysis of *C. elegans* with 1D 1^H nuclear magnetic resonance (NMR) spectroscopy

2.5.1 General procedure for metabolite extraction from whole *C. elegans* samples and analysis with 1D 1^H NMR spectroscopy

C. elegans metabolites were extracted from thawed worms in 50 % (v/v) water and ice-cold acetonitrile (AcN). Samples were kept on ice to prevent overheating and extraction was performed by sonication for 30 s durations with 30 s intervals at 10 % amplitude. Samples were vortexed for 30 s and then centrifuged for 5 min at 21,000 g, 4°C, to pellet insoluble components and cell debris. The metabolite containing supernatants were snap frozen in liquid nitrogen for 2 minutes and then lyophilised to completion with a Heto PowerDry LL1500 freeze dryer (ThermoFisher Scientific Inc). Metabolite containing supernatants and lipid-containing pellet samples were kept at -80°C for long-term storage, until required.

2.5.2 Metabolite extraction

After extraction was completed, but immediately prior to NMR acquisition, 200 μl of NMR buffer (89.8% ^2H_2O, 10% (v/v) 1 mM sodium phosphate (pH 7.4), 0.1% (v/v)

100 mM selectively deuterated (d4) trimethylsilyl-^{2}H$_4$-propionate (TSP), and 0.1% (v/v) 1.2 mM sodium azide) was added to each sample. All components were added to the buffer after metabolite extraction, except the reference compound, TSP, which was added prior to extraction to account for extraction-induced sample loss. After NMR buffer was added to samples, solutions were vortexed for 1 min and then centrifuged for 2 min at 12,000 g, 20°C to pellet remaining cell debris and insoluble components. 200 μl of the supernatant was then transferred to clean 3 mm NMR SampleJet tubes (Bruker BioSpin Gmbh).

2.5.3 Lipid extraction

Lipid containing cell pellets were resuspended in 500 μl chloroform (C$_1$HCl$_3$, Sigma) and vortexed for 30 s. Samples were then incubated for 5 min at -20°C before being centrifuged for 5 min at 21,500 g, 4°C. The lower lipophilic layer was transferred to new Eppendorf tubes before being snap frozen in liquid N$_2$. Immediately prior to NMR acquisition, 200 μl CDCl$_3$ was added to lyophilised samples, before being vortexed for 30 s. Samples were centrifuged for 2 min at 12,000 g, 20°C, before transferring 200 μl into 3 mm NMR tubes.

2.5.4 Spectra acquisition

1D ^{1}H NMR spectra were acquired on a Bruker Avance III HD 700 MHz spectrometer equipped with a 5 mm TCI cryoprobe at pH 7.4 and 25°C. For polar metabolites, 1D ^{1}H standard Carr-Purcell-Meiboom-Gill (CPMG)-type metabolomica experiment with optimal water suppression was acquired with cpmgpr1d filters for

small molecules via a CPMG sequence. For non-polar (lipid) metabolites, 1D 1H-NMR Nuclear Overhauser Effect Spectroscopy (NOESY) standard vendor pulse sequence (noesgppr1d – all parameters constant between samples) was used. Polar spectra were acquired with 256 transients at 15 ppm spectral width, 32 k points, 9.6 ms echo time, a 3.1 s acquisition time, and a 4 s interscan delay. Lipid spectra were acquired with 256 transients at 25 ppm spectral width at 15°C to offset the volatility of the chloroform.

2.5.5 Spectra inclusion criteria

All spectra was subjected to strict quality control (QC) (309) using TopSpin™ version 3.6.3 (Bruker BioSpin Gmbh). Baseline phasing was checked and manually corrected if required. All polar peaks were referenced to the resonance of TSP at 0 ppm, and lipid peaks were referenced to the resonance of the chloroform peak at 7.26 ppm. The reference peak line width for each sample was measured at half height to ensure it was within the upper (mean line width + standard deviation) and lower (mean line width – standard deviation) limits. In metabolite samples, width of the water peak was also measured, ensuring it was present at 7.4 Hz. Any samples that failed QC were acquired again on the spectrometer up to a maximum of 3 times.

2.5.6 Spectra processing

A representative spectrum was used to create a pattern file, defining 'bin' boundaries for all peak positions. The pattern file was then validated using the TameNMR Galaxy toolkit (https://github.com/PGB-LIV/tameNMR) and used to integrate spectral peak data into numerous bins for statistical analysis.

2.6 NMR statistical analysis

All data was normalised by probabilistic quotient normalisation (PQN), described below, and auto scaled (each bin is mean centred and then divided by the standard deviation for that bin). One-way ANOVA analysis was performed, followed by Tukey's multiple comparisons test. Multivariate principal component analysis (PCA) was performed on all spectra and partial least squares discriminant analysis (PLS-DA) was performed if sample number exceeded 6. Statistical analysis was conducted using in-house scripts which were implemented using the mixOmics R package.

2.6.1 Data normalisation

Normalisation is essential for omics analysis to correct any variance on sample preparation. PQN was the method chosen in this investigation, which normalises each spectrum by a reference one such as the median spectrum. The PQN normalisation function first includes creating a reference spectrum by calculating the median spectrum using the bins in the whole dataset. The quotients are created, and all spectra are divided by the reference spectra. The median of the quotients is then used to calculate the normalisation factor, after which the raw data is divided by the normalisation factor (310).

2.6.2 Principal component analysis (PCA)

A PCA is an orthogonal data transformation which returns unobserved variables, known as principal components (PC). Each PC demonstrates a proportion of the

variance within the data, with the first PC explaining the most variance. The second

PC then explains the most variance which cannot explained by the first PC. The

second PC however follows a direction that is orthogonal and not correlated to the

first PC. This process continues for subsequent PCs (311). As a result, uncorrelated

PCs explain the variance within the dataset, and will usually only require the first few

PCs to explain all the variance. This investigation used a PCA to identify any hidden

structures within the data of different strains, allowing identification of how each

sample separates out from each other. Furthermore, a PCA loadings plot provides

an association between differences to metabolites by showing the variability between

different metabolites within the dataset (310).

2.6.3 Partial least square discriminant analysis (PLS-DA)

A PLS-DA is a variation of partial least squares (PLS) regression. It is a supervised

statistical model often applied to multivariate datasets to make predictive models

between two matrices. The first matrix is the input data which acts as the predictors

(training), and the second matrix is the response where the output is observed (test).

A PLS-DA model projects predicted and observable variables using a linear

regression model in latent variables known as variates, or PCs. NMR spectra

demonstrates multicollinearity as single metabolites can often be represented by

multiple peaks, making a PLS-DA model suitable for establishing variance.

Supervised statistical models, like the PLS-DA, require the model to be trained on

data prior to prediction, which has a large impact on the observed outcome.

Therefore, PLS-DA models benefit from larger data sets with sufficient data for

training (310).

As the PLS-DA uses part of the data for training, the test prediction can return four results: true positive, false positive, true negative, and false negative. The sensitivity of the model coincides with the true positive rate, while the specificity is associated with the model's ability to correctly rule out the false positive. To understand the performance of the model, a receiver operating characteristic (ROC) curve can be used, which plots the true positive rate versus the false positive rate for the considered classifier at different threshold values. The performance of the classifier is measured using the corresponding area under the curve (AUC). A classifier with no predicting value (random prediction) would have an AUC of 0.5, while a perfect classifier would have an AUC of 1. A classifier with some predictive power would be in the region of 0.8 (311). As such, the closer to 1 the AUC value, the better predicting power of the model.

Chapter 3: *dgk-1 loss-of-function* is necessary, but not sufficient, for the *unc-18* rescue phenotype

3.1 Introduction

The neuromuscular system for locomotion in the worm is made up of 75 motoneurons which are divided into six excitatory cholinergic, and two inhibitory GABAergic classes that innervate the dorsal and ventral groups of muscle cells (312,313), making the worm an excellent model for studying neurotransmission. The alternating wave of contraction and relaxation drives the dorsoventral body bends that are characteristic of *C. elegans* locomotion (289,314). *unc-18* is expressed in motor neurons and has been implicated as a key part of the exocytic machinery with a role at multiple stages of the process such as priming, docking, and fusion (41). Mutations that disrupt neurotransmission in *C. elegans*, such as those in *unc-18*, produce an uncoordinated phenotype and resistance to inhibitors of cholinesterase (203,226,284). While the exact role of *unc-18* within these processes has been heavily debated, *unc-18* mutants demonstrate defects in trafficking of *unc-64* (syntaxin-1) and a reduction in the size of the readily releasable pool and number of docked vesicles (168,181), highlighting the importance of *unc-18* for neurotransmitter release.

Coordinated locomotion in *unc-18* null mutants can be rescued by wild-type expression of *unc-18*, Munc18-1, *unc-18* point mutations that block closed-conformation syntaxin, and rescue of mutant Munc18-1 with various chemical chaperones (10,181,306,315). However, mutants in which N-terminal binding to syntaxin is deficient remain paralysed. In chromaffin cells, Munc18-1 defects in docking can be rescued through overexpression of SNAP-25 (316), while in *unc-18* null mutants, docking defects can be partially improved with a *unc-18;tom-1* double

mutation (204). To date, however, resumption of synaptic transmission in the absence of *unc-18* has not been demonstrated.

Prior work has identified an *unc-18* rescue mutant in which locomotion is restored, despite the presence of the *unc-18 (e81)* null mutation. Additionally, the presence of two novel mutations in *dgk-1* and *sorf-2,* postulated to be involved in the restoration of locomotion in *unc-18* rescue mutants, were identified. In this study, I first focused on the involvement of *dgk-1*, the homologue for mammalian DGKθ, which acts as a negative regulator of synaptic vesicle exocytosis by phosphorylating diacylglycerol (DAG) into phosphatidic acid (PA) in motor neurons (224). It plays an important role in the serotonin inhibition of both locomotion and acetylcholine release (224), processes which are severely reduced in *unc-18* null mutants (168,317). The nonsense mutation *(ulv1)* in *dgk-1* identified in *unc-18* rescue mutants resides within the kinase domain of the gene. Previously, missense mutations within this domain have been found to severely affect *dgk-1* function, assessed through egg laying and dopamine-induced paralysis, with more severe effects observed in *dgk-1* null mutants. As *dgk-1* functions as a negative regulator of synaptic transmission, its *loss-of-function* results in increased acetylcholine release, likely due to the accumulation of DAG (100,224). This investigation hypothesised a role of the *dgk-1 (ulv1)* mutation in the *unc-18* rescue phenotype through a truncation and/or *loss-of-function.*

The *C. elegans* nematode is a useful organism to study the molecular mechanisms of neurotransmission due to its responsiveness to genetic and pharmacological manipulations (318). This chapter describes a series of behavioural and electrophysiological experiments conducted to characterise the successful rescue of

locomotion in *unc-18* rescue worms. We then aimed to investigate the necessity of the *dgk-1 (ulv1)* mutation for the rescue phenotype observed in these mutants before addressing whether the *dgk-1 (ulv1)* mutation would be sufficient to produce the rescue phenotype if present alone with *unc-18 (e81)* mutation.

3.2 Results

3.2.1 Locomotion of *unc-18 (e81)* null mutants was successfully restored following EMS mutagenesis

Quantification of locomotion using body bends is a well-established behavioural phenotype to investigate *C. elegans* strains in which neuronal processes are defective. Locomotion rate was assessed to characterise the rescue phenotype observed in *unc-18* rescue mutants. This was investigated by quantifying the number of sinusoidal movements (body bends) produced in one minute on a solid NGM surface in the absence of OP50 (*E. coli*) (Figure 3.1A). Wild-type (WT) locomotion was observed to be 14 body bends per minute, consistent with previous literature (306). *unc-18 (e81)* null mutants failed to produce any body bends within one minute of measurement, while *unc-18* rescue worms moved in a coordinated manner similar to WT (12.6 body bends per minute, p>0.05) and significantly better than *unc-18 (e81)* null mutants (p<0.0001) (Figure 3.1C, Figure 3.1D).

Following confirmation of the successful restoration of locomotion in *unc-18* rescue mutants, the necessity of the *dgk-1 (ulv1)* nonsense mutation was investigated. Wild-type *dgk-1* was introduced back into the *unc-18* rescue mutant through synaptic expression driven by the *rab-3* promoter (*unc-18* rescue + *dgk-1*). These mutants show a reversal in the restoration of locomotion, failing to produce any body bends within the measured time (0 body bends per minute). Next, we wanted to assess the sufficiency of the *dgk-1 (ulv1)* mutation through an alternative method, however, as *unc-18* and *dgk-1* both reside on chromosome X, making a compound mutation proved to be difficult. Thus, a compound mutation was created with *gain-of-function egl-30 (js126)* (*unc-18 (e81)* null + DAG) to mimic the hypothesised effects of the *dgk-1 (ulv1)* mutation – excess DAG. Mimicking this effect failed to improve

locomotion as worms remained immobile during the time measured (Figure 3.1D).

When *C. elegans* move across an agar surface, body bends are interrupted by reversal movements or brief periods of pausing where there is no movement. However, when placed in solution, the wavelength and frequency of *C. elegans* locomotion changes and instead the worms move from side to side in the plane of their transverse movements (314) (Figure 3.1B). In this medium, locomotion of wild-type worms is constant and occurs at a high-frequency (226), so measuring locomotion in solution provides an alternative measure to quantify neuronal defects. When placed in solution, WT worms swam at a rate of 85 thrashes per minute, while *unc-18 (e81)* null mutants remained immobile and did not produce any thrashes (p<0.0001). Similarly, *unc-18* rescue mutants thrashed significantly less compared to WT worms, producing 1.73 thrashes per minute (p<0.0001). *unc- 18 (e81) null* + DAG and *unc-18* rescue + *dgk-1* mutants did not thrash significantly different to *unc-18 (e81)* null and *unc-18* rescue worms as both mutants did not produce any thrashes and remained immobile during the assay time (Figure 3.1E). It is interesting that *unc-18* rescue mutants were not significantly different from *unc-18 (e81)* null mutants in thrashing, despite being significantly different when crawling on a surface. Crawling and swimming are distinguished by different kinematics and distinct underlying patterns of neuromuscular activity (319) which may explain these results. It is possible that some neuromuscular pathways involved in swimming remain defective in *unc-18* rescue mutants, and so the two assays should be interpreted as different mechanisms of locomotion.
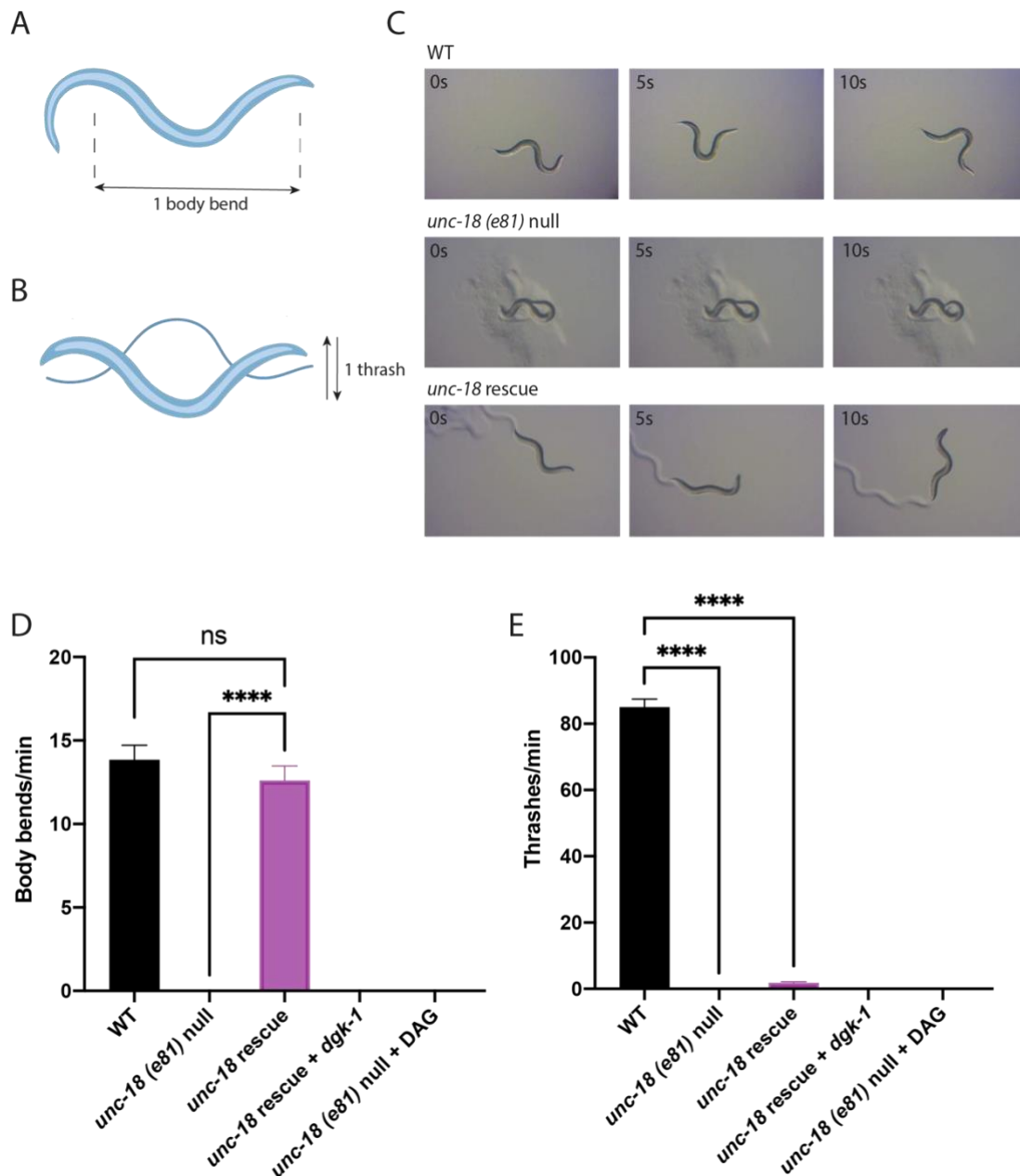
Figure 3.1 Behavioural analysis of *C. elegans*. A) Illustration of one sinusoidal body bend movement. B) Illustration of a single thrashing movement. C) Video stills of WT, *unc-18 (e81)* null and *unc-18* rescue worms at 0, 5 and 10 seconds while crawling on an unseeded agar surface. D) Locomotion on a surface was quantified by measuring the number of body bends produced per minute while crawling on an unseeded agar plate. *unc-18* rescue worms show a significant improvement in locomotion compared to *unc-18 (e81)* null mutants. *unc-18* rescue + *dgk-1* and *unc-18 (e81)* null + DAG mutants failed to produce any body bends during the assay time. E) Locomotion in solution was quantified by counting the number of thrashes in Dent's solution. All mutants thrashed significantly lower compared to WT worms, with no thrashes observed in *unc-18 (e81)* null, and *unc-18* rescue + *dgk-1* RNAi, and *unc-18 (e81)* null + DAG mutants. A total of 10 worms were analysed in each experiment with a total of 3 independent experiments (n=30 worms per strain). Data is shown as mean ± standard error of the mean. Statistical data analysis was performed using one-way analysis of variance, followed by Tukey's multiple comparisons test. ****$p \leq 0.0001$.

3.2.2 Acetylcholine release is restored in *unc-18* rescue mutants

C. elegans locomotion is driven by the presynaptic release of GABA and acetylcholine, which stimulates muscle contraction (320). Exposure to aldicarb, an acetylcholinesterase inhibitor, leads to the accumulation of acetylcholine (ACh) in the neuromuscular junction (NMJ), eventually resulting in hypercontraction and paralysis (Figure 3.2A). This provides a useful tool to investigate the mechanisms of synaptic transmission, as the time taken for paralysis to be reached is dependent on the efficacy of cholinergic release (321). It has long been established that mutants with defective neurotransmitter release, such as *unc-18* mutants, have lower levels of acetylcholine at the NMJ and take longer to reach paralysis (226). These mutants are termed to be resistant to inhibitors of cholinesterase (RIC), while mutants with higher levels of neurotransmitter release reach paralysis quicker in comparison to wild-type worms and are termed to be hyper-sensitive to inhibitors of cholinesterase (HIC). The latter is characteristic of *dgk-1* mutants, with the HIC phenotype being attributed to the heightened levels of DAG (224).

As the *unc-18* rescue worm is mutant for *dgk-1* and null for *unc-18*, there was a question of whether mutating *dgk-1* was sufficient to rescue neurotransmitter release and alter aldicarb sensitivity in these mutants. Based on characteristics of *dgk-1* mutants, it was hypothesised that the presence of the *dgk-1* mutation would result in hypersensitivity to aldicarb in comparison to *unc- 18 (e81)* null mutants. *unc-18 (e81)* null mutants demonstrated a RIC phenotype and were significantly more resistant to 1 mM aldicarb in comparison to WT worms ($p<0.0001$), in line with current literature (226,315,322). The RIC phenotype is rescued in *unc-18* rescue mutants, and despite the presence of the *unc-18 (e81)* mutation, the worms

demonstrate a HIC phenotype consistent with characteristics of *dgk-1* mutants (323). *unc-18* rescue mutants reached a state of paralysis significantly quicker compared to *unc-18 (e81)* null ($p < 0.0001$) and WT mutants ($p < 0.01$). Next, the necessity of the *dgk-1 (ulv1)* mutation was confirmed as expression of WT *dgk-1* in *unc-18* rescue mutants reversed the HIC phenotype to a level of resistance similar to *unc-18 (e81)* null mutants ($p < 0.0001$ vs *unc-18* rescue). Conversely, increasing levels of DAG in *unc-18 (e81)* null + DAG mutants through expression of *egl-30 (js126)* increased hypersensitivity to aldicarb, resulting in a phenotype that was not significantly different from *unc-18* rescue mutants ($p > 0.05$) (Figure 3.2B). This HIC phenotype was consistent with mutants with enhanced *egl-30* activity (100), although to a lesser extent which is likely due to the presence of the resistant *unc-18 (e81)* mutation. These findings together suggest that the HIC phenotype observed in *unc-18* rescue mutants is due to the presence of the *dgk-1 (ulv1)* mutation.
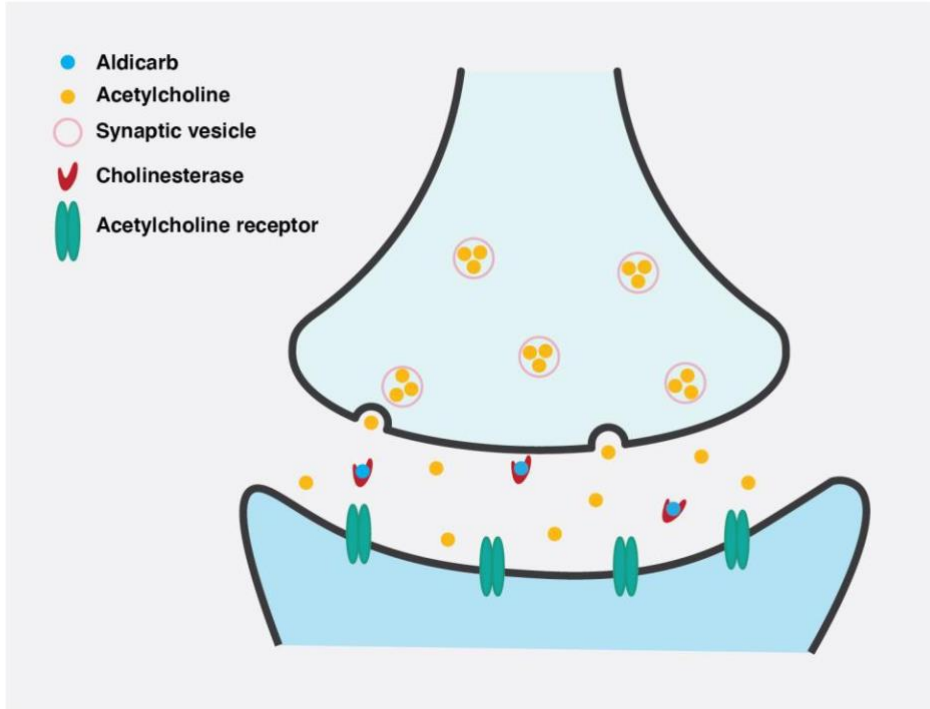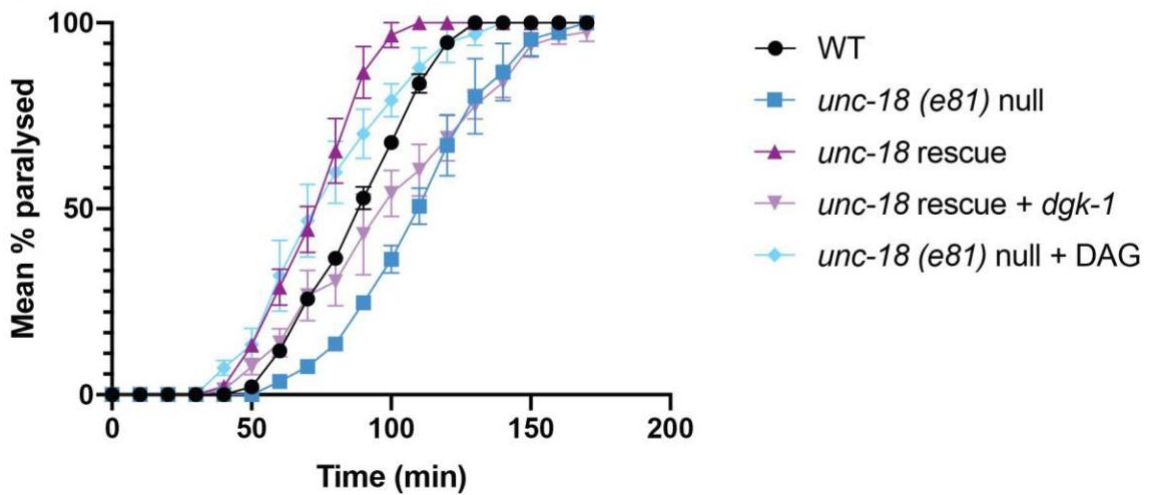
Figure 3.2. Neuronal impairments of mutant worms with defective *unc-18* A) Schematic of aldicarb action. B) Aldicarb sensitivity of mutant *C. elegans* following treatment with 1 mM aldicarb. 25–40 worms were assayed in each experiment and a total of 3 experiments were conducted for each strain. Curves on the graph are representative of triplicate experiments. Statistical analysis was done using a log-rank test for Kaplan Meier followed by the Bonferroni comparisons test.

3.2.3 Extracellular recordings of pharyngeal activity

Following confirmation that locomotion and cholinergic release is improved in *unc-18* rescue mutants compared to *unc-18 (e81)* null mutants, we next wanted to validate these findings through extracellular measurements of pharyngeal activity. Electropharyngeogram (EPG) recordings provide information about the activity of the pharynx. These recordings measure the excitation and relaxation of the corpus and terminal bulbs, while also measuring the activity of M3 motoneurons (291,295), providing an indirect measure of neuronal activity.

Output measurements of EPGs include the mean frequency of pumping and mean pump duration which measures the time from an excitatory peak to a relaxation peak. These measurements provide insight into the contraction and relaxation of pharyngeal muscles. The output results can also provide information about the regularity of pumping by measuring the inter-pump interval duration standard deviation (IPI duration SD), which represents the time between one excitatory peak to the next (Figure 3.3A). In addition to this, information can be derived from the pump parameters, such as the pump duration coefficient of variation, which is a threshold set for the maximum amount of acceptable variation in pump duration. Due to the defective nature of the mutants studied, the pump duration coefficient of variation was set to a threshold of 50% and only recordings that fit within this threshold were analysed. Analysis of these different variables can therefore be informative of the regularity and efficacy of neuromuscular transmission.

Wild-type worms displayed consistent, rhythmic pharyngeal pumping with a mean frequency of 3.75 Hz. Pharyngeal pumping frequency in *unc-18* rescue mutants was significantly increased compared to *unc-18 (e81)* null mutants (2.79 Hz and 2.20 Hz, respectively; p<0.05). *unc-18* rescue + *dgk-1* mutants show a significant reduction in pharyngeal pumping compared to *unc-18* rescue worms, with a mean frequency of 1.31 Hz (p<0.0001) (Figure 3.3B). WT worms pumped with an IPI duration SD of 76.92 ms. This measure was not significantly different in *unc-18* rescue mutants (91.95 ms, p>0.05). Pumping in *unc-18 (e81)* null and *unc-18* rescue + *dgk-1* mutants was irregular and IPI duration SD was significantly higher in both mutants compared to WT (430.86 ms and 336.22 ms, respectively; p<0.0001) (Figure 3.3C). *unc-18 (e81)* null + DAG mutants were too small to fit in the microfluidic recording chamber so EPG recordings could not be made.

Furthermore, the mean pump duration of WT and *unc-18* rescue worms was not significantly different from each other (113.70 ms and 139.29 ms, respectively; p>0.05), however, only WT worms were significantly different to *unc-18 (e81)* null mutants which had a mean pump duration of 165.27 ms (p=0.0001). The mean pump duration of *unc-18* rescue + *dgk-1* mutants was significantly higher compared to *unc-18* rescue mutant worms (184.79 ms; p<0.001), but not significantly different from *unc-18 (e81)* null mutants (p>0.05) (Figure 3.3D). The mean pump duration coefficient of variation was significantly higher in *unc-18 (e81)* null mutants (10.29%) compared to WT worms (7.26%, p<0.05). The mean pump duration coefficient of variation was 8.88% in *unc-18* rescue mutants and 7.66% in *unc-18* rescue + *dgk-1* mutants (p>0.05). Neither mutant was significantly different from WT and *unc-18* null mutants in this measure (p>0.05) (Figure 3.3E).

A

Wild-type
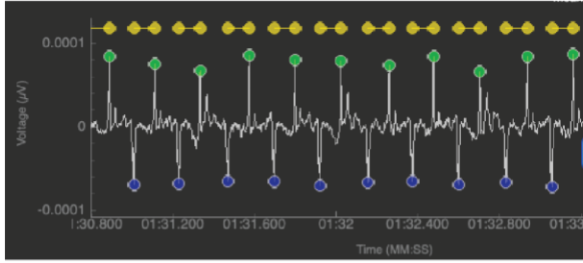
unc-18 Rescue

unc-18 (e81) null

unc-18 Rescue + dgk-1

B

Mean Frequency (Hz)

WT — unc-18 (e81) null — unc-18 rescue — unc-18 rescue + dgk-1

** ****

C

IPI duration standard deviation (ms)

WT — unc-18 (e81) null — unc-18 rescue — unc-18 rescue + dgk-1

**** ****

D

Mean pump duration (Hz)

WT — unc-18 (e81) null — unc-18 rescue — unc-18 rescue + dgk-1

ns ns ***

E

Pump Duration Coefficient of Variation (%)

WT — unc-18 (e81) null — unc-18 rescue — unc-18 rescue + dgk-1

*

94
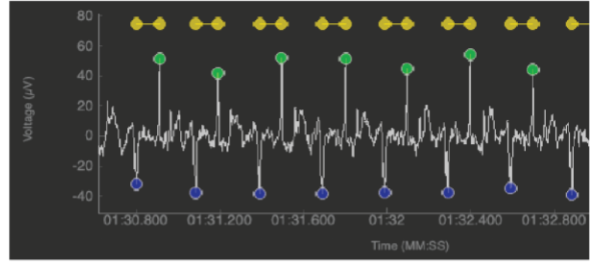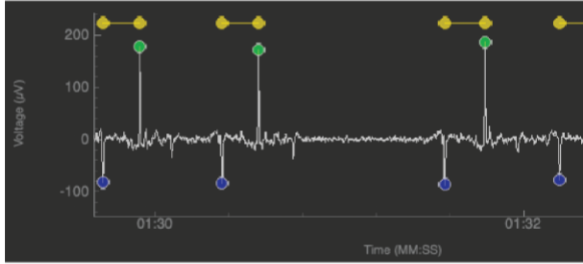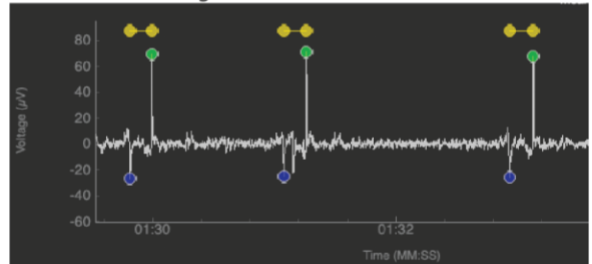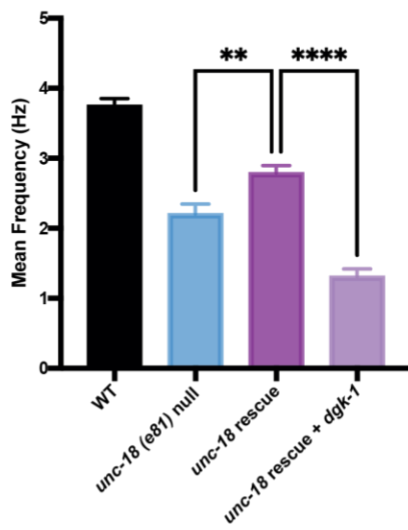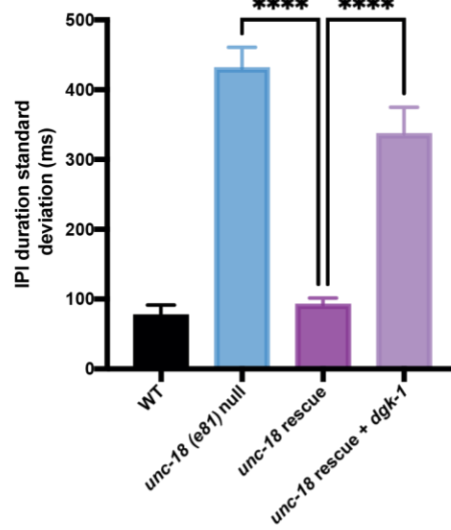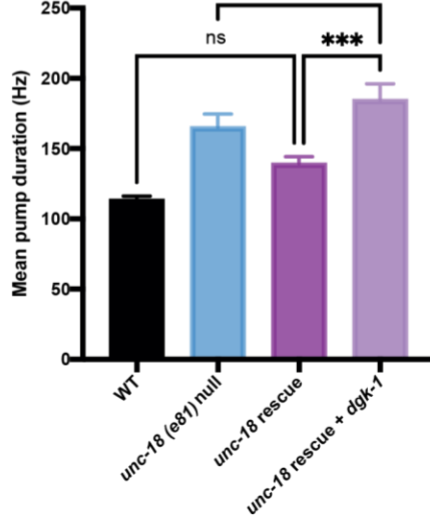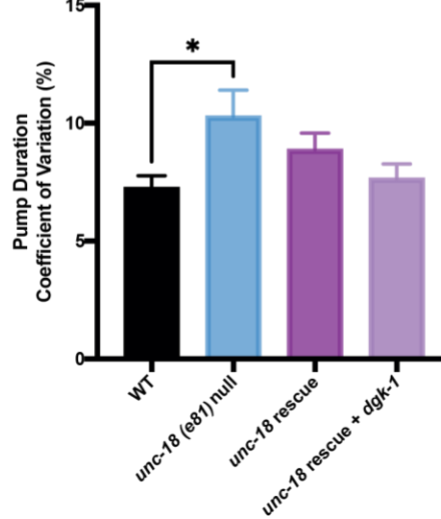
Figure 3.3. Electropharyngeogram (EPG) recordings from *unc-18* worms. A) Representative EPG traces from wild-type (WT), *unc-18 (e81)* null, *unc-18* rescue, and *unc-18* rescue + *dgk-1* worms. These traces show information from EPG traces such as waveform, excitatory (green circles) and relaxatory (blue circles) pumps, pump frequency, pump duration (yellow circles) and amplitude. B) *unc-18* rescue worms showed significantly increased mean pump frequency compared to *unc-18 (e81)* null mutants. This was significantly reduced in *unc-18* rescue + *dgk-1* mutants compared to *unc-18* rescue worms. C) The inter-pump interval duration standard deviation (IPI duration SD) did not significantly differ between WT and *unc-18* rescue mutants, or between *unc-18 (e81)* null and *unc-18* rescue + *dgk-1* mutants. D) *unc-18 (e81)* null mutants had a mean pump duration significantly higher compared to WT mutants. *unc-18* rescue + *dgk-1* RNAi mutants had a mean duration significantly higher than wild-type and *unc-18* rescue worms. E) Pump duration coefficient of variation was significantly higher in *unc-18 (e81)* null worms compared to WT worms. There was no other significant difference in this measure between mutants. Fifteen animals per strain were analysed and data are shown as mean ± standard error of the mean. Statistical analysis was performed using a one-way analysis of variance with Tukey's multiple comparisons test. *$p \leq 0.05$, ** $p \leq 0.01$, **** $p \leq 0.0001$.

3.2.4 Phorbol 12-myristate 13-acetate treatment on *unc-18 (e81)* null mutants fails to improve locomotion

Previous investigations of the effects of DAG were conducted genetically through the expression of *egl-30 (js126)*. While *egl-30* acts in motor neurons and leads to the production of DAG, it functions upstream of DAG by activating *egl-8* (321). *dgk-1* on the other hand negatively regulates synaptic transmission by directly phosphorylating DAG into PA (224,321). Studies involving *egl-30 (js126)* therefore provide a limited representation of the *dgk-1 (ulv1)* mutation and its effects. As such, a pharmacological approach was deemed to be an alternative method to investigate the effects of increased DAG resulting from the *dgk-1 (ulv1)* mutation. Phorbol esters such as phorbol 12-myristate 13-acetate (PMA) are analogues of DAG, which directly binds to C1 domains of DAG-binding proteins, such as PKC and the subsequently identified, *unc-13* (324–326). This leads to their activation, and as a result, acetylcholine release at the NMJ is stimulated. Phorbol esters, for this reason, have been widely used to investigate the mechanism of DAG and its downstream effects.

In 1986, phorbol esters were shown to potentiate synaptic transmission in the rat hippocampus through activation of PKC (327), a finding that has been supported by several subsequent studies (328–331). Evidence that PKC inhibitors failed to block the phorbol ester effect of enhanced secretion suggested an alternative mechanism of action for these compounds through Munc13 (332,333). This role of phorbol ester action was highlighted following the finding that reducing the availability of Munc13 through binding to a synthetic peptide, reduced the effect of phorbol esters on neurotransmitter release (332). Increased synaptic transmission can be clearly observed in WT worms treated with PMA, which exhibit hypersensitivity to aldicarb

(Figure 3.4A). Similarly, PMA has been found to restore the HIC phenotype in *egl-30* mutants (100).

In the current study, increased DAG predicted to result from the *dgk-1 (ulv1)* mutation was mimicked through PMA treatment, addressing the question of whether excess DAG is sufficient to produce the rescue phenotype. *unc-18 (e81)* null mutants were treated with 2 μg/ml PMA for two hours before being assessed for sensitivity to aldicarb. *unc-18 (e81)* null mutants demonstrated a RIC phenotype, which was statistically significantly different from the hypersensitive phenotype of *unc-18 (e81)* null + DAG mutants (p<0.0001). Following PMA treatment, *unc-18 (e81)* null mutants demonstrated hypersensitivity to aldicarb at a level that was not statistically significant from *unc-18 (e81)* null + DAG mutants (p>0.05) (Figure 3.4B). While PMA resulted in increased hypersensitivity in *unc-18 (e81)* null mutants, the full effect of PMA was muted as hypersensitivity did not reach levels observed in WT worms treated with PMA. Similar to *unc-18 (e81)* null + DAG and *unc-18* rescue mutants, this muted effect is likely due to the presence of the *unc-18 (e81)* null mutation.

Following evidence that neurotransmitter release is increased in *unc-18 (e81)* null mutants, body bends were measured following PMA treatment to investigate whether the increase in ACh release results in increased locomotion (Figure 3.4C). WT worms treated with PMA demonstrated significantly increased locomotion compared to untreated worms (24.9 vs. 14.27 body bends per minute, respectively; p<0.0001),

consistent with previous findings of PMA-treated WT worms (100,334). In contrast, PMA treatment on *unc-18* rescue worms significantly reduced locomotion from 18.17 body bends per minute to 10.7 body bends per minute (p<0.0001). Locomotion rates in *unc-18 (e81)* null mutants showed no change following treatment with PMA despite demonstrating a HIC phenotype. PMA treatment on mutants in which DAG levels are already heightened either through *egl-30 (js126)* expression or with RNAi of *dgk-1* (*unc-18 (e81)* null + DAG, and *unc-18* null + *dgk-1* RNAi) also failed to improve locomotion as worms remained immobile for the time measured.
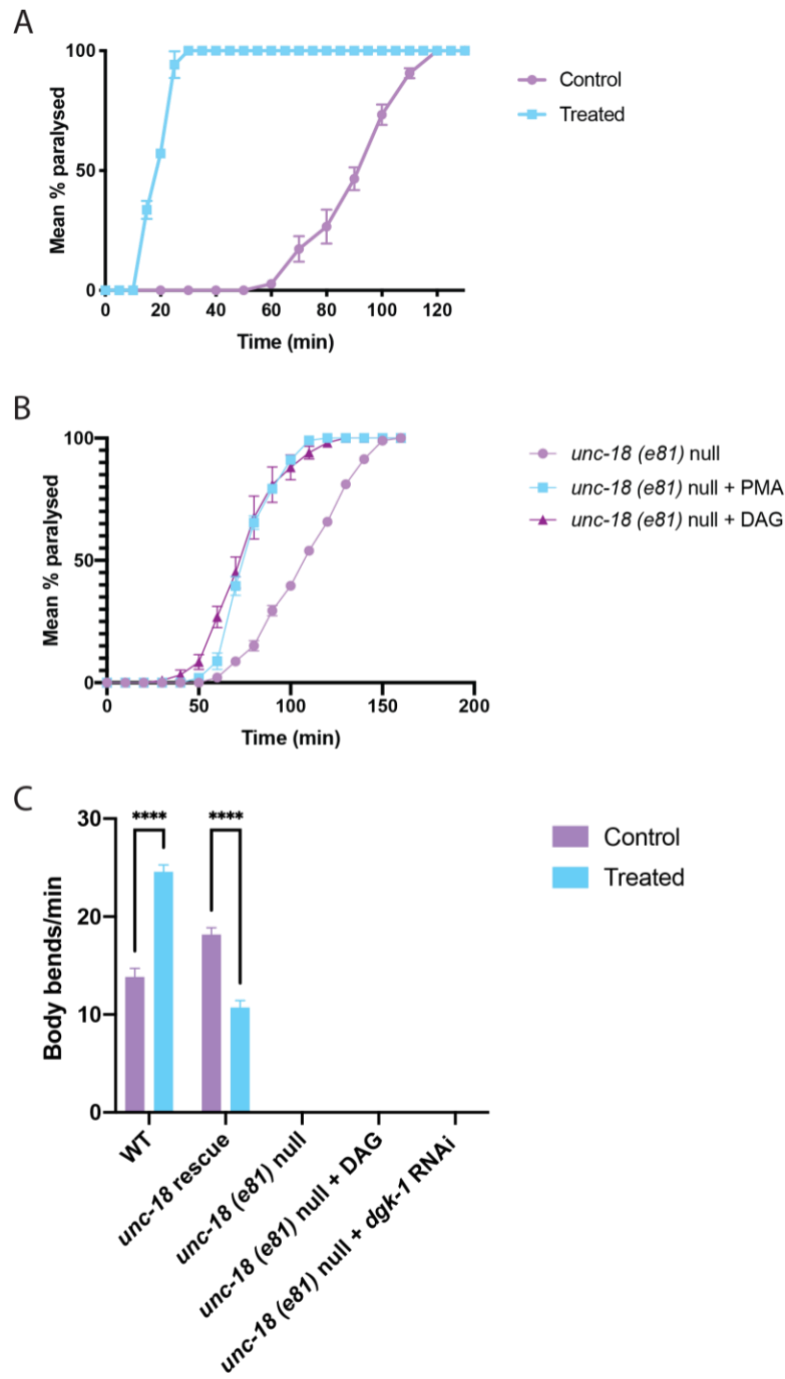
Figure 3.4. PMA treatment of *unc-18* mutant *C. elegans*. A) PMA treatment (2 μg/ml) on WT worms causes hypersensitivity to aldicarb. B) PMA treatment of *unc-18 (e81)* null mutants increased hypersensitivity to aldicarb. C) PMA treatment of WT and *unc-18* mutants. For body bends, a total of 10 worms were analysed in each experiment with a total of 3 independent experiments (n = 30 worms per strain). For aldicarb assays, 25-40 worms were assessed in each experiment, with a total of 3 experiments. Curves on the graph are representative of triplicate experiments. Data are shown as mean ± standard error of the mean. Statistical analysis of body bends was performed using a one-way analysis of variance followed by Tukey's multiple comparison test. Statistical analysis of aldicarb assays was performed using a log-rank test for Kaplan Meier followed by Bonferroni corrections test. ****$p<0.0001$.

3.2.5 *dgk-1 loss-of-function* alone is not sufficient to restore locomotion in *unc-18 (e81)* null mutants

As PMA acts as an analogue of DAG, its exposure results in the activation of downstream effectors of DAG. PMA provides a restricted representation of the *dgk-1 (ulv1)* mutation itself, as was found with studies which utilised the *egl-30 (js126)* mutation. This is because the use of PMA addresses the hypothesised excess of DAG, but does not address *loss-of-function* of *dgk-1*. *C. elegans* treated with PMA may have heightened levels of DAG, however, *dgk-1* continues to function as normal and produces phosphatidic acid (PA) through DAG phosphorylation. This, therefore, blocks interpretations which may be drawn from the different effects of the *ulv1* mutation which cannot be observed through increased DAG alone. To address this issue, DGK inhibitor II (R59949) was used to recreate the effects of the *dgk-1 (ulv1)* mutation more accurately, and re-address the question of whether the *ulv1* mutation alone is sufficient to produce the *unc-18* rescue phenotype.

As hypersensitivity to aldicarb and an increase in locomotion rate results from *dgk-1 loss-of-function* (224), a dose-response assay would allow the determination of a concentration that produces a hypersensitive phenotype similar to what is observed in *dgk-1* null mutant *C. elegans*. To establish the correct dose of inhibitor for treatment, a dose-response assay was performed on WT worms, in which worms were exposed to varying concentrations of R59949 for two hours before being assessed for aldicarb sensitivity. Increasing the dose of R59949 from 0 μM–1 μM increased hypersensitivity to aldicarb in WT worms. However, exceeding the dose of R59949 above 1 μM reversed aldicarb sensitivity, with 10 μM resulting in an aldicarb phenotype similar to that of untreated WT worms (Figure 3.5A). None of the doses tested produced a phenotype as strong as that seen in PMA-treated WT mutants or in

untreated *dgk-1 (ok1462)* loss-of-function mutants. Locomotion in WT worms was also assessed following treatment with the various doses tested, finding that increasing R59949 concentration from 0.01 μM to 0.1 μM significantly increased locomotion rate from 20.4 body bends per minute to 24.5 body bends per minute (p<0.01). Further increasing concentration to 1 μM only slightly increased locomotion rate to 24.7 body bends per minute. Treatment with 10 μM R59949 significantly reduced locomotion rate to 15.2 body bends per minute (p<0.0001), while 100 μM resulted in paralysis (Figure 3.5B).
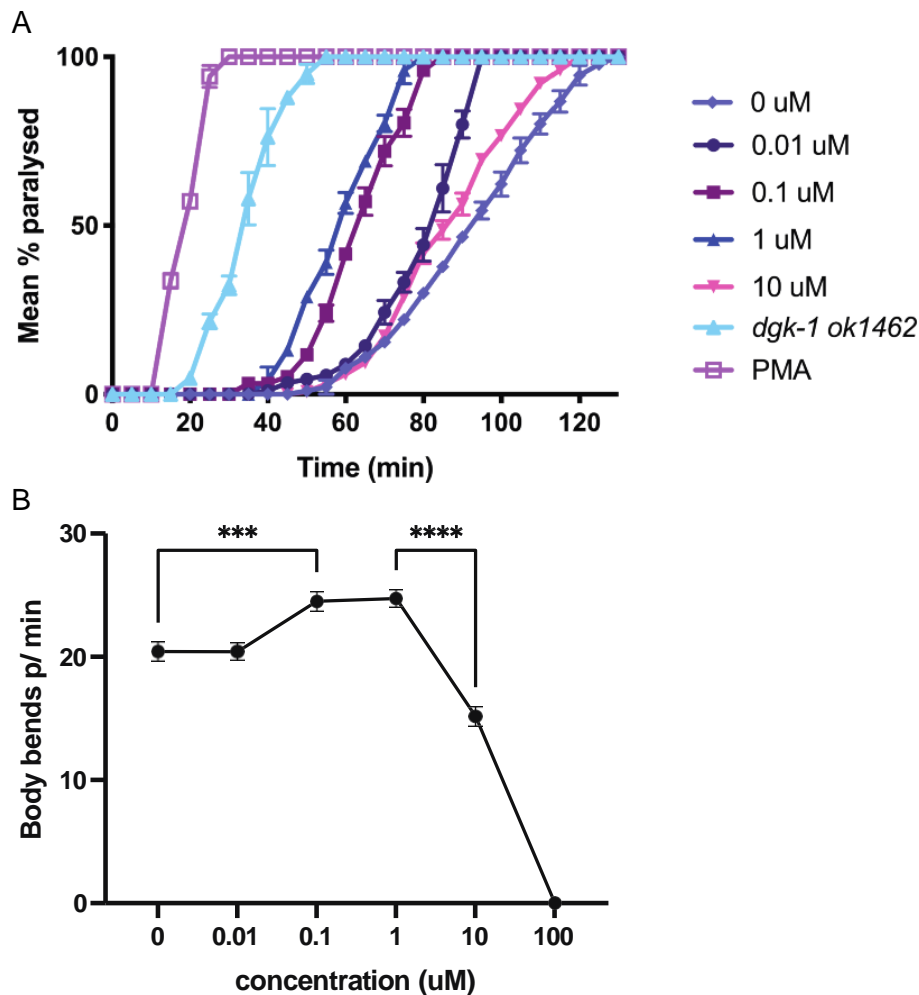
Figure 3.5. Dose-response analysis of DGK inhibitor II (R59949) treated WT worms. A) WT worms treated with 0.01 μM, 0.1 μM, and 1 μM become more hypersensitive compared to untreated worms. 0.1 μM and 1 μM resulted in the most hypersensitive phenotype, while treatment with 10 μM reversed the hypersensitive phenotype back to similar levels in untreated worms. B) Increasing R59949 concentration from 0 μM to 0.1 μM significantly increased body bends. Increasing concentration above 1 μM significantly reduced body bends. In aldicarb assays, 25–40 worms were assessed in each experiment and a total of 3 experiments were conducted for each drug, concentration, or strain. Curves on the graph are representative of triplicate experiments. For body bends, a total of 10 worms were analysed in each experiment with a total of 3 independent experiments (n=30 worms per strain). Data are shown as mean ± standard error of the mean. Statistical analysis on body bends was performed using a two-way analysis of variance followed by Tukey's multiple comparisons test. *** p<0.001, **** p<0.0001.

Following the results of the R59949 dose-response assays, 1 μM was chosen as the appropriate dose to use in future assays as this produced the most hypersensitive phenotype to aldicarb compared to all the doses that were tested. Consistent with observations in PMA-treated WT worms, R59949 significantly increased hypersensitivity to aldicarb in WT worms (p<0.0001; Figure 3.6A), and significantly increased locomotion from 13.8 body bends per minute to 24.6 body bends per minute (p<0.0001).

unc-18 rescue mutants were treated with R59949 to test the hypothesis that the *dgk-1 (ulv1)* mutation results in *loss-of-function.* A slight hypersensitive phenotype was observed in *unc-18* rescue mutants yet to a lesser extent compared to WT worms (p<0.001; Figure 3.6B). Interestingly, body bends in these mutants increased from 12.6 body bends per minute to 20.2 body bends per minute following exposure to R59949 (p<0.0001; Figure 3.6D).

Next, *unc-18 (e81)* null mutants were treated with R59949 to address the question of whether pharmacologically inhibiting *dgk-1* is sufficient to rescue synaptic transmission defects in *unc-18 (e81)* null mutants. R59949 treatment resulted in a shift towards aldicarb hypersensitivity compared to untreated worms (p<0.01; Figure 3.6C), yet failed to improve locomotion, as worms remained immobile during the time measured (Figure 3.6D). These results are consistent with observations following PMA treatment in *unc-18 (e81)* null mutants (Figure 3.4C).
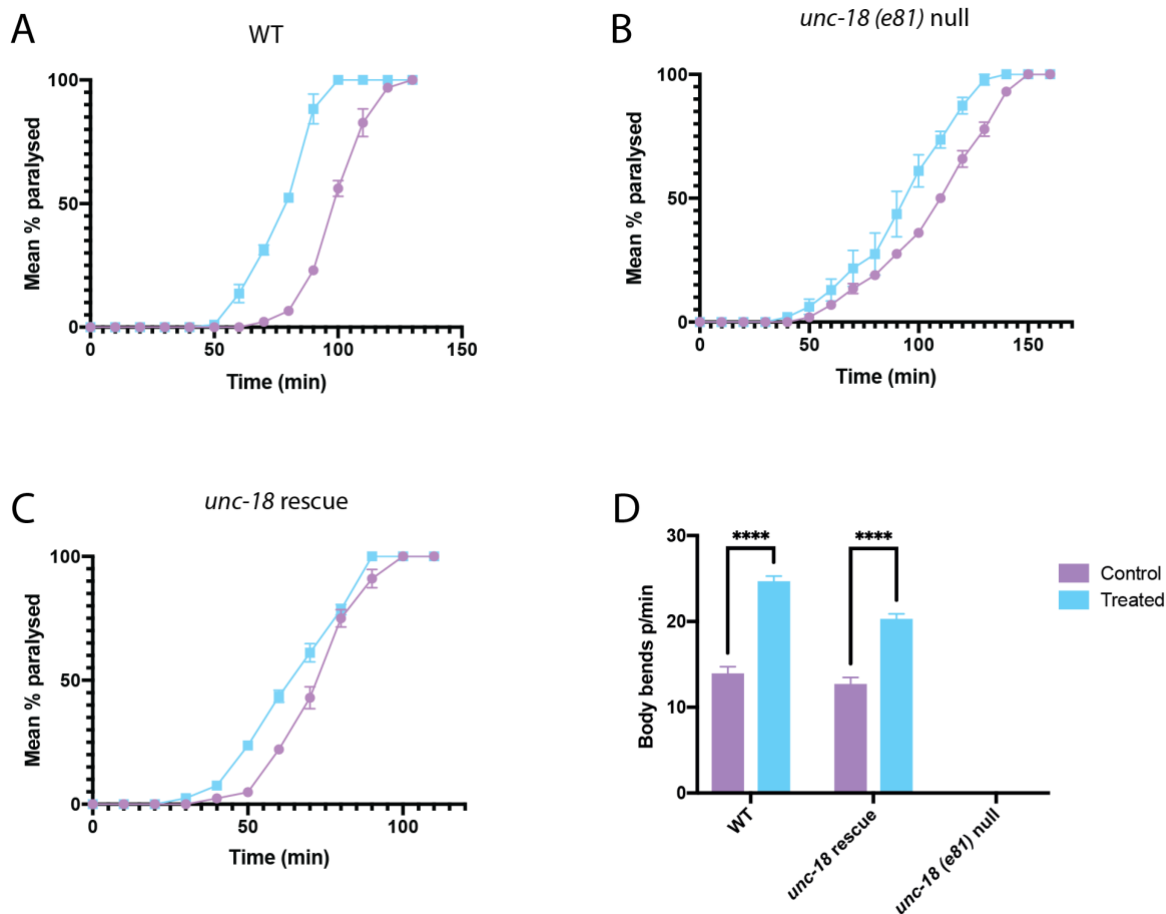
Figure 3.6. Locomotion and aldicarb sensitivity of untreated and R59949 treated worms. A–C) Aldicarb sensitivity of N2, *unc-18 (e81)* null and *unc-18* rescue mutants following R59949 treatment. D) Locomotion rate of N2, *unc-18 (e81)* null and *unc-18* rescue mutants following R59949 treatment. All assays were conducted after 2-hour treatment with R59949. For body bends, a total of 10 worms were analysed in each experiment with a total of 3 independent experiments (n=30 worms per strain). In aldicarb assays, 25–40 worms were assessed in each experiment, with a total of 3 experiments. Curves on the graph are representative of triplicate experiments. Data are shown as mean ± standard error of the mean. Statistical analysis on body bends was performed using a two-way ANOVA followed by Tukey's multiple comparisons test. Statistical analysis on aldicarb assays was performed using a log-rank test for Kaplan-Meier followed by Bonferroni corrections test. ****$p < 0.0001$.

3.3 Discussion

This study aimed to characterise the restoration of locomotion of *unc-18 (e81)* null mutants and investigate the necessity and sufficiency of the *dgk-1(ulv1)* mutation for the rescue phenotype of *unc-18* rescue. Previous studies have shown full or partial rescue of *unc-18 (e81)* null mutants with transgenic expression of wild-type *unc-18* (315), human Munc18-1 (306), or *unc-18* with point mutations that block closed-form syntaxin (181), and rescue of Munc18-1 using various chemical chaperones (10). While these studies stabilise or restore the function of the protein, the current study investigates a model in which the function of *unc-18* has been bypassed through alternative mechanisms to restore neurotransmission within *unc-18 (e81)* null *C. elegans.*

The results of this study categorically demonstrate successful restoration of locomotion and improved neurotransmission in *unc-18* rescue mutants containing the *unc-18 (e81)* mutation (Figure 3.1D, 3.2B, 3.3), suggesting that *unc-18* is not required for coordinated movement. Additionally, we show that *dgk-1 loss-of-function* through the *ulv1* nonsense mutation within the kinase domain, alongside other contributing factors, bypassed *unc-18* function and enhanced ACh release in *unc-18* rescue mutants. However, the *dgk-1 (ulv1)* mutation alone is not sufficient to produce the rescue phenotype observed, as mimicking the hypothesised effects of the mutation through increased DAG genetically, or pharmacologically, failed to improve locomotion in *unc-18 (e81)* null mutants. Understanding the role of *dgk-1* in synaptic transmission, and how mutating the kinase domain affects transmission is vital for understanding how the *ulv1* mutation allows the bypass of *unc-18* function. *dgk-1 loss-of-function* inhibits the phosphorylation of DAG into PA, leading to DAG

accumulation (224), which is consistent with the current findings of this study. DAG functions as a positive regulator of exocytosis activating downstream targets such as PKC and MUNC13 (89,90,100,335), two proteins that are closely linked to UNC-18 and its function. PKC-mediated enhancement of neurotransmission occurs through the phosphorylation of various substances.

Particularly, PKC has been found to phosphorylate Munc18-1/UNC-18 (336), with evidence that this reduces its binding affinity to syntaxin (213,214,337). As a result, this positively regulates exocytosis by increasing the availability of syntaxin for SNARE complex formation (213). Additionally, phosphorylation of Munc18-1 increases the vesicle pool replenishment (338), while also regulating exocytosis kinetics (214). PKC phosphorylation of Munc18-1 also inhibits interactions between SNAP-25 and syntaxin (339) which would enhance exocytosis by dissociating the SNARE complex (340). As there is no discernible UNC-18 protein in *unc-18 (e81)* null mutants (168), it is unlikely that this mechanism contributes to the *unc-18* rescue phenotype. However, PKC is known to phosphorylate a host of proteins. *In vitro* and *in vivo*, synaptotagmin-1 acts as a substrate for PKC, which potentially increases its affinity to bind to Ca^{2+} or the SNARE complex (340). Another known target of PKC phosphorylation is SNAP-25, which impacts its association with syntaxin (339). Other substrates for PKC include myristoylated alanine-rich C-kinase substrate (MARCKS), neuromodulin, and dynamin-1 (341). Munc13 on the other hand facilitates exocytosis by binding to the Munc18-1- syntaxin-1 complex, releasing Munc18-1 and enabling SNARE complex formation (101). Both the PKC and UNC-13 pathways have been implicated in vesicle secretion (85,335), and it is likely that they facilitate the production of the *unc-18* rescue phenotype. While many of these functions described require functional *unc- 18*, research has found that Munc13 promotes the proper

106

configuration of syntaxin- 1A/synaptobrevin-2 independent of Munc18-1 (3), increasing interest in *unc-13* for a potential role in the bypass of *unc-18*. Future work may investigate the involvement of PKC and *unc-13* in the *unc-18* rescue phenotype by examining whether the phenotype remains intact when the function of *unc-13* or PKC is reduced in these mutants.

As one focus of this study is increased levels of DAG in *unc-18* rescue mutants, any protein containing DAG-binding C1 domains should be considered as a possible contributing factor for the restoration of locomotion. In addition to PKC and Munc13-1, several other C1 domain-containing proteins exist, however not all function in the regulation of neurotransmitter release (342). Another potential protein that may play a role in the *unc-18* rescue phenotype is protein kinase D (PKD), which like PKC, belongs to a family of serine/threonine kinases that are activated by DAG and regulate various processes including cell differentiation, vesicle trafficking, and apoptosis (343–346). PKDs contain two DAG-binding C1 domains (C1a and C1b) with preferential binding of DAG to the C1a domain (347) in the *trans*-Gogli network (348). DAG regulates PKD activity by either binding to its C1 domain and regulating its localisation, or by inducing its activation by PKC-dependent phosphorylation (349,350). It is the binding of PKC to the PH domain of PKDs which phosphorylates its activation loop, resulting in its activation (349). Following the production of DAG, various DAG receptors are translocated to membrane compartments, where both PKD and PKC are present. The role of PKD however has been implicated in the endocytic pathway (351) with little evidence of its function in the exocytic pathway, and so there is little confidence in a role of PKD in the *unc-18* rescue phenotype compared to the possible involvement of PKC and/or *unc-13*.

In this study, genetically (*gain-of-function egl-30* mutation), or pharmacologically

enhancing (through PMA) DAG levels in *unc-18 (e81)* null mutants failed to improve

locomotion (Figure 3.1D, 3.1E, 3.2C). However, while these methods produced the

hypothesised effects of the *dgk-1 (ulv1)* nonsense mutation, they did not directly alter

dgk-1 activity. *dgk-1* activity is vital for maintaining the balance between DAG and

PA levels (216,352,353). In *unc-18 (e81)* null mutants in which DAG levels were

enhanced, *dgk-1* remained functional and continued to phosphorylate DAG into PA.

As this process is hindered in *unc-18* rescue mutants, this investigation does not

accurately encapsulate the exact effects of the *dgk-1 (ulv1)* mutation. It is possible

that the rescue phenotype is due to alterations in PA levels rather than the

enhancement of DAG alone. PA is a second messenger lipid with targets distinctive

from those of DAG, including Raf-1 kinase (354), PKC-ξ (355), phosphatidylinositol

phosphate 5-kinase (356,357), and protein tyrosine phosphatase (358,359).

Additionally, downstream targets of PA exceed the number of targets for DAG, likely

due to the lack of a common binding motif, such as the DAG-binding C1 domains

present in DAG-binding proteins (360). Studies of DGKs in mammals have found

that various species of PA are generated by DGK isoenzymes which are isozyme-

and cell/stimulation dependent. For example, PA generated by DGKζ enhances

mTOR function (361) and PIP5KIα (362), while PA generated by DGKθ strongly

binds to α-synuclein (363). These studies suggest that the downstream effects of PA

and the consequences of changes in its level may facilitate the *unc-18* rescue

phenotype. Additionally, Xie and colleagues found that PA restored granule

exocytosis in DGK-inhibited cells in which granule fusion was defective, while

supplementation with DAG failed to do so (58). This supports the hypothesis that the

unc-18 rescue phenotype may require alterations in levels of PA, as well as DAG,

and could explain the lack of improvement observed in *unc-18 (e81)* null mutants in

which DAG levels were elevated, either through genetic manipulation or PMA treatment. The complexity of PA and its interactions within cellular processes, together, with evidence that PA is involved in membrane fusion (364), suggest an important role for PA in producing the *unc-18* rescue phenotype, and should be explored in future studies.

Mimicking the effects of the *dgk-1 (ulv1)* mutation more accurately using R59949 treatment in *unc-18 (e81)* null mutants did not improve locomotion (Figure 3.6D), consistent with findings in which DAG levels had been enhanced in *unc-18 (e81)* null mutants (Figure 3.1D, 3.1E, 3.2C). Before discussing the implications of these findings, the efficacy of R59949 as a DGK inhibitor must be considered. In *C. elegans*, five classes of DGKs have been identified, while in humans, ten classes of the kinase exist, sharing between them conserved regions such as C1 and catalytic domains. While all DGKs facilitate the phosphorylation of DAG into PA, it is the differences in regulatory domains of the different DGKs which determine localisation (353), and 'when' and 'how' they are activated (223). The expression of DGKs is ubiquitous, with differential tissue specificity between isozymes (216,353,360), and has been discussed previously (Section 1.6). R59949 inhibition of DGKs is not selective and so its use results in a cascade of molecular changes which cannot be distinguished from one another. *In vitro* studies of purified or cloned DGK isozymes finding R59949 only inhibits type I, Ca^{2+} activated DGKs (DGKα, β, and γ), while only moderately attenuating the activity of type II DGKθ and κ (365,366). Deletion of the Ca^{2+}-binding EF motif of these isotypes did not alter inhibition as R59949 was instead found to act on the catalytic domain (365). In *C. elegans, dgk-3*, the DGKβ homologue, is predicted to be involved in olfactory behaviour and thermotaxis, however, there are currently no *C. elegans* homologues identified for DGKα, γ, and

κ. As the *dgk-1 (ulv1)* mutation resides within the catalytic domain, R59949 was selected as a suitable method to mimic the effects of the mutation. However, R59949 has not been investigated in *C. elegans*, so the exact effects of the compound on the five classes of DGKs remain enigmatic and findings from mammalian studies cannot be translated to the DGKs existing within *C. elegans*. It is possible that R59949 inhibition of different DGKs in *C. elegans* generates various species of PA which create distinct downstream effects that are not consistent with the effects of *dgk-1 (ulv1)* mutation.

In the present study, R59949 treatment results in hypersensitivity to aldicarb in wild-type worms, a phenotype that is characteristic of *dgk-1* mutants, suggesting that R59949 does in fact inhibit *dgk-1*. However, it should be noted that a R59949 concentration of 10 μM seemed to be toxic to the worms. Therefore, it is a possibility that the observed hypersensitivity to aldicarb may in fact be a consequence of the toxicity of R59949. Future work may determine the efficacy of R59949 on *dgk-1* inhibition more accurately through quantification of DAG activity in mutants treated with the drug. Nonetheless, the lack of improvement in locomotion following R59949 treatment, together with evidence that increasing DAG in *unc-18 (e81)* null mutants does not improve locomotion, supports insufficiency of the *dgk-1 (ulv1)* mutation for the *unc-18* rescue phenotype. Therefore, it is hypothesised that another mutation, potentially *sorf-2 (ulv2),* works alongside or directly with the *dgk-1 (ulv1)* mutation to produce the observed *unc-18* rescue phenotype.

Another notable finding following R59949 treatment in *unc-18* rescue mutants was the observed increase in locomotion. This is interesting as a complete l*oss-of-function* was hypothesised as a result of the *dgk-1 (ulv1)* mutation. If this was the

case, an effect on locomotion would not be expected in these mutants. As an increase in locomotion was observed in *unc-18* rescue mutants following R59949 treatment, it is possible that some *dgk-1* activity may be intact in these mutants. Therefore, the *ulv1* mutation may lead to a truncated and/or partially active form of *dgk-1* rather than a complete *loss-of-function* in the gene. However, without isolating the *dgk-1 (ulv1)* mutation on a wild-type background, absent of the *sorf-2 (ulv2)* and *unc-18 (e81)* mutations, the resulting phenotype of the allele cannot fully be elucidated. If the *ulv1* mutation does result in a partially active form of *dgk-1*, further inhibition of the gene should result in an additional increase in DAG levels, which would have been identified through an increased HIC phenotype when exposed to aldicarb (Figure 3.6C). Excess DAG following PMA treatment produced the most hypersensitive phenotype in wild-type worms with increased locomotion, but in *unc-18* rescue mutants, resulted in reduced locomotion (Figure 3.4C). The different effects on locomotion in *unc-18* rescue mutants following PMA and R59949 treatment further support the idea that the *unc-18* rescue phenotype results from changes in both DAG, and PA rather than just enhanced DAG.

3.3.1 Summary

This study aimed to categorically confirm the successful restoration of synaptic transmission within *unc-18* rescue mutants and identify the necessity of the *dgk-1 (ulv1)* in the production of the rescue phenotype. *Unc-18* rescue worms were shown to have locomotion and neurotransmission at similar levels to wild-type worms. After validating this finding, we confirmed the need of the *dgk-1 (ulv1)* mutation in producing the rescue as wild-type *dgk-1* reversed the rescue phenotype. Identification that inhibiting *dgk-1* or enhancement of DAG is not sufficient to produce the rescue phenotype in *unc-18 (e81) null* mutants confirms the requirement of another mutation in the observed phenotype, such as the *sorf-2 (ulv2)* mutation. This raises the question of which changes within the biochemical exocytic machinery occur as a result of the *ulv1* and *ulv2* mutations to bypass the function of *unc-18* in exocytosis.

Chapter 4: The *unc-18* rescue phenotype requires both *sorf-2* and *dgk-1*

4.1 Introduction

Following the evidence that *dgk-1* does not by itself produce the *unc-18* rescue phenotype, we aimed to investigate the necessity and sufficiency of *sorf-2* for the observed improvement in behaviour. Whole genome SoLiD sequencing identified the novel *ulv2* missense mutation, located at the C-terminus of *sorf-2* (C>Y):III: 5333229G>A, and was validated in *unc-18* rescue mutants using Sanger sequencing (Figure 4.1). The role of *sorf-2* in neuronal processes has not yet been fully elucidated, so the exact effects of the *ulv2* mutation are unclear. Current literature, however, has implicated the gene in processes ranging from trafficking and endocytosis to neurogenesis (271,367). While research on *sorf-2* is still in its infancy, knowledge of its structure provides insight into how the gene functions within various biological processes. Generally, BEACH domain-containing proteins (BDCPs) are very large and function within vital processes of vesicle trafficking, signalling and membrane dynamics (276,368). The presence of WD40 repeats gives the proteins the ability to scaffold interactions between proteins for multiprotein complex formation (276), with protein functions ranging from signal transduction, vesicular trafficking, cell cycle control and cytoskeletal assembly (369,370).

As the *ulv2* mutation does not lie within the BEACH domain or WD40 repeats (Figure 4.1), it is difficult to ascertain the effects of the *ulv2* mutation on *sorf-2* function. Previous studies have identified that *sorf-2 loss-of-function* partially rescues impairments in endosome fusion in various *vps* deletion mutants, likely due to elevated phosphatidylinositol 3-phosphate (PtdIns3P) levels, which may compensate for its *loss-of-function* (271). It was suggested that this effect may occur through the

activation of PtdIns3P effectors such as RABS-5 and EEA-1, which facilitate SNARE complex formation (271). Thus, we hypothesise that the *sorf-2 ulv2* results in the *loss-of-function* of the gene which then aids successful synaptic transmission within *unc-18* rescue mutants. We further hypothesise a role of *sorf-2* in vesicular transport and exocytosis, consistent with functions of other BEACH domain-containing proteins (276).

Confirming a role for *sorf-2* in the *unc-18* rescue phenotype would identify a novel pathway through which the function of *unc-18* may be completely bypassed if dysfunctional. Investigation of how *dgk-1* and *sorf-2* work together to achieve this bypass would then provide insight into the role of *sorf-2* in synaptic transmission. This would be useful for understanding the role of its mammalian homologue, WDR81, in the neuronal disorders in which it has been implicated.
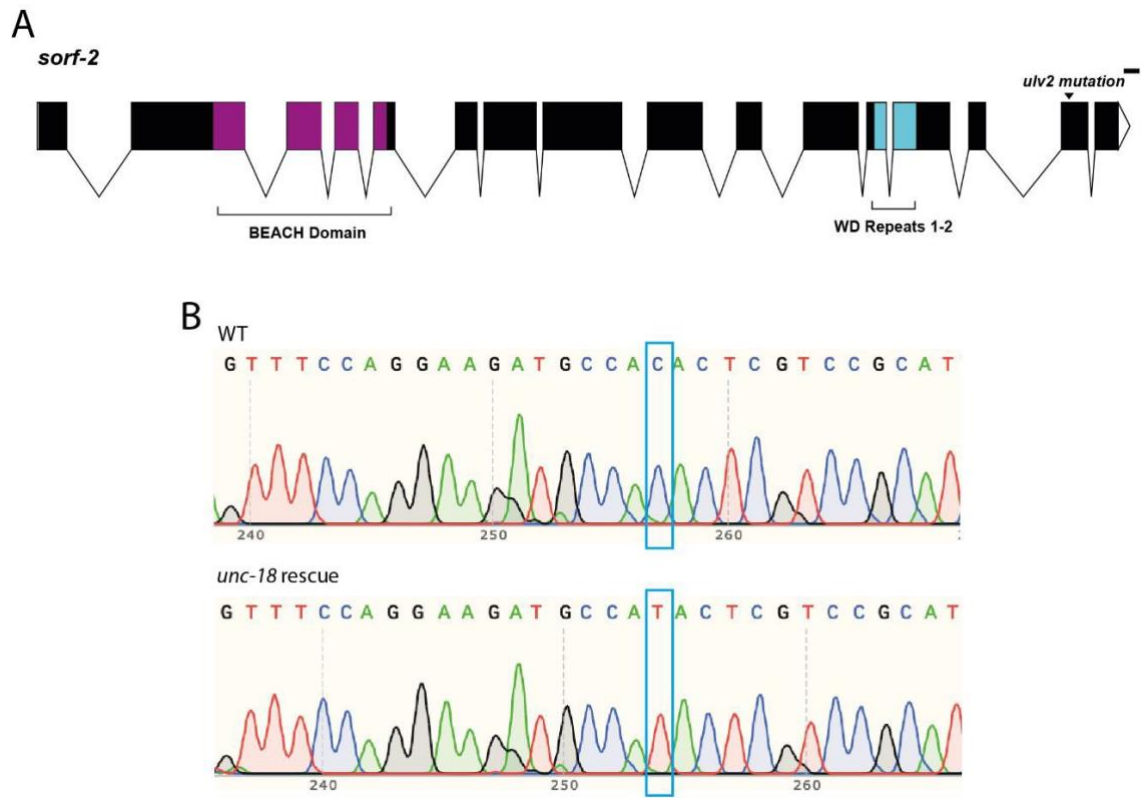
Figure 4.1. *A)* Schematic of *sorf-2* exon structure and location of the *ulv2* mutation sequenced in *unc-18* rescue and WT worms using a reverse primer. B) Chromatogram of the *sorf-2 (ulv2)* mutation in *unc-18* rescue mutants.

4.2 Results

4.2.1 *sorf-2* functions in the regulation of behavioural phenotypes

To better understand the role of *sorf-2* in neuronal mechanisms, I aimed to investigate the behavioural effects of *sorf-2* over-expression and under-expression (Figure 4.2). *sorf-2* was overexpressed in Bristol N2 WT through either a *rab3* promoter (*sorf-2* OE (neuronal)) or through its own endogenous promoter (*sorf-2* OE (global)). Under-expression of *sorf-2* was investigated using a lethal *sorf-2* null mutation (271) which is viable as heterozygous through a hT2 genetic balancer. Additionally, a novel mutant was isolated (*dgk-1 + sorf-2),* courtesy of Dr Jeff Barclay, in which the *dgk-1 (ulv1)* and *sorf-2 (ulv2)* mutations were present together, absent of the *unc-18 (e81)* mutation. Behavioural analysis of the *dgk-1 + sorf-2* mutant allows identification of effects created by the two mutations, without the limitation of being masked by the strong behavioural phenotypes resulting from the *unc-18 (e81)* null mutation.

Locomotion rate was not significantly different between mutants in which *sorf-2* was over-expressed neuronally (9.4 body bends per minute) or globally (8.3 body bends per minute, $p > 0.05$), however, both mutants moved at a rate significantly lower than WT (*sorf-2* OE (neuronal) $p < 0.001$, *sorf-2* OE (global) $p < 0.0001$) and *unc-18* rescue worms (*sorf-2* OE (neuronal) $p < 0.05$, *sorf-2* OE (global) $p < 0.001$). *sorf-2* heterozygous null mutants moved significantly slower compared to all other mutants investigated (5.3 body bends per minute), with the most significant differences observed in comparison to WT, *unc-18* rescue and *dgk-1 + sorf-2* worms (all $p < 0.0001$) (Figure 4.2A). As both over-expression and under-expression of *sorf-2*

117

reduce the locomotion of worms, combined with previous findings in this investigation, it is likely that *dgk-1 (ulv1)* contributes to the increase in locomotion at a greater extent than the *sorf-2 (ulv2)* mutation. *dgk-1 + sorf-2* mutants moved at a rate significantly higher compared to *unc-18* rescue mutants (17.9 body bends per minute vs 12.6 body bends per minute, respectively; $p<0.0001$). This was also significantly higher compared to WT worms which moved at a rate of 13.8 body bends per minute ($p<0.01$).
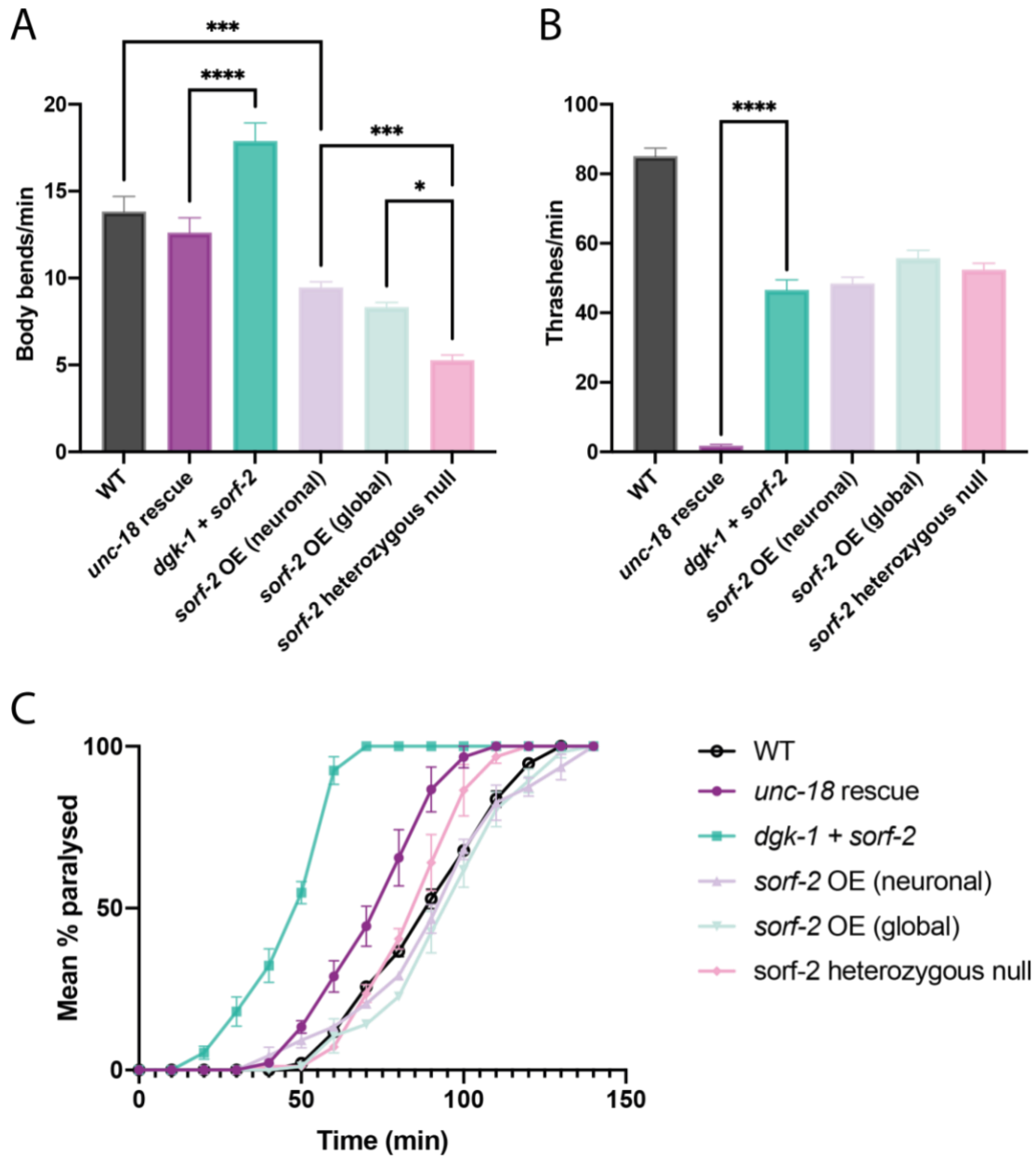
Figure 4.2. Behavioural analysis of *sorf-2* mutants. A) Locomotion rate of *sorf-2* mutants when crawling on a surface. B) Locomotion rate of *sorf-2* mutants in Dent's solution. C) Aldicarb sensitivity of *sorf-2* mutants. For body bends and thrashing assays, a total of 10 worms were analysed in each experiment with 3 independent experiments (n=30 worms per strain). For aldicarb assays, 25–50 worms were analysed in each experiment, with a total of 3 independent experiments. Data are shown as mean ± standard error of the mean. Statistical data analysis for body bends and thrashing was performed using a one-way analysis of variance, followed by Tukey's multiple comparisons test. Aldicarb data analysis was performed using a log-rank test for Kaplan-Meier followed by Bonferroni comparisons test. *p$\leq$0.05, ***p$\leq$0.001, ****p$\leq$0.0001.

unc-18 rescue worms moved significantly slower than WT worms when in solution

(Figure 3.1), despite moving at a rate that is not significantly different when on a

surface, so it was considered necessary to investigate the thrashing rate of all

mutants (Figure 4.2B). This would provide information about whether the low

thrashing frequency observed in *unc-18* rescue mutants is characteristic of *sorf-2*

mutants. *dgk-1 + sorf-2* mutants thrashed at a rate significantly less compared to WT

worms (46.5 thrashes per minute vs 85.0 thrashes per minute, $p<0.0001$), but

significantly higher in comparison to *unc-18* rescue mutants which produced 1.7

thrashes per minute ($p<0.0001$). *sorf-2* OE (neuronal) mutants thrashed at a rate of

48.3 thrashes per minute, which was not significantly different to *sorf-2* OE (global)

mutants (55.7 thrashes per minute), *sorf-2* heterozygous null mutants (52.3 thrashes

per minute) or *dgk-1 + sorf-2* mutants (all $p>0.05$). Thrashing in these worms,

however, was significantly less than WT ($p<0.0001$) and significantly higher than

unc-18 rescue mutants ($p<0.0001$). Similar results were observed in *sorf-2* OE

(global) mutants, with the difference that in these mutants, thrashing was significantly

higher compared to *dgk-1 + sorf-2* mutants ($p<0.05$). Thrashing in *sorf-2*

heterozygous null mutants was significantly lower than WT worms ($p<0.0001$), but

significantly higher than *unc-18* rescue mutants ($p<0.0001$). There was no significant

difference between thrashing in *sorf-2* heterozygous null mutants and *dgk-1 + sorf-2*

mutants ($p>0.05$). As *unc-18* rescue mutants thrashed significantly lower compared

with all other mutants for *sorf-2* (all $p<0.0001$), these findings suggest that the defect

in thrashing is not caused by *sorf-2* itself. These observations support the idea that

only some neuromuscular pathways are restored in the *unc-18* rescue mutant, while

others remain defective due to the *unc-18 (e81)* null mutation.

Next, acute sensitivity to aldicarb was assayed to investigate how cholinergic release

differs between mutants with varying expression of *sorf-2* (Figure 4.2C). This would

provide insight into whether *sorf-2* functions within the cholinergic pathway. Results

found that the aldicarb sensitivity of *sorf-2* OE (neuronal), *sorf-2* heterozygous null

and *sorf-2* OE (global) were not significantly different from WT worms (p>0.05). *unc-18* rescue mutants were significantly more hypersensitive to aldicarb than *sorf-2*

heterozygous null mutants, and both *sorf-2* overexpression mutants (p<0.01). This is

interesting as the *unc-18* rescue mutant contains the *unc-18 (e81)* null mutation

which has been shown to produce a RIC phenotype. Presence of the *sorf-2 (ulv2)*

and *dgk-1 (ulv1)* mutations, which produce a HIC phenotype, are able to partially

overcome the effects of the resistance resulting from the *unc-18 (e81)* null mutation.

The resistant effects of the *unc-18 (e81)* mutation can be clearly observed when

comparing the aldicarb sensitivity of *unc-18* rescue mutants to *dgk-1 + sorf-2*

mutants, which were significantly more hypersensitive to aldicarb compared to WT

worms, and all other *sorf-2* mutants investigated (p<0.0001), including *unc-18* rescue

mutants.

4.2.2 Relative expression of *unc-18, sorf-2* and *dgk-1* in mutant *C. elegans*

RT-qPCR was used to quantify the relative expression of *unc-18, sorf-2 and dgk-1* in mutant animals. This would provide information about whether the mutations present in *dgk-1* and *sorf-2* affect mRNA expression. As the function of *dgk-1* is well-established, the effects of the *dgk-1 (ulv1)* mutation can be hypothesised with some knowledge. However, as the role of *sorf-2* is still being established, hypothesising the effects of the *sorf-2 (ulv2)* mutation is more challenging. To better understand the role of *sorf-2* in neurotransmission, this study included two mutants with *sorf-2* overexpression (*sorf-2* OE (neuronal) and *sorf-2* OE (global)), and one *sorf-2* deletion mutant, which has been genetically balanced (*sorf- 2* heterozygous null). The mean relative expression of *sorf-2* was significantly higher than WT in *unc-18 (e81)* null mutants (1.75; p<0.05) and *sorf-2* heterozygous null mutants (0.54; p<0.01), but not in *unc-18* rescue mutants (1.52), *sorf-2* OE (neuronal) (5.59), or *sorf-2* OE (global) (4.63) mutants (p>0.05). *unc-18* relative expression was significantly reduced in both *unc-18 (e81)* null (0.29), *unc-18* rescue (0.12), and *sorf-2* heterozygous null mutants (0.40) (p<0.001), but not in *sorf-2* OE (neuronal) (2.00), or *sorf-2* OE (global) (1.39) mutants (p>0.05). *dgk-1* relative expression was significantly lower than WT in *unc-18* rescue mutants (0.31; p<0.05), and *sorf-2* heterozygous null mutants (0.12; p<0.001), but not in *unc-18 (e81)* null mutants (0.74), *sorf-2* OE (neuronal) (1.15), or *sorf-2* OE (global) (0.97) mutants (p>0.05) (Figure 4.3).
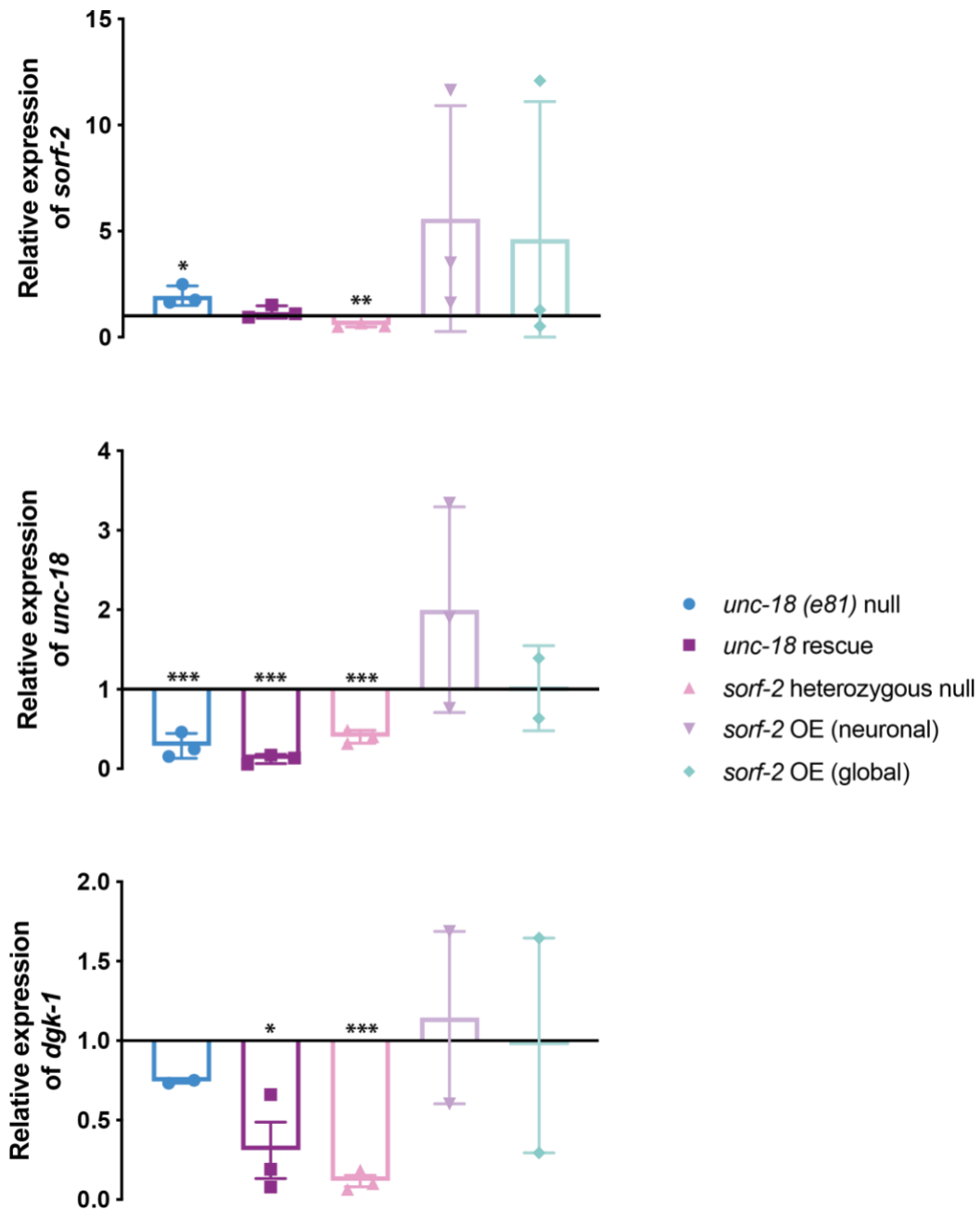
Figure 4. Quantitative PCR analysis showing relative expression of *sorf-2, unc-18* and *dgk-1* in mutant *C. elegans,* normalised against expression in WT worms. Data are displayed as mean values ± standard error of the mean. n=3 for all results, except for *unc-18 (e81)* null and *sorf-2* OE neuronal mutants which have n=2 for *dgk-1* analysis, and *sorf-2* OE global mutants which have n=2 for *unc-18* and *dgk-1* analysis. Data were analysed using one-way ANOVA followed by Tukey's multiple comparisons test. *p≤0.05, **p≤0.01, *** p≤0.001.

4.2.3 Present together, *dgk-1 (ulv1)* and *sorf-2 (ulv2)* alter pharyngeal pumping

unc-18 rescue mutants previously demonstrated an improvement in neuronal activity through measurements of EPG recordings. Thus, EPG recordings of *dgk-1 + sorf-2* mutants were made to investigate whether the same results were observed when the *dgk-1 (ulv1)* and *sorf-2 (ulv2)* mutations were isolated without the *unc-18 (e81)* mutations (Figure 4.4). This would provide insight into whether the two mutations together result in increased neuronal activity and would support the hypothesis that the two mutations are responsible for the improved synaptic transmission observed in *unc-18* rescue mutants. *sorf-2* over-expression and under-expression mutants were also recorded to investigate whether altering *sorf-2* expression has an effect on neuronal activity, as was observed in the investigation of behavioural phenotypes.

dgk-1 + sorf-2 mutants pumped at a mean frequency that was not significantly different than *unc-18* rescue mutants (2.54 Hz vs 2.79 Hz, $p > 0.05$) or *sorf-2* heterozygous null mutants (2.73 Hz, $p < 0.05$). However, in comparison with WT worms (3.75 Hz), the mean frequency of pumping was significantly lower in *dgk-1 + sorf-2* worms ($p < 0.0001$). A similar result was found when compared with *sorf-2* OE (neuronal) mutants (3.51 Hz, $p < 0.0001$), and *sorf-2* OE (global) mutants (3.12 Hz, $p < 0.05$). Consistent with findings from locomotion and aldicarb assays, there was no significant difference in mean pumping frequency between the two *sorf-2* over-expression mutants ($p > 0.05$). However, differences were observed when compared with the mean pumping frequency of other mutants. In comparison to *sorf-2* heterozygous null mutants, mean pumping frequency was significantly higher in *sorf-2* OE (neuronal) mutants ($p < 0.001$), however, *sorf-2* OE (global) mutants did not

significantly differ in this measure. In comparison with WT worms, *sorf-2* OE (neuronal) mutants were not significantly different, while *sorf-2* OE global mutants pumped at a mean frequency that was significantly lower than WT (p<0.05) (Figure 4.4A).
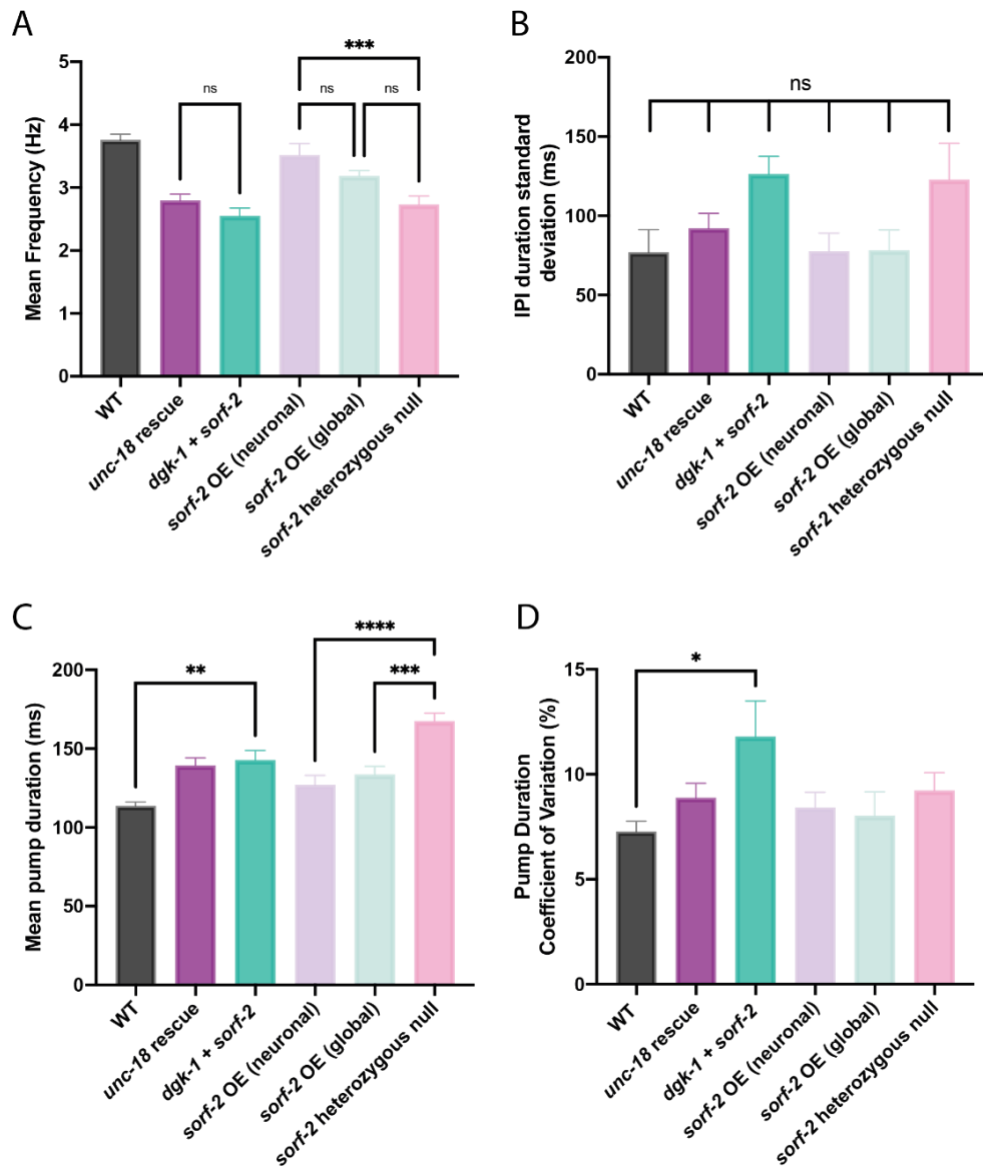
Figure 4.4. Electropharyngeogram (EPG) recordings of *sorf-2* mutants. A) *unc-18* rescue worms and *dgk-1 + sorf-2* mutants did not significantly differ in mean pump frequency. *sorf-2* heterozygous null mutants pumped significantly lower compared to *sorf-2* OE (neuronal) mutants. B) The inter-pump interval duration standard deviation (IPI duration SD) did not significantly differ between any of the mutants investigated. C) *dgk-1 + sorf-2* had a significantly higher mean pump duration than wild-type mutants. *sorf-2* heterozygous null mutants had a mean pump duration significantly higher than both *sorf-2* over-expression mutants. D) Pump duration coefficient of variation was significantly higher in *dgk-1 + sorf-2* worms compared to wild-type worms. There was no other significant difference in this measure between mutants. No significant differences were observed between *sorf-2* OE (neuronal) and *sorf-2* OE (global) mutants for any of the outcomes. Fifteen animals per strain were analysed, and data are shown as mean ± standard error of the mean. Statistical analysis was performed using a one-way analysis of variance with Tukey's multiple comparisons test. *p≤0.05, **p≤0.01, ***p≤0.001, ****p≤0.0001

As previously mentioned, the inter-pump interval duration standard deviation (IPI duration SD) provides information about the regularity of pumping by measuring the time between one excitatory pump to the next. There was no statistically significant difference found in this measure between any of the mutants investigated ($p > 0.05$) (Figure 4.4B). Mean pump duration measures are informative of the contraction and relaxation of pharyngeal muscles. Mean pump duration was significantly higher for *dgk-1 + sorf-2* mutants compared with WT worms (142.6 ms vs 113.7 ms, $p < 0.01$). This measure was not significantly different between *sorf-2* OE (neuronal) and *sorf-2* OE (global) mutants (126.7 ms vs 133.4 ms, $p > 0.05$), however, both mutants were significantly different from *sorf-2* heterozygous null mutants, which had a mean pump duration of 167.2 ms ($p < 0.0001$ and $p < 0.001$, respectively). The mean pump duration of *sorf-2* heterozygous null mutants was also significantly higher than WT and *unc-18* rescue mutants ($p < 0.0001$ and $p < 0.01$, respectively) (Figure 4.4C).

The pump duration coefficient of variation provides information about the variation between pump durations. This measure was significantly higher in *dgk-1 + sorf-2* mutants compared with WT worms (11.8% vs 7.3%, respectively; $p < 0.05$). *unc-18* rescue mutants had a pump duration coefficient of variation of 8.9%, while this measure was 9.2% in *sorf-2* heterozygous null mutants ($p > 0.05$). No significant difference was found between *sorf-2* OE (neuronal) and *sorf-2* OE (global) mutants (8.4% vs 8.0%, $p > 0.05$) (Figure 4.4D). These findings, along with findings from behavioural analysis support a neuronal nature of *sorf-2.*

4.2.4 Attempted isolation of the *dgk-1 (ulv1)* and *sorf-2 (ulv2)* mutations

Thus far, the mutations in *dgk-1* and *sorf-2* have only been investigated alongside each other, or in the presence of the *unc-18 (e81)* mutation, making it difficult to decipher the viability of the two mutations. I now aimed to genetically isolate the *dgk-1 (ulv1)* and *sorf-2 (ulv2)* from each other to allow a more accurate analysis of the individual effects of each mutation on synaptic transmission. To accomplish this, *dgk-1* + *sorf-2* hermaphrodite mutants were genetically crossed with WT male worms, and successful heterozygous mutant F1 offspring were isolated and allowed to self-fertilise.

It was hypothesised that an F1 offspring, heterozygous for both *dgk-1 (ulv1)* and *sorf-2 (ulv2)* would produce offspring with 9 different genotypes (Figure 4.5. Following the successful fertilisation of a single F1 heterozygous worm, approximately 80-100 F2 worms were isolated and genotyped. Genotyping for *sorf-2* and *dgk-1* unfortunately only returned 18 successful results in which both genes had been sequenced. Out of 9 expected genotypes, results identified the presence of only 3 (Figure 4.5). Double mutant *dgk-1* worms were observed as the most common, at a higher frequency than expected (66.6%). No wild-type worms were identified in the selected offspring.

Despite a low number of successful reads for both genes in a worm, we wanted to assess the frequency of each allele, as this could provide insight into the nature of the mutations. In total, there were 47 successful reads for *dgk-1*, all of which were heterozygous for *dgk-1 (ulv1)*. For *sorf-2*, there were 28 successful reads, of which 20 (71.4%) were heterozygous, 2 (7.1%) were homozygous for *sorf-2 (ulv2)*, and 6

(21.4%) were wild-type. These findings are interesting as there was no observation

of wild-type *dgk-1* or homozygous *dgk-1 (ulv1).* The lack of homozygous *dgk-1 (ulv1)*

reads suggests that present as a homozygous, the mutation may be lethal.

d s d s	d + d s	s + d s	s + d +
d + d s	d + d +	s + d +	+ + d +
s + d s	s + d +	s + s +	+ + s +
s + d +	+ + d +	+ + s +	+ + + +

	Expected (%)	Observed (%)
(black)	6.25	0
(magenta)	12.5	0
(teal)	12.5	11.1
(orange)	25	66.7
(light blue)	12.5	22.2
(pink-red)	12.5	0
(light pink)	6.25	0
(purple)	6.25	0
(blue)	6.25	0

Figure 4.5 Punnett square predicting genotypes of F2 offspring following successful genetic crossing of N2 wild-type male *C. elegans* with *dgk-1 + sorf-2* hermaphrodite worms. Expected and observed frequencies for each genotype are presented. 18 worms were successfully sequenced for both genes, *dgk-1* and *sorf-2*. Out of 9 possible genotypes, 3 were observed, with the initial *dgk-1 + sorf-2* heterozygous mutant identified at the highest frequency. d=*dgk-1 (ulv1)*; s=*sorf-2 (ulv2)*; +=wild-type.

This investigation aimed to isolate the *dgk-1 (ulv1)* and *sorf-2 (ulv2)* mutations from each other. Given the nature of the experiment, *dgk-1* resides on chromosome X and *sorf-2* resides on chromosome III. Therefore, it would be assumed that the separation of the two mutations would be unproblematic. However, this study was limited by the low number of samples with successful reads for both *dgk-1* and *sorf-2* in a single worm. This reduced the probability of observing genotypes which were already expected to exist at a low frequency, such as wild-type worms. In the interest of time, it was decided to abort this investigation.

4.2.5 Transgenic expression of *wild-type sorf-2* in *unc-18* rescue mutants reverses the rescue phenotype

Next, the necessity of the *sorf-2 ulv2* mutation for the *unc-18* rescue phenotype was addressed. In our hands, isolation of transgenic worms expressing wild-type *sorf-2* in the *unc-18* rescues, under the control of either a neuronal or constitutive promoter was not possible, and it was therefore hypothesised that this transgenic expression was not viable. This hypothesis fits with the observation that *unc-18 + DAG* mutant worms were poor growing. Therefore, wild-type *sorf-2* was subcloned into an expression vector under the control of a phsp16.48 heat-shock promoter (phsp16.48::*sorf-2*), which was then injected into *unc-18* rescue mutants (*unc-18* rescue + *sorf-2*). It was hypothesised that if mutant *sorf-2* was necessary for the *unc-18* rescue phenotype, a reduction in locomotion would result following the heat-shock induced expression of wild-type *sorf-2* in *unc-18* rescue worms. Additionally, reduced locomotion would suggest a reduced function of *sorf-2* resulting from the *ulv2* mutation.

Expression of wild-type *sorf-2* in the *unc-18* rescue worms following heat-shock significantly reduced locomotion from 17.2 body bends per minute to 9.4 body bends per minute in *unc-18* rescue + *sorf-2* mutants ($p<0.0001$). In *unc-18* rescue mutants, heat shock resulted in a slight yet significant increase in locomotion from 17.2 body bends per minute to 18.7 body bends per minute ($p<0.05$) (Figure 4.6) indicating that exposure to the heat shock protocol itself was not deleterious. However, as over-expression of *sorf-2* (in *sorf-2* OE (global) and *sorf-2* OE (neuronal) mutants), and under-expression of *sorf-2* (in *sorf-2* heterozygous null mutants) result in reduced locomotion, these results do not provide complete evidence about whether the *sorf-2 (ulv2)* mutation results in a *gain-of-* or *loss-of-function*.
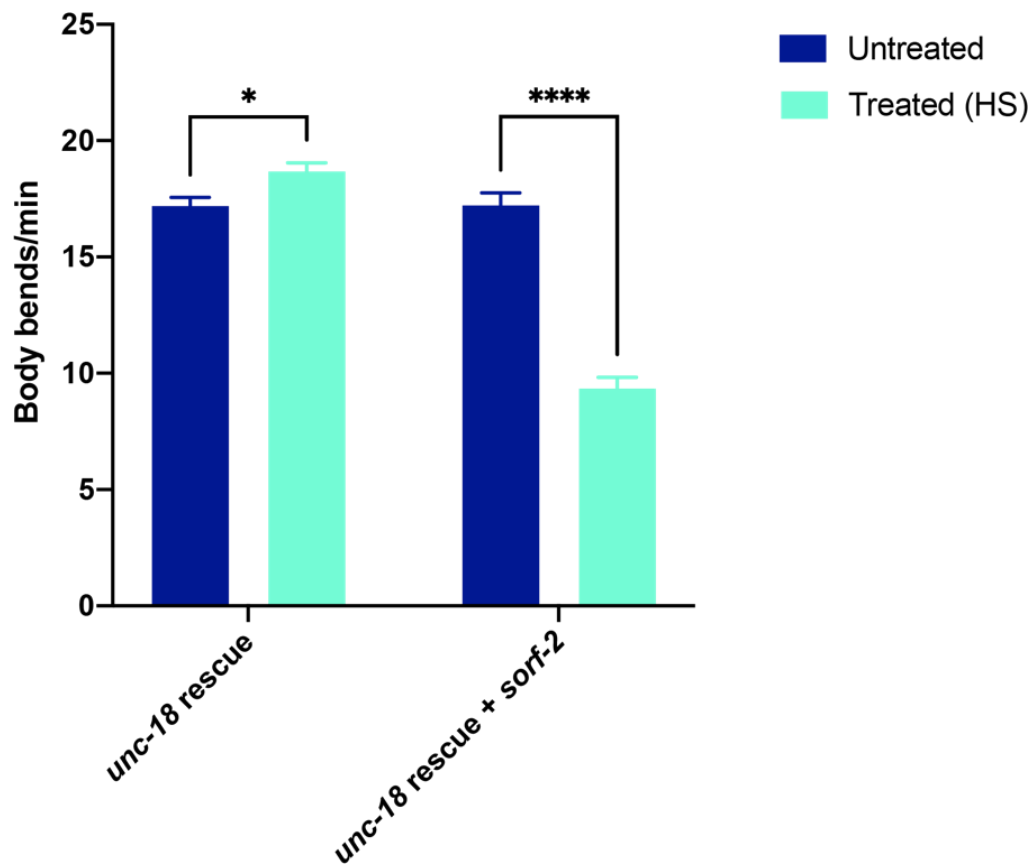
Figure 4.6. Expression of wild-type *sorf-2* in *unc-18* rescue mutants significantly reduces the locomotion of *unc-18* rescue + *sorf-2* mutants. A total of 10 worms were analysed in each experiment with a total of 3 independent experiments (n=30 worms per strain). Data are shown as mean ± standard error of the mean. Statistical data analysis was performed using two-way ANOVA, followed by Tukey's multiple comparisons test. *p≤*0.05,* **** p≤0.0001.

Behavioural analysis thus far suggests that the hypersensitive phenotype of *unc-18* rescue mutants is owed to the *dgk-1 (ulv1)* mutation. Therefore, cholinergic release in *unc-18* rescue + *sorf-2* mutants following heat shock was also investigated to address the question of whether the expression of wild-type *sorf-2* reversed the improved acetylcholine release which is observed in *unc-18* rescue mutants. This would provide support for *sorf-2* function within the cholinergic pathway and would support the current findings that *sorf-2* is neuronal in nature. Heat-shock induced expression of wild-type *sorf-2* did not significantly alter aldicarb sensitivity in *unc-18* rescue or *unc-18* rescue + *sorf-2* mutants (p>0.05) (Figure 4.7A).

The expression of *sorf-2* was validated and quantified using RT-qPCR. Analysis showed that expression of *sorf-2* following heat shock was significantly higher in *unc-18* rescue + *sorf-2* mutants (0.71 vs. 2.03, p<0.01) (Figure 4.7B). Relative expression of *unc-18* and *dgk-1* were also analysed to see if *sorf-2* expression altered the mRNA expression of other genes. There was no significant change in *unc-18* relative expression following heat shock (0.59 vs 0.79, p>0.05), however, a significant increase was observed in *dgk-1* relative expression following heat shock (0.21 vs 1.40, p<0.01) (Figure 4.7B).
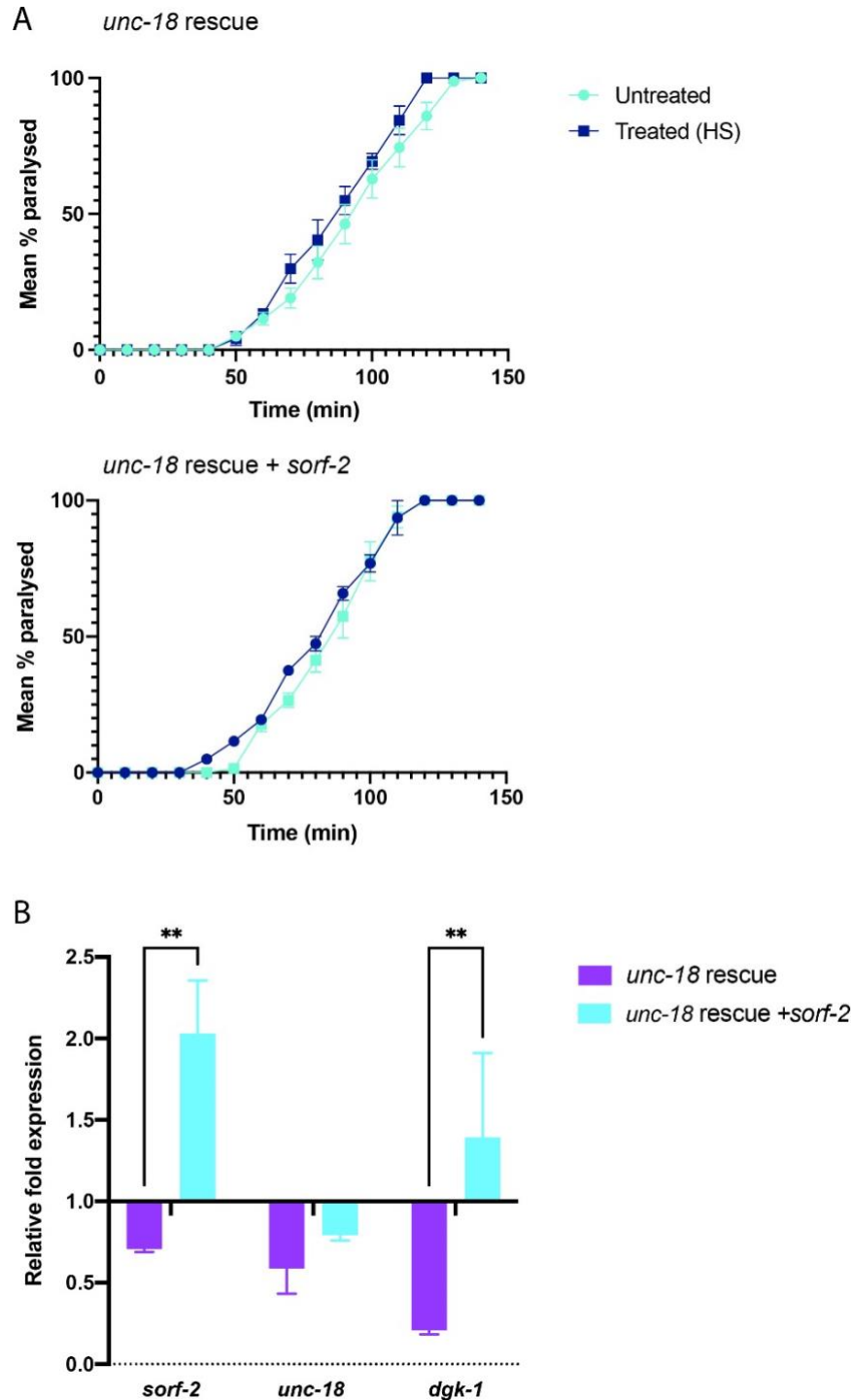
Figure 4.7. A) Aldicarb sensitivity of *unc-18* rescue + *sorf-2* mutants before and after heat shock. Wild-type expression of *sorf-2* did not significantly alter sensitivity to aldicarb in *unc-18* rescue or *unc-18* rescue + *sorf-2* mutants. B) Relative expression of *sorf-2, unc-18* and *dgk-1* in *unc-18* rescue and *unc-18* rescue + *sorf-2* after heat-shock, normalised to relative expression before heat-shock. For aldicarb assays, 25–50 worms were used in each experiment and a total of 3 independent experiments were conducted. For RT-qPCR analysis, n=3, except for *unc-18* rescue control mutants, which are n=2 for *sorf-2* and *dgk-1* analysis. Body bend data were analysed using one-way ANOVA, followed by Tukey's multiple comparisons test, and aldicarb data were analysed using a log-rank test for Kaplan Meier followed by the Bonferroni corrections test. **p$\leq$0.001.

4.2.6 *sorf-2* RNAi and R59949 together rescue locomotion defects in *unc-18 (e81)* null mutants

Following the evidence that the *dgk-1 (ulv1)* and *sorf-2 (ulv2)* mutations are involved in the rescue phenotype, we wanted to investigate the possibility of reproducing the rescue phenotype through alternative methods. To mimic the *dgk-1 (ulv1)* mutation, DGK inhibitor, R59949 was used as previous experiments have demonstrated the success of the inhibitor in producing behavioural effects similar to those of *dgk-1* mutants (Figure 3.5) (226). Despite not accurately reproducing the effects of *dgk-1 (ulv1)* mutation, PMA was also investigated in this study to support the hypothesis that DAG is increased as a result of mutant *dgk-1 (ulv1).* Results from this study so far demonstrate that wild-type expression of *sorf-2* in *unc-18* rescue mutants reduces locomotion (Figure 4.6), suggesting that the *ulv2* mutation within *sorf-2* results in *loss-of-function.* Thus, *sorf-2* RNAi was selected as the method to mimic the *sorf-2 (ulv2)* mutation. To recreate the effect of the *dgk-1 (ulv1)* and *sorf-2 (ulv2)* mutation, *unc-18 (e81)* null mutants were subjected to *sorf-2* RNAi and then treated with R59949 or PMA, as previously described.

In contrast to what we have previously observed with *unc-18 (e81)* null mutants (Figure 3.4, Figure 3.6), R59949 and PMA treatment alone produced a slight increase in body bends in these mutants to 0.47 and 0.67 body bends per minute, respectively. However, this difference was not significant (p>0.05). The usual feeding *E. coli* OP50 was replaced with an empty feeding RNAi vector (L4440) which may have affected the outcomes of R59949 and PMA treatment. *sorf-2* RNAi and treatment with R59949 significantly increased body bends in *unc-18 (e81)* null mutants from 0.13 body bends per minute to 3.00 body bends per minute (p<0.0001). A significant increase in locomotion to 3.53 body bends per minute was

also observed with *sorf-2* RNAi and PMA treatment (p<0.0001). There was no significant difference between PMA and R59949 treatment for either control (empty vector – L4440) or *sorf-2* RNAi treated worms (Figure 4.8A). The success of *sorf-2* RNAi was validated and quantified using RT-qPCR which found *sorf-2* relative expression to be 0.52 in *unc-18 (e81)* null worms following RNAi (Figure 4.8B). These findings not only confirm the necessity of *dgk-1 (ulv1)* and *sorf-2 (ulv2)* for the *unc-18* rescue phenotype, but they also suggest that this phenotype results, at least in part, from a reduced function of *sorf-2* and an increase in DAG.
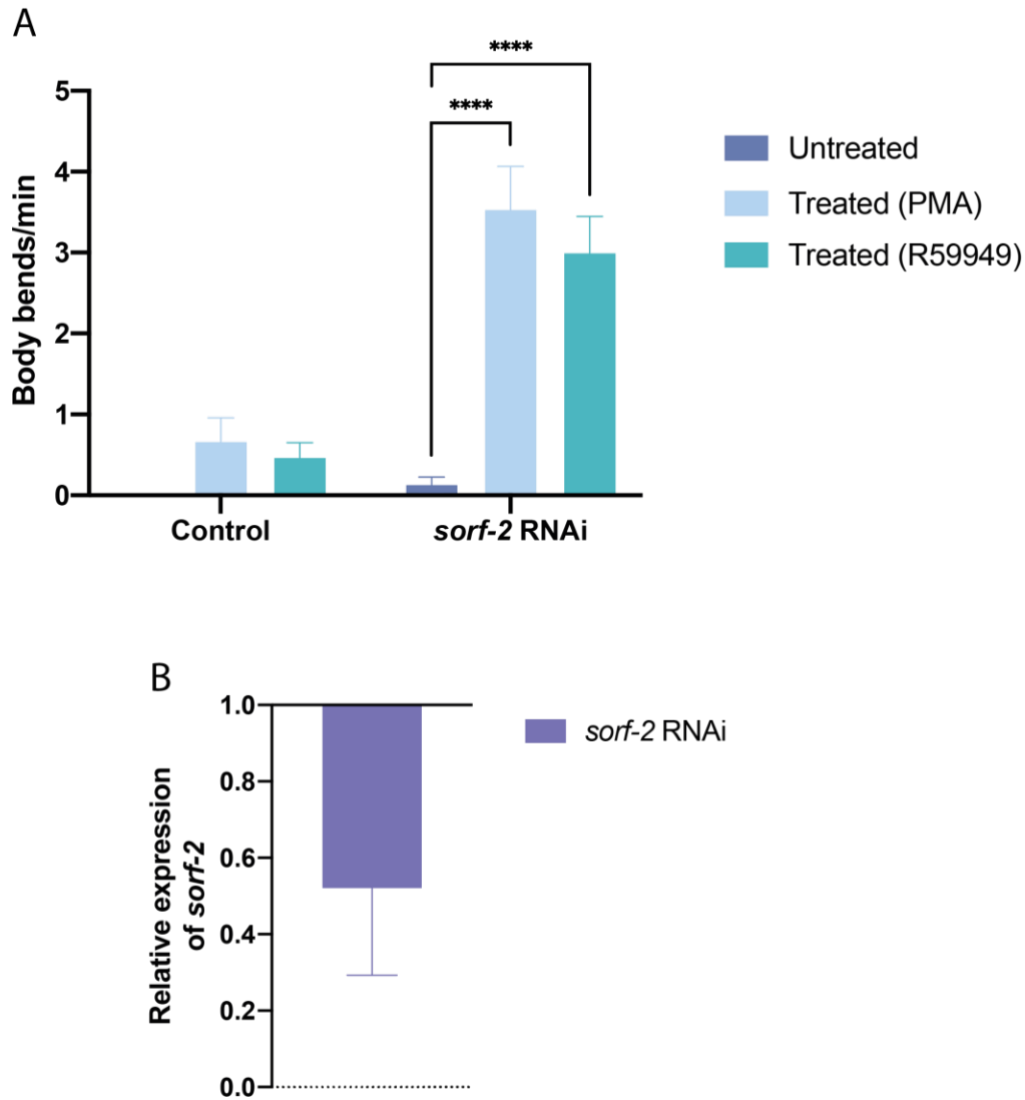
Figure 4.8. A) Locomotion of *unc-18 (e81)* null mutants subjected to *sorf-2* RNAi or L4440 empty vector RNAi (control), and treatment with either PMA or R59949. A total of 10 worms were analysed in each experiment with a total of 3 independent experiments (n=30 worms per strain). Data are shown as mean ± standard error of the mean. Statistical data analysis was performed using one-way ANOVA, followed by Tukey's multiple comparisons test. B) Quantitative PCR for *sorf-2* following *sorf-2* RNAi in *unc-18 (e81)* null mutants. Relative expression of *sorf-2* was measured to be 0.52 in *unc-18 (e81)* null mutants following *sorf-2* RNAi, relative to *sorf-2* relative expression in *unc-18 (e81)* null mutant controls. ****$p \leq 0.0001$

Previously, this study demonstrated that *unc-18* rescue mutants are hypersensitive to aldicarb (HIC) in comparison to *unc-18 (e81)* null mutants which are characteristically resistant to aldicarb (RIC) (Figure 3.4). Thus, it was important to assess aldicarb sensitivity to determine whether *unc-18 (e81)* null mutants subjected to *sorf-2* RNAi and pharmacological treatment with either PMA or R59949 produce improvements in cholinergic release consistent with those in *unc-18* rescue mutants. *sorf-2* RNAi alone did not significantly change aldicarb sensitivity in *unc-18 (e81)* null mutants ($p > 0.05$). PMA treatment and *sorf-2* RNAi together significantly increased aldicarb resistance in these mutants ($p < 0.0001$). An opposite effect was observed in mutants treated with R59949 following *sorf-2* RNAi, although aldicarb sensitivity was not significantly altered ($p > 0.05$) (Figure 4.9). It is evident that PMA and R59949 increase aldicarb sensitivity, consistent with findings that DAG produces a HIC phenotype in *unc-18 (e81)* null mutants (Figure 3.4, Figure 3.6). The observation that *sorf-2* had no effect on aldicarb, supports the notion that *sorf-2* may function to restore the neuromuscular response following successful neurotransmitter release.
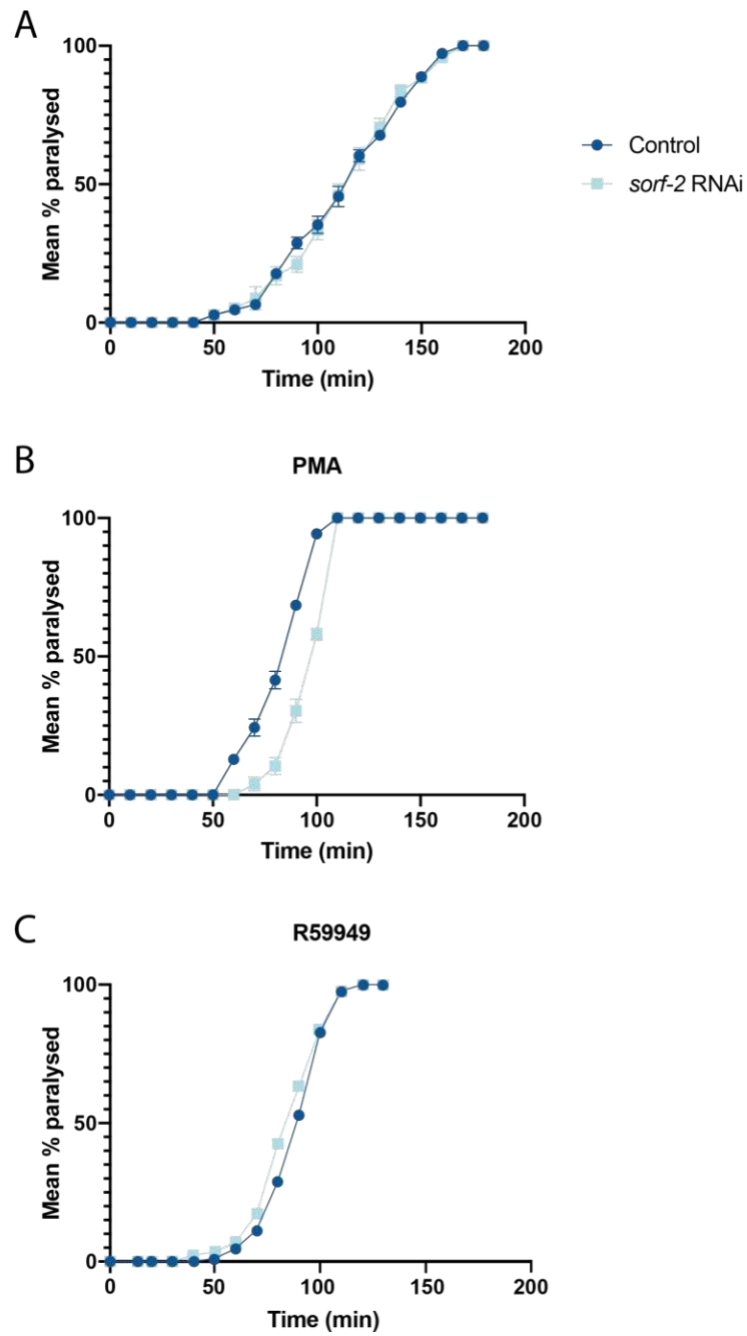
Figure 4.9 A–C) Aldicarb sensitivity of *unc-18 (e81)* null mutants following *sorf-2* RNAi or L4440 empty vector RNAi (control) with and without pharmacological treatment with R59949 or PMA. 25–50 worms were analysed in each experiment, with a total of 3 independent experiments. Data are displayed as mean ± standard error of the mean. Data were analysed using a log-rank test for Kaplan-Meier followed by Bonferroni corrections test.

Next, this study wanted to investigate more directly the effects of *sorf-2* RNAi and pharmacological treatment on the neuronal activity of *unc-18 (e81)* null mutants. Thus, EPG recordings were made to assess whether *sorf-2* RNAi and treatment with either PMA or R59949 could improve pharyngeal pumping as was observed in *unc-18* rescue mutants.

The mean frequency of pumping in *unc-18 (e81)* null mutants following RNAi treatment with an empty RNAi feeding vector (control) was 2.42 Hz, consistent with previous results of EPG recordings in *unc-18 (e81)* null worms (Figure 3.3). In *unc-18 (e81)* null mutants following *sorf-2* RNAi alone, the mean frequency of pumping was 2.78 Hz, which was not significantly higher compared to control worms ($p > 0.05$). In comparison to worms that were not treated with any pharmacological drug, R59949 treatment significantly improved the mean frequency of pumping in both the control group and *sorf-2* RNAi group to 3.89 Hz and 3.69, respectively, ($p < 0.0001$). However, there was no significant difference in mean frequency of pumping between the two groups following R59949 treatment ($p > 0.05$). Next, the effects of PMA were investigated to explore whether increasing DAG could produce changes in pharyngeal pumping in line with R59949-mediated *dgk-1* inhibition. Unlike R59949, PMA alone did not significantly alter the mean frequency of pumping in *unc-18 (e81)* null mutants (2.27 Hz) compared to untreated control mutants ($p > 0.05$). *sorf-2* RNAi and PMA-treated worms did not significantly differ from those in the control group treated with PMA alone (2.32 Hz, $p > 0.05$) (Figure 4.10A). Interestingly, these findings are not consistent with investigations of locomotion, which found that PMA and R59949 alone increased locomotion, which was then significantly increased by the addition of *sorf-2* RNAi to both PMA and R59949 treatment (Figure 4.8).

No significant differences were found in IPI duration SD within groups following *sorf-2* RNAi treatment. In untreated control *unc-18 (e81)* null mutants, the mean IPI duration SD was 177.32 ms, which then reduced to 104.29 ms following *sorf-2* RNAi. In the R59949 group, the mean IPI duration SD reduced from 64.97 ms to 38.99 ms following *sorf-2* RNAi. Interestingly, in the PMA-treated group, *sorf-2* RNAi resulted in an increase in mean IPI duration SD from 164.00 ms to 240.87 ms (Figure 4.10B). In these mutants, a significant increase in mean pump duration was observed following *sorf-2* RNAi from 111.82 ms to 159.79 ms ($p < 0.01$). There were no significant differences observed within other groups. Mean pump duration of *unc-18 (e81)* null mutants slightly decreased from 150.33 ms to 136.31 ms following *sorf-2* RNAi ($p > 0.05$). In R59949 treated worms, the mean pump duration slightly increased from 108.01 ms to 119.91 ms following *sorf-2* RNAi ($p > 0.05$) (Figure 4.10C). The mean pump duration coefficient of variation significantly decreased from 10.78% to 6.02% when *unc-18 (e81)* null mutants were subjected to *sorf-2* RNAi ($p < 0.05$). There were no significant differences observed within other treatment groups. In R59949 treated worms, *sorf-2* RNAi resulted in a slight decrease in the mean pump duration coefficient of variation from 7.99% to 4.38%; while in PMA-treated worms, a slight increase was observed from 11.20% to 14.82% ($p > 0.05$) (Figure 4.10D).
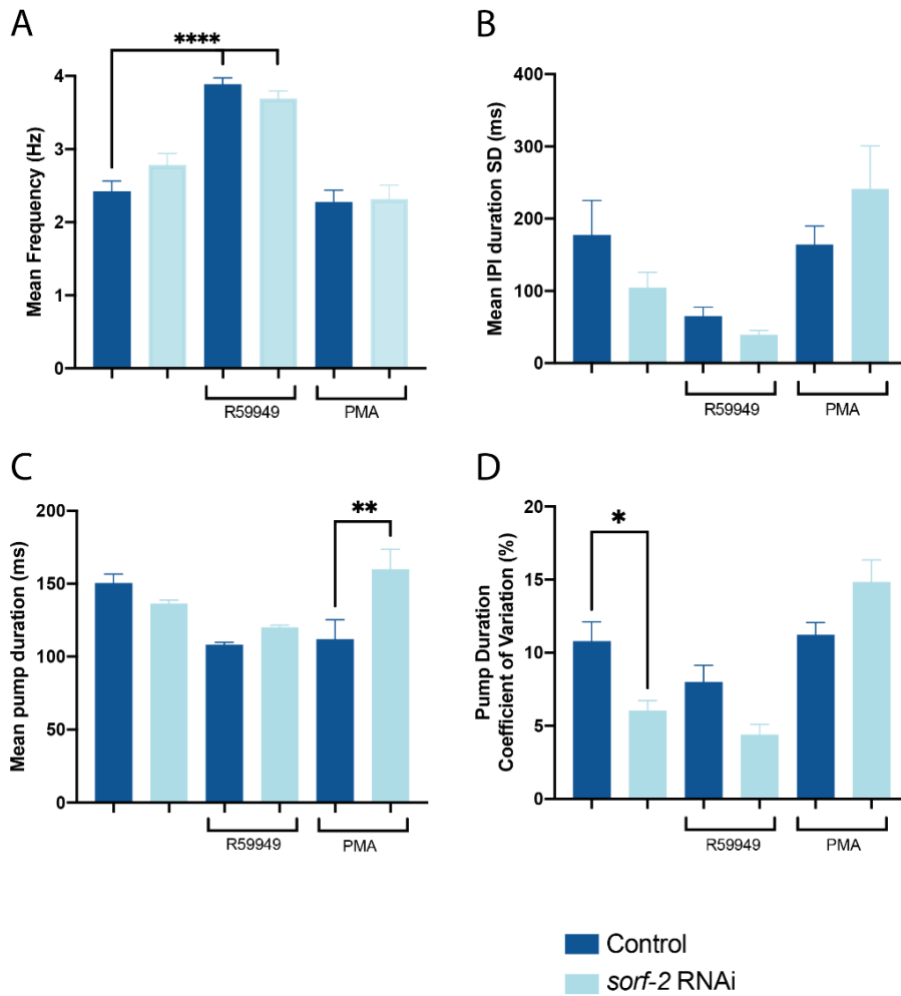
Figure 4.10. EPG recordings of *unc-18 (e81)* null mutants treated with *sorf-2* RNAi and either R59949 or PMA. A) *sorf-2* RNAi did not significantly alter mean pumping frequency in the untreated, R59949, or PMA treatment groups. B) *sorf-2* RNAi did not significantly alter mean inter-pump interval duration standard deviation (IPI duration SD) in any of the three treatment groups. C) *sorf-2* RNAi produced a significant increase in mean pump duration in the PMA treated groups, but not in the untreated and R59949 treated groups. D) *sorf-2* RNAi resulted in a significant decrease in the mean pump duration coefficient of variation of untreated *unc-18 (e81)* null worms. Fifteen animals per strain were analysed and data is shown as mean ± standard error of the mean. Statistical analysis was performed using a one-way ANOVA, followed by Tukey's multiple comparisons test. *p≤0.05, **p≤0.01, ****p≤0.0001.

4.2.7 The *unc-18* rescue phenotype may be specific to the *unc-18 (e81)* mutation

Following the evidence that *sorf-2* RNAi together with R59949 treatment

successfully improved locomotion in *unc-18 (e81)* null mutants, we wanted to

address the question of whether locomotion defects of other *unc-18* null mutants

could also be rescued through the same mechanism. This would provide strong

evidence towards a novel pathway through which *unc-18* function may be

completely bypassed. To investigate this, two additional *unc- 18* null mutants were

used: *unc-18* true deletion (containing a full reading frame deletion) (a kind gift from

Chris Hopkins, InVivo Biosystems) and *unc-18 ulv12* null (containing a 7 bp

deletion) (306).

sorf-2 RNAi and R59949 treatment failed to improve locomotion in *unc-18* true

deletion and *unc-18 ulv12* null mutants, as both strains remained immobile during the

assay time ($p > 0.05$) (Figure 4.11A). It was hypothesised that the lack of

improvement in locomotion may be due to insufficient knockdown of *sorf-2* following

RNAi, as previous evidence has shown that *sorf-2* RNAi resulted in approximately a

50% reduction in relative expression (Figure 4.8B). Therefore, to enhance the effects

of RNAi, double mutants for each *unc-18* null strain were made by genetic crossing

with *rrf-3* male mutants and selecting paralysed F2 progeny of a heterozygote F1

mutant. *rrf-3* + *unc-18* null double mutants were then subjected to *sorf-2* RNAi before

being treated with R59949, as previously described.

R59949 treatment alone significantly increased body bends of *rrf-3* control mutants

from 17.31 body bends per minute to 22.22 body bends per minute ($p < 0.0001$),

validating previous evidence from this study that *dgk-1* inhibition increases

locomotion (Figure 3.6), as well as findings from literature (224,321). *sorf-2* RNAi alone significantly increased *rrf-3* locomotion, yet to a lesser extent (19.96 body bends per minute, p<0.01), contrasting with previous findings in this investigation which found that *sorf-2 loss-of-function* in *sorf-2* heterozygous null mutants results in reduced locomotion (Figure 4.3A, 4.3B). *sorf-2* RNAi and treatment with R59949 together resulted in the largest improvement in body bends (24.52 body bends per minute, p<0.0001). This improvement was also significant compared with either R59949 treatment or *sorf-2* RNAi alone (p<0.01 and p<0.0001, respectively). There was no improvement in locomotion observed in any of the *unc-18* null mutants for any of the conditions investigated (Figure 4.12A), suggesting that the *unc-18* rescue phenotype may be specific to the *e81* mutation.

To assess the efficiency of *sorf-2* RNAi and *dgk-1* inhibition following R59949 treatment, RT-qPCR was performed to quantify the relative expression of *sorf-2* and *dgk-1*. Results found a significant decrease in relative *sorf-2* expression in all mutants investigated, with the most significant reduction surprisingly observed in *unc-18* true deletion and *unc-18 ulv12* null mutants (0.17 and 0.34, respectively; p<0.0001). Relative expression of *sorf-2* was similar between *rrf-3 + unc-18* true deletion (0.40) and *rrf-3 + unc-18 ulv12* null mutants (0.46, p<0.001). The least significant reduction in *sorf-2* relative expression was observed in *rrf-3* mutants (0.56, p<0.01).

Relative expression of *dgk-1* did not significantly change in *rrf-3* mutants following *sorf-2* RNAi (1.06, p>0.05) or *rrf-3 + unc-18 ulv12* null mutants (2.04, p>0.05). However, the relative expression of *dgk-1* in *rrf-3 + unc-18* true deletion worms was significantly different following *sorf-2* RNAi (3.39, p<0.05). *sorf-2* RNAi in *unc-18* true

deletion worms and *unc-18 ulv12* null mutants did not significantly alter *dgk-1* relative expression compared to untreated worms (0.55 and 0.47, respectively, p>0.05). Relative expression of *unc-18* was 0.83 in *rrf-3* mutants, 1.64 in *rrf-3 + unc-18* true deletion mutants, 0.96 in *rrf-3 + unc-18 ulv12* null worms, 2.00 in *unc-18* true deletion mutants and 0.94 in *unc-18 ulv12* null mutants. There was no significant change in *unc-18* relative expression in any of the mutants compared to untreated mutants.
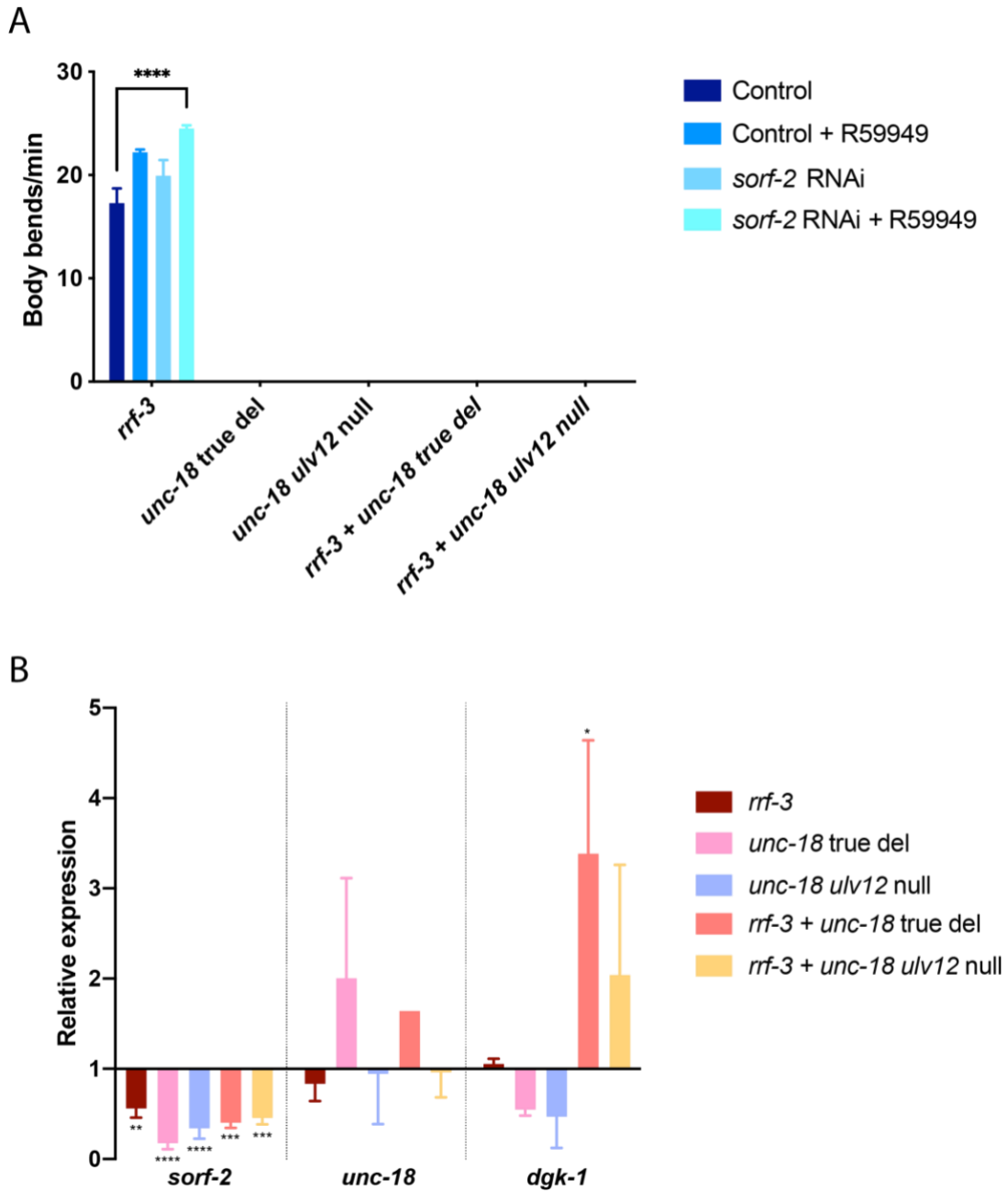
Figure 4.11. A) Locomotion rate of *unc-18* mutants following *sorf-2* RNAi and R59949 treatment. B) Quantitative real-time PCR analysis showing relative expression of *sorf-2, unc-18* and *dgk-1* in *unc-18* mutants following *sorf-2* RNAi and R59949 treatment. Data are displayed as mean values ± standard error of the mean, n=3. Data were analysed using two-way ANOVA, followed by Tukey's multiple comparisons test. *p≤0.05, **p≤0.01, ***p≤0.001, ****p≤0.0001.

4.2.8 Identification of a second *sorf-2* mutation, *ulv3,* which is necessary for the *unc-18* rescue phenotype

The results so far show that *sorf-2* RNAi in addition to either PMA or R59949 treatment, significantly improves locomotion in *unc-18 (e81)* null mutants, while failing to produce a significant effect in other *unc-18* null mutants (*unc-18* true deletion and *unc-18 ulv12* mutants). These findings suggest that the *unc-18* rescue phenotype may be strain specific. To further investigate this, the whole genome SoLiD sequencing results of *unc-18 (e81)* null and *unc-18* rescue mutants were re-analysed, finding the presence of a second mutation (*ulv3*) in *sorf-2* which resides in *unc-18 (e81)* null, *unc-18* rescue, and *dgk-1 + sorf-2* mutants. The *ulv3* mutation is an N-terminal missense mutation (D>N):III: 5328539G>A, located within the BEACH domain. The identification of this mutation suggests that it produces effects which were unable to be reproduced in additional *unc-18* null mutants using *sorf-2* RNAi. To investigate whether the *sorf-2 (ulv3)* mutation is required for the *unc-18* rescue phenotype, *unc-18 (e81)* null mutants were genetically crossed with WT worms to isolate the *unc-18 (e81)* mutation from the *sorf-2 (ulv3)* mutation (courtesy of Dr Jeff Barclay) and will be referred to as *unc-18 (e81)* null - *ulv3* mutants from this point forward. *unc-18 (e81)* null and *unc-18 (e81)* null - *ulv3* mutants were treated with R59949 following *sorf-2* RNAi to assess whether the improvement in locomotion, as has been seen previously (Figure 4.8A), could be produced in the absence of the *sorf-2 (ulv3)* mutation. Results found that *sorf-2* RNAi and R59949 did not produce a change in locomotion in *unc-18 (e81)* null - *ulv3* mutants, however, locomotion in *unc-18 (e81)* null mutants, which contains the *ulv3* mutation, successfully improved to 2.6 body bends per minute (p<0.0001) (Figure 4.12, consistent with previous findings (Figure 4.8A). Although this increase in locomotion is still one fifth of the locomotion rate of *unc-18* rescue mutants (12.6

body bends per minute; Figure 3.1), this finding supports a role of the *sorf-2 (ulv3)* mutation in the *unc-18* rescue phenotype and suggests that the mutation produces effects which then facilitate the improvement of locomotion in *unc-18* rescue mutants.
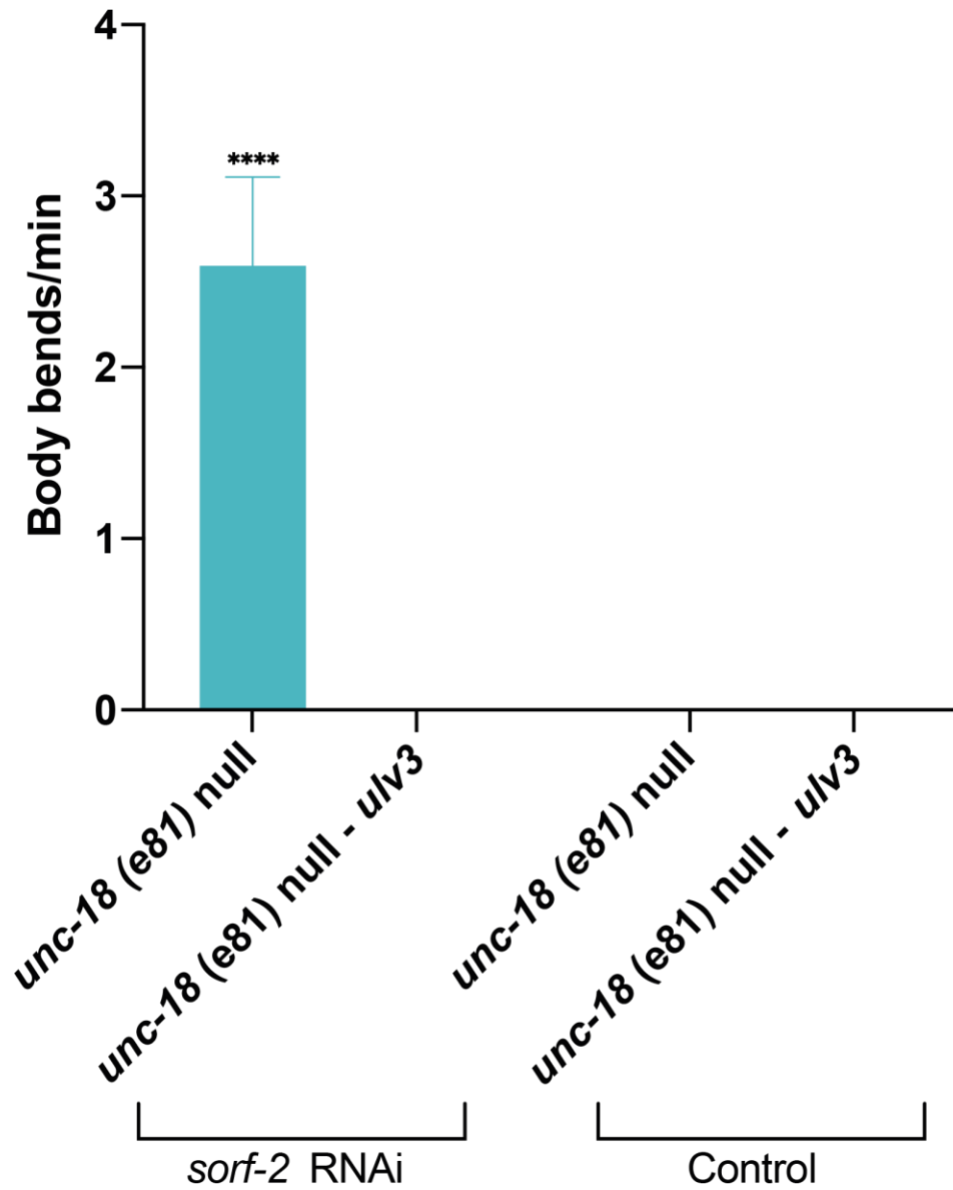
Figure 4.12. Locomotion of *unc-18 (e81)* null and *unc-18 (e81)* null - *ulv3* mutants following *sorf-2* RNAi and R59949 treatment. *sorf-2* RNAi and R59949 significantly improved locomotion in *unc-18 (e81)* null mutants but did not alter the locomotion of *unc-18 (e81)* null - *ulv3* worms. A total of 10 worms were analysed in each experiment with 3 independent experiments (n=30 worms per strain). Data are shown as mean ± standard error of the mean. Statistical data analysis was performed using a two-way analysis of variance, followed by Tukey's multiple comparisons test. ****p≤0.0001.

4.3 Discussion

The current study aimed to validate a role of *sorf-2* in the *unc-18* rescue phenotype. We then aimed to investigate the effects of the *sorf-2 ulv2* and *ulv3* mutations in order to understand better the function of *sorf-2* within neurotransmission. The current findings support the hypothesis that the *dgk-1 (ulv1), sorf-2 (ulv2) and sorf-2 (ulv3)* mutations are necessary for the *unc-18* rescue phenotype. This investigation also identified possible *unc-18 (e81)* specificity for the observed *unc-18* rescue phenotype, owing to the *sorf-2 (ulv3)* mutation which resides in both the *unc-18 (e81)* null and *unc-18* rescue mutants.

Isolation of the *dgk-1 (ulv1)*, and *sorf-2 (ulv2 and ulv3)* mutations in *dgk-1 + sorf-2* mutants confirmed that the three mutations together are viable; the latter of which was identified in later experiments. Attempts to isolate the *dgk-1 (ulv1)* and *sorf-2 (ulv2)* mutations individually, however, were unsuccessful (Figure 4.5), suggesting a synergistic association of the two mutations. The potential lethality of the *dgk-1 (ulv1)* or the *sorf-2 (ulv2* and *ulv3)* mutations cannot, therefore, be ruled out. Current evidence of other existing *dgk-1* mutants suggests that *dgk-1 loss-of-function* is not lethal, but results in hyperactive locomotion and hyperactive egg-laying behaviour (224,321). In mice, ablation of the *dgk-1* homologue, DGKθ, impaired recycling kinetics of synaptic vesicles, despite the mice showing no phenotypic defects (371). In this investigation, the *dgk-1 (ulv1)* nonsense mutation resides within the kinase domain of *dgk-1*, with phenotypic effects which may be distinct from other null mutations that have previously been investigated. On the other hand, lethality of *sorf-*

2 *loss-of-function* following a 1189 base pair deletion has previously been confirmed (271), supporting the possibility that the *ulv2* and *ulv3* mutations in *sorf-2* may be lethal. Detrimental effects of mutations in the *sorf-2* homologue, WDR81, have also been described. WDR81 mutations in patients with microcephaly implicate the gene in normal cell proliferation. Similarly, in *Drosophila*, downregulation of the *sorf-2* homologue, CG6734, resulted in an increased mitotic index in neuroblasts from the central brain (372). Together, the current data suggest a vital role of *sorf-2* in neuronal processes, increasing the likelihood that the *ulv2* and *ulv3* mutations alone may result in lethality.

The necessity of *sorf-2* for the *unc-18* rescue phenotype was confirmed following evidence that wild-type expression of *sorf-2* reduced the locomotion of *unc-18* rescue worms (Figure 4.6). Firstly, this experiment was limited due to lack of a WT control in which WT *sorf-2* was also expressed, allowing identification of any effects of the plasmid. In addition, as both overexpression and underexpression of *sorf-2* in wild-type worms were found to reduce locomotion, this study does not provide a clear-cut answer about whether the mutations within *sorf-2* result in a *loss of-* or *gain-of* function in *unc-18* rescue mutants. Furthermore, locomotion defects in *unc-18* rescue + *sorf-2* mutants were not as severe as those in *unc-18 (e81)* null mutants. Expression of the phsp16.48 promoter, which was utilised in this study, has been identified in all stages of the worm lifecycle from embryo to adult, with expression found in all cell types such as in neurons, intestine, muscles, and hypodermis (373). It is possible that the reduction in locomotion observed in these mutants is not at the same levels as *unc-18 (e81)* null mutants due to the levels of *sorf-2* expression following heat-shock, as demonstrated by the low increase in relative expression (Figure 4.6), however, the general expression profile of

phsp16.48 promoter may also be a contributing factor. Wild-type expression of *sorf-2* in *unc-18* rescue mutants through a neuronal promoter, such as *rab3* would provide a more accurate representation of the neuronal *sorf-2* function. Nevertheless, the difference in locomotion of *unc-18* rescue + *sorf-2* and *unc-18 (e81)* null mutants supports the idea that the mutations within *sorf-2* do not solely produce a *loss-of-function.*

This study was limited by the fact that the initial chosen concentration of the phsp16.48::*sorf-2* plasmid for *C. elegans* injection (20 ng/μl) was deemed to be toxic to the worms, producing no viable offspring. The concentration was incrementally reduced until a final injection concentration of 5 ng/μl was selected and found to be successful in producing viable offspring. Reducing the injection concentration may have reduced the level of expression of wild-type *sorf-2* following heat shock. If higher injection concentrations were viable, it is possible that there would be a higher level of *sorf-2* expression and thus, a larger reduction in locomotion following its expression. With this in mind, wild- type expression of *sorf-2* in *unc-18* rescue mutants essentially results in an *unc-18 (e81)* and *dgk-1 (ulv1)* double mutant. As found previously, increasing levels of DAG in *unc-18 (e81)* null mutants, such as those with *gain-of-function egl-30 (js126)* expression (*unc-18* (*e81*) null + DAG mutants), produce slow-growing and unhealthy worms. This would explain why the isolation of *unc-18* (*e81*) and *dgk-1* (*ulv1*) was not viable and necessitated the use of a heat-shock promoter. Additionally, this could explain why higher levels of transgenic expression of WT *sorf-2* was not observed in *unc-18* rescue + *sorf-2* worms.

Next, recreation of the *unc-18* rescue phenotype was attempted using alternative methods which replicate the effects of the *sorf-2 (ulv2)* and *dgk-1 (ulv1)* mutations.

sorf-2 RNAi paired with either pharmacological inhibition of *dgk-1* (R59949), or increased DAG (PMA), significantly improved locomotion in *unc-18 (e81)* null mutants. This investigation was pivotal for confirming that the *unc-18* rescue phenotype requires both mutant forms of *dgk-1* and *sorf-2*. However, the improvement in locomotion did not reach the level observed in *unc-18* rescue mutants (Figure 3.1; Figure 4.8A). Initially, it was thought that extent of *sorf-2* RNAi knockdown was not efficacious, however, RT- qPCR analysis found that *sorf-2* RNAi in *unc-18 (e81)* null mutants resulted in lower levels of *sorf-2* relative expression compared to that of *unc-18* rescue mutants (Figure 4.8B). Reduced expression does not necessarily indicate *loss-of-function*, and so it cannot be said whether *sorf-2* RNAi alters *sorf-2* expression to the same extent as the *sorf-2* mutations in *unc-18* rescue mutants. *sorf-2* RNAi addresses the hypothesis that there is a *sorf-2 loss-of-function* in *unc-18* rescue mutants. As *sorf-2* RNAi with R59949/PMA failed to improve locomotion in *unc-18 (e81)* null mutants lacking the *sorf-2 (ulv3)* mutation, it was hypothesised that the *ulv2* mutation produces a *loss-of-function*, while the *ulv3* mutation produces a *change-of* or *gain- of-function*. These findings suggest that the use of *sorf-2* RNAi replicates the effects *sorf-2 (ulv2)* mutation but negates the opposing effects of the *ulv3* mutation.

Interestingly, observations of locomotion following R59949 or PMA treatment were not consistent with EPG recordings. In the latter, R59949 and PMA treatment alone were sufficient to rescue the frequency of pharyngeal pumping (Figure 4.10A), however when measuring locomotion, R59949 or PMA treatment has little to no effect (Figure 4.8A). The effect of R59949/PMA on locomotion is consistent with observations in *unc-18 (e81)* null + DAG worms which are hypersensitive to aldicarb despite remaining completely immobile (Figure 3.2). It is evident that R59949 and

154

PMA are sufficient to increase cholinergic release and potentiate muscular activity within the pharynx of *unc-18 (e81)* null mutants, but not in the body of worm. To support this notion, extrapharyngeal activity of other *unc-18* null and *unc-18 (e81)* null – *ulv 3* mutants following R59949 or PMA treatment should also be investigated. This was attempted, with the hypothesis that R59949 and PMA alone would improve pharyngeal pumping and cholinergic release in these mutants, as was observed in *unc-18 (e81)* null mutants. However, the number of EPG recordings that passed the quality control measures was not sufficient for analysis.

Previous literature has found that abolishing pharyngeal neurons does not completely inhibit pharyngeal pumping, while the abolishment of cholinergic synaptic transmission does (375), highlighting the importance of the cholinergic pathway for pharyngeal pumping. In this investigation, locomotion on a surface, specifically, is only improved following the addition of the *sorf-2 ulv2* and *ulv3* mutations, or *sorf-2* RNAi. As *unc-18* rescue mutants still demonstrate defects in thrashing, *sorf-2* may function in the muscular response of locomotion following neurotransmission in distinct neuromuscular pathways. This idea is supported by evidence of quadrupedal locomotion in patients with mutated WDR81 (269). The alternating activation of cholinergic and GABAergic motorneurons controls the contraction and relaxation of muscles. Cholinergic neurons form dyadic synapses and innervate both muscles and GABAergic neurons projecting to the opposing side of the body (289,376). However, as the morphology of GABA motor neurons is normal in *unc-18 (e81)* null mutants (168), it would be assumed that rescue of cholinergic release in these mutants would be sufficient to see an improvement in locomotor behaviour. As this is not the case, a question remains about how *sorf-2* functions in the *unc-18* rescue phenotype.

The results of this study confirm that both *dgk-1* and *sorf-2* are involved in the *unc-18* rescue phenotype and implicate the enigmatic *sorf-2* in the exocytic pathway. As discussed previously, *dgk-1* is a negative regulator of synaptic transmission (224), thus it is not surprising that its *loss-of-function* positively regulates synaptic transmission. While it is known that *dgk-1* resides in ventral cord motor neurons (224), the localisation of *sorf-2* is not fully elucidated. Available literature suggests that *sorf-2* is localised in NSM neurons which reside in the pharynx anterior bulb, with branches running within the dorsal nerve cord and the subventral nerve cord (377). In *C. elegans*, *sorf-2* expression has been observed in coelomocytes (271), and in mice, *Wdr81* mRNA expression has been identified within several tissues of the CNS, including the cerebellum, brain, and spinal cord. Additionally, WDR81 was detected in the cerebral cortex where it colocalised with the Purkinje cell marker, calbindin (270). The results of this study are in line with current literature, implicating *sorf-2* in neuronal processes (270,271,367,372).

Initially *sorf-2* was hypothesised to function in the cholinergic pathway. However, *sorf-2* RNAi in *unc-18 (e81)* null mutants, with or without the predicted effects of the *dgk-1 (ulv1)* mutation (*dgk-1* inhibition or elevated DAG) did not alter aldicarb sensitivity. These findings were inconsistent with a previous study which utilised a *dgk-1* suppressor screen, finding that *sorf-2* RNAi on a *dgk-1* mutant background produced resistance to aldicarb (374). It is possible that the lack of aldicarb effect is due to the *unc-18 (e81)* null mutant background, with several other mutations potentially impacting the outcome of *sorf-2* RNAi. For a more definite investigation of the effects of *sorf-2* RNAi on aldicarb sensitivity, it would be important to subject WT worms to *sorf-2* RNAi, with and without the presence of R59949 or PMA. However, overexpression of *sorf-2* (*sorf-2* OE mutants) and *loss-of-function* of *sorf-2* (*sorf-2*

heterozygous null mutants) also did not significantly alter aldicarb sensitivity (Figure 4.4). It is therefore hypothesised that *sorf-2* functions extend beyond the cholinergic pathway. Currently, *sorf-2* is implicated in the endocytic pathway (271), with little evidence about its role in the synaptic vesicle exocytic pathway. Nonetheless, synaptic transmission relies on careful coordination between the two processes (378). After exocytosis, synaptic vesicles must be recycled by endocytosis to allow maintenance of successful exocytosis (4). Lipids are vital for this process, particularly phosphoinositides which are minority phospholipids within cellular membranes (239). These lipids are implicated in the DAG pathway, as well as the pathway in which *sorf-2* functions. Phosphatidylinositol-4,5-bisphosphate (PI $(4,5)P_2$) is a substrate for the DAG-producing phospholipase C, and is also produced from PA that results from *dgk-1* mediated DAG phosphorylation. PI$(4,5)P_2$ regulates synaptic vesicle priming through binding to Munc13 and CAPS (238), while also regulating synaptic vesicle recycling through recruitment and activation of molecules such as synaptotagmin at the presynaptic membrane (238,378). On the other hand, limited evidence suggests that *sorf-2* regulates phosphatidylinositol 3-phosphate (PtdIns3P) levels, which is important for the fusion of early endosomes, as well as the sorting and recycling of lysosomes (271). Interestingly, in studies of yeast vacuole fusion, both PtdIns3P and PI$(4,5)P_2$ were found to enhance the capacity of membrane-bound SNAREs to drive fusion in the absence of SNARE chaperones (379). This provides a potential mechanism that may allow *dgk-1* and *sorf-2* to bypass *unc-18* function. Furthermore. PtdIns3P is implicated in the priming stage of exocytosis (379); a step in which Munc18-1/*unc-18* also functions. During this stage, Munc18-1 binds to closed-state syntaxin-1 and enables the conformational transition to open-state syntaxin-1, which then allows the formation of the SNARE complex (185,206,208). This transition is accelerated by Munc13-1 binding to the syntaxin-1

SNARE motif through its MUN domain (101). It can therefore be speculated that the *unc-18* rescue phenotype occurs through elevation of DAG, and *unc-13* activation, which then bypasses the function of *unc-18* in SNARE complex formation. With the knowledge of Munc18/*unc-18* and DAG in priming, there is reason to suggest a potential role of *sorf-2* in priming as well. Given what is known about *sorf-2*, it is likely that the mutations residing within *dgk-1* and *sorf-2* create distinct changes within the lipid pathways which may affect *unc-18* function at different stages of the exocytic vesicle cycle. Munc18-1/*unc-18* interactions with syntaxin and the SNARE complex are important for the docking and fusion of vesicles, however, its interactions with other accessory proteins such as Mint1, phospholipase D, and Rab3 remain under investigation (203). Future investigations may aim to investigate the impact of the *dgk-1 (ulv1)* and *sorf-2 (ulv2 and ulv3)* mutations on the activity of such accessory proteins.

We then aimed to investigate whether the same improvement in phenotype could be observed in other *unc-18* null mutants *sorf-2* RNAi and R59949 or PMA treatment (Figure 4.11). *sorf-2* RNAi and R59949/PMA treatment did not improve locomotion in *unc-18* true deletion and *unc-18 ulv12* null mutants, suggesting that the *unc-18* rescue phenotype may be specific to the *unc-18 (e81)* null mutation. Evidence that *sorf-2* RNAi and R59949 treatment failed to improve locomotion in *unc-18 (e81)* null mutants lacking the *ulv3* mutation (*unc-18 (e81)* null - *ulv3*) confirmed this hypothesis (Figure 4.12). *sorf-2* RNAi in *unc-18 (e81)* null mutants provided an insight into the possible role of the *sorf-2 (ulv2)* mutation in the *unc-18* rescue phenotype, however a *gain-of-function* was not investigated, leaving a question regarding the effects of the *ulv3* mutation.

One limitation of this study that should be addressed is the use of controls. Often, for body bend assays, different strains were analysed on different days. It is important that when drawing comparisons between two strains, the data is collected at the same time to ensure the control is accurate as possible. Additionally, for aldicarb experiments following drug treatments (PMA/R59949), the possible effects of the drug on aldicarb sensitivity were not addressed. This could have been mitigated through assessment of aldicarb sensitivity of untreated control worms alongside those treated with the drug (Figure 4.9). The limitation of controls is also evident in analysis of EPG recordings following drug treatment (Figure 4.10). In this investigation, the 'untreated' controls used were worms subjected to *sorf-2* RNAi or empty vector feeding, however an additional control which would improve analysis would be worms that have not been treated with a drug, and have only been fed the original OP50 food source. Moreover, the identified mutations within *dgk-1* and *sorf-2* were investigated as the most likely novel mutations within genes with a known function, or possible function in neurotransmission. The *unc-18 (e81)* null mutant however contains a plethora of other mutations which were deemed unlikely to be involved in the *unc-18* rescue phenotype. It is possible that the presence of these mutations may provide favourable circumstances which allow mutant *dgk-1* and *sorf-2* to produce the observed improvement in locomotion. One method to test this hypothesis would be to express the *sorf-2 (ulv3)* mutation in other *unc-18* null mutants and repeat *sorf-2* RNAi with R59949/PMA treatment. However, to categorically confirm that the *unc-18* rescue phenotype is produced by only the three genes investigated in this study, the best approach would be to isolate the *unc-18*, *dgk-1* and *sorf-2* mutations completely on a wild-type background, although based on current findings, this may be limited due to the viability of worms.

4.3.1 Summary

This investigation aimed to first explore the necessity of the *sorf-2 (ulv2)* mutation in the *unc-18* rescue phenotype, which was confirmed by a reduction in locomotion following transgenic expression of the wild-type *sorf-2*. Next, we aimed to determine the effects of the *sorf-2 (ulv2)* mutation, however, isolation of the *dgk-1 (ulv2)* and *unc-18 (e81)* mutations with wild-type *sorf-2* was not possible, suggesting potential lethality of the *dgk-1* and/or *sorf-2* mutations. A third aspect of this investigation aimed to recreate the effects of the *dgk-1 (ulv1)* and *sorf-2 (ulv2)* mutations through alternative methods – DGK inhibition and *sorf-2* RNAi, respectively. DGK inhibition and *sorf-2* RNAi together successfully improved locomotion in *unc-18 (e81)* null mutants, but not in other *unc-18* null mutants, resulting in the identification of a third *sorf-2* mutation – *ulv3*, required for the *unc-18* rescue phenotype. Together these findings confirm that *dgk-1* and *sorf-2* are required together for the *unc-18* rescue phenotype and suggests the involvement of lipid pathways. To establish whether this is the case, differences in lipid composition between *unc-18 (e81)* null mutants and *unc-18* rescue mutants should be investigated.

Chapter 5: 1H NMR discriminates between lipid and polar metabolites in C. elegans mutant strains

5.1 Introduction

Lipids are an abundant class of molecules found in all organisms with a diverse range of roles (381). Traditionally, the role of lipids in synaptic transmission has been believed to be passive (382). However, there is emerging evidence that lipids are essential for cellular processes, ranging from signalling and membrane composition to cell metabolism, energy storage, and protein anchoring (383). In the membrane, cholesterol and sphingolipids contribute to membrane fluidity and trafficking of membrane proteins through the creation of 'lipid rafts' (234). At the pre-synapse, lipids support protein interactions and function during the synaptic vesicle cycle (384,385). In addition to diacylglycerol (DAG) and phosphatidic acid (PA), which have been previously discussed, phosphatidylinositol 4,5-bisphosphate ($PI(4,5)P_2$) functions as a key regulator of vesicle trafficking and synaptic transmission through its phosphorylation and dephosphorylation (246). Furthermore, lipids such as arachidonic acid (ARA) and sphingosine facilitate exocytosis through direct interaction (257). Therefore, understanding lipid composition of mutant organisms can provide deeper insight into the functions of the molecular machinery at the synapse.

The results of this investigation thus far have confirmed a role of *dgk-1* and *sorf-2* in the *unc-18* rescue phenotype, with evidence to support a reduced function of *dgk-1.* As *dgk-1* phosphorylates DAG into PA, there is reason to hypothesise a role of these lipids in the restoration of locomotion. The involvement of *sorf-2* in the *unc-18* rescue phenotype also suggests an additional involvement of lipids, given its known function as a negative regulator of phosphatidylinositol 3-phosphate (PtdIns3P) in endosomal conversion (271). This investigation aimed to explore the lipid profiles of *unc-18* rescue mutants in comparison to *unc-18 (e81)* null and WT worms. This would allow

the identification of any changes within lipid metabolites and would provide further insight into the pathway involved in the *unc-18* rescue phenotype.

To date, several techniques exist to investigate lipid profiles of organisms and tissues. [1]H-Nuclear Magnetic Resonance (NMR) provides a time-efficient and highly reproducible method to investigate lipids within a range of samples (383). While chromatography-coupled mass spectrometry (MS) provides spectra with better molecular separation and sensitivity compared to NMR, it requires complex quality control procedures and samples are destroyed during analysis. MS, therefore, lacks reproducibility for lipid analysis, which often have variable levels of ionisation, and reduces the ability to run multiple analyses on the same sample. In addition to this, molecular identification is done more easily with NMR using either databases or self-consistent analyses of 1D and 2D spectra between ^{1}H and [13]C (386). For these reasons, ^{1}H-NMR was chosen as the most suitable method for the initial analysis of lipids in *unc-18 (e81)* null, *unc-18* rescue, and WT *C. elegans*. For accurate analysis of spectra, a robust working protocol, developed by Dr. Phelan at the University of Liverpool (387), was followed to maximise the quality and reproducibility of spectra. Here we used a two-stage extraction method in which the polar and nonpolar (lipid) metabolites were separated from each other. DAG is made up of two fatty acid chains covalently bonded to a glycerol molecule through ester linkages and would be expected to be identified within the lipid subset. However, PA, has a similar structure with the addition of a phosphate head group (388), the latter of which would be expected to be identified in the polar subset. Likewise, several other polar lipids are amphiphilic, containing hydrophobic tails and hydrophilic heads (389). Therefore, it was deemed important to analyse both the lipid and polar metabolite profiles of each strain.

5.2 Results

5.2.1 Strain specific differences were observed in lipid profiles of *unc-18 (e81)* null, *unc-18* rescue, and wild-type worms

Lipid spectral peaks were separated into 154 bins, of which 59 were unknown metabolites. Representative peaks for lipid metabolites were identified according to the latest annotation provided by Amiel et al. (2019) (390). The selected peaks represented 13 different lipids or lipid classes – fatty acids, unsaturated fatty acids (UFA), monounsaturated fatty acids (MUFA), polyunsaturated fatty acids (PUFA), free cholesterol, cholesterol ester, arachidonic acid (ARA), eicosapentaenoic acid (EPA), linoleic acid, docosahexaenoic acid (DHA), phosphatidylethanolamine (PE), phosphatidylcholine (PC), triglycerides (TG), and phospholipids (PL).

Differences in lipid profiles of each sample were analysed using a principal component analysis (PCA). A PCA is an unsupervised model which uses linear transformation to reduce the dimensions of the data. In doing so, a PCA explains the variance of the data using 'principal components' (PCs), where the first PC explains the majority of the data, and subsequent PCs explain the majority of the variance that could not explained by the prior PC, in a manner that is orthogonal to the prior PCs (311). A PCA, therefore, is a simplified tool to establish the major variances within the data. The PCA consolidated over 66.0% explained variance in the first two components (PC1, 50.8%; PC2, 16.1%), showing weak clustering of the three strains (Figure 5.1A). A total of 6 components were required to explain 95% of the variance. Across PC1, approximately half of the variance showed WT samples cluster separately to *unc-18 (e81)* null and *unc-18* rescue worms. Interestingly, WT worms demonstrated larger variance across PC1 compared to PC2, while both *unc-18 (e81)* null and *unc-18* rescue mutants showed larger variance across PC2 than PC1.
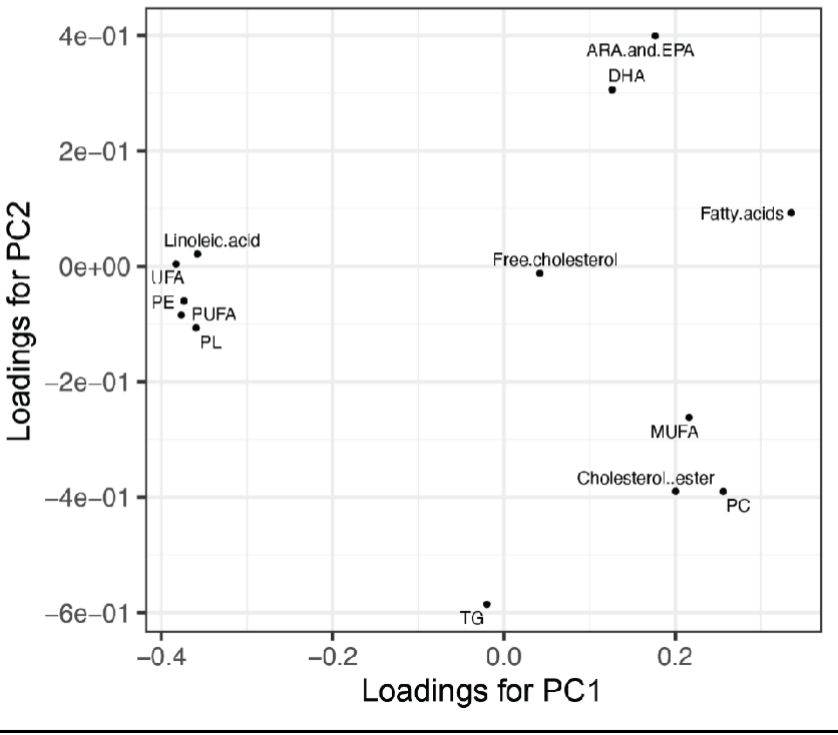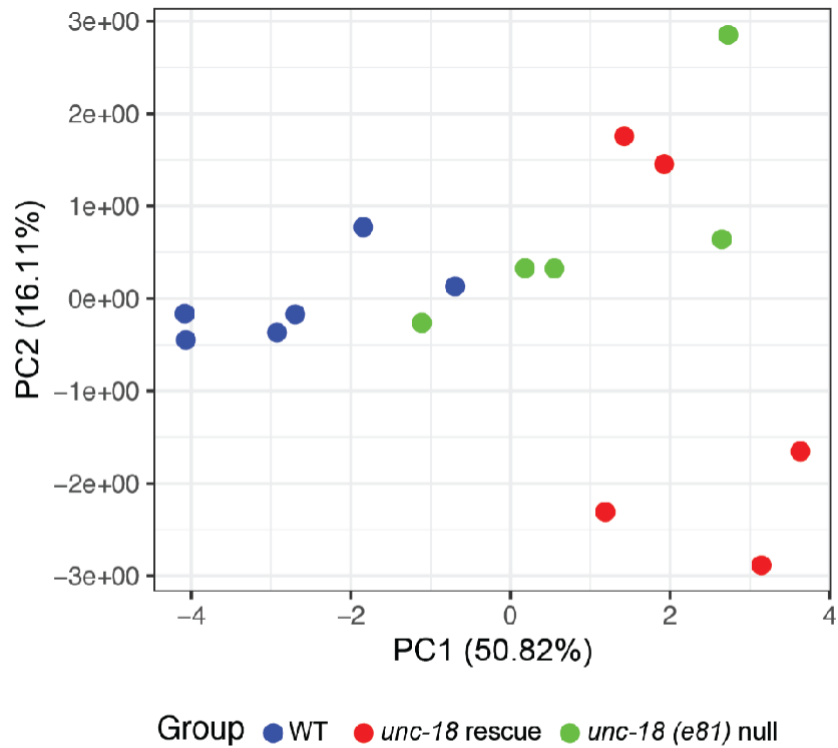
Figure 5.1. A) PCA scores of PC1 (50.82%) against PC2 (16.11%) from WT (n=6), *unc-18* rescue (n=5), and *unc-18 (e81)* null (n=5) samples. A total of 6 PCs were used to achieve 95% explained variance. B) PCA loadings plot of metabolites contributing to the variance across PC1 and PC2. ARA=arachidonic acid, DHA=docosahexaenoic acid, EPA-eicosapentaenoic acid, MUFA=monounsaturated fatty acids, PC=phosphatidylcholine, PE=phosphatidylethanolamine, PL=phospholipids, PUFA=polyunsaturated fatty acids, TG=triglycerides, UFA=unsaturated fatty acids.

When considering the overall metabolic profile of the samples, two of the five *unc-18* rescue samples separated from the remaining three *unc-18* rescue samples across PC2. This suggests that the biological variance between the samples across PC2 is higher for *unc-18* rescue mutants and raised the question of whether the two isolated samples should be classed as anomalous. While these samples are potential anomalies, it is also possible that this is the natural intrinsic variation within the strain. Due to the small sample number, the reason for variation cannot be confidently confirmed so the analysis was proceeded with all five *unc-18* rescue samples. The PCA loadings plot provides information about which metabolites contribute to variance observed using PC1 and PC2 (Figure 5.1B). Analysis of the loadings plot identified monounsaturated fatty acids, cholesterol ester, and phosphatidylcholine as the metabolites contributing to the variation of the three *unc-18* rescue samples which separated from the other two *unc-18* rescue mutant samples. The loadings plot also identified polyunsaturated fatty acids, unsaturated fatty acids, linoleic acid, phosphatidylethanolamine, and phospholipids as the metabolites explaining the major variation of WT from the two mutant strains.

To gain a metabolite level understanding of differences between the strains, metabolite levels were compared using fold-change analysis and visualised using heatmaps (Figure 5.2). Significant differences between metabolite levels were established using a one-way ANOVA with Tukey's multiple comparisons test. Of the 13 lipid groups, 7 were significantly different between the strains. In comparison with WT worms, *unc-18 (e81)* null mutants exhibited significantly lower abundance of polyunsaturated fatty acids ($p<0.05$), phosphatidylethanolamine ($p<0.001$), phospholipids ($p<0.001$), and unsaturated fatty acids ($p<0.05$). *unc-18* rescue mutants however demonstrated significantly lower abundance of linoleic acid

(p<0.05), polyunsaturated fatty acids (p<0.01), phosphatidylethanolamine (p<0.001), phospholipids (p<0.001), and unsaturated fatty acids (p<0.01). The abundance of monounsaturated fatty acids and phosphatidylcholine were significantly higher in *unc-18* rescue mutants than WT worms (p<0.01 and p<0.05, respectively). ANOVA followed by Tukey's multiple comparisons test did not identify any significant differences between *unc-18* rescue and *unc-18 (e81)* null mutants. While some differences were hypothesised, this is not surprising as the *unc-18* rescue mutant is derived from the *unc-18 (e81)* null mutant. Interestingly, *unc-18* rescue mutants significantly differed from WT in levels of monounsaturated fatty acids, phosphatidylcholine, and linoleic acid, while *unc-18 (e81)* null mutants did not. This suggests that these changes in metabolite abundance may have arisen by novel mutations in the *unc-18* rescue mutant which are not in the *unc-18 (e81)* null, such as the *dgk-1 (ulv1)* and *sorf-2 (ulv2).* Overall, these results confirm that the *unc-18* rescue mutant still shares much of its lipid metabolite composition with the *unc-18 (e81)* null mutant and suggest that identification of more subtle differences between the samples would require a much larger sample number, which was beyond the scope of this study.
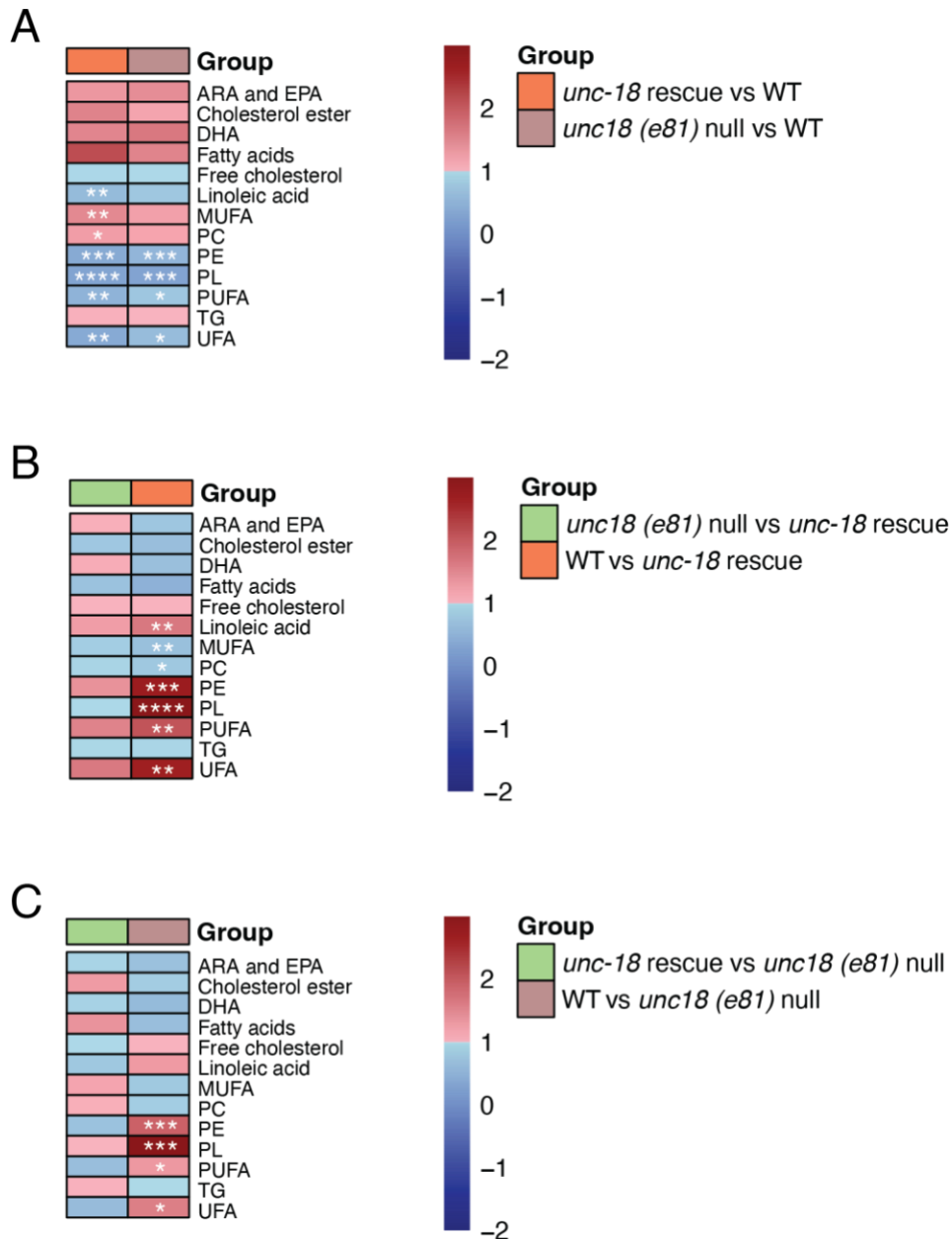
Figure 5.2. Fold change analysis of key lipids between WT, *unc-18 (e81)* null and *unc-18* rescue mutants. A) Lipid changes for *unc-18* rescue and *unc-18 (e81)* null mutants in relation to WT. B) Lipid changes for *unc-18 (e81)* null and WT worms in relation to *unc-18* rescue mutants. C) Lipid changes for *unc-18* rescue and WT worms in relation to *unc-18 (e81)* null mutants. Red cells indicate a fold-change increase, blue cells indicate a fold-change decrease. Statistical analysis was done using a one-way ANOVA and Tukey's multiple comparisons test. $*p<0.05$, $**p<0.01$, $***p<0.001$, $****p<0.0001$. ARA=arachidonic acid, DHA=docosahexaenoic acid, EPA=eicosapentaenoic acid, MUFA=monounsaturated fatty acids, PC=phosphatidylcholine, PE=phosphatidylethanolamine, PL=phospholipids, PUFA=polyunsaturated fatty acids, TG=triglycerides, UFA=unsaturated fatty acids.

5.2.2 Strain specific differences in polar metabolite profiles of *unc-18 (e81)* null, *unc-18* rescue, and wild-type worms

The polar metabolite annotation identified 371 bins, of which 170 were attributed to unknown metabolites. 126 bins were attributed to more than one metabolite (overlapping peaks), of which 62 overlapped with an unknown metabolite. To simplify analysis and reduce the number of variables, a correlation reliability score (CRS) (310) was calculated to confirm annotation and select representative metabolite bins using the highest correlation score within multiple peaks of the same metabolite. In each case, a singlet peak was selected if available, however, if no singlet peak was available, the overlapping peak with the highest correlation was selected (Appendix 1). 65 representative bins attributing to 65 metabolites were selected, of which 43 were singlet bins and 22 were overlapping bins. Overall differences in polar metabolite profiles were analysed using a PCA. The PCA consolidated 43.1% of the variance (PC1, 24.7%; PC2, 18.4%), with strong clustering of *unc-18 (e81)* null and *unc-18* rescue samples (Figure 5.3). A total of 15 components were required to explain 95% of the variation, indicating greater data complexity in comparison to lipids. WT worms exhibited the greatest variance across PC1 (with samples distributed across the whole component) and PC2, with almost half of WT samples clustering separately from *unc-18 (e81)* null and *unc-18* rescue mutants. There was no clear separation of *unc-18 (e81)* null and *unc-18* rescue mutants from each other, and both mutants showed limited variation across PC1 with more variation in PC2 for *unc-18 (e81)* null mutants than *unc-18* rescue mutants. Due to the large number of polar metabolites, the PCA loadings plot did not clearly indicate the overall differences in metabolites between the three strains investigated.
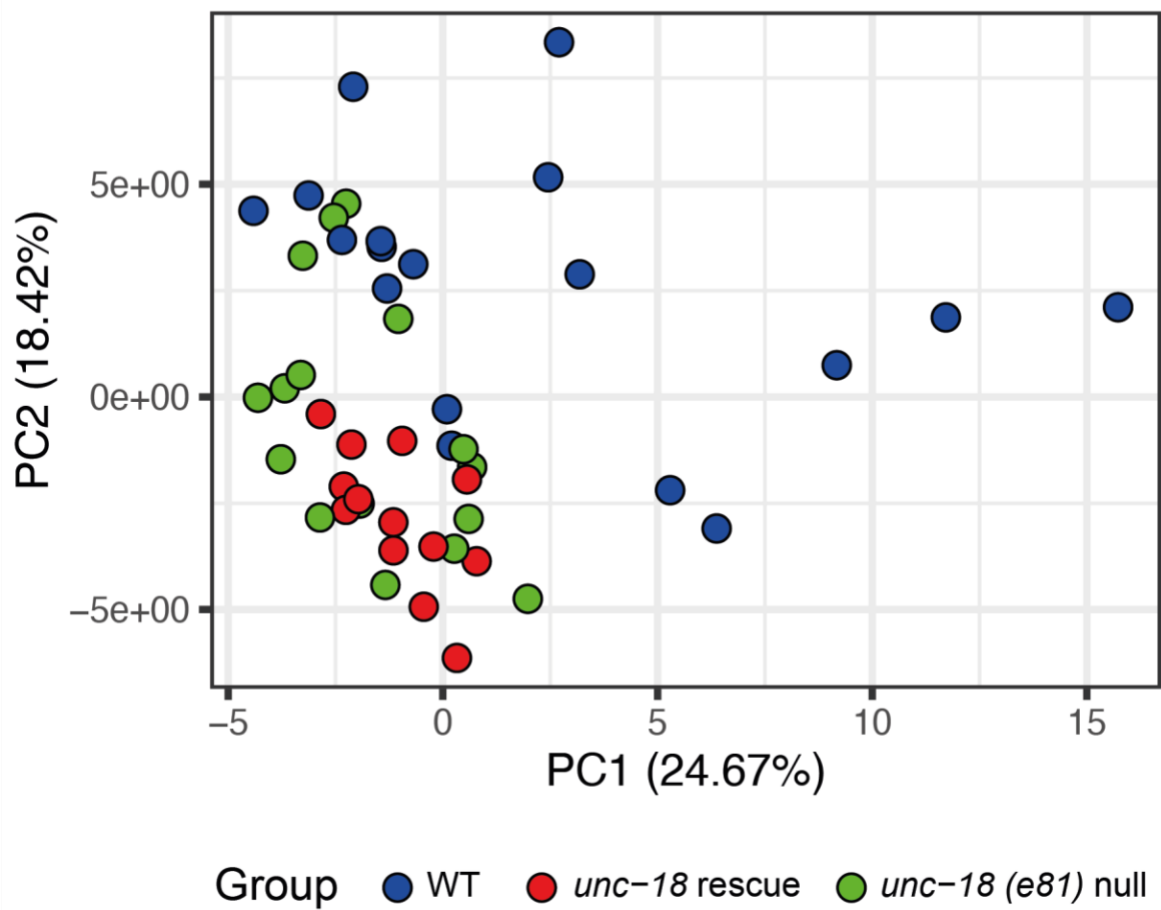
Figure 5.3. PCA scores of PC1 (24.67%) against PC2 (18.42%) from WT (n=18), *unc-18* rescue (n=13), and *unc-18 (e81)* null (n=16) samples. A total of 15 PC was used to achieve 95% explained variance.

Next PLS-DA was performed to probe deeper and uncover effects that may be masked by other components. A PLS-DA is a supervised model – which utilises a proportion of the dataset to train itself, and then tests the training on the remaining dataset – offers better discrimination of the dataset compared to a PCA. However, a valid PLS-DA model requires a modest amount of data for adequate training and testing (311). In this study, a PLS-DA was only performed if sample numbers exceeded 6, which was only the case for the dataset of polar metabolites. 3 PLS-DA models were performed to reveal differences between strains. One model to uncover differences between WT and *unc-18 (e81)* null worms, one model to investigate differences between WT and *unc-18* rescue worms and a third model to investigate differences between *unc-18 (e81)* null and *unc-18* rescue mutants. Following a PLS-DA models, variable importance in projection (VIP) scores were calculated for all the representative bins, with a VIP scores greater than one indicative of metabolites with greater than average influence in the model.

In the first WT and *unc-18 (e81)* null 2-component PLSDA model (Figure 5.4A), 20/65 (35.1%) bins scored higher than the VIP threshold. A receiver operating characteristic (ROC) curve was obtained using cross validation. A perfect discriminatory model would score 100% for both specificity and sensitivity. ROC values were 0.88 for component 1 and 0.68 for component 2, suggesting a weak-to- moderate model for discriminating between the two strains. In the second model, *unc-18* rescue and WT samples separated out completely from each other using a 2- component PLS-DA model (Figure 5.4B). 24/65 (36.9%) bins scored higher than the VIP threshold. Cross validation using the ROC curve found the model to score 100% for both specificity and sensitivity, with ROC scores of 1 for both components, suggesting that the model was a strong model for discriminating between WT and *unc-18* rescue samples.
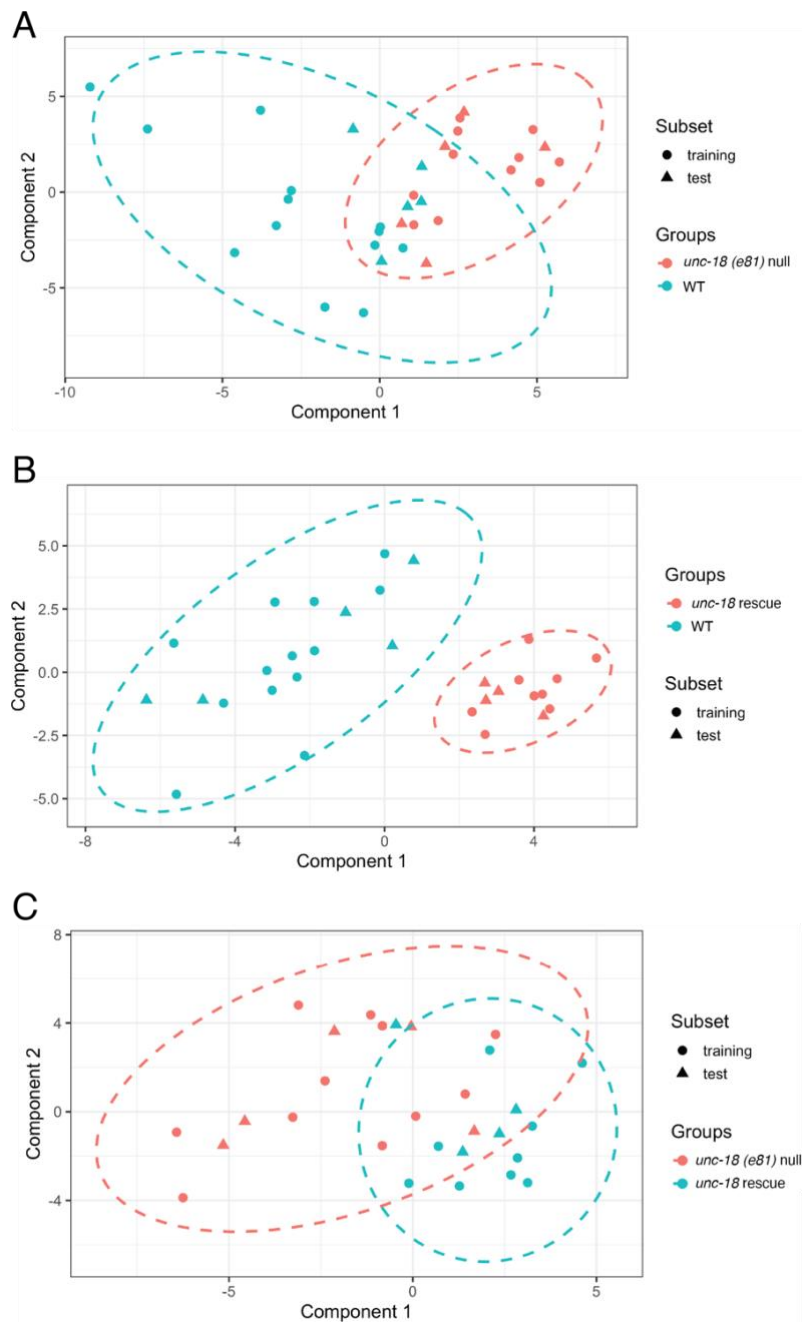
Figure 5.4. Variates one and two of PLS-DA models for comparisons between A) *unc-18 (e81)* null and WT samples, B) *unc-18* rescue and WT samples, and C) *unc-18 (e81)* null and *unc-18* rescue samples. Ellipses represent 95% confidence region. Training samples represent those used to train the PLS-DA model, and test models represent those on which the PLS-DA model tested the trained discrimination.

In the third 2 component PLSDA model, *unc-18* rescue, and *unc-18 (e81)* null

samples (Figure 5.4C) 23/65 (35.4%) bins scored higher than the VIP threshold.

ROC scores were 0.8 and 0.9 for component 1 and component 2, respectively,

suggesting that the PLS-DA was modest in discriminating between *unc-18* rescue

and *unc-18 (e81)* null samples.

Variance in projections (VIPs), and fold change analysis visualised using heatmaps,

allowed identification of key metabolites for each discriminant model. Significant

differences between metabolite levels were established using a one-way ANOVA

and Tukey's multiple comparisons test (Figure 5.5A). 23/65 (35.4%) bins were VIP

>1 between the three strains. In addition, there were five significant bins between

unc-18 (e81) null and *unc-18* rescue worms, 18 between WT and *unc-18 (e81)* null

mutants, and 22 between WT and *unc-18* rescue. In comparison with WT worms,

unc-18 (e81) null mutants had significantly higher abundance of beta-alanine

($p<0.05$), citric acid ($p<0.01$), creatine ($p<0.0001$), DMF ($p<0.01$), glutathione

($p<0.001$), histamine ($p<0.01$), L-carnitine ($p<0.01$), L- tryptophan ($p<0.01$), N-

carbamoyl aspartate ($p<0.05$), NADP ($p<0.01$), O- phosphocholine ($p<0.0001$),

phosphocreatine ($p<0.05$), and TMAO ($p<0.05$). In contrast, abundance of ADP

($p<0.01$), formate ($p<0.05$), fumarate ($p<.01$), L-isoleucine ($p<0.01$), and 5,6-

dihydrothymine ($p<0.01$) were significantly lower in *unc-18 (e81)* null mutants than in

WT worms (Figure 5.5A).
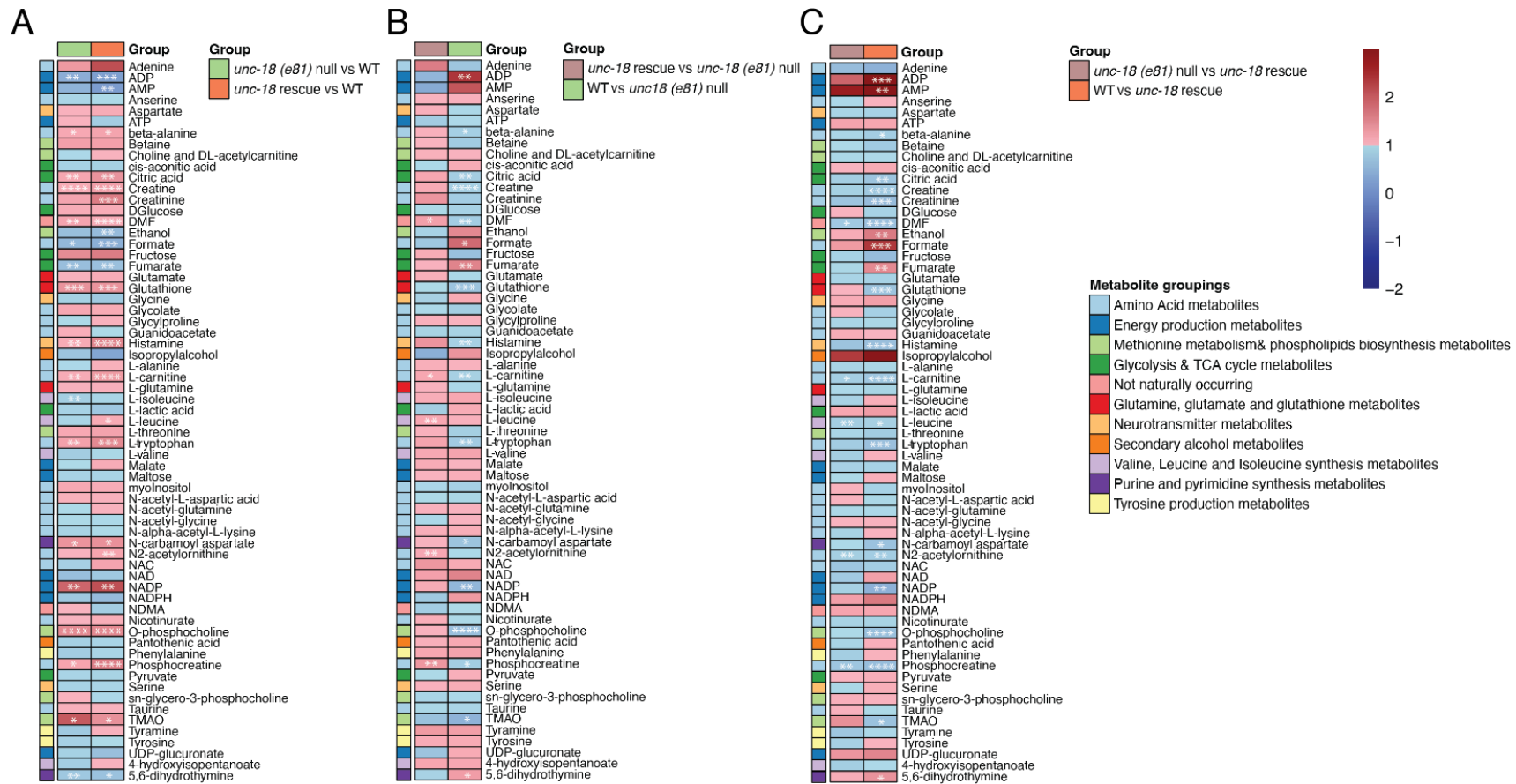
Figure 5.5. Fold change analysis of key metabolites for *unc-18 (e81)* null, *unc-18* rescue, and WT worms. Fold change analysis of A) *unc-18 (e81)* null and *unc-18* rescue mutants with respect to WT worms; B) *unc-18* rescue and WT worms with respect to *unc-18 (e81)* null mutants; and C) *unc-18 (e81)* null and WT worms with respect to *unc-18* rescue mutants. Metabolites are grouped according to key metabolic processes. Red cells indicate a fold increase, blue cells indicate a fold decrease. ADP=adenosine diphosphate, AMP=adenosine monophosphate, ATP=adenosine triphosphate, DMF=N,N-dimethylformamide, NAC=N-acetylcysteine, NAD=nicotinamide adenine dinucleotide, NADP= nicotinamide adenine dinucleotide phosphate, NADPH=nicotinamide adenine nucleotide phosphate, NDMA=N-nitrosodimethylamine, TMAO=trimethylamine N-oxide, UDP=uridine diphosphate. Asterisks represent Tukey's multiple comparisons p-values - *p≤0.05, **p≤0.01, ***p≤0.001, ****p≤0.0001.

Compared with WT worms, *unc-18* rescue mutants had significantly higher abundance of beta-alanine ($p<0.05$), citric acid ($p<0.01$), creatine ($p<0.0001$), creatinine ($p<0.001$), DMF ($p<0.0001$), glutathione ($p<0.001$), histamine ($p<0.0001$), L-carnitine ($p<0.0001$), L-leucine ($p<0.05$), L-tryptophan ($p<0.001$), N-carbamoyl aspartate ($p<0.05$), N2-acetylornithine ($p<0.01$), NADP ($p<0.01$), O-phosphocholine ($p<0.0001$), phosphocreatine ($p<0.0001$), and TMAO ($p<0.05$). In contrast, the abundance of ADP ($p<0.001$), AMP ($p<0.01$), ethanol ($p<0.01$), formate ($p<0.001$), fumarate ($p<0.01$), and 5,6-dihydrothymine ($p<0.05$) were significantly lower in *unc-18* rescue mutants than in WT worms (Figure 5.5B). In comparison with *unc-18 (e81)* null mutants, *unc-18* rescue mutants exhibited significantly higher abundance of DMF ($p<0.05$), L-carnitine ($p<0.05$), L-leucine ($p<0.01$), N2-acetylonithine ($p<0.01$), and phosphocreatine ($p<0.01$). No metabolites were found to be significantly lower in abundance in *unc-18* rescue mutants compared to *unc-18 (e81)* null mutants (Figure 5.5C).

Overall, polar and lipid analysis demonstrated differences between the wild-type, *unc-18 (e81)* null, and *unc-18* rescue strains, however there was no clear observable pattern of difference.

5.3 Discussion

This investigation aimed to establish differences in metabolite abundance between WT, *unc-18 (e81)* null and *unc-18* rescue worms using ^{1}H NMR. In recent years, NMR has been widely used in *C. elegans* to investigate various biological functions from gene function to analysis of processes involved in diet and growth (297,304,391). However, the use of NMR in *C. elegans* is still evolving compared to its well-established use in mammalians. The current results demonstrate that ^{1}H NMR can successfully discriminate between lipid groups in *C. elegans*, identifying significant differences between mutants in several lipid groups with roles in neuronal processes. Additionally, ^{1}H NMR was able to successfully quantify the abundance of several polar metabolites with good discrimination between the three strains investigated.

Lipid analysis identified significant changes in the majority of the lipid groups attributed to spectral bins. Overall, significant differences were observed between the strains in levels of linoleic acid, monounsaturated fatty acids (MUFA), polyunsaturated fatty acids (PUFA), unsaturated fatty acids (UFA), phosphatidylcholine (PC), phosphatidylethanolamine (PE), phospholipids (PL), and triglycerides (TG). In the human brain, fatty acids are abundant, with established roles in neuronal processes (392–394). Particularly important for synaptic signalling are PUFA, which are released by phospholipase A2 (PLA2) and form important structural components of membrane phospholipids (392,395,396). The importance of PUFA for neuronal function is evident as disruption in the metabolism of these fatty acids has been associated with neurodevelopmental and neurodegenerative disorders (392). Several types of these fatty acids exist, however arachidonic acid

175

(ARA) and docosahexaenoic acid (DHA) are the most abundant, and some of the most investigated forms (396). In addition to PUFA, this investigation also found significant differences in abundance of linoleic acid, which acts as the precursor of ARA; while α-linoleic acid acts as the precursor of EPA and DHA (396). Of all these lipids ARA is particularly important in SNARE function and was the first signalling lipid to be identified with a direct interaction with SNARE proteins. In this pivotal study, ARA was found to activate syntaxin-1 through a direct mechanism, even in the presence of Munc18 (253). It is now well established that ARA are rich at the plasma membrane, enhancing exocytosis by targeting syntaxin-1 and facilitating the formation of SNARE complexes (254). Additionally, ARA has been found to activate PKC which in turn phosphorylates growth associated protein-43 (GAP-43), a protein involved in neuronal growth and plasticity (397). This suggests that some differences in PUFA composition may be due to the *dgk-1* and *sorf-2* mutations, however as significant differences were also observed in *unc-18 (e81)* null, other factors would be contributing to PUFA abundance, which requires further investigation.

In humans, the ARA NMR spectra comprise five peak clusters. Therefore, it is possible that differences in ARA abundance may contribute to the significant differences observed in PUFA levels between the three strains, despite ARA being attributed to a separate bin. Significant differences in PUFA compared to WT were observed for both mutant strains, with a larger difference in *unc-18* rescue mutants than *unc-18 (e81)* null mutants. Together these findings show that the metabolic profile of the two mutants investigated differ from WT, a finding that may be owing to the mutations present in each strain. Interestingly, the activity of unsaturated fatty acids has been found to be synergistic to DAG activity for the activation of PKC,

even when Ca^{2+} abundance is low (398). Additionally, in *C. elegans*, synthesis of PUFA requires saturated fatty acids obtained from their *E. coli* diet (263), making possible that in addition to the mutations, there may have been intrinsic variance within each strain due to different feeding behaviours.

The current investigation also identified significant differences between strains in abundance of phospholipids, phosphatidylcholine and phosphatidylethanolamine. In the brain, phospholipids usually contain two PUFAs (399). Mostly DHA is found in ethanolamine plasmalogen, phosphatidylserine and phosphatidylethanolamine, whereas ARA is esterified in phosphatidylcholine (400). In association with each other, phospholipids and PUFA play important roles in membrane structure by determining flexibility and curvature of the lipid bilayer (396). In addition, other forms of fatty acids in which significant differences were observed (MUFA and UFA), are highly important for membrane fluidity, suggesting alterations in general membrane composition. *unc-18 (e81)* null, *unc-18* rescue, and WT worms differ in the rate of cholinergic release, with higher levels observed in WT and *unc-18* rescue worms. Thus, differences in lipids involved in membrane composition were expected.

C. elegans are able to synthesise and use a diverse range of head groups, giving rise to a number of lipid classes, such as phosphatidic acids, phosphatidylcholines, phosphatidylethanolamines, phosphatidylserines, phosophatidylglycerols and glycerolphosphates, and phosphatidylinositols (303). In the current investigation, the *C. elegans* lipid spectra labelled representative bins for phosphatidylcholines, phosphatidylethanolamines, and also phospholipids more generally; all of which were found to be significantly different between the strains. As DAG is associated with several of the lipid classes investigated, it is difficult to determine whether significant differences observed are solely due to changes in DAG. Nonetheless,

177

both *unc-18* rescue, and *unc-18 (e81)* null mutants were significantly different from WT in abundance of phospholipids and phosphatidylethanolamine, however only *unc-18* rescue mutants differed from WT in abundance of phosphatidylcholine. While the presence of many significant differences in these metabolites occur in both mutant strains, suggesting that the changes are unlikely due to the *dgk-1* and *sorf-2* mutations, the significant difference observed in phosphatidylcholine, monounsaturated fatty acids and linoleic acid in *unc-18* rescue mutants (and not *unc-18 (e81)* null mutants) mutants suggest that these may be due to the mutations which are novel to the *unc-18* rescue strain. To now, evidence of this investigation suggested an increase in DAG levels in *unc-18* rescue mutants compared to *unc-18 (e81)* null mutants. Therefore, the original hypothesis of this investigation expected to observe differences in DAG, which is generated during a range of metabolic reactions. Triacylglycerol is one precursor of DAG which contains three fatty acids esterified to the trihydric alcohol glycerol, presenting three possible sites of hydrolysis. In result, this produces distinct DAG isoforms. Phospholipase C (PLC) releases the phospholipid headgroup from membrane phospholipids, giving rise to DAG which is anchored to the membrane by two hydrophobic carbon chains (265). Alternatively, hydrolysis of phosphatidylcholine by phospholipase D (PLD) produces the choline head group and phosphatidic acid; the latter of which is hydrolysed into DAG by phosphatidic acid phosphohydrolase (265). In another pathway, termed the Kennedy pathway, phosphatidylcholine is synthesised from choline in a three-step reaction, which requires DAG in the final stage (Figure 5.6) (401). This provides a possible explanation for the observed changes in phosphatidylcholine abundance in *unc-18* rescue mutants compared to WT worms. Disruption of the *dgk-1* mediated phosphorylation of DAG to PA may in turn impact related pathways (Figure 5.6).
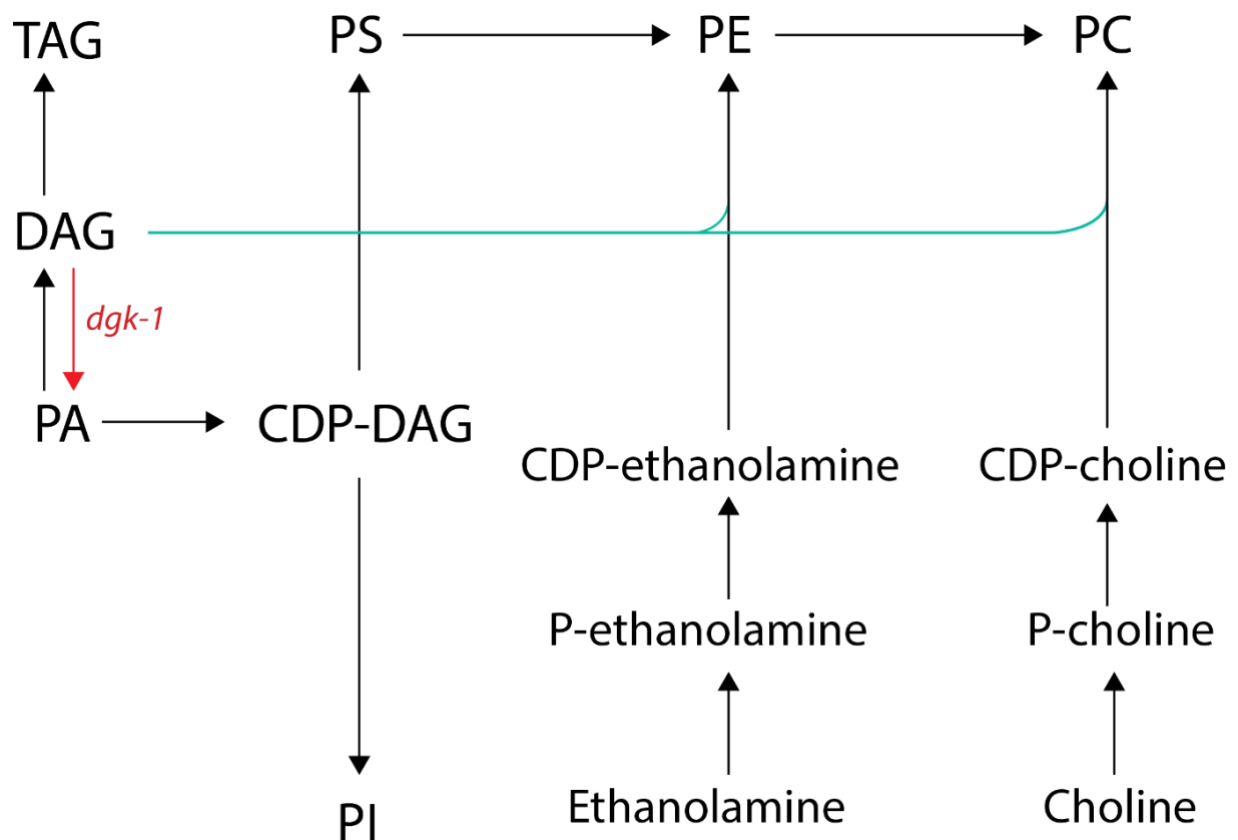
Figure 5.6. The general pathway for phospholipid synthesis through the Kennedy pathway. Two branches of the pathway include the synthesis of phosphatidylethanolamine from ethanolamine, and synthesis of phosphatidylcholine from choline. In the first pathway, ethanolamine kinase catalyses the phosphorylation of ethanolamine in an ATP-dependent manner, forming P-ethanolamine and by-product ADP. CTP:phosphoethanolamine cytidylyltransferase uses phosphoethanolamine and CTP to form CDP-ethanolamine, releasing pyrophosphate. In the third step, CDP-ethanolamine:1,2,diacylglycerol ethanolaminephosphotransferase uses CDP-ethanolamine and DAG to form PE, with CMP as a by-product. The second branch of the Kennedy pathway is analogous, using similar reactions which involve choline instead of ethanolamine. The DAG used in the third step of each reaction is produced by PA. The red line denotes the pathway which is affected by the *dgk-1 (ulv1)* mutation, and the green lines denote the pathways which may be affected as a result of the *ulv1* mutation. CDP-choline=cytidine-diphosphocholine; CDP-DAG=cytidine diacylglycerol; CDP-ethanolamine=cytidine-diphosphoethanolamine; DAG=diacylglycerol; PA=phosphatidic acid; PC=phosphatidylcholine; PE=phosphatidylethanolamine; PI=phosphatidylinositol; PS=phosphatidylserine; TAG=triacylglycerol.

Although the polar subset of metabolites was not the primary aim of the study, ^{1}H NMR showed potential to discriminate between several metabolites involved in key physiological processes. These metabolites were categorised in relation to the key processes that they are involved in, with differences identified in metabolites involved in all categories except for those involved in tyrosine production. When looking at the whole metabolic profile, the PLS-DA found *unc-18* rescue samples to separate out from WT samples, while *unc-18 (e81)* null samples failed to separate out from either WT or *unc-18* rescues. The initial hypothesis expected *unc-18* rescue and *unc-18 (e81)* null mutants to separate out from each other, however, as the physiological roles of polar metabolites vary significantly, these results are of little surprise. Some differences in metabolites involved in neuronal process were observed, which may have been linked to *unc-18, dgk-1* and *sorf-2* mutations. Glutamate and glutamine function in pathways including energy provision, protein synthesis, and the synthesis of chemicals such as N-acetylaspartate, N-acetylaspatylglutamate, GABA, and glutathione. Investigation of peaks corresponding to glutamate and glutamine have been used as markers for degeneration in both preclinical and clinical studies (402). Furthermore, glycine is an activator of glycine receptors and a co-agonist for glutamate excitatory transmission through NMDA receptors, exhibiting a dual role as an inhibitory neurotransmitter (403). Compounds containing choline are important for the synthesis of membrane lipids, and act as precursors for acetylcholine biosynthesis. However, in the mammalian brain, it has been reported that choline levels are below the detection limit of NMR, with the majority of the signal attributed to glycerylphosphorylcholine and phosphorylcholine (403,404). It is possible that for the *C. elegans* metabolome, the abundance of some metabolites may also have been below the detection limit. Nonetheless, the findings of this investigation provide further support that metabolic

processes within the two mutant strains are significantly altered compared to WT worms.

To date, the use of NMR to investigate the lipidome of *C. elegans* is limited. While several studies have used ^{1}H NMR to understand polar metabolites, there are currently very few studies that have used ^{1}H NMR to investigate the lipidome of *C. elegans.* Our findings suggest that following further optimisation, there is potential for ^{1}H NMR to provide insight into novel pathways affected by genetic mutations in *C. elegans*. We have identified differences between several lipids involved in neuronal processes, as well as polar metabolites involved in a range of physiological functions. There are however several limitations to the present investigation. Firstly, the protocol utilised in this study extracted metabolites from whole worms, rather than from neuronal specific regions. In *C. elegans,* membranes are largely made up of sphingolipids and glycerophospholipids, with a smaller abundance of cholesterol (302,405). In the metabolites that make up glycerophospholipids, 54.5% contain ethanolamine, 32.3% contain choline, 8.1% contain sphingomyelin, and 5.1% contain other metabolites. Additionally, the lipid composition of the plasma membrane varies between different tissue types and will differ from the lipid composition of organelle membranes. For example, mitochondrial membranes are largely made up of phosphatidylcholine, phosphatidylethanolamine, and cardiolipin, whereas in comparison, the ER consists larger amounts of phosphatidylcholine, with lower amounts of phosphatidylethanolamine, and small amounts of phosphatidylinositol (406,407). Synaptic membranes on the other hand are highly enriched in polyunsaturated fatty acids, as has been discussed (392). These are all factors which could have contributed to the significant differences in lipid abundance observed between *unc-18 (e81)* null, *unc-18* rescue, and WT worms. Furthermore, lipids are not only important for membrane structure and neuronal signalling, but they also play

important roles in processes such as inflammation, stress response, and development, suggesting that other physiological differences beyond those caused by the mutations of interest will have contributed to observed results. It should also be noted that the *unc-18 (e81)* null mutant, from which the *unc-18* rescue mutant is derived, contained several other mutations which were not investigated in this study. Therefore, as ^{1}H NMR identifies differences in the whole metabolome, it is possible that the background mutations present and differences in physiology between strains considerably contributed to the differences observed.

Secondly, the lipid analysis was limited due to low sample number, meaning a PLS-DA could not be performed. Therefore, interpretation of differences in lipid profiles between the strains was limited to the unsupervised PCA. A supervised PLS-DA model would have shown better discrimination between the samples and may have resolved differences that were not observed in the PCA. Despite preparing over 30 samples per strain for lipid analysis, the low sample number arose from difficulties during the sample preparation. Lipid samples are highly temperature sensitive and are required to stay frozen during sample preparation. In the currently study, these samples were prepared in large batches, resulting in some samples defrosting during the process of transfer for lyophilisation. As a result, several samples were degraded and following NMR acquisition, failed spectra quality control. Another factor which reduced the sample number is variation in spectra quality between batches. As samples were prepared across several days, large amounts of variation in the worm cultures were found to affect spectra quality, consistent with previous findings of NMR in *C. elegans* (391). These variances may have arisen from differences in the cleanliness of plates, age of worms, or feeding behaviour. For instance, the protocol used for metabolite extraction involved several washes of the worm plate to remove

any unwanted debris, exposing worms to a level of stress (391). This suggests that worms on dirtier plates may have been more stressed due to more washes required to gain a clean sample. Therefore, for the final analysis, only the spectra of highest quality were selected.

This study also utilised a scoring system based on the correlation of signals – correlation reliability score (CRS) – to identify representative bins for each polar metabolite (310). While this method allows selection of the best representative peak for a metabolite, this approach is limited to metabolites which are represented by more than one peak. Metabolites represented by a singlet peak always scored 100% using the CRS, even if the signal was not accurate. Therefore, analysis of these metabolites should be interpreted with caution. Furthermore, a common limitation of ^{1}H NMR spectroscopy is the presence of overlapping peaks in both polar and lipid spectra. This adds complexity to the data as individual levels of metabolites are represented in several peaks within the spectra. Interpretations of 1D NMR can be enhanced through extension to 2D NMR which can validate interpretations and improve identification of metabolites. Particularly, the identification of metabolites relies on a well-established pattern file of known metabolites, however, there is currently no centralised database for the *C. elegans* lipidome (303). In the present analysis, the lipid pattern file was adapted from *Danio rerio* annotation (408). As the annotation was not specific to *C. elegans*, the lipid and polar spectra in the present investigation contained a high number of unknown peaks, especially within the lipid sample. The high number of unknowns limited the number of peaks which were analysed. This increased the possibility that important differences in metabolite abundance between the strains could not be attributed to specific metabolites, and statistical power could not be improved by subsetting data for single representative

peak per identity via CRS. This study aimed to investigate differences between strains in abundance of DAG and PA. However, the ability of ^{1}H NMR to detect individual lipids is limited due to several factors including the presence of overlapping peaks, the complexity of lipids and the sample, and the sensitivity of NMR. Therefore, the use of ^{1}H NMR in this investigation failed to address the question of interest. To investigate individual lipid levels, ^{1}H NMR may be complimented with more robust techniques such as mass spectrometry.

The use of model organisms in biological research has enhanced our understanding of physiology and disease and has advanced the medical field. Establishing robust metabolomics and lipidomic methods in model organisms, such as *C. elegans* can further contribute to these advancements. In 2015, the Metabolomics Society's Model Organism Metabolomes (MOM) task group was launched with aims to identify and map all metabolites onto metabolic pathways, develop quantitative metabolic models for several model organisms, and to relate metabolic pathways within the context of evolutionary metabolomics (409). This study utilised a previously optimised protocol for *C. elegans* polar metabolite extraction (410), however the current *C. elegans* lipid analysis will be informative for future lipidomic studies to further optimise and utilise the benefits of ^{1}H NMR. With a *C. elegans* specific pattern file, and a larger sample number, ^{1}H NMR may be able to distinguish additional polar and lipid metabolites with increased sensitivity. Additionally, with more time, and better mapping of metabolic pathways in *C. elegans,* outcomes of ^{1}H NMR may be cross-validated with 2D NMR and orthogonal techniques such as mass-spectrometry. ^{1}H NMR is usually the preferred method of choice for metabolic profiling due to the nuclei's high natural abundance (99.9%), and prevalence in endogenous metabolites compared to other nuclei such as ^{13}C, ^{15}N, and ^{31}P. A caveat for 1D NMR is the presence of overlapping peaks in which less abundant

metabolites are hidden beneath peaks of those that are more abundant (411). 2D NMR may therefore offer a more optimal technique to separate different metabolites. MS on the other hand offers increased sensitivity to NMR, as well as the ability to detect a higher number of metabolites (412). Future work therefore should not replace the use of ^{1}H NMR but take advantage of other techniques to enhance its findings.

5.3.1 Summary

The aim of this investigation was to utilise 1D ^{1}H NMR to investigate the metabolome of *unc-18 (e81)* null, *unc-18* rescue and WT *C. elegans,* with a focus on DAG and PA. In doing so, we aimed to identify possible pathways involved in the *unc-18* rescue phenotype. As there is currently no annotation for the *C. elegans* metabolome using NMR, this investigation utilised a *Danio rerio* annotation of metabolites. ^{1}H NMR identified significant differences in the abundance of polar and lipid metabolites between the strains investigated, many of which were involved in neuronal processes. However, ^{1}H NMR was unable to detect individual lipids and did not address the question of whether DAG and/or PA levels were different between strains. While it was not possible to identify specific metabolic changes owing to the *dgk-1* and *sorf-2* mutations, this investigation supports the idea that with a collective research effort, a ^{1}H NMR approach for the investigation of *C. elegans* can be established in which the variation of external confounding factors is minimised, allowing accuracy in discrimination of genetic differences.

Chapter 6. General discussion

6.1 Summary of findings

Munc18-1 (also known as STXBP1) has been established as an indispensable protein, with a crucial role in synaptic vesicle fusion and neurotransmitter release (198,202,205,210). As such, mutations in Munc18-1 have been linked to several epileptic neurodevelopmental disorders (known as STXBP1-encephalopathy), schizophrenia, movement disorders (Parkinson's disease), and neurodegeneration (Alzheimer's disease) (8,413,414, 415). Null mutations of Munc18-1 and its homologues in several organisms are unviable (13,179). However, in *C. elegans*, null mutations are viable yet result in neurotransmitter and locomotor defects (paralysis). Previous studies have demonstrated rescue of locomotor defects in these organisms through expression of wild-type *unc- 18* or Munc18-1, *unc-18* point mutations that block binding to closed-conformation syntaxin, or chemical chaperones which restore gene function (10,181,306,315).

This investigation wanted to identify and characterise whether Munc18-1/*unc-18* function can be bypassed if it is completely dysfunctional. Due to their viability with *unc-18* null mutations, genetic tractability, and reproducible nature, *C. elegans* were chosen as the optimal organism for this investigation. Prior to the work carried out in this project, ethyl methanesulfonate (EMS) mutagenesis of *unc-18 (e81)* null mutants identified a novel mutant (*unc-18* rescue) in which locomotion had been restored. Whole genome SoLiD sequencing identified three mutations with putative involvement in the alteration of synaptic transmission in *unc-18* rescue mutants – a novel mutation, *ulv1,* in diacylglycerol kinase-1 (*dgk-1*), a novel mutation, *ulv2,* in suppressor of organelle function-2 (*sorf-2*), and a second mutation (*ulv3)* in *sorf-2* which is also present in the *unc-18 (e81)* null mutant. In this study, the successful

restoration of locomotion (rescue phenotype) in *unc-18* rescue mutants was validated and the necessity of both the *dgk-1* and *sorf-2* mutations in the rescue phenotype was confirmed. In *unc-18 (e81)* null mutants containing the *sorf-2 (ulv3)* mutation (but not in those lacking the mutation), inhibition of *dgk-1* or mimicking excess DAG using PMA, in addition to *sorf-2* RNAi significantly improved locomotion suggesting that the *dgk-1* (*ulv1*) mutation results in a *loss-of-function*, likely altering DAG levels, while the *sorf-2* (*ulv2* and *ulv3*) mutations pointed towards a *loss-of-function*, and change of function, respectively.

6.2 Contributions to the field

To date, it is widely accepted that *unc-18* plays two key functions during the synaptic vesicle cycle, one as a chaperone for syntaxin-1 (1,180,181), and one as an activator of SNARE-mediated fusion during the priming stage (6). *unc-18* binding to the N-terminus of syntaxin-1 has been shown to be essential for normal locomotion and neurotransmitter release (181,416), while other studies have shown that Munc18-1 and Munc13, together, chaperone SNARE complex assembly and prevent SNARE complex misassembly (3,67,101). Together, these studies suggest that Munc18-1/*unc-18* function for vesicle fusion and coordinated locomotion is an absolute. The findings of this investigation identify the existence of an alternative mechanism through which the function of *unc-18* may be bypassed, challenging the idea that *unc-18* is required for coordinated movement. The identified mechanism may compensate for the function of *unc-18* on syntaxin-1 and SNARE complex assembly. This investigation also found evidence supporting a crucial role of lipids (i.e., DAG) within neuronal signalling, as demonstrated by the successful use of PMA to enhance locomotion in *unc-18 (e81)* null mutants subjected to *sorf-2* RNAi.

The use of ^{1}H NMR further complimented the findings through discovery of lipid differences between wild-type worms and mutant *C. elegans* in which synaptic transmission was altered. This study is among the first studies to show the utility of ^{1}H NMR for lipid analysis in *C. elegans*, demonstrating that with correct optimisation, the technique has potential to discriminate between several lipids within the *C. elegans.*

Furthermore, the present work contributes to the understanding of *sorf-2*, which is still in its infancy. Following identification of its mammalian homologue, WDR81, in 2011, WDR81/*sorf-2* has been suggested to function in endosomal fusion, autophagy, aggrephagy, mitosis and neurogenesis (270–272,274,417). Our findings add to the evidence of its role in fusion and suggest that *sorf-2* may also function within the exocytic pathway, with direct or indirect association with *dgk-1* and *unc-18*. This is a novel finding which requires further exploration to better understand *sorf-2* function within neurons.

The outcomes of this study challenge what is currently understood about the *unc-18 (e81)* null mutation, and its effects on overall *unc-18* function, with evidence that *unc-18* function can be bypassed. So, what is the mechanism of bypass? While the exact mechanisms remain unclear, the present findings have highlighted possible molecular components which may play a role (Figure 6.1). In current literature, *dgk-1* and *sorf-2* have not been directly associated with each other, however both are associated with phospholipids. Based on the current findings, we emphasise a role of signalling lipids in the *unc-18* rescue phenotype, such as excess DAG resulting from *dgk-1 loss-of-function*. In addition, *loss-of-function* of *dgk-1* presumably also affects levels of phosphatidic acid at the presynaptic membrane. phosphatidylinositol 3-kinase (PI3K)

phosphorylates phosphatidylinositol (4,5)- bisphosphate (PI(4,5)P_2) into phosphatidylinositol (3,4,5)-biphosphate (PIP$_3$). Hydrolysis of PI(4,5)P_2 produces DAG and inositol (1,4,5)-trisphosphate (Ins(1,4,5)P_3). PI(4,5)P_2 is particularly essential for the priming stage of the vesicle fusion cycle, with evidence that sites at the plasma membrane containing both PI(4,5)P_2 and CAPS have a likely chance (70%) of containing docked vesicles. Also, an inhibitory role of PI(4,5)P_2 on SNARE-dependent fusion was identified in the absence of CAPS (418). The importance of PI(4,5)P_2 is also demonstrated through its function to recruit syntaxin-1, synaptotagmin-1 and Docβ to the plasma membrane (419). It is now well established that PI(4,5)P_2 is a key lipid component for synaptic transmission, and should be investigated further in regard to the *unc-18* rescue phenotype.

Furthermore, once DAG is produced, it activates PKC and PKD. Activation of PKD produces a series of signalling reactions, including the production of phosphatidylinositol 4-phosphate. This allows the delivery of cholesterol and ceramide to the Golgi complex, where they are converted to sphingomyelin and DAG (345). Alternatively, and possibly more relevant to the current investigation, DAG binds the C1 domain of PKC, while Ins(1,4,5)P_3 releases intracellular Ca^{2+}, facilitating the tethering of PKC to the membrane. At the membrane, PKC phosphorylates Munc-18/*unc-18*, a process which is believed to be essential for DAG-dependent synaptic transmission (420). Specifically in *C. elegans,* phosphorylation by PKC *in vitro* on UNC-18 Ser322 reduces binding to closed-conformation syntaxin (421). In addition to PKC, DAG facilitates synaptic transmission through binding to the C1 domain of Munc13, while the C2 domain of Munc13 binds PI(4,5)P_2. Through C1C2 domain binding, Munc13 plays a crucial role in bridging the vesicle and plasma membrane. In addition, Munc13 cooperates with Munc18 to facilitate the

transition of the Munc18-1/syntaxin complex to the tertiary SNARE complex (3,67,87,90,94,101). Like PI(4,5)P$_2$, it is predicted that both PKC and Munc13 exert their functions during the priming stages of the synaptic vesicle cycle. As Munc18 is believed to be required for vesicle priming and chaperoning syntaxin-1 to the plasma membrane, the role of PKC and Munc13/*unc-13* in the *unc-18* rescue phenotype should also be investigated in future studies. It is possible that through the action of Munc13 and/or PKC, along with lipid activity, the priming defects owing to the *unc-18 (e81)* null mutation are rescued, sufficient to increase vesicle exocytosis. This hypothesis would support a bypass of *unc-18* function, as *unc-18 loss-of-function* has been found to partially reduce syntaxin levels at the synapse (168,181,204), suggesting that some syntaxin is still available for SNARE complex formation in *unc-18* null mutants. Thus, it would be assumed that the *dgk-1* and *sorf-2* mutations compensate for the role of *unc-18* in priming rather than the role of a syntaxin chaperone.

In another line of research, *sorf-2* has been found to negatively regulate phosphatidylinositol-3-phosphate levels in endosomal conversion, with *sorf-2 loss-of-function* resulting in elevated PI3K levels (271). This investigation has identified clear differences in phospholipid abundance in *unc-18 (e81)* null and *unc-18* rescue mutants compared with WT worms. While the conclusions are speculative, the involvement of *dgk-1* and *sorf-2* both indicate that phospholipids may also play a key role in the *unc-18* rescue phenotype and should be explored further. It is important that future studies aim to better dissect the individual *dgk-1, sorf-2* and *unc-18* pathways to understand the mechanism through which the bypass of *unc-18* function occurs.
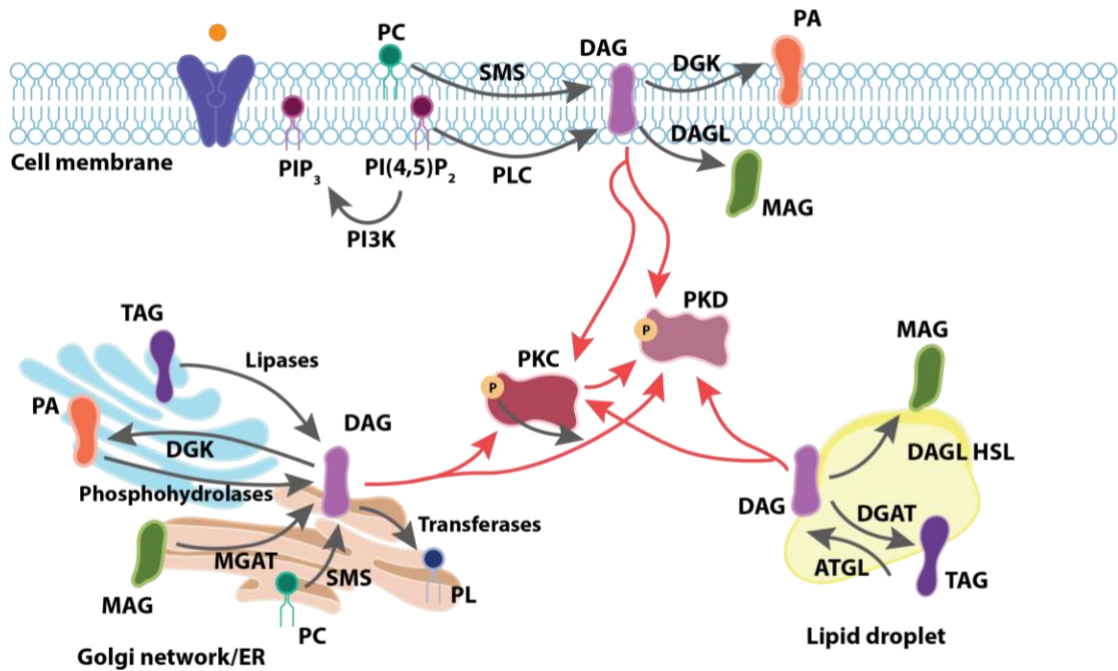
Figure 6.1. Schematic of potential lipid pathways affected by the *dgk-1* and *sorf-2* mutations. A detailed description of the pathways is provided in the text. There are several sources of DAG within the cell – it is produced through *de novo* biosynthesis of TAG and PL, and during catabolism of TAG which is stored in cytoplasmic or ER-associated lipid droplets, or PL within the plasma membrane of Golgi complex. It is also produced from hydrolysis of PIP_2 by PLC. DAG then activates PKC and PKD. ATGL =adipose triglyceride lipase; DAGK=diacylglycerol kinase; DAGL=diacylglycerol lipase; DGAT=diglyceride acyltransferase; ER=endoplasmic reticulum; HSL=hormone-sensitive lipase; MAG=monoacylglycerol; MGAT=monoacylglycerol-O-acyltransferase; PA=phosphatidic acid; PC=phosphatidylcholine; $PI(4,5)P_2$=phosphatidylinositol (4,5)-bisphosphate; PIP_3=phosphatidyl (3,4,5)-biphosphate; PI3K=phosphatidylinositol 3-kinase; PKC=protein kinase C; PKD=protein kinase D; PLC=phospholipase; SMS=sphingomyelin synthase; TAG=triacylglycerol. Adapted from Kolszynsca et al. 2020.

6.3 Evaluation of methodology and future directions

While this investigation presents novel findings, it is important that the limitations of the study are acknowledged. Firstly, the *C. elegans* was the only organism utilised for the investigation and so general limitations of the organism will first be discussed. *C. elegans* were the first multicellular organism in which the whole genome was sequenced, and has since often been used as the first point of investigation for genetic studies (422,423). *C. elegans* are a relatively simple organism with a limited number of tissues, making it difficult to investigate the effects of mutations on more complex organ systems that are found in other organisms. Additionally, these nematodes do not usually exceed 1 mm in length and are difficult to use in cell culture. Therefore, biochemistry and metabolomic studies will rely on whole worm extracts, which increases difficulty in identifying tissue-specific signalling and pathways.

The viability of *unc-18* null *C. elegans* is unlike other organisms. Therefore, it cannot be said with certainty that the conclusions drawn from this investigation will be applicable in other invertebrate or mammalian models. While the function of SM proteins is conserved between species, like any study, it is important that findings are validated using different models to establish biological relevance. The *unc-18 (e81)* null mutant contains an excessive number of other mutations which were also found in the *unc-18* rescue mutant, however their role was not analysed any further. Therefore, conclusions regarding the possible roles of the *dgk-1* and *sorf-2* mutations should still consider either direct or indirect influence from one or many of the other mutations present. This possibility was highlighted by the finding that R59949 and *sorf-2* RNAi, together, significantly improved locomotion in *unc-18 (e81)*

null mutants, but not in other *unc-18* null mutants. As a result of this, our investigation identified the *ulv3* mutation in *sorf-2*, which is present in both *unc-18 (e81)* null, and *unc-18* rescue mutants and is required for the *unc-18* rescue phenotype (Figure 4.12). This raises the question of which other mutations may be present which aid the rescue phenotype. Due to the complexity of the genetic profile of *unc-18* rescue mutants, this investigation found it difficult to isolate the individual mutations (Figure 4.5). Outcomes from the analysis of the offspring following crossing suggested that the mutations in isolation as single or double mutants may be unviable. Additional difficulty arose from the absence of a direct observable phenotype (except for the loopy phenotype of *dgk-1* mutants) or visual marker to identify the required mutations, resulting in reliance on Sanger sequencing. To increase the probability of identifying mutants in which the *dgk-1* and *sorf-2* mutations were isolated, approximately 100 offspring were selected for sequencing before the plate became outgrown. Therefore, if the results were inconclusive, or did not return the desired genotype, the genetic cross had to be reperformed. Due to these limitations, *C. elegans* research will often remain broad and will always require further validation in higher organisms.

An aspect of this investigation, which was not possible in the time available, aimed to validate the findings using a mammalian cellular model and electrophysiology. This would provide more certainty that the current observations are not specific to the *C. elegans* organism and would support the idea that the mechanism of bypass identified may be conserved between species. Further investigation in cellular models from other organisms will allow more complex biochemistry and will enhance the understanding of the association between these mutations beyond the behavioural level. Future approaches may also utilise more targeted methods such

as CRISPR-Cas9 or expressing the mutations with the aid of a genetic balancer. Additionally, incorporation of a visual marker, such as a fluorescent tag, to identify each mutation would streamline future investigations further.

Another limitation to this study arose from the level of understanding of *sorf-2*. To understand the contribution of a mutation to a particular phenotype often requires some understanding of the physiological role of a gene, especially in cases where the phenotype is formed by the combined function of several genes. We initially hypothesised a *loss-of-function* of *sorf-2* resulting from the *ulv2* mutation, and so approaches to recreate the effects of the mutation focused on this outcome. *sorf-2* RNAi, alongside DGK inhibition, improved locomotion in *unc-18 (e81)* null mutants but not in other *unc-18* null mutants (Figure 4.8, Figure 4.11). As *dgk-1* alone failed to improve locomotion in *unc-18 (e81)* null mutants (which contain the *sorf-2 (ulv3)* mutation), it was hypothesised that *sorf-2 (ulv2)* mutation produces a *loss-of-function*, while the sorf-2 *(ulv3)* mutation produces a change of function. However, understanding *sorf-2* function in present analysis was further convoluted following the finding that overexpression of *sorf-2*, and *loss-of-function* of *sorf-2*, both reduced locomotion in wild-type worms (Figure 4.3). Therefore, it is important for future approaches to investigate a potential *gain-of-function* owing to the *ulv2* and/or *ulv3* mutations.

Furthermore, the approaches utilised in this study were largely focused on behavioural phenotypes and indirect methods to investigate neurotransmitter release. While it is presumed that the paralysed phenotype of *unc-18* null mutants is due to reduced neurotransmitter release (168,416), there are several other molecular abnormalities present at the synapse which may contribute to the phenotype. These

include mislocalisation of syntaxin-1 (181), and reductions in the number of primed and docked vesicles (168); defects which are also present in Munc18-1 knockout models (1,179). To identify a mechanism through which *unc-18* function is bypassed would be to investigate more closely its role within vesicle fusion. From the observed improvement in cholinergic release in *unc-18* rescue mutants, it may be inferred that the number of primed and docked vesicles has improved. However, the effects of the *dgk-1* and *sorf-2* mutations on synaptic transmission were not investigated at the cellular level. For this reason, these claims cannot be made and require more thorough investigation. This investigation has focused on and drawn conclusions regarding the presynaptic molecular machinery. The use of PMA and R59949 increased aldicarb sensitivity and altered pharyngeal pumping in mutant strains. As a result, it was concluded that the two compounds are sufficient to increase cholinergic release. However, the potential effects of the compounds on postsynaptic machinery were not addressed. It is possible that PMA and/or R49949 increase the sensitivity of ACh receptors on the postsynapse. Therefore, the observed changes in behavioural phenotypes may be a result of increased receptor sensitivity rather than increased ACh release. Future studies may aim to investigate the differential effects of PMA and R59949 on presynaptic and postsynaptic machinery to allow clearer conclusions to be drawn. Additionally, in the present analysis, locomotion was successfully restored in *unc-18* rescue mutants, however, the thrashing rate remained defective. This suggests that some defects in the synaptic physiology of *unc-18* rescue mutants may still be present. Addressing this was not possible within the scope of this investigation, leaving a question of whether these defects are also completely restored in *unc-18* rescue mutants.

Finally, the key limitations of the NMR should be reviewed. ^{1}H NMR showed

potential to discriminate between lipid and polar metabolites in *C. elegans*, despite

using a low number of samples. However, the conclusions drawn from the

investigation remain speculative. One major limitation of the investigation was the

low sample number used, which may have lowered the power of comparisons

between the strains and reduced accuracy of the statistical models used (PCA and

PLS-DA). This said, the use of a PLS-DA model in this study has its own caveats. A

PLS-DA model relies on using a part of the data to train the model and the

remainder of the data to validate and test the model. Ideally, 60% of the data is used

for training, 20% for validating and 20% for testing (310). This requires larger

amounts of data than was attained in this project, reducing the validity of the model

used. Future studies should consider these limitations when using 1D ^{1}H NMR in *C.

elegans* research. To enhance the use of NMR in *C. elegans*, it is important that the

C. elegans research community continue to build on what is currently known about

the metabolic profile of this organism.

6.4 Final remarks

The work presented here accentuates the benefits of *C. elegans* as a model

organism for investigating synaptic function and exocytosis, while also highlighting

the potential of ^{1}H NMR for investigating the metabolome of the organism. We have

identified a mutant *C. elegans* strain in which the paralysed phenotype resulting from

the *unc-18 (e81)* mutation has been rescued, while *unc-18* function remains

defective. Currently, treatments for early infantile encephalopathy rely on seizure

and behavioural control, however, there is no treatment that specifically targets

Munc18 (9). In recent years, research has attempted to restore Munc18 function

through wild- type expression, or the use of chemical chaperones (10,306). Our

findings suggest that *unc-18* function can be bypassed, likely through the function of *dgk-1* and *sorf-2*. Particularly, the importance of lipids has been emphasised throughout this study and should not be overlooked when understanding the pathway through which *unc-18* function is bypassed. The mechanism of bypass may offer a potential novel therapeutic target for early infantile epileptic encephalopathy, which would allow better treatments of the disorder that goes beyond symptom control.

References

1. Arunachalam L, Han L, Tassew NG, He Y, Wang L, Xie L, et al. Munc18-1 is critical for plasma membrane localisation of syntaxin1 but not of SNAP-25 in PC12 cells. Mol Biol Cell. 2008 Feb;19(2):722–34.

2. Park S, Bin NR, Yu B, Wong R, Sitarska E, Sugita K, et al. UNC-18 and tomosyn antagonistically control synaptic vesicle priming downstream of UNC-13 in *caenorhabditis elegans*. J Neurosci. 2017 Sep 6;37(36):8797–815.

3. Lai Y, Choi UB, Leitz J, Rhee HJ, Lee C, Altas B, et al. Molecular mechanisms of synaptic vesicle priming by Munc13 and Munc18. Neuron. 2017 Aug 2;95(3):591-607.e10.

4. Südhof TC. The synaptic vesicle cycle. Annu Rev Neurosci. 2004;27:509–47.

5. Söllner T. Regulated exocytosis and SNARE function (Review). Mol Membr Biol. 2003 Jan 1;20(3):209–20.

6. Südhof TC, Rothman JE. Membrane Fusion: Grappling with SNARE and SM Proteins. Science. 2009 Jan 23;323(5913):474–7.

7. Chen Y, Scheller R. SNARE-mediated membrane fusion. Nat Rev Mol Cell Biol. 2001 Feb;2(2):98–106.

8. Saitsu H, Kato M, Mizuguchi T, Hamada K, Osaka H, Tohyama J, et al. *De novo* mutations in the gene encoding STXBP1 (MUNC18-1) cause early infantile epileptic encephalopathy. Nat Genet. 2008 Jun;40(6):782–8.

9. Stamberger H, Nikanorova M, Willemsen MH, Accorsi P, Angriman M, Baier H, et al. STXBP1 encephalopathy: a neurodevelopmental disorder including epilepsy. Neurology. 2016 Mar 8;86(10):954–62.

10. Guiberson NGL, Pineda A, Abramov D, Kharel P, Carnazza KE, Wragg RT, et al. Mechanism-based rescue of Munc18-1 dysfunction in varied encephalopathies by chemical chaperones. Nat Commun. 2018 Dec;9(1):3986.

11. Halachmi N, Lev Z. The Sec1 family: a novel family of proteins involved in synaptic transmission and general secretion. J Neurochem. 1996 Mar;66(3):889–97.

12. Voets T, Toonen RF, Brian EC, de Wit H, Moser T, Rettig J, et al. Munc18-1 promotes large dense-core vesicle docking. Neuron. 2001;31(4):581–92.

13. Harrison SD, Broadie K, Goor J van de, Rubin GM. Mutations in the *drosophila* Rop gene suggest a function in general secretion and synaptic transmission. Neuron. 1994 Sep 1;13(3):555–66.

14. Feizi A, Gatto F, Uhlen M, Nielsen J. Human protein secretory pathway genes are expressed in a tissue-specific pattern to match processing demands of the secretome. Npj Syst Biol Appl. 2017 Aug 18;3(1):1–9.

15. Pelham HRB. SNAREs and the secretory pathway - lessons from yeast. Exp Cell Res. 1999 Feb 25;247(1):1–8.

16. Almers W. Exocytosis. Annu Rev Physiol. 1990;52(1):607–24.

17. Katz B. The release of neural transmitter substances. Springfield, Ill.: Thomas; 1969. 60 p. (Sherrington lectures).

18. Tooze SA, Martens GJM, Huttner WB. Secretory granule biogenesis: rafting to the SNARE. Trends Cell Biol. 2001 Mar 1;11(3):116–22.

19. Burgoyne R, Morgan A. Regulated exocytosis. Biochem J. 1993 Jul 15;293(Pt 2):305–16.

20. Hille B, Billiard J, Babcock DF, Nguyen T, Koh DS. Stimulation of exocytosis without a calcium signal. J Physiol. 1999 Oct 1;520(Pt 1):23–31.

21. Südhof TC. The presynaptic active zone. Neuron. 2012 Jul 12;75(1):11–25.

22. Bruns D, Jahn R. Real-time measurement of transmitter release from single synaptic vesicles. Nature. 1995 Sep;377(6544):62–5.

23. Bar-Peled M, Bassham DC, Raikhel NV. Transport of proteins in eukaryotic cells: more questions ahead. Plant Mol Biol. 1996 Oct;32(1–2):223–49.

24. Barlowe C, Orci L, Yeung T, Hosobuchi M, Hamamoto S, Salama N, et al. COPII: a membrane coat formed by Sec proteins that drive vesicle budding from the endoplasmic reticulum. Cell. 1994 Jun 17;77(6):895–907.

25. Horton AC, Ehlers MD. Secretory trafficking in neuronal dendrites. Nat Cell Biol. 2004 Jul;6(7):585–91.

26. Ramírez OA, Couve A. The endoplasmic reticulum and protein trafficking in dendrites and axons. Trends Cell Biol. 2011 Apr 1;21(4):219–27.

27. Valenzuela JI, Perez F. Diversifying the secretory routes in neurons. Front Neurosci. 2015 Oct 7;9:358.

28. Tsukita S, Ishikawa H. Three-dimesnional distribution of smooth endoplasmic reticulum in myelinated axons. J Electron Microsc (Tokyo). 1976 Jan 1;25(3):141–9.

29. Broadwell RD, Cataldo AM. The neuronal endoplasmic reticulum: its cytochemistry and contribution to the endomembrane system. I. Cell bodies and dendrites. J Histochem Cytochem. 1983 Sep 1;31(9):1077–88.

30. Spacek J, Harris KM. Three-dimensional organisation of smooth endoplasmic reticulum in hippocampal CA1 dendrites and dendritic spines of the immature and mature rat. J Neurosci. 1997 Jan 1;17(1):190–203.

31. Gardiol A, Racca C, Triller A. Dendritic and postsynaptic protein synthetic machinery. J Neurosci. 1999 Jan 1;19(1):168–79.

32. Appenzeller-Herzog C, Hauri HP. The ER-Golgi intermediate compartment (ERGIC): in search of its identity and function. J Cell Sci. 2006 Jun 1;119(11):2173–83.

33. Cooper GM. The Golgi Apparatus. The cell: A molecular approach. 2nd Ed. 2000 [cited 2022 Dec 30]

34. Jackson CL. Mechanisms of transport through the Golgi complex. J Cell Sci. 2009 Feb 15;122(Pt 4):443–52.

35. Mogelsvang S, Marsh BJ, Ladinsky MS, Howell KE. Predicting function from structure: 3d structure studies of the mammalian golgi complex. Traffic. 2004;5(5):338–45.

36. James Morré D, Mollenhauer HH. Microscopic morphology and the origins of the membrane maturation model of Golgi apparatus function. Int Rev Cytol. 2007;262:191–218.

37. Rambourg A, Jackson CL, Clermont Y. Three dimensional configuration of the secretory pathway and segregation of secretion granules in the yeast Saccharomyces cerevisiae. J Cell Sci. 2001 Jun;114(Pt 12):2231–9.

38. Matsuura-Tokita K, Takeuchi M, Ichihara A, Mikuriya K, Nakano A. Live imaging of yeast Golgi cisternal maturation. Nature. 2006 Jun 22;441(7096):1007–10.

39. Sudhof TC, Rizo J. Synaptic vesicle exocytosis. Cold Spring Harb Perspect Biol. 2011 Jan 12;3(12):a005637.

40. Jung JH, Szule JA, Marshall RM, McMahan UJ. Variable priming of a docked synaptic vesicle. Proc Natl Acad Sci. 2016 Feb 23;113(8):E1098–107.

41. Calahorro F, Izquierdo PG. The presynaptic machinery at the synapse of C. elegans. Invert Neurosci. 2018 [cited 2020 Apr 15];18(2). Available from:

42. Rizo J, Rosenmund C. Synaptic vesicle fusion. Nat Struct Mol Biol. 2008;15(7):665–74.

43. Lin RC, Scheller RH. Mechanisms of synaptic vesicle exocytosis. Annu Rev Cell Dev Biol. 2000;16:19–49.

44. Haucke V, Neher E, Sigrist SJ. Protein scaffolds in the coupling of synaptic exocytosis and endocytosis. Nat Rev Neurosci. 2011 Mar;12(3):127–38.

45. Balch WE, Dunphy WG, Braell WA, Rothman JE. Reconstitution of the transport of protein between successive compartments of the golgi measured by the coupled incorporation of N-acetylglucosamine. Cell. 1984 Dec;39(2):405–16.

46. Ungar D, Hughson FM. SNARE protein structure and function. Annu Rev Cell Dev Biol. 2003;19:493–517.

47. Jahn R, Scheller RH. SNAREs--engines for membrane fusion. Nat Rev Mol Cell Biol. 2006 Sep;7(9):631–43.

48. Bennett MK, Calakos N, Scheller RH. Syntaxin: a synaptic protein implicated in docking of synaptic vesicles at presynaptic active zones. Science. 1992 Jul 10;257(5067):255–9.

49. Oyler GA, Higgins GA, Hart RA, Battenberg E, Billingsley M, Bloom FE, et al. The identification of a novel synaptosomal-associated protein, SNAP-25, differentially expressed by neuronal subpopulations. J Cell Biol. 1989 Dec;109(6 Pt 1):3039–52.

50. Südhof TC, Baumert M, Perin MS, Jahn R. A synaptic vesicle membrane protein is conserved from mammals to Drosophila. Neuron. 1989 May;2(5):1475–81.

51. Baumert M, Maycox PR, Navone F, De Camilli P, Jahn R. Synaptobrevin: an integral membrane protein of 18,000 daltons present in small synaptic vesicles of rat brain. EMBO J. 1989 Feb;8(2):379–84.

52. Trimble WS, Cowan DM, Scheller RH. VAMP-1: a synaptic vesicle-associated integral membrane protein. Proc Natl Acad Sci U S A. 1988 Jun;85(12):4538–42.

53. Söllner T, Whiteheart SW, Brunner M, Erdjument-Bromage H, Geromanos S, Tempst P, et al. SNAP receptors implicated in vesicle targeting and fusion. Nature. 1993 Mar 25;362(6418):318–24.

54. Fasshauer D, Sutton RB, Brunger AT, Jahn R. Conserved structural features of the synaptic fusion complex: SNARE proteins reclassified as Q- and R-SNAREs. Proc Natl Acad Sci U S A. 1998 Dec 22;95(26):15781–6.

55. Saifee O, Wei L, Nonet ML. The *Caenorhabditis elegans unc-64* locus encodes a syntaxin that interacts genetically with synaptobrevin. Mol Biol Cell. 1998 Jun;9(6):1235–52.

56. Fang Q, Lindau M. How could SNARE proteins open a fusion pore? Physiology. 2014 Jul;29(4):278–85.

57. Lonart G, Sudhof TC. Assembly of SNARE core complexes prior to neurotransmitter release sets the readily releasable pool of synaptic vesicles. J Biol Chem. 2000;275(36):27703–7.

58. Weimer RM, Jorgensen EM. Controversies in synaptic vesicle exocytosis. J Cell Sci. 2003;116:3661–6.

59. Sutton RB, Fasshauer D, Jahn R, Brunger AT. Crystal structure of a SNARE complex involved in synaptic exocytosis at 2.4 A resolution. Nature. 1998 Sep 24;395(6700):347–53.

60. Broadie K, Prokop A, Bellen HJ, O'Kane CJ, Schulze KL, Sweeney ST. Syntaxin and synaptobrevin function downstream of vesicle docking in *Drosophila*. Neuron. 1995 Sep;15(3):663–73.

61. Schulze KL, Broadie K, Perin MS, Bellen HJ. Genetic and electrophysiological studies of *Drosophila* syntaxin-1A demonstrate its role in nonneuronal secretion and neurotransmission. Cell. 1995 Jan 27;80(2):311–20.

62. Nonet ML, Saifee O, Zhao H, Rand JB, Wei L. Synaptic transmission deficits in *Caenorhabditis elegans* synaptobrevin mutants. J Neurosci Off J Soc Neurosci. 1998 Jan 1;18(1):70–80.

63. Deitcher DL, Ueda A, Stewart BA, Burgess RW, Kidokoro Y, Schwarz TL. Distinct requirements for evoked and spontaneous release of neurotransmitter are revealed by mutations in the *Drosophila* gene neuronal-synaptobrevin. J Neurosci Off J Soc Neurosci. 1998 Mar 15;18(6):2028–39.

64. Washbourne P, Thompson PM, Carta M, Costa ET, Mathews JR, Lopez-Benditó G, et al. Genetic ablation of the t-SNARE SNAP-25 distinguishes mechanisms of neuroexocytosis. Nat Neurosci. 2002 Jan;5(1):19–26.

65. Schoch S, Deák F, Königstorfer A, Mozhayeva M, Sara Y, Südhof TC, et al. SNARE function analysed in synaptobrevin/VAMP knockout mice. Science. 2001 Nov 2;294(5544):1117–22.

66. Fiebig KM, Rice LM, Pollock E, Brunger AT. Folding intermediates of SNARE complex assembly. Nat Struct Biol. 1999 Feb;6(2):117–23.

67. Ma C, Su L, Seven AB, Xu Y, Rizo J. Reconstitution of the vital functions of Munc18 and Munc13 in neurotransmitter release. Science. 2013 Jan 25;339(6118):421–5.

68. Xiao W, Poirier MA, Bennett MK, Shin YK. The neuronal t-SNARE complex is a parallel four-helix bundle. Nat Struct Biol. 2001 Apr;8(4):308–11.

69. Zhang F, Chen Y, Kweon DH, Kim CS, Shin YK. The four-helix bundle of the neuronal target membrane SNARE complex is neither disordered in the middle nor uncoiled at the C-terminal region. J Biol Chem. 2002 Jul 5;277(27):24294–8.

70. Poirier MA, Xiao W, Macosko JC, Chan C, Shin YK, Bennett MK. The synaptic SNARE complex is a parallel four-stranded helical bundle. Nat Struct Biol. 1998 Sep;5(9):765–9.

71. Sørensen JB, Wiederhold K, Müller EM, Milosevic I, Nagy G, de Groot BL, et al. Sequential N- to C-terminal SNARE complex assembly drives priming and fusion of secretory vesicles. EMBO J. 2006 Mar 8;25(5):955–66.

72. Yang Y, Shin JY, Oh JM, Jung CH, Hwang Y, Kim S, et al. Dissection of SNARE-driven membrane fusion and neuroexocytosis by wedging small hydrophobic molecules into the SNARE zipper. Proc Natl Acad Sci U S A. 2010 Dec 21;107(51):22145–50.

73. Lou X, Shin YK. SNARE zippering. Biosci Rep. 2016 May 6;36(3):e00327.

74. Yoon TY, Munson M. SNARE complex assembly and disassembly. Curr Biol. 2018 Apr;28(8):R397–401.

75. Söllner T, Bennett MK, Whiteheart SW, Scheller RH, Rothman JE. A protein assembly-disassembly pathway in vitro that may correspond to sequential steps of synaptic vesicle docking, activation, and fusion. Cell. 1993 Nov 5;75(3):409–18.

76. Schweizer FE, Dresbach T, DeBello WM, O'Connor V, Augustine GJ, Betz H. Regulation of neurotransmitter release kinetics by NSF. Science. 1998 Feb 20;279(5354):1203–6.

77. Littleton JT, Chapman ER, Kreber R, Garment MB, Carlson SD, Ganetzky B. Temperature-sensitive paralytic mutations demonstrate that synaptic exocytosis requires SNARE complex assembly and disassembly. Neuron. 1998 Aug;21(2):401–13.

78. Hanson PI, Roth R, Morisaki H, Jahn R, Heuser JE. Structure and conformational changes in NSF and its membrane receptor complexes visualised by quick-freeze/deep- etch electron microscopy. Cell. 1997 Aug 8;90(3):523–35.

79. Nagiec EE, Bernstein A, Whiteheart SW. Each domain of the N-ethylmaleimide-sensitive fusion protein contributes to its transport activity. J Biol Chem. 1995 Dec 8;270(49):29182–8.

80. Whiteheart SW, Rossnagel K, Buhrow SA, Brunner M, Jaenicke R, Rothman JE. N-ethylmaleimide-sensitive fusion protein: a trimeric ATPase whose hydrolysis of ATP is required for membrane fusion. J Cell Biol. 1994 Aug;126(4):945–54.

81. Hohl TM, Parlati F, Wimmer C, Rothman JE, Söllner TH, Engelhardt H. Arrangement of Subunits in 20 S Particles consisting of NSF, SNAPs, and SNARE complexes. Mol Cell. 1998 Nov 1;2(5):539–48.

82. Huang X, Sun S, Wang X, Fan F, Zhou Q, Lu S, et al. Mechanistic insights into the SNARE complex disassembly. Sci Adv. 2019 Apr 10;5(4):eaau8164.

83. Littleton J, Barnard RJO, Titus SA, Slind J, Chapman ER, Ganetzky B. SNARE-complex disassembly by NSF follows synaptic-vesicle fusion. Proc Natl Acad Sci U S A. 2001 Oct 9;98(21):12233–8.

84. You Y, Katti S, Yu B, Igumenova TI, Das J. Probing the diacylglycerol binding site of presynaptic Munc13-1. Biochemistry. 2021 Apr 27;60(16):1286–98.

85. Betz A, Ashery U, Rickmann M, Augustin I, Neher E, Südhof TC, et al. Munc13-1 is a presynaptic phorbol ester receptor that enhances neurotransmitter release. Neuron. 1998 Jul 1;21(1):123–36.

86. Xu J, Camacho M, Xu Y, Esser V, Liu X, Trimbuch T, et al. Mechanistic insights into neurotransmitter release and presynaptic plasticity from the crystal structure of Munc13-1 C1C2BMUN. eLife. 2017 Feb 8;6:e22567.

87. Basu J, Shen N, Duluvova I, Lu J, Guan R, Guryev O, et al. A minimal domain responsible for Munc13 activity. Nat Struct Mol Biol. 2005 Nov;12(11):1017–8.

88. Junge HJ, Rhee JS, Jahn O, Varoqueaux F, Spiess J, Waxham MN, et al. Calmodulin and Munc13 form a Ca2+ sensor/effector complex that controls short-term synaptic plasticity. Cell. 2004 Aug 6;118(3):389–401.

89. Basu J, Betz A, Brose N, Rosenmund C. Munc13-1 C1 Domain activation lowers the energy barrier for synaptic vesicle fusion. J Neurosci. 2007 Jan 31;27(5):1200–10.

90. Rhee JS, Betz A, Pyott S, Reim K, Varoqueaux F, Augustin I, et al. Beta phorbol ester- and diacylglycerol-induced augmentation of transmitter release is mediated by Munc13s and not by PKCs. Cell. 2002 Jan 11;108(1):121–33.

91. Betz A, Thakur P, Junge HJ, Ashery U, Rhee JS, Scheuss V, et al. Functional interaction of the active zone proteins Munc13-1 and RIM1 in synaptic vesicle priming. Neuron. 2001 Apr;30(1):183–96.

92. Duluvova I, Lou X, Lu J, Huryeva I, Alam A, Schneggenburger R, et al. A Munc13/RIM/Rab3 tripartite complex: from priming to plasticity? EMBO J. 2005 Aug 17;24(16):2839–50.

93. Lu J, Machius M, Dulubova I, Dai H, Südhof TC, Tomchick DR, et al. Structural Basis for a Munc13–1 Homodimer to Munc13–1/RIM Heterodimer Switch. PLoS Biol. 2006 Jul;4(7):e192.

94. Shin OH, Lu J, Rhee JS, Tomchick DR, Pang ZP, Wojcik SM, et al. Munc13 C2B domain is an activity-dependent Ca2+ regulator of synaptic exocytosis. Nat Struct Mol Biol. 2010 Mar;17(3):280–8.

95. Xu T, Binz T, Niemann H, Neher E. Multiple kinetic components of exocytosis distinguished by neurotoxin sensitivity. Nat Neurosci. 1998 Jul;1(3):192–200.

96. Aravamudan B, Fergestad T, Davis WS, Rodesch CK, Broadie K. *Drosophila* Unc-13 is essential for synaptic transmission. Nat Neurosci. 1999 Nov;2(11):965–71.

97. Brose N, Hofmann K, Hata Y, Südhof TC. Mammalian homologues of *Caenorhabditis elegans unc-13* gene define novel family of C2-domain proteins. J Biol Chem. 1995 Oct 20;270(42):25273–80.

98. Richmond JE, Davis WS, Jorgensen EM. UNC-13 is required for synaptic vesicle fusion in C. elegans. Nat Neurosci. 1999 Nov;2(11):959–64.

99. Augustin I, Rosenmund C, Südhof TC, Brose N. Munc13-1 is essential for fusion competence of glutamatergic synaptic vesicles. Nature. 1999 Jul;400(6743):457–61.

100. Lackner MR, Nurrish SJ, Kaplan JM. Facilitation of Synaptic Transmission by EGL-30 Gqα and EGL-8 PLCβ: DAG Binding to UNC-13 is required to stimulate acetylcholine release. Neuron. 1999 Oct 1;24(2):335–46.

101. Ma C, Li W, Xu Y, Rizo J. Munc13 mediates the transition from the closed syntaxin–Munc18 complex to the SNARE complex. Nat Struct Mol Biol. 2011 May;18(5):542–9.

102. Wang S, Li Y, Gong J, Ye S, Yang X, Zhang R, et al. Munc18 and Munc13 serve as a functional template to orchestrate neuronal SNARE complex assembly. Nat Commun. 2019 08;10(1):69.

103. Hammarlund M, Palfreyman MT, Watanabe S, Olsen S, Jorgensen EM. Open syntaxin docks synaptic vesicles. PLOS Biol. 2007 Jul 17;5(8):e198.

104. Liu X, Seven AB, Camacho M, Esser V, Xu J, Trimbuch T, et al. Functional synergy between the Munc13 C-terminal C1 and C2 domains. eLife. 2016 May 23;5:e13696.

105. Schoch S, Castillo PE, Jo T, Mukherjee K, Geppert M, Wang Y, et al. RIM1α forms a protein scaffold for regulating neurotransmitter release at the active zone. Nature. 2002 Jan;415(6869):321–6.

106. Koushika SP, Richmond JE, Hadwiger G, Weimer RM, Jorgensen EM, Nonet ML. A post-docking role for active zone protein Rim. Nat Neurosci. 2001 Oct;4(10):997–1005.

107. Gracheva EO, Hadwiger G, Nonet ML, Richmond JE. Direct interactions between C. elegans RAB-3 and Rim provide a mechanism to target vesicles to the presynaptic density. Neurosci Lett. 2008 Oct 24;444(2):137–42.

108. Castillo PE, Schoch S, Schmitz F, Südhof TC, Malenka RC. RIM1alpha is required for presynaptic long-term potentiation. Nature. 2002 Jan 17;415(6869):327–30.

109. Calakos N, Schoch S, Südhof TC, Malenka RC. Multiple roles for the active zone protein RIM1α in late stages of neurotransmitter Release. Neuron. 2004 Jun 24;42(6):889–96.

110. Deng L, Kaeser PS, Xu W, Südhof TC. RIM proteins activate vesicle priming by reversing autoinhibitory homodimerisation of Munc13. Neuron. 2011 Jan 27;69(2):317–31.

111. Sauvola CW, Littleton JT. SNARE regulatory proteins in synaptic vesicle fusion and recycling. Front Mol Neurosci. 2021 Aug 6;14:733138.

112. Gallegos ME, Balakrishnan S, Chandramouli P, Arora S, Azameera A, Babushekar A, et al. The C. elegans Rab family: identification, classification and toolkit construction. PLOS ONE. 2012 Nov 21;7(11):e49387.

113. Bennett MK, Scheller RH. The molecular machinery for secretion is conserved from yeast to neurons. Proc Natl Acad Sci. 2006;90:2559–63.

114. Schlüter OM, Khvotchev M, Jahn R, Südhof TC. Localisation versus function of Rab3 proteins: evidence for a common regulatory role in controlling fusion. J Biol Chem. 2002 Oct 25;277(43):40919–29.

115. Fischer von Mollard G, Stahl B, Walch-Solimena C, Takei K, Daniels L, Khoklatchev A, et al. Localisation of Rab5 to synaptic vesicles identifies endosomal intermediate in synaptic vesicle recycling pathway. Eur J Cell Biol. 1994 Dec 1;65(2):319–26.

116. Khvotchev MV, Ren M, Takamori S, Jahn R, Südhof TC. Divergent functions of neuronal Rab11b in Ca2+-regulated versus constitutive exocytosis. J Neurosci. 2003 Nov 19;23(33):10531–9.

117. Geppert M, Bolshakov VY, Siegelbaum SA, Takei K, De Camilli P, Hammer RE, et al. The role of Rab3A in neurotransmitter release. Nature. 1994 Jun;369(6480):493–7.

118. Nonet ML, Staunton JE, Kilgard MP, Fergestad T, Hartwieg E, Horvitz HR, et al. *Caenorhabditis elegans rab-3* mutant synapses exhibit impaired function and are partially depleted of vesicles. J Neurosci. 1997 Nov 1;17(21):8061–73.

119. Littleton JT, Bai J, Vyas B, Desai R, Baltus AE, Garment MB, et al. synaptotagmin mutants reveal essential functions for the C2B domain in Ca2+-triggered fusion and recycling of synaptic vesicles in vivo. J Neurosci Off J Soc Neurosci. 2001 Mar 1;21(5):1421–33.

120. Rizo J, Chen X, Araç D. Unraveling the mechanisms of synaptotagmin and SNARE function in neurotransmitter release. Trends Cell Biol. 2006 Jul 1;16(7):339–50.

121. Chapman ER. Synaptotagmin: A Ca2+ sensor that triggers exocytosis? Nat Rev Mol Cell Biol. 2002 Jul;3(7):498–508.

122. Chapman ER, Jahn R. Calcium-dependent interaction of the cytoplasmic region of synaptotagmin with membranes. Autonomous function of a single C2-homologous domain. J Biol Chem. 1994 Feb 25;269(8):5735–41.

123. Brose N, Petrenko AG, Südhof TC, Jahn R. Synaptotagmin: a calcium sensor on the synaptic vesicle surface. Science. 1992 May 15;256(5059):1021–5.

124. Elferink LA, Peterson MR, Scheller RH. A role for synaptotagmin (p65) in regulated exocytosis. Cell. 1993 Jan 15;72(1):153–9.

125. Fukuda M, Moreira JE, Lewis FM, Sugimori M, Niinobe M, Mikoshiba K, et al. Role of the C2B domain of synaptotagmin in vesicular release and recycling as determined by specific antibody injection into the squid giant synapse preterminal. Proc Natl Acad Sci U S A. 1995 Nov 7;92(23):10708–12.

126. Mikoshiba K, Fukuda M, Moreira JE, Lewis FM, Sugimori M, Niinobe M, et al. Role of the C2A domain of synaptotagmin in transmitter release as determined by specific antibody injection into the squid giant synapse preterminal. Proc Natl Acad Sci U S A. 1995 Nov 7;92(23):10703–7.

127. Bommert K, Charlton MP, DeBello WM, Chin GJ, Betz H, Augustine GJ. Inhibition of neurotransmitter release by C2-domain peptides implicates synaptotagmin in exocytosis. Nature. 1993 May 13;363(6425):163–5.

128. Nonet ML, Grundahl K, Meyer BJ, Rand JB. Synaptic function is impaired but not eliminated in *C. elegans* mutants lacking synaptotagmin. Cell. 1993 Jul 2;73(7):1291–305.

129. DiAntonio A, Parfitt KD, Schwarz TL. Synaptic transmission persists in synaptotagmin mutants of *Drosophila*. Cell. 1993 Jul 2;73(7):1281–90.

130. Littleton JT, Stern M, Schulze K, Perin M, Bellen HJ. Mutational analysis of *Drosophila* synaptotagmin demonstrates its essential role in Ca(2+)-activated neurotransmitter release. Cell. 1993 Sep 24;74(6):1125–34.

131. Geppert M, Goda Y, Hammer RE, Li C, Rosahl TW, Stevens CF, et al. Synaptotagmin I: a major Ca2+ sensor for transmitter release at a central synapse. Cell. 1994 Nov 18;79(4):717–27.

132. Chen X, Tomchick DR, Kovrigin E, Araç D, Machius M, Südhof TC, et al. Three-dimensional structure of the complexin/SNARE complex. Neuron. 2002 Jan 31;33(3):397–409.

133. Xue M, Reim K, Chen X, Chao HT, Deng H, Rizo J, et al. Distinct domains of complexin I differentially regulate neurotransmitter release. Nat Struct Mol Biol. 2007 Oct;14(10):949–58.

134. Maximov A, Tang J, Yang X, Pang ZP, Südhof TC. Complexin controls the force transfer from SNARE complexes to membranes in fusion. Science. 2009 Jan 23;323(5913):516–21.

135. Kaeser-Woo YJ, Yang X, Südhof TC. C-terminal complexin sequence is selectively required for clamping and priming but not for Ca2+ triggering of synaptic exocytosis. J Neurosci Off J Soc Neurosci. 2012 Feb 22;32(8):2877–85.

136. Martin JA, Hu Z, Fenz KM, Fernandez J, Dittman JS. Complexin has opposite effects on two modes of synaptic vesicle fusion. Curr Biol CB. 2011 Jan 25;21(2):97–105.

137. Tang J, Maximov A, Shin O, Dai H, Rizo J, Südhof TC. A complexin/synaptotagmin 1 switch controls fast synaptic vesicle exocytosis. Cell. 2006 Sep 22;126(6):1175–87.

138. Imig C, Min SW, Krinner S, Arancillo M, Rosenmund C, Südhof TC, et al. The morphological and molecular nature of synaptic vesicle priming at presynaptic active zones. Neuron. 2014 Oct 22;84(2):416–31.

139. Hobson RJ, Liu Q, Watanabe S, Jorgensen EM. Complexin maintains vesicles in the primed state in C. elegans. Curr Biol CB. 2011 Jan 25;21(2):106–13.

140. Malsam J, Bärfuss S, Trimbuch T, Zarebidaki F, Sonnen AFP, Wild K, et al. Complexin suppresses spontaneous exocytosis by capturing the membrane-proximal regions of VAMP2 and SNAP25. Cell Rep. 2020 Jul 21;32(3):107926.

141. Fujita Y, Shirataki H, Sakisaka T, Asakura T, Ohya T, Kotani H, et al. Tomosyn: a syntaxin-1-binding protein that forms a novel complex in the neurotransmitter release process. Neuron. 1998 May;20(5):905–15.

142. Hatsuzawa K, Lang T, Fasshauer D, Bruns D, Jahn R. The R-SNARE motif of tomosyn forms SNARE core complexes with syntaxin 1 and SNAP-25 and down-regulates exocytosis. J Biol Chem. 2003 Aug 15;278(33):31159–66.

143. Masuda ES, Huang BC, Fisher JM, Luo Y, Scheller RH. Tomosyn binds t-SNARE proteins via a VAMP-like coiled coil. Neuron. 1998 Sep;21(3):479–80.

144. Mcewen JM, Madison JM, Dybbs M, Kaplan JM. Antagonistic regulation of synaptic vesicle priming by tomosyn and UNC-13. Neuron. 2006 Aug 3;51(3):303–15.

145. Ann K, Kowalchyk JA, Loyet KM, Martin TFJ. Novel Ca2+-binding Protein (CAPS) Related to UNC-31 Required for Ca2+-activated Exocytosis. J Biol Chem. 1997 Aug 8;272(32):19637–40.

146. Sadakata T, Washida M, Iwayama Y, Shoji S, Sato Y, Ohkura T, et al. Autistic-like phenotypes in Cadps2-knockout mice and aberrant CADPS2 splicing in autistic patients. J Clin Invest. 2007 Apr;117(4):931–43.

147. Rizo J, Südhof TC. C2-domains, structure and function of a universal Ca2+-binding domain. J Biol Chem. 1998 Jun 26;273(26):15879–82.

148. Lemmon MA. Membrane recognition by phospholipid-binding domains. Nat Rev Mol Cell Biol. 2008 Feb;9(2):99–111.

149. Grishanin RN, Kowalchyk JA, Klenchin VA, Ann K, Earles CA, Chapman ER, et al. CAPS acts at a prefusion step in dense-core vesicle exocytosis as a PIP2 binding protein. Neuron. 2004 Aug 19;43(4):551–62.

150. Speidel D, Varoqueaux F, Enk C, Nojiri M, Grishanin RN, Martin TFJ, et al. A family of Ca2+-dependent activator proteins for secretion: comparative analysis of structure, expression, localisation, and function. J Biol Chem. 2003 Dec 26;278(52):52802–9.

151. Speese S, Petrie M, Schuske K, Ailion M, Ann K, Iwasaki K, et al. UNC-31 (CAPS) is required for dense-core vesicle but not synaptic vesicle exocytosis in *Caenorhabditis elegans*. J Neurosci Off J Soc Neurosci. 2007 Jun 6;27(23):6150–62.

152. Jockusch WJ, Speidel D, Sigler A, Sørensen JB, Varoqueaux F, Rhee JS, et al. CAPS-1 and CAPS-2 are essential synaptic vesicle priming proteins. Cell. 2007 Nov 16;131(4):796–808.

153. Renden R, Berwin B, Davis W, Ann K, Chin CT, Kreber R, et al. *Drosophila* CAPS is an essential gene that regulates dense-core vesicle release and synaptic vesicle fusion. Neuron. 2001 Aug 16;31(3):421–37.

154. Liu Y, Schirra C, Edelmann L, Matti U, Rhee J, Hof D, et al. Two distinct secretory vesicle–priming steps in adrenal chromaffin cells. J Cell Biol. 2010 Sep 20;190(6):1067–77.

155. Kabachinski G, Yamaga M, Kielar-Grevstad DM, Bruinsma S, Martin TFJ. CAPS and Munc13 utilise distinct PIP2-linked mechanisms to promote vesicle exocytosis. Mol Biol Cell. 2014 Feb;25(4):508–21.

156. Zhou H, Wei Z, Wang S, Yao D, Zhang R, Ma C. Structural and functional analysis of the CAPS SNARE-binding domain required for SNARE complex formation and exocytosis. Cell Rep. 2019 Mar 19;26(12):3347-3359.e6.

157. Novick P, Field C, Schekman R. Identification of 23 complementation groups required for post-translational events in the yeast secretory pathway. Cell. 1980 Aug;21(1):205–15.

158. Aalto MK, Jäntti J, Östling J, Keränen S, Ronne H. Mso1p: A yeast protein that functions in secretion and interacts physically and genetically with Sec1p. Proc Natl Acad Sci. 1997 Jul 8;94(14):7331–6.

159. Ossig R, Dascher C, Trepte HH, Schmitt HD, Gallwitz D. The yeast SLY gene products, suppressors of defects in the essential GTP-binding Ypt1 protein, may act in endoplasmic reticulum-to-Golgi transport. Mol Cell Biol. 1991 Jun;11(6):2980–93.

160. Wada Y, Kitamoto K, Kanbe T, Tanaka K, Anraku Y. The SLP1 gene of Saccharomyces cerevisiae is essential for vacuolar morphogenesis and function. Mol Cell Biol. 1990 May;10(5):2214–23.

161. Cowles CR, Emr SD, Horazdovsky BF. Mutations in the VPS45 gene, a SEC1 homologue, result in vacuolar protein sorting defects and accumulation of membrane vesicles. J Cell Sci. 1994 Dec 1;107(12):3449–59.

162. Novick P, Schekman R. Secretion and cell-surface growth are blocked in a temperature- sensitive mutant of Saccharomyces cerevisiae. Proc Natl Acad Sci. 1979 Apr;76(4):1858–62.

163. Peng R, Gallwitz D. Sly1 protein bound to Golgi syntaxin Sed5p allows assembly and contributes to specificity of SNARE fusion complexes. J Cell Biol. 2002 May 13;157(4):645–55.

164. Aalto MK, Ronne H, Keränen S. Yeast syntaxins Sso1p and Sso2p belong to a family of related membrane proteins that function in vesicular transport. EMBO J. 1993 Nov;12(11):4095–104.

165. Garcia EP, McPherson PS, Chilcote TJ, Takei K, De Camilli P. rbSec1A and B colocalise with syntaxin 1 and SNAP-25 throughout the axon, but are not in a stable complex with syntaxin. J Cell Biol. 1995 Apr;129(1):105–20.

166. Hosono R, Kamiya Y. Additional genes which result in an elevation of acetylcholine levels by mutations in *Caenorhabditis elegans*. Neurosci Lett. 1991 Jul 22;128(2):243–4.

167. Nguyen M, Alfonso A, Johnson CD, Rand JB. *Caenorhabditis elegans* mutants resistant to inhibitors of acetylcholinesterase. Genetics. 1995 Jun;140(2):527–35.

168. Weimer RM, Richmond JE, Davis WS, Hadwiger G, Nonet ML, Jorgensen EM. Defects in synaptic vesicle docking in *unc-18* mutants. Nat Neurosci. 2003;6(10).

169. Sassa T, Harada S ichi, Ogawa H, Rand JB, Maruyama IN, Hosono R. Regulation of the UNC-18–*Caenorhabditis elegans* syntaxin complex by UNC-13. J Neurosci. 1999 Jun 15;19(12):4772–7.

170. Gengyo-Ando K, Kamiya Y, Yamakawa A, Kodaira K, Nishiwaki K, Miwa J, et al. The *C. elegans unc-18* gene encodes a protein expressed in motor neurons. Neuron. 1993 Oct;11(4):703–11.

171. Salzberg A, Cohen N, Halachmi N, Kimchie Z, Lev Z. The *Drosophila* Ras2 and Rop gene pair: a dual homology with a yeast Ras-like gene and a suppressor of its loss-of- function phenotype. Dev Camb Engl. 1993 Apr;117(4):1309–19.

172. Wu MN, Fergestad T, Lloyd TE, He Y, Broadie K, Bellen HJ. Syntaxin 1A interacts with multiple exocytic proteins to regulate neurotransmitter release *in vivo.* Neuron. 1999 Jul 1;23(3):593–605.

173. Hata Y, Binz T, Niemann H, McMahon H, Hayashi T, Südhof TC, et al. Synaptic vesicle membrane fusion complex: action of clostridial neurotoxins on assembly. EMBO J. 1994;13(21):5051–61.

174. Pevsner J, Hsu SC, Scheller RH. n-Sec1: a neural-specific syntaxin-binding protein. Proc Natl Acad Sci. 1994 Feb 15;91(4):1445–9.

175. Pevsner J, Hsu SC, Braun JEA, Calakos N, Ting AE, Bennett MK, et al. Specificity and regulation of a synaptic vesicle docking complex. Neuron. 1994 Aug 1;13(2):353–61.

176. Calakos N, Bennett MK, Peterson KE, Scheller RH. Protein-protein interactions contributing to the specificity of intracellular vesicular trafficking. Science. 1994 Feb 25;263(5150):1146–9.

177. Misura KMS, Scheller RH, Weis WI. Three-dimensional structure of the neuronal-Sec1–syntaxin 1a complex. Nature. 2000;404(6776):355–62.

178. Gengyo-Ando K, Kamiya Y, Yamakawa A, Kodaira K, Nishiwaki K, Miwa J, et al. The *C. elegans unc-18* gene encodes a protein expressed in motor neurons. Neuron. 1993 Oct;11(4):703–11.

179. Verhage M, Maia AS, Plomp JJ, Brussaard AB, Heeroma JH, Vermeer H, et al. Synaptic assembly of the brain in the absence of neurotransmitter secretion. Science. 2000 Feb;287(5454):864–864.

180. Rowe J, Corradi N, Malosio ML, Taverna E, Halban P, Meldolesi J, et al. Blockade of membrane transport and disassembly of the Golgi complex by expression of syntaxin 1A in neurosecretion-incompetent cells: prevention by rbSEC1. J Cell Sci. 1999 Jun;112 (Pt 12):1865–77.

181. Mcewen JM, Kaplan JM. UNC-18 promotes both the anterograde trafficking and synaptic function of syntaxin. Mol Biol Cell. 2008;19:3836–46.

182. Shen J, Tareste DC, Paumet F, Rothman JE, Melia TJ. Selective activation of cognate SNAREpins by Sec1/Munc18 proteins. Cell. 2007 Jan 12;128(1):183–95.

183. Rodkey TL, Liu S, Barry M, McNew JA. Munc18a scaffolds SNARE assembly to promote membrane fusion. Mol Biol Cell. 2008 Dec;19(12):5422–34.

184. Toonen RF, Kochubey O, de Wit H, Gulyas-Kovacs A, Konijnenburg B, Sørensen JB, et al. Dissecting docking and tethering of secretory vesicles at the target membrane. EMBO J. 2006/08/10 ed. 2006 Aug;25(16):3725–37.

185. Duluvova I, Sugita S, Hill S, Hosaka M, Fernandez I, Südhof TC, et al. A conformational switch in syntaxin during exocytosis: role of Munc18. EMBO J. 1999 Aug;18(16):4372–82.

186. Pérez-Branguli F, Muhaisen A, Blasi J. Munc 18a Binding to syntaxin 1A and 1B isoforms defines its localisation at the plasma membrane and blocks SNARE assembly in a three-hybrid system Assay. Mol Cell Neurosci. 2002 Jun 1;20(2):169–80.

187. Schulze KL, Littleton JT, Salzberg A, Halachmi N, Stern M, Lev Z, et al. rop, a Drosophila homolog of yeast Sec1 and vertebrate n-Sec1/Munc-18 proteins, is a negative regulator of neurotransmitter release *in vivo*. Neuron. 1994 Nov;13(5):1099–108.

188. Wu MN, Littleton JT, Bhat MA, Prokop A, Bellen HJ. ROP, the *Drosophila* Sec1 homolog, interacts with syntaxin and regulates neurotransmitter release in a dosage- dependent manner. EMBO J. 1998 Jan 2;17(1):127–39.

189. Chen X, Lu J, Dulubova I, Rizo J. NMR Analysis of the closed conformation of Syntaxin-1. J Biomol NMR. 2008 May;41(1):43–54.

190. Burkhardt P, Hattendorf DA, Weis WI, Fasshauer D. Munc18a controls SNARE assembly through its interaction with the syntaxin N-peptide. EMBO J. 2008 Apr 9;27(7):923–33.

191. Medine C, Rickman C, Chamberlain L, Duncan R. Munc18-1 prevents the formation of ectopic SNARE complexes in living cells. J Cell Sci. 2008 Jan 1;120:4407–15.

192. Rickman C, Medine CN, Bergmann A, Duncan RR. Functionally and spatially distinct modes of Munc18-syntaxin 1 interaction. J Biol Chem. 2007 Apr 20;282(16):12097–103.

193. Martinez-Arca S, Proux-Gillardeaux V, Alberts P, Louvard D, Galli T. Ectopic expression of syntaxin 1 in the ER redirects TI-VAMP- and cellubrevin-containing vesicles. J Cell Sci. 2003 Jul 1;116(13):2805–16.

194. Graham ME, Barclay JW, Burgoyne RD. Syntaxin/Munc18 interactions in the late events during vesicle fusion and release in exocytosis. J Biol Chem. 2004;279(31):32751–60.

195. Toonen RFG, De Vries KJ, Zalm R, Südhof TC, Verhage M. Munc18–1 stabilises syntaxin 1, but is not essential for syntaxin 1 targeting and SNARE complex formation. J Neurochem. 2005;93(6):1393–400.

196. Richmond JE, Weimer RM, Jorgensen EM. An open form of syntaxin bypasses the requirement for UNC-13 in vesicle priming. Nature. 2001 Jul 19;412(6844):338–41.

197. Munson M, Chen X, Cocina AE, Schultz SM, Hughson FM. Interactions within the yeast t-SNARE Sso1p that control SNARE complex assembly. Nat Struct Biol. 2000;7(10):9.

198. Dulubova I, Khvotchev M, Liu S, Huryeva I, Südhof TC, Rizo J. Munc18-1 binds directly to the neuronal SNARE complex. Proc Natl Acad Sci. 2007 Feb 20;104(8):2697–702.

199. Carr CM, Grote E, Munson M, Hughson FM, Novick PJ. Sec1p binds to snare complexes and concentrates at sites of secretion. J Cell Biol. 1999 Jul 26;146(2):333–44.

200. Scott BL, Van Komen JS, Irshad H, Liu S, Wilson KA, McNew JA. Sec1p directly stimulates SNARE-mediated membrane fusion *in vitro*. J Cell Biol. 2004 Oct 11;167(1):75–85.

201. Graham M, Handley MTW, Barclay JW, Ciufo LF, Barrow SL, Morgan A, et al. A *gain-of-function* mutant of Munc18-1 stimulates secretory granule recruitment and exocytosis and reveals a direct interaction of Munc18-1 with Rab3. Biochem J. 2007 Dec 21;409(2):407–16.

202. Burgoyne RD, Barclay JW, Ciufo LF, Graham ME, Handley MTW, Morgan A. The functions of Munc18-1 in regulated exocytosis. Ann N Y Acad Sci. 2009 Jan;1152:76–86.

203. Graham ME, Prescott GR, Johnson JR, Jones M, Walmesley A, Haynes LP, et al. Structure-function study of mammalian Munc18-1 and *C. elegans* UNC-18 implicates domain 3b in the regulation of exocytosis. PLoS ONE. 2011;6(3). Available from: www.plosone.org

204. Gracheva EO, Maryon EB, Berthelot-Grosjean M, Richmond JE. Differential regulation of synaptic vesicle tethering and docking by UNC-18 and TOM-1. Front Synaptic Neurosci. 2010;2(141).

205. Lee S, Shin J, Jung Y, Son H, Shin J, Jeong C, et al. Munc18-1 induces conformational changes of syntaxin-1 in multiple intermediates for SNARE assembly. Sci Rep. 2020 Jul 15;10(1):11623.

206. Dawidowski D, Cafiso DS. Munc18-1 and the Syntaxin-1 N terminus regulate open-closed states in a t-SNARE Complex. Struct Lond Engl 1993. 2016 Mar 1;24(3):392–400.

207. Baker RW, Jeffrey PD, Zick M, Phillips BP, Wickner WT, Hughson FM. A direct role for the Sec1/Munc18-family protein Vps33 as a template for SNARE assembly. Science. 2015 Sep 4;349(6252):1111–4.

208. Jiao J, He M, Port SA, Baker RW, Xu Y, Qu H, et al. Munc18-1 catalyses neuronal SNARE assembly by templating SNARE association. eLife. 2018 Dec 12;7:e41771.

209. Shu T, Jin H, Rothman JE, Zhang Y. Munc13-1 MUN domain and Munc18-1 cooperatively chaperone SNARE assembly through a tetrameric complex. Proc Natl Acad Sci. 2020 Jan 14;117(2):1036–41.

210. Rizo J, Südhof TC. SNAREs and Munc18 in synaptic vesicle fusion. Nat Rev Neurosci. 2002 Aug;3(8):641–53.

211. Li W, Ma C, Guan R, Xu Y, Tomchick DR, Rizo J. The crystal structure of a Munc13 C-terminal module exhibits a remarkable similarity to vesicle tethering factors. Struct Lond Engl 1993. 2011 Oct 12;19(10):1443–55.

212. Shuang R, Zhang L, Fletcher A, Groblewski GE, Pevsner J, Stuenkel EL. Regulation of Munc-18/syntaxin 1A interaction by cyclin-dependent kinase 5 in nerve endings. J Biol Chem. 1998 Feb 27;273(9):4957–66.

213. Fujita Y, Sasaki T, Fukui K, Kotani H, Kimura T, Hata Y, et al. Phosphorylation of Munc-18/n-Sec1/rbSec1 by protein kinase C: its implication in regulating the interaction of Munc-18/n-Sec1/rbSec1 with syntaxin. J Biol Chem. 1996 Mar 29;271(13):7265–8.

214. Barclay JW, Craig TJ, Fisher RJ, Ciufo LF, Evans GJO, Morgan A, et al. Phosphorylation of Munc18 by Protein Kinase C Regulates the Kinetics of Exocytosis. J Biol Chem. 2003 Mar;278(12):10538–45.

215. Hokin LE, Hokin MR. Effects of acetylcholine on the turnover of phosphoryl units in individual phospholipids of pancreas slices and brain cortex slices. Biochim Biophys Acta. 1955 Sep;18(1):102–10.

216. Sakane F, Imai SI, Kai M, Yasuda S, Kanoh H. Diacylglycerol kinases: why so many of them? Biochim Biophys Acta. 2007 Jul;1771(7):793–806.

217. van Blitterswijk WJ, Houssa B. Properties and functions of diacylglycerol kinases. Cell Signal. 2000 Oct;12(9–10):595–605.

218. Sanjuán MA, Jones DR, Izquierdo M, Mérida I. Role of Diacylglycerol Kinase α in the Attenuation of Receptor Signaling. J Cell Biol. 2001 Apr 2;153(1):207–20.

219. Nagaya H, Wada I, Jia YJ, Kanoh H. Diacylglycerol Kinase δ Suppresses ER-to-Golgi Traffic via Its SAM and PH Domains. Mol Biol Cell. 2002 Jan;13(1):302–16.

220. Topham MK, Bunting M, Zimmerman GA, McIntyre TM, Blackshear PJ, Prescott SM. Protein kinase C regulates the nuclear localisation of diacylglycerol kinase-zeta. Nature. 1998 Aug 13;394(6694):697–700.

221. Topham MK, Prescott SM. Mammalian diacylglycerol kinases, a family of lipid kinases with signaling functions *. J Biol Chem. 1999 Apr 23;274(17):11447–50.

222. Klauck TM, Xu X, Mousseau B, Jaken S. Cloning and characterisation of a glucocorticoid-induced diacylglycerol kinase *. J Biol Chem. 1996 Aug 16;271(33):19781–8.

223. Merida IM´, Avila-Flores A, Merino E. Diacylglycerol kinases: at the hub of cell signalling. Biochem J. 2008;409:1–18.

224. Nurrish S, Ségalat L, Kaplan JM. Serotonin inhibition of synaptic transmission: Galpha(0) decreases the abundance of UNC-13 at release sites. Neuron. 1999 Sep;24(1):231–42.

225. McMullan R, Hiley E, Morrison P, Nurrish SJ. Rho is a presynaptic activator of neurotransmitter release at pre-existing synapses in C. elegans. Genes Dev. 2006 Jan 1;20(1):65–76.

226. Miller KG, Alfonso A, Nguyen M, Crowell JA, Johnson CD, Rand JB. A genetic selection for *Caenorhabditis elegans* synaptic transmission mutants. Proc Natl Acad Sci U S A. 1996 Oct;93(22):12593–8.

227. Jose AM, Koelle MR. Domains, amino acid residues, and new isoforms of caenorhabditis elegans diacylglycerol kinase 1 (DGK-1) important for terminating diacylglycerol signaling *in vivo*. J Biol Chem. 2005 Jan 28;280(4):2730–6.

228. Raghu P, Usher K, Jonas S, Chyb S, Polyanovsky A, Hardie RC. Constitutive activity of the light-sensitive channels TRP and TRPL in the *Drosophila* diacylglycerol kinase mutant, rdgA. Neuron. 2000 Apr 1;26(1):169–79.

229. Hardie RC, Martin F, Chyb S, Raghu P. Rescue of light responses in the *Drosophila* "null" phospholipase c mutant, norpAP24, by the diacylglycerol kinase mutant, rdgA, and by metabolic inhibition *. J Biol Chem. 2003 May 23;278(21):18851–8.

230. Horn A, Jaiswal JK. Structural and signaling role of lipids in plasma membrane repair. Curr Top Membr. 2019;84:67–98.

231. Lang T, Halemani ND, Rammner B. Interplay between lipids and the proteinaceous membrane fusion machinery. Prog Lipid Res. 2008 Nov;47(6):461–9.

232. Kooijman EE, Chupin V, de Kruijff B, Burger KNJ. Modulation of membrane curvature by phosphatidic acid and lysophosphatidic acid. Traffic Cph Den. 2003 Mar;4(3):162–74.

233. Chernomordik L, Chanturiya A, Green J, Zimmerberg J. The hemifusion intermediate and its conversion to complete fusion: regulation by membrane composition. Biophys J. 1995 Sep;69(3):922–9.

234. Salaün C, James DJ, Chamberlain LH. lipid rafts and the regulation of exocytosis. Traffic Cph Den. 2004 Apr;5(4):255–64.

235. Simons K, Ikonen E. Functional rafts in cell membranes. Nature. 1997 Jun;387(6633):569–72.

236. Simons K, Toomre D. Lipid rafts and signal transduction. Nat Rev Mol Cell Biol. 2000 Oct;1(1):31–9.

237. Cremona O, De Camilli P. Phosphoinositides in membrane traffic at the synapse. J Cell Sci. 2001 Mar;114(Pt 6):1041–52.

238. Martin TFJ. Role of PI(4,5)P2 in vesicle exocytosis and membrane fusion. Subcell Biochem. 2012;59:111–30.

239. Falkenburger BH, Jensen JB, Dickson EJ, Suh BC, Hille B. Phosphoinositides: lipid regulators of membrane proteins. J Physiol. 2010 Sep 1;588(Pt 17):3179–85.

240. Wenk MR, De Camilli P. Protein-lipid interactions and phosphoinositide metabolism in membrane traffic: Insights from vesicle recycling in nerve terminals. Proc Natl Acad Sci. 2004 Jun;101(22):8262–9.

241. Koch M, Holt M. Coupling exo- and endocytosis: an essential role for PIP$_2$ at the synapse. Biochim Biophys Acta. 2012 Aug;1821(8):1114–32.

242. Milosevic I, Sørensen JB, Lang T, Krauss M, Nagy G, Haucke V, et al. Plasmalemmal phosphatidylinositol-4,5-bisphosphate level regulates the releasable vesicle pool size in chromaffin cells. J Neurosci. 2005 Mar 9;25(10):2557–65.

243. Gong LW, Di Paolo G, Diaz E, Cestra G, Diaz ME, Lindau M, et al. Phosphatidylinositol phosphate kinase type I gamma regulates dynamics of large dense- core vesicle fusion. Proc Natl Acad Sci U S A. 2005 Apr 5;102(14):5204–9.

244. Olsen HL, Hoy M, Zhang W, Bertorello AM, Bokvist K, Capito K, et al. Phosphatidylinositol 4-kinase serves as a metabolic sensor and regulates priming of secretory granules in pancreatic beta cells. Proc Natl Acad Sci U S A. 2003 Apr 29;100(9):5187–92.

245. Raben DM, Barber CN. Phosphatidic acid and neurotransmission. Adv Biol Regul. 2017 Jan;63:15–21.

246. Rohrbough J, Broadie K. Lipid regulation of the synaptic vesicle cycle. Nat Rev Neurosci. 2005 Mar 1;6:139–50.

247. Cremona O, Di Paolo G, Wenk MR, Lüthi A, Kim WT, Takei K, et al. Essential role of phosphoinositide metabolism in synaptic vesicle recycling. Cell. 1999 Oct 15;99(2):179–88.

248. Martin TFJ. PI(4,5)P2 regulation of surface membrane traffic. Curr Opin Cell Biol. 2001 Aug 1;13(4):493–9.

249. Salaün C, Gould GW, Chamberlain LH. Lipid Raft Association of SNARE proteins regulates exocytosis in PC12 Cells *. J Biol Chem. 2005 May 20;280(20):19449–53.

250. Puri N, Roche PA. Ternary SNARE complexes are enriched in lipid rafts during mast cell exocytosis. Traffic. 2006;7(11):1482–94.

251. Veit M, Becher A, Ahnert-Hilger G. Synaptobrevin 2 Is palmitoylated in synaptic vesicles prepared from adult, but not from embryonic brain. Mol Cell Neurosci. 2000 Apr 1;15(4):408–16.

252. Chamberlain LH, Burgoyne RD. Cysteine-String Protein: The chaperone at the synapse. J Neurochem. 2008 Jul 30;74(5):1781–9.

253. Rickman C, Davletov B. Arachidonic acid allows SNARE complex formation in the presence of Munc18. Chem Biol. 2005 May;12(5):545–53.

254. Connell E, Darios F, Broersen K, Gatsby N, Peak-Chew SY, Rickman C, et al. Mechanism of arachidonic acid action on syntaxin–Munc18. EMBO Rep. 2007 Apr;8(4):414–9.

255. Darios F, Wasser C, Shakirzyanova A, Giniatullin A, Goodman K, Munoz-Bravo JL, et al. Sphingosine facilitates SNARE complex assembly and activates synaptic vesicle exocytosis. Neuron. 2009 Jun 11;62(5):683–94.

256. Camoletto PG, Vara H, Morando L, Connell E, Marletto FP, Giustetto M, et al. Synaptic vesicle docking: sphingosine regulates syntaxin 1 interaction with Munc18. PloS One. 2009;4(4):e5310.

257. Garcia-Martinez V, Gimenez-Molina Y, Villanueva J, Darios FD, Davletov B, Gutiérrez LM. Emerging evidence for the modulation of exocytosis by signalling lipids. FEBS Lett. 2018;592(21):3493–503.

258. García-Martínez V, Villanueva J, Torregrosa-Hetland CJ, Bittman R, Higdon A, Darley-Usmar VM, et al. Lipid metabolites enhance secretion acting on SNARE microdomains and altering the extent and kinetics of single release events in bovine adrenal chromaffin cells. PLoS ONE. 2013 Sep 20;8(9):e75845.

259. Flašker A, Jorgačevski J, Calejo AI, Kreft M, Zorec R. Vesicle size determines unitary exocytic properties and their sensitivity to sphingosine. Mol Cell Endocrinol. 2013 Aug 25;376(1):136–47.

260. Amatore C, Arbault S, Bouret Y, Guille M, Lemaître F, Verchier Y. Regulation of exocytosis in chromaffin cells by trans-insertion of lysophosphatidylcholine and arachidonic acid into the outer leaflet of the cell membrane. Chembiochem Eur J Chem Biol. 2006 Dec;7(12):1998–2003.

261. Morgan A, Burgoyne RD. Relationship between arachidonic acid release and Ca2(+)- dependent exocytosis in digitonin-permeabilised bovine adrenal chromaffin cells. Biochem J. 1990 Nov 1;271(3):571–4.

262. Meloni I, Muscettola M, Raynaud M, Longo I, Bruttini M, Moizard MP, et al. FACL4, encoding fatty acid-CoA ligase 4, is mutated in nonspecific X-linked mental retardation. Nat Genet. 2002 Apr;30(4):436–40.

263. Watts JL, Browse J. Genetic dissection of polyunsaturated fatty acid synthesis in *Caenorhabditis elegans*. Proc Natl Acad Sci U S A. 2002 Apr 30;99(9):5854–9.

264. Lesa GM, Palfreyman M, Hall DH, Clandinin MT, Rudolph C, Jorgensen EM, et al. Long chain polyunsaturated fatty acids are required for efficient neurotransmission in *C. elegans*. J Cell Sci. 2003 Dec 15;116(Pt 24):4965–75.

265. Darios F, Connell E, Davletov B. Phospholipases and fatty acid signalling in exocytosis. J Physiol. 2007 Dec 15;585(Pt 3):699–704.

266. Balsinde J, Winstead MV, Dennis EA. Phospholipase A(2) regulation of arachidonic acid mobilization. FEBS Lett. 2002 Oct 30;531(1):2–6.

267. Winstead MV, Balsinde J, Dennis EA. Calcium-independent phospholipase A2: structure and function. Biochim Biophys Acta BBA - Mol Cell Biol Lipids. 2000 Oct 31;1488(1):28–39.

268. Gülsüner S, Tekinay AB, Doerschner K, Boyaci H, Bilguvar K, Unal H, et al. Homozygosity mapping and targeted genomic sequencing reveal the gene responsible for cerebellar hypoplasia and quadrupedal locomotion in a consanguineous kindred. Genome Res. 2011 Dec;21(12):1995–2003.

269. Gülsüner S. Quadrupedal gait in humans : identification and partial characterization of a novel gene WD repeat domain 81 (WDR81) [Thesis]. Bilkent University; 2011 [cited 2023 Apr 24]. Available from: http://repository.bilkent.edu.tr/handle/11693/15223

270. Elbaz B, Kidd GJ, Popko B, Millen KJ, Traka M, Collins D, et al. WDR81 Is Necessary for Purkinje and Photoreceptor Cell Survival. J Neurosci. 2013;33(16):6834–44.

271. Liu K, Jian Y, Sun X, Yang C, Gao Z, Zhang Z, et al. Negative regulation of phosphatidylinositol 3-phosphate levels in early-to-late endosome conversion. J Cell Biol. 2016 Jan 18;212(2):181–98.

272. Han X, Xing R, Wang M, Guo W, Yang C, Liu X, et al. WDR81 regulates adult hippocampal neurogenesis through endosomal SARA-TGFβ signaling. Mol Psychiatry. 2018;

273. Tadayoni Nia A, Bazi Z, Khosravi A, Oladnabi M. WDR81 Gene Silencing Can Reduce Exosome Levels in Human U87-MG Glioblastoma Cells. J Mol Neurosci MN. 2021 Aug;71(8):1696–702.

274. Liu X, Li Y, Wang X, Xing R, Liu K, Gan Q, et al. The BEACH-containing protein WDR81 coordinates p62 and LC3C to promote aggrephagy. J Cell Biol. 2017;216(5):1301–20.

275. Nagle DL, Karim MA, Woolf EA, Holmgren L, Bork P, Misumi DJ, et al. Identification and mutation analysis of the complete gene for Chediak–Higashi syndrome. Nat Genet. 1996 Nov;14(3):307–11.

276. Cullinane AR, Schäffer AA, Huizing M. The BEACH is hot: A LYST of emerging roles for BEACH-domain containing proteins in human disease. Traffic Cph Den. 2013 Jul;14(7):10.1111/tra.12069.

277. Wang JW, Gamsby JJ, Highfill SL, Mora LB, Bloom GC, Yeatman TJ, et al. Deregulated expression of LRBA facilitates cancer cell growth. Oncogene. 2004 May;23(23):4089–97.

278. Lopez-Herrera G, Tampella G, Pan-Hammarström Q, Herholz P, Trujillo-Vargas CM, Phadwal K, et al. Deleterious mutations in LRBA are associated with a syndrome of immune deficiency and autoimmunity. Am J Hum Genet. 2012 Jun 8;90(6):986–1001.

279. Castermans D, Wilquet V, Parthoens E, Huysmans C, Steyaert J, Swinnen L, et al. The neurobeachin gene is disrupted by a translocation in a patient with idiopathic autism. J Med Genet. 2003 May;40(5):352–6.

280. Chen J, Lu Y, Xu J, Huang Y, Cheng H, Hu G, et al. Identification and characterization of NBEAL1, a novel human neurobeachin-like 1 protein gene from fetal brain, which is up regulated in glioma. Mol Brain Res. 2004 Jun 18;125(1):147–55.

281. Albers CA, Cvejic A, Favier R, Bouwmans EE, Alessi MC, Bertone P, et al. Exome sequencing identifies NBEAL2 as the causative gene for Gray Platelet Syndrome. Nat Genet. 2011 Jul 17;43(8):735–7.

282. Kahr WH, Hinckley J, Li L, Schwertz H, Christensen H, Rowley JW, et al. Mutations in NBEAL2, encoding a BEACH protein, cause gray platelet syndrome. Nat Genet. 2011 Jul 17;43(8):738–40.

283. Zhao H, Yang W, Qiu R, Li J, Xin Q, Wang X, et al. An intronic variant associated with systemic lupus erythematosus changes the binding affinity of Yinyang1 to downregulate WDFY4. Genes Immun. 2012 Oct;13(7):536–42.

284. Brenner S. The genetics of *Caenorhabditis elegans*. Genetics. 1974 May;77(1):71–94.

285. Alvarez J, Alvarez-Illera P, García-Casas P, Fonteriz RI, Montero M. The role of Ca2+ signaling in aging and neurodegeneration: insights from *Caenorhabditis elegans* models. Cells. 2020 Jan;9(1):204.

286. Barclay JW, Morgan A, Burgoyne RD. Neurotransmitter release mechanisms studied in *Caenorhabditis elegans.* Cell Calcium. 2012 Sep 1;52(3):289–95.

287. White JG, Southgate E, Thomson JN, Brenner S. The structure of the nervous system of the nematode *Caenorhabditis elegans*. Philos Trans R Soc Lond B Biol Sci. 1986;314(1165):1–340.

288. Sulston JE, Horvitz HR. Post-embryonic cell lineages of the nematode, *Caenorhabditis elegans*. Dev Biol. 1977 Mar;56(1):110–56.

289. Thapliyal S, Babu K. *C. elegans* locomotion: finding balance in imbalance. Adv Exp Med Biol. 2018;1112:185–96.

290. Mahoney TR, Luo S, Nonet ML. Analysis of synaptic transmission in *Caenorhabditis elegans* using an aldicarb-sensitivity assay. Nat Protoc. 2006;1(4):1772–7.

291. Raizen DM, Avery L. Electrical activity and behavior in the pharynx of *Caenorhabditis elegans.* Neuron. 1994 Mar;12(3):483–95.

292. Albertson DG, Thomson JN. The pharynx of *Caenorhabditis elegans*. Philos Trans R Soc Lond B Biol Sci. 1976 Aug 10;275(938):299–325.

293. Seymour MK, Wright KA, Doncaster CC. The action of the anterior feeding apparatus of *Caenorhabditis elegans* (Nematoda: Rhabditida). J Zool. 1983;201(4):527–39.

294. Avery L, Horvitz HR. Pharyngeal pumping continues after laser killing of the pharyngeal nervous system of *C. elegans*. Neuron. 1989 Oct;3(4):473–85.

295. Dillon J, Andrianakis I, Bull K, Glautier S, O'Connor V, Holden-Dye L, et al. AutoEPG: software for the analysis of electrical activity in the microcircuit underpinning feeding behaviour of *Caenorhabditis elegans*. Brezina V, editor. PLoS ONE. 2009 Dec 29;4(12):e8482.

296. Ashrafi K. Obesity and the regulation of fat metabolism. WormBook: The Online Review of C. elegans Biology [Internet]. WormBook; 2007 [cited 2023 Jan 29]. Available from: https://www.ncbi.nlm.nih.gov/books/NBK19757/

297. Castro C, Sar F, Shaw WR, Mishima M, Miska EA, Griffin JL. A metabolomic strategy defines the regulation of lipid content and global metabolism by Δ9 desaturases in *Caenorhabditis elegans*. BMC Genomics. 2012 Jan 20;13(1):36.

298. Yilmaz LS, Walhout AJM. A *Caenorhabditis elegans* genome-scale metabolic network model. Cell Syst. 2016 May 25;2(5):297–311.

299. Gebauer J, Gentsch C, Mansfeld J, Schmeißer K, Waschina S, Brandes S, et al. A genome-scale database and reconstruction of *Caenorhabditis elegans* metabolism. Cell Syst. 2016 May;2(5):312–22.

300. Reed LK, Baer CF, Edison AS. Considerations when choosing a genetic model organism for metabolomics studies. Curr Opin Chem Biol. 2017 Feb 1;36:7–14.

301. Perez CL, Van Gilst MR. A 13C isotope labeling strategy reveals the influence of insulin signaling on lipogenesis in *C. elegans.* Cell Metab. 2008 Sep;8(3):266–74.

302. Watts JL, Ristow M. Lipid and carbohydrate metabolism in *Caenorhabditis elegans*. Genetics. 2017 Oct;207(2):413–46.

303. Witting M, Schmitt-Kopplin P. The *Caenorhabditis elegans* lipidome: A primer for lipid analysis in *Caenorhabditis elegans*. Arch Biochem Biophys. 2016 Jan 1;589:27–37.

304. Cravero BH, Prez G, Lombardo VA, Binolfi A, Mendoza D de. Unsaturated fatty acids profiling in live *C. elegans* using real-time NMR spectroscopy. bioRxiv; 2021 Apr 2: p. 2021.04.02.438181.

305. Van Assche R, Temmerman L, Dias DA, Boughton B, Boonen K, Braeckman BP, et al. Metabolic profiling of a transgenic *Caenorhabditis elegans* Alzheimer model. Metabolomics. 2015 Apr 1;11(2):477–86.

306. Zhu B, Mak JCH, Morris AP, Marson AG, Barclay JW, Sills GJ, et al. Functional analysis of epilepsy-associated variants in STXBP1/Munc18-1 using humanised Caenorhabditis elegans. Epilepsia. 2020 Apr;61(4):810–21.

307. Tsalik EL, Hobert O. Functional mapping of neurons that control locomotory behavior in *Caenorhabditis elegans*. J Neurobiol. 2003 Aug;56(2):178–97.

308. Kamath RS, Ahringer J. Genome-wide RNAi screening in *Caenorhabditis elegans*. Methods San Diego Calif. 2003 Aug;30(4):313–21.

309. Sumner LW, Amberg A, Barrett D, Beale MH, Beger R, Daykin CA, et al. Proposed minimum reporting standards for chemical analysis Chemical Analysis Working Group (CAWG) Metabolomics Standards Initiative (MSI). Metabolomics Off J Metabolomic Soc. 2007 Sep;3(3):211–21.

310. Grosman R. NMR metabolic profiling of mosquito species to understand insecticide resistance [Thesis]. University of Liverpool; 2019 [cited 2023 Apr 24]. Available from: https://livrepository.liverpool.ac.uk/3067218

311. Corsaro C, Vasi S, Neri F, Mezzasalma AM, Neri G, Fazio E. NMR in Metabolomics: From Conventional Statistics to Machine Learning and Neural Network Approaches. Appl Sci. 2022 Jan;12(6):2824.

312. Deng L, Denham JE, Arya C, Yuval O, Cohen N, Haspel G. Inhibition underlies fast undulatory locomotion in *Caenorhabditis elegans*. eNeuro [Internet]. 2021 Mar 1 [cited 2023 Jan 10];8(2). Available from: https://www.eneuro.org/content/8/2/ENEURO.0241-20.2020

313. Gjorgjieva J, Biron D, Haspel G. Neurobiology of *Caenorhabditis elegans* locomotion: where do we stand? Bioscience. 2014 Jun 1;64(6):476–86.

314. Gray J, Lissmann HW. The locomotion of nematodes. J Exp Biol 1964;41 (1):135–154.

315. Graham ME, Edwards MR, Holden-Dye L, Morgan A, Burgoyne RD, Barclay JW. UNC-18 modulates ethanol sensitivity in *Caenorhabditis elegans*. Mol Biol Cell. 2009 Jan 1;20(1):43–55.

316. de Wit H, Walter AM, Milosevic I, Gulyás-Kovács A, Riedel D, Sørensen JB, et al. Synaptotagmin-1 docks secretory vesicles to Syntaxin-1/SNAP-25 acceptor complexes. Cell. 2009 Sep;138(5):935–46.

317. Brenner S. The genetics of *Caenorhabditis elegans*. Genetics. 1974 May;77(1):71–94.

318. Blazie SM, Jin Y. Pharming for genes in neurotransmission: combining chemical and genetic approaches in *Caenorhabditis elegans*. ACS Chem Neurosci. 2018 Aug 15;9(8):1963–74.

319. Pierce-Shimomura JT, Chen BL, Mun JJ, Ho R, Sarkis R, McIntire SL. Genetic analysis of crawling and swimming locomotory patterns in *C. elegans*. Proc Natl Acad Sci. 2008 Dec 30;105(52):20982–7.

320. Guiberson NGL, Pineda A, Abramov D, Kharel P, Carnazza KE, Wragg RT, et al. Mechanism-based rescue of Munc18-1 dysfunction in varied encephalopathies by chemical chaperones. Nat Commun. 2018 Dec;9(1):3986.

321. Miller KG, Emerson MD, Rand JB. Goα and diacylglycerol kinase negatively regulate the Gqα Pathway in *C. elegans*. Neuron. 1999 Oct;24(2):323–33.

322. Johnson JR, Kashyap S, Rankin K, Barclay JW. *Rab-3* and *unc-18* interactions in alcohol sensitivity are distinct from synaptic transmission. PLOS ONE. 2013 Nov 14;8(11):e81117.

323. Miller KG, Emerson MD, Rand JB. Goα and diacylglycerol kinase negatively regulate the Gqα pathway in *C. elegans*. Neuron. 1999;24(2):323–33.

324. Maruyama IN, Brenner S. A phorbol ester/diacylglycerol-binding protein encoded by the *unc-13* gene of *Caenorhabditis elegans*. Proc Natl Acad Sci U S A. 1991 Jul 1;88(13):5729–33.

325. Silinsky EM, Searl TJ. Phorbol esters and neurotransmitter release: more than just protein kinase C? Br J Pharmacol. 2003;138(7):1191–201.

326. Lou X, Korogod N, Brose N, Schneggenburger R. phorbol esters modulate spontaneous and Ca2+-evoked transmitter release via acting on both Munc13 and protein kinase C. J Neurosci. 2008 Aug 13;28(33):8257–67.

327. Malenka RC, Madison DV, Nicoll RA. Potentiation of synaptic transmission in the hippocampus by phorbol esters. Nature. 1986 May;321(6066):175–7.

328. Shapira R, Silberberg SD, Ginsburg S, Rahamimoff R. Activation of protein kinase C augments evoked transmitter release. Nature. 1987 Jan;325(6099):58–60.

329. Segal M. Synaptic transmission between cultured rat hippocampal neurons is enhanced by activation of protein kinase-C. Neurosci Lett. 1989 Jun 19;101(2):169–74.

330. Parfitt KD, Madison DV. Phorbol esters enhance synaptic transmission by a presynaptic, calcium-dependent mechanism in rat hippocampus. J Physiol. 1993 Nov;471:245–68.

331. Stevens CF, Sullivan JM. Regulation of the readily releasable vesicle pool by protein kinase C. Neuron. 1998 Oct 1;21(4):885–93.

332. Redman RS, Searl TJ, Hirsh JK, Silinsky EM. Opposing effects of phorbol esters on transmitter release and calcium currents at frog motor nerve endings. J Physiol. 1997 May 15;501(Pt 1):41–8.

333. Searl TJ, Silinsky EM. Increases in acetylcholine release produced by phorbol esters are not mediated by protein kinase C at motor nerve endings. J Pharmacol Exp Ther. 1998 Apr;285(1):247–51.

334. Miller KG, Emerson MD, McManus JR, Rand JB. RIC-8 (Synembryn): a novel conserved protein that is required for G(q)alpha signaling in the *C. elegans* nervous system. Neuron. 2000 Aug;27(2):289–99.

335. Sieburth D, Madison JM, Kaplan JM. PKC-1 regulates secretion of neuropeptides. Nat Neurosci. 2007 Jan;10(1):49–57.

336. Sassa T, Ogawa H, Kimoto M, Hosono R. The synaptic protein UNC-18 is phosphorylated by protein kinase C. Neurochem Int. 1996 Nov;29(5):543–52.

337. de Vries KJ, Geijtenbeek A, Brian EC, de Graan PN, Ghijsen WE, Verhage M. Dynamics of Munc18-1 phosphorylation/dephosphorylation in rat brain nerve terminals. Eur J Neurosci. 2000 Jan;12(1):385–90.

338. Nili U, De Wit H, Gulyas-Kovacs A, Toonen RF, Sørensen JB, Verhage M, et al. Munc18-1 phosphorylation by protein kinase C potentiates vesicle pool replenishment in bovine chromaffin cells. Neuroscience. 2006 Dec;143(2):487–500.

339. Shimazaki Y, Nishiki T, Omori A, Sekiguchi M, Kamata Y, Kozaki S, et al. Phosphorylation of 25-kDa synaptosome-associated protein. Possible involvement in

protein kinase C-mediated regulation of neurotransmitter release. J Biol Chem. 1996 Jun 14;271(24):14548–53.

340. Hilfiker S, Augustine GJ. Regulation of synaptic vesicle fusion by protein kinase C. J Physiol. 1999 Feb 15;515(Pt 1):1.

341. Liu JP. Protein kinase C and its substrates. Mol Cell Endocrinol. 1996 Jan 15;116(1):1– 29.

342. Colón-González F, Kazanietz MG. C1 domains exposed: from diacylglycerol binding to protein-protein interactions. Biochim Biophys Acta. 2006 Aug;1761(8):827–37.

343. Ellwanger K, Hausser A. Physiological functions of protein kinase D in vivo. IUBMB Life. 2013 Feb;65(2):98–107.

344. Steinberg SF. Regulation of protein kinase D1 activity. Mol Pharmacol. 2012 Mar;81(3):284–91.

345. Fu Y, Rubin CS. Protein kinase D: coupling extracellular stimuli to the regulation of cell physiology. EMBO Rep. 2011 Aug;12(8):785–96.

346. Johnson JR, Barclay JW. *C. elegans dkf-1* (Protein Kinase D1) mutants have age-dependent defects in locomotion and neuromuscular transmission. MicroPubl Biol. 2023 Apr 4;2023:10.17912/micropub.biology.000800.

347. Chen J, Deng F, Li J, Wang QJ. Selective binding of phorbol esters and diacylglycerol by individual C1 domains of the PKD family. Biochem J. 2008 Mar 27;411(2):333–42.

348. Yeaman C, Ayala MI, Wright JR, Bard F, Bossard C, Ang A, et al. Protein kinase D regulates basolateral membrane protein exit from trans-Golgi network. Nat Cell Biol. 2004 Feb;6(2):106–12.

349. Wang QJ. PKD at the crossroads of DAG and PKC signaling. Trends Pharmacol Sci. 2006 Jun;27(6):317–23.

350. Zugaza JL, Sinnett-Smith J, Van Lint J, Rozengurt E. Protein kinase D (PKD) activation in intact cells through a protein kinase C-dependent signal transduction pathway. EMBO J. 1996 Nov 15;15(22):6220–30.

351. Oueslati Morales CO, Ignácz A, Bencsik N, Sziber Z, Rátkai AE, Lieb WS, et al. Protein kinase D promotes activity-dependent AMPA receptor endocytosis in hippocampal neurons. Traffic. 2021;22(12):454–70.

352. Sakane F, Kanoh H. Diacylglycerol kinase. Int J Biochem Cell Biol. 1997 Oct 1;29(10):1139–43.

353. Xie S, Naslavsky N, Caplan S. Diacylglycerol kinases in membrane trafficking. Cell Logist. 2015 Apr 3;5(2):e1078431.

354. Ghosh S, Strum JC, Sciorra VA, Daniel L, Bell RM. Raf-1 kinase possesses distinct binding domains for phosphatidylserine and phosphatidic acid. J Biol Chem. 1996 Apr;271(14):8472–80.

355. Limatola C, Schaap D, Moolenaar WH, van Blitterswijk WJ. Phosphatidic acid activation of protein kinase C-zeta overexpressed in COS cells: comparison with other protein kinase C isotypes and other acidic lipids. Biochem J. 1994 Dec 15;304(Pt 3):1001–8.

356. Moritz A, De Graan PN, Gispen WH, Wirtz KW. Phosphatidic acid is a specific activator of phosphatidylinositol-4-phosphate kinase. J Biol Chem. 1992 Apr 15;267(11):7207–10.

357. Honda A, Nogami M, Yokozeki T, Yamazaki M, Nakamura H, Watanabe H, et al. Phosphatidylinositol 4-phosphate 5-kinase α is a downstream effector of the small g protein ARF6 in membrane ruffle formation. Cell. 1999 Nov 24;99(5):521–32.

358. Zhao Z, Shen SH, Fischer EH. Stimulation by phospholipids of a protein-tyrosine-phosphatase containing two src homology 2 domains. Proc Natl Acad Sci U S A. 1993 May 1;90(9):4251–5.

359. Frank C, Keilhack H, Opitz F, Zschörnig O, Böhmer FD. Binding of phosphatidic acid to the protein-tyrosine phosphatase SHP-1 as a basis for activity modulation. Biochemistry. 1999 Sep 1;38(37):11993–2002.

360. Sakane F, Hoshino F, Murakami C. New era of diacylglycerol kinase, phosphatidic acid and phosphatidic acid-binding protein. Int J Mol Sci. 2020 Jan;21(18):6794.

361. Ávila-Flores A, Santos T, Rincón E, Mérida I. Modulation of the mammalian target of rapamycin pathway by diacylglycerol kinase-produced phosphatidic acid. J Biol Chem. 2005 Mar;280(11):10091–9.

362. Luo B, Prescott SM, Topham MK. Diacylglycerol kinase zeta regulates phosphatidylinositol 4-phosphate 5-kinase Ialpha by a novel mechanism. Cell Signal. 2004 Aug;16(8):891–7.

363. Mizuno S, Sasai H, Kume A, Takahashi D, Satoh M, Kado S, et al. Dioleoyl-phosphatidic acid selectively binds to α-synuclein and strongly induces its aggregation. FEBS Lett. 2017;591(5):784–91.

364. Zeniou-Meyer M, Zabari N, Ashery U, Chasserot-Golaz S, Haeberlé AM, Demais V, et al. Phospholipase D1 production of phosphatidic acid at the plasma membrane promotes exocytosis of large dense-core granules at a late stage. J Biol Chem. 2007 Jul;282(30):21746–57.

365. Jiang Y, Sakane F, Kanoh H, Walsh JP. Selectivity of the diacylglycerol kinase inhibitor 3-{2-(4-[bis-(4-fluorophenyl)methylene]-1-piperidinyl)ethyl}-2,3-dihydro-2-thioxo-4(1H)quinazolinone (R59949) among diacylglycerol kinase subtypes. Biochem Pharmacol. 2000 Apr 1;59(7):763–72.

366. Day P, Burrows L, Richards D, Fountain SJ. Inhibitors of DAG metabolism suppress CCR2 signalling in human monocytes. Br J Pharmacol. 2019 Aug;176(15):2736–49.

367. Rapiteanu R, Davis LJ, Williamson JC, Timms RT, Paul Luzio J, Lehner PJ. A genetic screen identifies a critical role for the WDR81-WDR91 complex in the trafficking and degradation of tetherin. Traffic. 2016;17:940–58.

368. Jogl G, Shen Y, Gebauer D, Li J, Wiegmann K, Kashkar H, et al. Crystal structure of the BEACH domain reveals an unusual fold and extensive association with a novel PH domain. EMBO J. 2002 Sep 16;21(18):4785–95.

369. Smith TF, Gaitatzes C, Saxena K, Neer EJ. The WD repeat: a common architecture for diverse functions. Trends Biochem Sci. 1999 May;24(5):181–5.

370. Li D, Roberts R. WD-repeat proteins: structure characteristics, biological function, and their involvement in human diseases. Cell Mol Life Sci CMLS. 2001 Dec;58(14):2085–97.

371. Tu-Sekine B, Goldschmidt HL, Raben DM. DGK-θ: Structure, Enzymology, and Physiological Roles. Front Cell Dev Biol. 2016 [cited 2022 Sep 18];4. Available from: https://www.frontiersin.org/articles/10.3389/fcell.2016.00101

372. Reilly ML, Poirier K, Rio M, Doco-Fenzy M, Attie-Bitach T, Rujano MA, et al. WDR81 mutations cause extreme microcephaly and impair mitotic progression in human fibroblasts and *Drosophila* neural stem cells. Brain. 2017;140:2597–609.

373. Stringham EG, Dixon DK, Jones D, Candido EP. Temporal and spatial expression patterns of the small heat shock (hsp16) genes in transgenic *Caenorhabditis elegans*. Mol Biol Cell. 1992 Feb;3(2):221–33.

374. Sieburth D, Ch'ng Q, Dybbs M, Tavazoie M, Kennedy S, Wang D, et al. Systematic analysis of genes required for synapse structure and function. Nature. 2005 Jul 28;436(7050):510–7.

375. Trojanowski NF, Raizen DM, Fang-Yen C. Pharyngeal pumping in *Caenorhabditis elegans* depends on tonic and phasic signaling from the nervous system. Sci Rep. 2016 Mar 15;6:22940.

376. Zhen M, Samuel AD. C. elegans locomotion: small circuits, complex functions. Curr Opin Neurobiol. 2015 Aug 1;33:117–26.

377. Axäng C, Rauthan M, Hall DH, Pilon M. Developmental genetics of the *C. elegans* pharyngeal neurons NSML and NSMR. BMC Dev Biol. 2008 Apr 9;8(1):38.

378. Goldschmidt HL, Tu-Sekine B, Volk L, Anggono V, Huganir RL, Raben DM. DGKθ catalytic activity is required for efficient recycling of presynaptic vesicles at excitatory synapses. Cell Rep. 2016;14(2):200–7.

379. Schink KO, Raiborg C, Stenmark H. Phosphatidylinositol 3-phosphate, a lipid that regulates membrane dynamics, protein sorting and cell signalling. BioEssays News Rev Mol Cell Dev Biol. 2013 Oct;35(10):900–12.

380. Wang X, Gong J, Zhu L, Wang S, Yang X, Xu Y, et al. Munc13 activates the Munc18-1/syntaxin-1 complex and enables Munc18-1 to prime SNARE assembly. EMBO J. 2020 Aug 17;39(16):e103631.

381. Fahy E, Cotter D, Sud M, Subramaniam S. Lipid classification, structures and tools. Biochim Biophys Acta. 2011 Nov;1811(11):637–47.

382. Postila PA, Róg T. A perspective: active role of lipids in neurotransmitter dynamics. Mol Neurobiol. 2020;57(2):910–25.

383. Gil M, Samino S, Barrilero R, Correig X. Lipid Profiling Using 1H NMR Spectroscopy. Methods Mol Biol Clifton NJ. 2019;2037:35–47.

384. Puchkov D, Haucke V. Greasing the synaptic vesicle cycle by membrane lipids. Trends Cell Biol. 2013 Oct 1;23(10):493–503.

385. Yang Z, Gou L, Chen S, Li N, Zhang S, Zhang L. Membrane Fusion Involved in Neurotransmission: Glimpse from Electron Microscope and Molecular Simulation. Front Mol Neurosci. 2017 [cited 2023 Jan 17];10. Available from: https://www.frontiersin.org/articles/10.3389/fnmol.2017.00168

386. Li J, Vosegaard T, Guo Z. Applications of nuclear magnetic resonance in lipid analyses: an emerging powerful tool for lipidomics studies. Prog Lipid Res. 2017 Oct 1;68:37–56.

387. Wong SQ, Pontifex MG, Phelan MM, Pidathala C, Kraemer BC, Barclay JW, et al. α-Methyl-α-phenylsuccinimide ameliorates neurodegeneration in a *C. elegans* model of TDP-43 proteinopathy. Neurobiol Dis. 2018 Oct;118:40–54.

388. Stillwell W. Chapter 20 - Bioactive Lipids. In: Stillwell W, editor. An Introduction to Biological Membranes (Second Edition). Elsevier; 2016 [cited 2022 Oct 13]. p. 453–78. Available from: https://www.sciencedirect.com/science/article/pii/B9780444637727000208

389. Zheng L, Fleith M, Giuffrida F, O'Neill BV, Schneider N. Dietary polar lipids and cognitive development: a narrative review. Adv Nutr. 2019 Nov 1;10(6):1163–76.

390. Amiel A, Tremblay-Franco M, Gautier R, Ducheix S, Montagner A, Polizzi A, et al. Proton NMR enables the absolute quantification of aqueous metabolites and lipid classes in unique mouse liver samples. Metabolites. 2019 Dec 21;10(1):9.

391. Blaise BJ, Giacomotto J, Triba MN, Toulhoat P, Piotto M, Emsley L, et al. Metabolic profiling strategy of Ca*enorhabditis elegans* by whole-organism nuclear magnetic resonance. J Proteome Res. 2009 May;8(5):2542–50.

392. Bazinet RP, Layé S. Polyunsaturated fatty acids and their metabolites in brain function and disease. Nat Rev Neurosci. 2014 Dec;15(12):771–85.

393. Romano A, Koczwara JB, Gallelli CA, Vergara D, Micioni Di Bonaventura MV, Gaetani S, et al. Fats for thoughts: An update on brain fatty acid metabolism. Int J Biochem Cell Biol. 2017 Mar 1;84:40–5.

394. Falomir-Lockhart LJ, Cavazzutti GF, Giménez E, Toscani AM. fatty acid signaling mechanisms in neural cells: fatty acid receptors. Front Cell Neurosci. 2019 Apr 24;13:162.

395. Kahn-Kirby AH, Dantzker JLM, Apicella AJ, Schafer WR, Browse J, Bargmann CI, et al. Specific polyunsaturated fatty acids drive TRPV-dependent sensory signaling *in vivo*. Cell. 2004 Dec 17;119(6):889–900.

396. Miceli MD, Bosch-Bouju C, Layé S. PUFA and their derivatives in neurotransmission and synapses: a new hallmark of synaptopathies. Proc Nutr Soc. 2020 Nov;79(4):388–403.

397. Schaechter J, Benowitz L. Activation of protein kinase C by arachidonic acid selectively enhances the phosphorylation of GAP-43 in nerve terminal membranes. J Neurosci. 1993 Oct 1;13(10):4361–71.

398. Shinomura T, Asaoka Y, Oka M, Yoshida K, Nishizuka Y. Synergistic action of diacylglycerol and unsaturated fatty acid for protein kinase C activation: its possible implications. Proc Natl Acad Sci U S A. 1991;88(12):5149–53.

399. Takamori S, Holt M, Stenius K, Lemke EA, Grønborg M, Riedel D, et al. Molecular anatomy of a trafficking organelle. Cell. 2006 Nov 17;127(4):831–46.

400. Wassall SR, Stillwell W. Polyunsaturated fatty acid–cholesterol interactions: Domain formation in membranes. Biochim Biophys Acta BBA - Biomembr. 2009 Jan 1;1788(1):24–32.

401. Gibellini F, Smith TK. The Kennedy pathway—*de novo* synthesis of phosphatidylethanolamine and phosphatidylcholine. IUBMB Life. 2010;62(6):414–28.

402. Duarte JMN, Lei H, Mlynárik V, Gruetter R. The neurochemical profile quantified by in vivo 1H NMR spectroscopy. NeuroImage. 2012 Jun 1;61(2):342–62.

403. Betz H, Laube B. Glycine receptors: recent insights into their structural organisation and functional diversity. J Neurochem. 2006 Jun;97(6):1600–10.

404. Klein J. Membrane breakdown in acute and chronic neurodegeneration: focus on choline-containing phospholipids. J Neural Transm Vienna Austria 1996. 2000;107(8–9):1027–63.

405. Merris M, Wadsworth WG, Khamrai U, Bittman R, Chitwood DJ, Lenard J. Sterol effects and sites of sterol accumulation in *Caenorhabditis elegans*. J Lipid Res. 2003 Jan 1;44(1):172–81.

406. Horvath SE, Daum G. Lipids of mitochondria. Prog Lipid Res. 2013 Oct 1;52(4):590–614.

407. Hou NS, Gutschmidt A, Choi DY, Pather K, Shi X, Watts JL, et al. Activation of the endoplasmic reticulum unfolded protein response by lipid disequilibrium without disturbed proteostasis in vivo. Proc Natl Acad Sci. 2014 Jun 3;111(22):E2271–80.

408. Morgan RS, Walmsley G, Peffers MJ, Barrett-Jolley R, Phelan MM. A robust method for performing 1H-NMR lipidomics in embryonic zebrafish. 2021 May [cited 2021 Sep 15] p. 2021.05.26.445770. Available from: https://www.biorxiv.org/content/10.1101/2021.05.26.445770v1

409. Edison AS, Hall RD, Junot C, Karp PD, Kurland IJ, Mistrik R, et al. The time is right to focus on model organism metabolomes. Metabolites. 2016 Feb 15;6(1):8.

410. Wong SQ. Using *Caenorhabditis elegans* to identify succinimide-based neuroprotective compounds and their mechanisms of action [Thesis]. University of Liverpool; 2017 [cited 2023 Apr 24]. Available from: https://livrepository.liverpool.ac.uk/3017944

411. Van QN, Issaq HJ, Jiang Q, Li Q, Muschik GM, Waybright TJ, et al. Comparison of 1D and 2D NMR Spectroscopy for Metabolic Profiling. J Proteome Res. 2008 Feb 1;7(2):630–9.

412. Emwas AHM. The strengths and weaknesses of NMR spectroscopy and mass spectrometry with particular focus on metabolomics research. In: Bjerrum JT, editor. Metabonomics: Methods and Protocols. New York, NY: Springer; 2015 [cited 2023 Jan 17]. p. 161–93. (Methods in Molecular Biology). Available from: https://doi.org/10.1007/978-1-4939-2377-9_13

413. Stamberger H, Crosiers D, Balagura G, Bonardi CM, Basu A, Cantalupo G, et al. Natural history study of STXBP1-developmental and epileptic encephalopathy into adulthood. Neurology. 2022 Jul 19;99(3):e221–33.

414. Chen W, Cai ZL, Chao ES, Chen H, Longley CM, Hao S, et al. Stxbp1/Munc18-1 haploinsufficiency impairs inhibition and mediates key neurological features of STXBP1 encephalopathy. Monteggia LM, Dulac C, Missler M, editors. eLife. 2020 Feb 19;9:e48705.

415. Ramos-Miguel A, Hercher C, Beasley CL, Barr AM, Bayer TA, Falkai P, et al. Loss of Munc18-1 long splice variant in GABAergic terminals is associated with cognitive decline and increased risk of dementia in a community sample. Mol Neurodegener. 2015 Dec 2;10(1):65.

416. Johnson JR, Barclay JW, Lian LY, Morgan A, Burgoyne RD, Ferdek P. Binding of UNC-18 to the N-terminus of syntaxin is essential for neurotransmission in *Caenorhabditis elegans*. Biochem J. 2008;418:73–80.

417. Cavallin M, Rujano MA, Bednarek N, Medina-Cano D, Bernabe Gelot A, Drunat S, et al. WDR81 mutations cause extreme microcephaly and impair mitotic progression in human fibroblasts and *Drosophila* neural stem cells. Brain J Neurol. 2017 Oct 1;140(10):2597–609.

418. James DJ, Khodthong C, Kowalchyk JA, Martin TFJ. Phosphatidylinositol 4,5-bisphosphate regulates SNARE-dependent membrane fusion. J Cell Biol. 2008 Jul 21;182(2):355–66.

419. Katan M, Cockcroft S. Phosphatidylinositol(4,5)bisphosphate: diverse functions at the plasma membrane. Essays Biochem. 2020 Sep;64(3):513–31.

420. Wierda KDB, Toonen RFG, de Wit H, Brussaard AB, Verhage M. Interdependence of PKC-dependent and PKC-independent pathways for presynaptic plasticity. Neuron. 2007 Apr 19;54(2):275–90.

421. Edwards MR, Johnson JR, Rankin K, Jenkins RE, Maguire C, Morgan A, et al. PKC-2 phosphorylation of UNC-18 Ser322 in AFD neurons regulates temperature dependency of locomotion. J Neurosci. 2012 May 16;32(20):7042–51.

422. Meneely PM, Dahlberg CL, Rose JK. Working with Worms: *Caenorhabditis elegans* as a Model Organism. Curr Protoc Essent Lab Tech. 2019;19(1):e35.

423. *C. elegans* Sequencing Consortium. Genome sequence of the nematode *C. elegans*: a platform for investigating biology. Science. 1998 Dec 11;282(5396):2012–8.

424. Debik J, Sangermani M, Wang F, Madssen TS, Giskeødegård GF. Multivariate analysis of NMR-based metabolomic data. NMR Biomed. 2022;35(2):e4638.

Appendices

Appendix 1: CRS scores of polar metabolites

Metabolite	Bin	CRS (%)	Representative bin
NAD	1 15* 16* 55 56	64.90 62.21 69.07 46.78 67.89	56
AMP	6* 12 51 52* 53* 77* 78* 79*	48.07 45.57 31.52 42.05 39.64 28.91 22.34 22.90	12
ADP	7*	unique	7
Formate	8	Unique	8
ATP	13* 52* 53* 73* 74*	33.96 15.82 14.48 37.01 30.19	13
Adenine	14* 16*	69.37 69.37	14
UDP-glucuronic acid	23* 24* 65*	58.19 56.02 15.70	23
UDP-glucose	23* 24* 59* 65*	62.04 60.17 60.17 10.40	23
Histamine	25* 181* 183* 211* 213*	79.34 87.95 92.34 90.40 90.45	183
L-tryptophan	26* 32* 38* 177 178*	85.44 61.98 85.27 84.09 86.03	177
L-phenylalanine	35 36* 37* 38*	99.56 99.40 99.53 99.42	35
L-tyrosine	41 44* 107*	89.60 86.94 88.70	41
Carnosine	42*	unique	42
Anserine	42* 135* 136*	90.93 94.86 93.68	135
Tyramine	44* 187* 188* 215* 217*	83.46 67.28 82.97 81.86 79.44	44
Fumaric acid	48	unique	48
NADPH	50* 59*	70.96 70.96	50

Maltose	69*	39.66	102
	102*	76.42	
	116*	77.37	
	119*	75.80	
	143*	76.19	
	146*	73.22	
	155*	68.49	
	167*	48.88	
	184*	73.87	
Glucose	69*	55.08	114
	111*	83.84	
	112*	74.44	
	114	88.25	
	115	88.96	
	116*	83.02	
	119*	73.09	
	121*	85.16	
	137*	81.40	
	163	84.16	
	164	84.18	
	165	87.78	
	166	68.02	
	170*	79.14	
	171	85.31	
	172	84.55	
	187*	83.06	
	188*	80.16	
NADP	73*	95.77	73
	74*	95.77	
Sn-glycero-3-phosphocholine	80*	84.24	143
	143*	85.56	
	189*	80.10	
N-carbamoyl-aspartate	82	86.42	83
	83	86.42	
	234*	84.78	
	235*	88.16	
	236*	78.82	
	253*	83.56	
	255*	86.53	
L-threonine	84	89.27	337
	154	90.89	
	337	90.90	
	339	89.59	
O-phosphocholine	87	87.60	87
	153	85.15	
	190	76.17	
L-lactic acid	89	78.99	340
	338	89.17	
	340	89.36	
Fructose	92*	unique	92
Myo-Inositol	93	92.51	152
	94*	92.40	
	150	93.83	
	151*	93.02	
	152	93.61	
	157	82.07	
	158*	91.46	
	160	93.18	
	183*	91.26	
	184*	91.08	
	185*	80.00	
Creatinine	94*	93.26	206
	206	91.68	
	208*	95.10	
Serine	101*	95.48	103
	103	96.93	

	104	96.89	
	105*	96.53	
	107*	94.92	
	120	94.03	
Nicotinurate	101*	unique	101
Phosphocreatine	105*	96.73	207
	207	96.73	
Glycylproline	105*	91.23	292
	155*	76.80	
	269*	92.31	
	290*	93.68	
	291*	87.84	
	292*	94.41	
	294*	93.92	
	295*	93.09	
Glycolate	106	unique	106
Creatine	108	unique	108
Betaine	111*	93.96	111
	185*	93.96	
Glutathione	126*	80.83	240
	127*	76.46	
	128*	80.74	
	129*	78.64	
	130*	80.43	
	212	89.12	
	214	87.47	
	215*	70.91	
	217*	63.07	
	218*	75.27	
	219*	87.93	
	237*	86.70	
	238	88.54	
	239	89.69	
	240	89.66	
	241*	88.99	
	243	86.49	
	244*	87.10	
	246*	87.70	
	248	87.06	
	277*	88.50	
	278*	87.52	
	279*	86.82	
	282	83.22	
Guanidinoacetate	128*	unique	128
L-alanine	128*	91.65	325
	130*	94.48	
	132*	92.44	
	325	88.27	
NDMA	128*	88.26	196
	196*	88.26	
L-glutamine	130*	85.13	257
	131*	84.36	
	133*	83.48	
	250	89.42	
	251*	89.34	
	252	88.23	
	253*	73.02	
	254*	90.66	
	255*	78.16	
	257	90.40	
	258*	85.70	
	260*	83.78	
	277*	90.33	
	278*	87.08	
	279*	87.14	
	280*	87.24	

	281*	88.94	
Glutamic acid	131*	80.59	265
	132*	78.49	
	133*	84.36	
	134	82.98	
	261*	82.70	
	262*	83.61	
	263*	85.28	
	264	83.51	
	265	85.43	
	266*	82.28	
	279*	76.86	
	280*	84.40	
	283	77.64	
	284*	0.71	
	286	81.02	
	287*	85.36	
N-acetyl-glycine	136	unique	136
L-isoleucine	145*	71.53	374
	294*	86.58	
	295*	87.01	
	346*	20.76	
	368	85.36	
	372	86.24	
	374	86.40	
	375*	85.79	
	376*	86.57	
Ethanol	146*	28.58	354
	167*	57.44	
	351	63.31	
	352	70.00	
	354	70.64	
L-valine	151*	96.35	369
	269*	98.19	
	366	98.21	
	367	98.29	
	369	98.37	
Glycine	156	unique	156
Pantothenic acid	162*	81.56	375
	375*	92.72	
	376*	91.33	
	379*	91.41	
Taurine	168	82.35	168
	169	80.10	
	185*	80.24	
	186	76.73	
Trimethylamine N-oxide (TMAO)	185*	unique	185
cis-Aconitic acid	187*	unique	187
	189*	78.80	254
	254*	88.86	
	256*	84.93	
Choline	191*	Unique	191
DL-acetylcarnitine	191*	unique	191
beta-Alanine	193	90.53	242
	194	88.94	
	196*	85.31	
	241	89.54	
	242	92.92	
	245*	89.09	
N,N-Dimethylformamide (DMF)	208*	93.37	208
	218*	93.37	
N-acetyl-L-cysteine (NAC)	216	81.23	216
	217*	84.16	
	218*	80.08	
	284*	53.55	

Aspartate	225 227 232*	97.32 97.08 94.56	225
Citric acid	232* 234* 244* 245* 246* 247	88.57 84.77 90.36 91.89 91.56 91.72	247
Malate	234 258 260 261 263	74.78 91.63 91.67 92.71 93.33	261
Pyruvate	262 263	97.45 97.45	262
N-acetyl-glutamine	287*	unique	286
N2-acetylornithine	287* 312 313 314	97.59 98.10 98.74 98.07	313
N-acetyl-L-aspartic acid	291*	unique	291
L-leucine	310 311 312* 313* 314* 315* 317* 370* 371*	96.44 98.22 97.96 97.80 96.90 98.26 97.07 97.00 97.13	311
N-alpha-acetyl-L-lysine	315* 317*	99.30 99.30	317
5,6-dihydrothimine	348 349	93.18 93.18	349
Isopropyl alcohol	353 355	99.88 99.88	355
4-hydroxyisopentanoate	370* 371*	99.98 99.98	371

Note: "234" appears in the top-right margin near the Citric acid row.